

1. Report No. FHWA/TX-04/4178-2	2. Government Accession No.	3. Recipient's Catalog No.	
4. Title And Subtitle Fatigue Strength of Signal Mast Arm Connections		5. Report Date August 2003	
		6. Performing Organization Code	
7. Author(s) Mark T. Koenigs, Tamer A. Botros, Dylan Freytag, and Karl H. Frank		8. Performing Organization Report No. Research Report 4178-2	
9. Performing Organization Name and Address Center for Transportation Research The University of Texas at Austin 3208 Red River, Suite 200 Austin, TX 78705-2650		10. Work Unit No. (TRAIS)	
		11. Contract or Grant No. Research Project 0-4178	
12. Sponsoring Agency Name and Address Texas Department of Transportation Research and Technology Implementation Office P.O. Box 5080 Austin, TX 78763-5080		13. Type of Report and Period Covered Research Report (9/99-8/01)	
		14. Sponsoring Agency Code	
15. Supplementary Notes Project conducted in cooperation with the U.S. Department of Transportation, Federal Highway Administration, and the Texas Department of Transportation			
16. Abstract Changes in the AASHTO Standard Specifications for Structural Supports for Highway Signs, Luminaires, and Traffic Signals and an increasing rate of fatigue related problems have raised awareness of fatigue concerns in traffic signal mast arms. Prior research has indicated that the most commonly used connection details exhibit poor fatigue performance. This study was initiated to confirm the previous research results, as well as to investigate a larger variety of connection details and a weld treatment method. During this study, 55 full-size mast arm connection detail specimens were tested for fatigue resistance. The present specifications were found to overestimate the fatigue life of connections with stiffeners. The results indicate that the Ultrasonic Impact Treatment weld treatment can significantly improve the fatigue life of a fillet-welded socket connection detail. Several other connection details exhibited improved fatigue lives; however, the improvements were not as significant as the UIT treated specimens. An extensive finite element analysis generated stress concentration factors for a variety of connection geometries. These finite element analyses extended the range of geometries beyond those included in the experimental study.			
17. Key Words fatigue, fillet welds, mast arms, socketed connections, finite element analysis, stiffeners		18. Distribution Statement No restrictions. This document is available to the public through the National Technical Information Service, Springfield, Virginia 22161.	
19. Security Classif. (of report) Unclassified	20. Security Classif. (of this page) Unclassified	21. No. of pages 218	22. Price

FATIGUE STRENGTH OF SIGNAL MAST ARM CONNECTIONS

by

Mark T. Koenigs, Tamer A. Botros, Dylan Freytag, and Karl H. Frank

Research Report 4178-2

Research Project 0-4178

FILLET WELD DETAILING FOR STIFFENER

conducted for the

Texas Department of Transportation

in cooperation with the

**U.S. Department of Transportation
Federal Highway Administration**

by the

**CENTER FOR TRANSPORTATION RESEARCH
BUREAU OF ENGINEERING RESEARCH
THE UNIVERSITY OF TEXAS AT AUSTIN**

August 2003

Research performed in cooperation with the Texas Department of Transportation and the U.S. Department of Transportation, Federal Highway Administration.

ACKNOWLEDGEMENTS

The research was sponsored by the Texas Department of Transportation. The Project Director was Heather Gilmer. Her help and guidance with the project is gratefully acknowledged. The specimens were welded by Mike Bell of the Ferguson Laboratory staff. The help and technical expertise of Blake Stasney, Dennis Phillip, and Ray Madonna also of the Ferguson Laboratory staff contributed to the success of the research.

DISCLAIMER

The contents of this report reflect the views of the authors, who are responsible for the facts and the accuracy of the data presented herein. The contents do not necessarily reflect the view of the Federal Highway Administration or the Texas Department of Transportation. This report does not constitute a standard, specification, or regulation.

NOT INTENDED FOR CONSTRUCTION,
PERMIT, OR BIDDING PURPOSES

K. H. Frank, P.E., Texas #48953
Research Supervisor

TABLE OF CONTENTS

CHAPTER 1: INTRODUCTION.....	1
1.1 BACKGROUND INFORMATION	1
1.2 WIND PHENOMENA AND RESULTING FATIGUE RELATED CONCERNS.....	3
1.2.1 Natural Wind Gusts	4
1.2.2 Truck Induced Wind Gusts	4
1.2.3 Vortex Shedding	5
1.2.4 Galloping.....	5
1.3 FATIGUE FAILURES OF TRAFFIC SIGNAL MAST-ARMS	6
1.3.1 TxDOT Mast-Arm Failure.....	7
1.4 CURRENT AASHTO SPECIFICATIONS.....	9
1.5 RESULTS OF RELATED RESEARCH	10
1.6 SCOPE.....	11
CHAPTER 2: TEST SETUP	13
2.1 TEST ASSUMPTIONS AND DESIGN DECISIONS.....	13
2.2 TEST SETUP DESIGN.....	14
2.3 SETUP LIMITATION - INSTABILITY UNDER COMPRESSIVE LOADING	15
CHAPTER 3: TEST SPECIMEN DESIGN	17
3.1 SPECIMEN DESIGN.....	17
3.1.1 Phase 1	17
3.1.2 Phase 2	26
3.2 SPECIMEN LABELS	35
CHAPTER 4: TESTING PROCEDURE	37
4.1 GENERAL TEST PROCEDURE	37
4.2 SPECIMEN PREPARATION	37
4.2.1 Cutting of Specimens	37
4.2.2 Attachment of Load Plates.....	38
4.2.3 Measurement and Strain Gauge Instrumentation.....	38
4.3 MEAN STRESS CALCULATIONS	38
4.4 GENERAL TESTING NOTES	39
4.5 STATIC TEST.....	40
4.6 DYNAMIC TEST	42
4.6.1 Determination of Loads for Limits of Dynamic Testing	42
4.6.2 Dynamic Test Procedure	43
4.6.3 Failure Definition.....	44
CHAPTER 5: RESULTS OF TENSILE TESTS, CHEMISTRY ANALYSES AND DYNAMIC STRAIN MONITORING.....	45
5.1 TENSILE TEST RESULTS	45
5.1.1 Process	45

5.2	CHEMISTRY ANALYSIS.....	47
5.3	DYNAMIC CORROBORATION OF STATIC TEST STRAINS	48
CHAPTER 6: STATIC TEST RESULTS		51
6.1	STATIC TESTING.....	51
6.2	UNEQUAL LEG FILLET-WELDED SOCKET CONNECTION SPECIMENS	52
6.3	STIFFENED SPECIMEN	57
6.3.1	<i>Vertical and Horizontally Oriented Stiffeners.....</i>	<i>57</i>
6.3.2	<i>Stiffeners Oriented 45° from Vertical.....</i>	<i>59</i>
6.4	UIT WELD TREATMENT PROCESS	61
6.5	UIT TREATED SPECIMENS	64
6.5.1	<i>Phase 1.....</i>	<i>64</i>
6.5.2	<i>Phase 2.....</i>	<i>66</i>
6.6	MISCELLANEOUS CONNECTION DETAILS AND VARIABLES.....	71
6.6.1	<i>Base Plate Thickness: VALNu 2 Series.....</i>	<i>71</i>
6.6.2	<i>Galvanizing: VALNu G Series.....</i>	<i>72</i>
6.6.3	<i>U-Rib Stiffener Connection – VALN UR Series.....</i>	<i>72</i>
6.6.4	<i>External Collar Connection Detail – VALN Col Series.....</i>	<i>73</i>
6.6.5	<i>Internal Collar Connection Detail: VALN IC Series.....</i>	<i>75</i>
6.6.6	<i>Full-Penetration Weld Detail – VALN W Series.....</i>	<i>77</i>
CHAPTER 7: FATIGUE TEST RESULTS.....		79
7.1	TESTING PROGRAM.....	79
7.2	FATIGUE LIFE COEFFICIENT, A, CALCULATION.....	80
7.3	CALCULATION OF REPORTED STRESS.....	81
7.4	FATIGUE TEST RESULTS.....	83
7.5	UNEQUAL LEG FILLET-WELDED SOCKET CONNECTION SPECIMENS	83
7.6	STIFFENED SPECIMENS.....	86
7.6.1	<i>Vertical Stiffeners.....</i>	<i>86</i>
7.6.2	<i>VALN 6x3/8@45 specimens.....</i>	<i>94</i>
7.6.3	<i>Protection of Socket Weld due to Addition of Stiffeners.....</i>	<i>96</i>
7.7	UIT WELD TREATED SPECIMENS.....	97
7.7.1	<i>Phase 1.....</i>	<i>97</i>
7.7.2	<i>Phase 2.....</i>	<i>101</i>
7.8	MISCELLANEOUS CONNECTION DETAILS AND VARIABLES.....	106
7.8.1	<i>Base Plate Thickness: VALNu 2 Series.....</i>	<i>107</i>
7.8.2	<i>Galvanizing: VALNu G Series.....</i>	<i>108</i>
7.8.3	<i>U-Rib Stiffener Connection – VALN UR Series.....</i>	<i>109</i>
7.8.4	<i>External Collar Connection Detail – VALN Col Series.....</i>	<i>112</i>
7.8.5	<i>Internal Collar Connection Detail – VALN IC Series.....</i>	<i>114</i>
7.8.6	<i>Full-Penetration Weld Detail – VALN W Series.....</i>	<i>115</i>
7.9	INFLUENCE OF MEAN STRESS	117
CHAPTER 8: RESULTS – VALUE BASED DESIGN ANALYSIS METHOD.....		121
8.1	VALUE BASED DESIGN APPROACH.....	121

8.1.1	<i>Comparison with Previous Analysis Methods</i>	122
8.2	ANALYSIS OF RESULTS USING VALUE BASED DESIGN APPROACH	122
8.2.1	<i>UIT Treated Specimens</i>	125
8.3	ANALYSIS OF ALTERNATIVE CONNECTION DETAILS USING VALUE BASED DESIGN APPROACH	125
8.3.1	<i>Socket Connection Details</i>	127
8.3.2	<i>Stiffeners Oriented 45° From Vertical - VALN 6x3/8@45 Series</i>	128
8.3.3	<i>External Collar Stiffeners - VALN Col Series</i>	128
8.3.4	<i>Internal Collar Stiffeners - VALN IC Series</i>	128
8.3.5	<i>U-Rib Stiffeners - VALN UR Series</i>	128
8.3.6	<i>Full-Penetration Weld Connections - VALN W Series</i>	128
8.4	BENEFITS OF USING VALUE BASED DESIGN APPROACH	129
CHAPTER 9: FINITE ELEMENT ANALYSIS OF CONNECTIONS.....		131
9.1	INTRODUCTION	131
9.1.1	<i>Geometric Variables Analyzed</i>	131
9.1.2	<i>Purpose</i>	132
9.2	ANALYSIS TOOLS AND TECHNIQUES	132
9.2.1	<i>Analysis Techniques</i>	132
9.3	STRESS CONCENTRATION FACTOR CALCULATION.....	134
9.4	GRAPHICAL EXPLANATION OF SCFS	135
9.5	STRESS CONCENTRATION FACTOR EVALUATION TECHNIQUES	138
9.5.1	<i>ABS Technique</i>	138
9.5.2	<i>DNV Technique</i>	139
9.5.3	<i>Mesh Refinement / Submodeling Technique</i>	139
9.5.4	<i>Example of Stress Extrapolation</i>	140
9.5.5	<i>Comparison of Stress Solutions</i>	140
9.6	UNSTIFFENED MODELS	142
9.6.1	<i>Effect of Non-linear Geometry</i>	143
9.6.2	<i>Unstiffened Model Results and Discussion</i>	145
9.6.3	<i>Effect of mast arm thickness and length on socket weld SCF</i>	146
9.6.4	<i>Effect of Solid Baseplate on Socket Weld SCF</i>	146
9.6.5	<i>Effect of Baseplate Thickness on Socket Weld SCF</i>	146
9.6.6	<i>Effect of Bolt Pattern on Socket Weld SCF</i>	148
9.7	STIFFENED MODELS.....	149
9.7.1	<i>Stiffened Model Results and Discussion</i>	150
9.7.2	<i>Effect of Mast Arm Wall Thickness on SCFs</i>	152
9.7.3	<i>Effect of Stiffener Length on SCFs</i>	152
9.7.4	<i>Effect of Stiffener Thickness on SCFs</i>	154
9.7.5	<i>Effect of Stiffener Thickness to Wall Thickness Ratio on SCFs</i>	154
9.7.6	<i>Effect of Baseplate Thickness on SCFs</i>	154
9.7.7	<i>Effect of number of Stiffeners and stiffener Offset ON SCFS</i>	156
9.8	COMPARISON OF STIFFENED AND UNSTIFFENED MODELS	156
9.9	CONCLUSIONS	157

CHAPTER 10: WELD SIZE MEASUREMENTS	159
10.1 INTRODUCTION	159
10.2 DESCRIPTION OF STUDY.....	159
10.2.1 <i>Results of Study: Leg Dimensions</i>	160
10.2.2 <i>Results of Study: Incident Angle onto Mast Arm</i>	163
10.2.3 <i>Results of Study: UIT Radius of Curvature</i>	165
10.3 DISCUSSION: LEG DIMENSIONS.....	165
10.4 DISCUSSION: INCIDENT ANGLE ONTO MAST ARM.....	166
10.5 DISCUSSION: UIT RADIUS OF CURVATURE	167
10.6 CONCLUSIONS	167
CHAPTER 11: CONCLUSIONS AND RECOMMENDED RESEARCH.....	169
11.1 CONCLUSIONS	169
11.2 FURTHER RESEARCH.....	170
11.2.1 <i>Loading Related Research</i>	170
11.2.2 <i>Resistance Related Research</i>	171
APPENDIX A: SUMMARY OF PREVIOUS TESTING	173
APPENDIX B: MEASURED DIMENSIONS OF TEST SPECIMENS	179
APPENDIX C: RESULT SUMMARY	189
APPENDIX D: CREATING THE SOLID MODELS IN AUTOCAD 2002.....	191
APPENDIX E: ABS TECHNIQUE.....	193
APPENDIX F: MEASURED DATA.....	195
REFERENCES	199

LIST OF FIGURES

Figure 1.1	Typical Cantilever Mast-Arm Traffic Signal Support Structure	1
Figure 1.2	Built-Up-Box Connection Detail.....	2
Figure 1.3	Fillet Welded Socket Connection Detail	3
Figure 1.4	Portion of Failed Mast-Arm from TxDOT	7
Figure 1.5	Pole Fatigue Fracture Surface of TxDOT Mast-Arm	8
Figure 1.6	Base Plate Fatigue Fracture Surface of TxDOT Mast-Arm	8
Figure 1.7	Failure Surface Transition Zone of TxDOT Mast-Arm.....	9
Figure 1.8	Test Setup for Tests Performed at Valmont Industries, Valley, NE.....	10
Figure 2.1	Moment Diagram on Cantilever Mast-Arm Traffic Signal	13
Figure 2.2	Test Setup Design with Simply Supported Beam Analogy	13
Figure 2.3	Test Setup.....	14
Figure 2.4	Double Restraint Fixture of Test Setup Design.....	15
Figure 2.5	Single Restraint Fixture of Test Setup Design	15
Figure 3.1	Test Specimen Drawing	18
Figure 3.2	Fillet Weld Detail	19
Figure 3.3	Stiffener Diagram with Critical Locations Indicated.....	21
Figure 3.4	Stiffener Detail	22
Figure 3.5	Base Plate Fabrication Drawing	26
Figure 3.6	Base Plate Fabrication Drawing with Stiffeners Offset at 45°Angles	28
Figure 3.7	External Collar Connection Detail	30
Figure 3.8	External Collar Stiffened Specimen	30
Figure 3.9	Inner Collar Detail.....	31
Figure 3.10	U-Rib Stiffener Plan Detail	32
Figure 3.11	U-Rib Stiffener Elevation Detail.....	32
Figure 3.12	U-Rib Stiffened Specimen.....	33
Figure 3.13	U-Rib Stiffened Specimen.....	33
Figure 3.14	Full-Penetration-Weld Connection Detail	34
Figure 3.15	Specimen Label Explanation Chart	36
Figure 4.1	Cutting Jig	37
Figure 4.2	Plot of Mean Stress vs. Mast-Arm Length due to Dead Load.....	39
Figure 4.3	Static Test Result – Up-and-Down Test – Typical Results	41
Figure 4.4	Static Test Result – Cyclic Test – Typical Results.....	41
Figure 4.5	Plot of Load vs. Deflection for First Test.....	43
Figure 5.1	Tensile Test Results for 3g (0.239" thickness) Steel Coupon – Entire Measured Behavior.....	45

Figure 5.2	Tensile Test Results for 3g (0.239" thickness) Steel Coupon – Closeup of Initial Portion of Graph.....	46
Figure 5.3	Dynamic Strain Monitoring of Top Gauge on Specimen VALN IC A	48
Figure 5.4	Dynamic Strain Monitoring of Top Gauge on Specimen VAL 3x1/4C	49
Figure 6.1	Static Test Results for VALu A.....	53
Figure 6.2	Strain Range vs. Height from Horizontal Axis Plot of Static Test Results for VALu A.....	54
Figure 6.3	Plot of Static Test Results for TxuA.....	55
Figure 6.4	Plot of Strain Range vs. Height for TXu A	55
Figure 6.5	Plot of Strain vs. Height for TXu A under the Minimum and Maximum Loads.....	56
Figure 6.6	Plot of Strain vs. Load for Strain Gauges Located inside the Pole of Specimen TXu A.....	57
Figure 6.7	Plot of Static Test Results for VAL 3x1/4 A.....	58
Figure 6.8	Plot of Static Test Results for VAL 6x3/8A.....	58
Figure 6.9	Plot of Static Test Results for TX 3x3/8 A.....	59
Figure 6.10	Plot of Strain vs. Height for TX 3x3/8 C.....	59
Figure 6.11	Plot of Static Test Results for VALN 6x3/8@45 A	60
Figure 6.12	Plot of Static Test Results for VALN 6x3/8@45 D	61
Figure 6.13	UIT Equipment.....	62
Figure 6.14	UIT Treatment Tool	62
Figure 6.15	UIT Treatment Tool Head.....	63
Figure 6.16	UIT Treatment in Progress	63
Figure 6.17	UIT Treated Socket Connection Specimen prior to testing.....	64
Figure 6.18	UIT Treated Stiffened Connection Specimen Prior to Testing (dashed line indicates the termination of the treated area).....	65
Figure 6.19	Plot of Static Test Results for VALu EP.....	65
Figure 6.20	Plot of Static Test Results for VAL 3x3/8 CP.....	66
Figure 6.21	UIT Treated Region of a VALNu PR Specimen.....	67
Figure 6.22	UIT Treatment of Heat Affected Region on VALNu PG Series	69
Figure 6.23	Static Test Results for VALNu 2 A.....	71
Figure 6.24	Static Test Results for Strain Gauges Located 3" from Termination of Stiffener on Specimen VALN UR A	72
Figure 6.25	Static Test Results of Strain Gauges located 3" from Socket Weld on Specimen VALN UR B. Includes Strain Gauge Located Inside the Stiffener and at 45°Angles from Vertical.	73
Figure 6.26	Static Test Results for VALN Col A.....	74
Figure 6.27	Static Test Results for Strain Gauge on the Collar of Specimen VALN Col B.....	74
Figure 6.28	Static Test Results for VALN IC A.....	75
Figure 6.29	Static Test Results for VALN IC A presented in a Strain Verses Height Plot.....	76
Figure 6.30	Static Test Results for VALN IC A SG beyond Collar	76
Figure 6.31	Static Test Results for the Strain Gauges Located Beyond the Backing Bar of Specimen VALN W B	77

Figure 6.32	Static Test Results for Strain Gauge Located within the Length of the Backing Bar on Specimen VALN W B.....	78
Figure 7.1	Failure of Socket Weld Connection Specimen.....	84
Figure 7.2	Failure of Socket Connection Specimen – Painted arrows indicate extents of visible cracking.....	84
Figure 7.3	S-N Plot of Unstiffened Socket Connection Results	85
Figure 7.4	Failure of VAL 3x1/4 Specimen	88
Figure 7.5	Failure of VAL 6x3/8 Specimen	88
Figure 7.6	Failure of TX 3x3/8 Specimen – Note: Paint line represents extent of visible cracking	89
Figure 7.7	Failure of TX 3x1/4 Specimen – Note: Paint line at termination of stiffener represents extent of visible cracking, and painted arrows indicate visible crack tips in socket weld toe	89
Figure 7.8	Failure of VAL 3x1/4 Specimen – Note: Paint line at termination of stiffener represents extent of visible cracking, and painted arrows indicate visible crack tips in socket weld toe.....	90
Figure 7.9	S-N Plot of Stiffened VAL (thin pole wall) Connection Results.....	93
Figure 7.10	S-N Plot of Stiffened TX (thick pole wall) Connection Results.....	94
Figure 7.11	Failure of VALN 6x3/8@45 Specimen – Painted line indicates extent of visible cracking, specimen tested at 6 ksi stress range	95
Figure 7.12	Failure of VALN 6x3/8@45 Specimen – Paint lines at termination of stiffeners represent extents of visible cracking, and painted arrows indicate visible crack tips in socket weld toe, specimen tested at 12 ksi stress range	95
Figure 7.13	S-N Plot of Protection Provided by TX 6x3/8 Stiffeners – Plotted on a Semi-Log Plot	97
Figure 7.14	Failure of UIT Treated Socket Connection Specimen – Painted line indicates extent of visible cracking.....	98
Figure 7.15	Failure of UIT Treated Socket Connection Specimen.....	99
Figure 7.16	S-N Plot of Results of UIT Treated Specimens - Phase 1	100
Figure 7.17	Failure of TX 3x3/8 CP Specimen – Note: Paint lines represent extent of visible cracking at termination of stiffener and socket weld toe.....	101
Figure 7.18	S-N Plot of UIT Specimen Phase 2	103
Figure 7.19	Failure of UIT Retrofit Specimen after Unloading and Retesting – VALNu PR ul Specimen	103
Figure 7.20	Failure of Specimen VALNu GP B - Arrow points to weld start/stop in critical location	105
Figure 7.21	Failure of UIT Prior to Galvanization Specimen.....	106
Figure 7.22	S-N Plot of Base Plate Thickness Variable	107
Figure 7.23	S-N Plot of Influence of Galvanizing	108
Figure 7.24	Failure of U-Rib Stiffened Specimen – Note: Painted lines represent extent of visible cracking	110
Figure 7.25	Failure of U-Rib Stiffened Specimen	111
Figure 7.26	S-N Plot of Results of U-Rib Stiffened Specimens	112
Figure 7.27	Failure of Externally Stiffened Collar Specimen.....	112
Figure 7.28	Crack Observed in Interior Weld of External Collar Stiffened Specimen.....	113
Figure 7.29	S-N Plot of Results of Alternative Connection Specimens	114
Figure 7.30	Failure of Internal Collar Stiffened Specimen.....	114

Figure 7.31	Failure of Full-Penetration Welded Connection Detail Specimen – Paint arrows indicate extent of visible cracking	115
Figure 7.32	Failure of Full-Penetration Welded Connection Detail Specimen	116
Figure 7.33	S-N Plot of All Available Test Results.....	117
Figure 7.34	S-N Plot of All Available Stiffened Connection Detail Test Results	118
Figure 7.35	S-N Plot of All Available Test Results for Stiffened and Unstiffened Socket Connection Details	119
Figure 8.1	Graph of A as Calculated by the Nominal Stress Fatigue Life Method and the Value Based Design Method for All Series of Specimens Tested.....	125
Figure 8.2	Graph of AVBDM/AE' for All Series of Specimens Tested	127
Figure 8.3	Graph of AVBDM/AE' for Each Series of Specimens Tested Excluding UIT Treated Series	127
Figure 9.1	Coordinate System and Symmetric Model.....	133
Figure 9.2	Typical ABS and DNV Meshing Scheme for Unstiffened Models.....	133
Figure 9.3	Typical ABS and DNV Meshing Scheme for Stiffened Models	133
Figure 9.4	Typical Refined Meshing Scheme for an Unstiffened Model	134
Figure 9.5	Typical Submodeling Meshing Scheme for Stiffened Models.....	134
Figure 9.6	Example of SCF Calculation	135
Figure 9.7	Mast Arm Deformations and Local Curvature (100x Deformation using Mesh Refinement Approach).....	136
Figure 9.8	Longitudinal Stress Range Along Top of Mast Arm.....	136
Figure 9.9	Stress vs. Height at Socket Weld Toe.....	137
Figure 9.10	Stress vs. Height at 1.00 in. from Face of Baseplate	137
Figure 9.11	Affect of Mesh Size on Stress Singularity.....	138
Figure 9.12	Example of Stress Extrapolation	140
Figure 9.13	Comparison of ABS, DNV, and Mesh Refinement Solutions around Stiffener.....	141
Figure 9.14	Bending vs. Principal Stress Range.....	142
Figure 9.15	Location of Maximum SCF.....	143
Figure 9.16	Effect of Non-linear Geometry on Stress Range at Stiffener Toe	144
Figure 9.17	Effect of Non-linear Geometry on Stress Range at Socket Weld Toe.....	144
Figure 9.18	SCFs for Analyzed Models	145
Figure 9.19	Effect of Shear and Mast Arm Thickness on Socket Weld SCF	146
Figure 9.20	Influence of Solid Baseplate on Socket Weld SCF	147
Figure 9.21	Influence of Baseplate Thickness on Socket Weld SCF.....	147
Figure 9.22	Influence of Bolt Pattern on Socket Weld SCF	148
Figure 9.23	Influence of Baseplate Thickness on Baseplate Deformation (100x Deformation using Mesh Refinement Approach)	149
Figure 9.24	Influence of Baseplate Thickness on Mast Arm Wall Deformation (100x Deformation using Mesh Refinement Approach)	149
Figure 9.25	Typical Locations of SCFs on Stiffened Models.....	151

Figure 9.26	Socket Weld SCFs for Stiffened Model	151
Figure 9.27	Stiffener SCFs for Stiffened Models	152
Figure 9.28	Effect of Mast Arm Wall Thickness on SCFs	153
Figure 9.29	Influence of Stiffener Length on SCFs.....	153
Figure 9.30	Influence of Stiffener Thickness on SCFs.....	154
Figure 9.31	Influence of Thickness Ratio on SCFs	155
Figure 9.32	Influence of Baseplate Thickness on Socket Weld SCF.....	155
Figure 9.33	Influence of Stiffener Offset on Socket Weld SCF	156
Figure 9.34	Comparison of Stiffened and Unstiffened Socket Weld SCFs	157
Figure 10.1	Length Dimensions of Interest	159
Figure 10.2	Global Angle	159
Figure 10.3	Local Angle	160
Figure 10.4	View of Pins on UIT Tool Head.....	160
Figure 10.5	Curvature Due to UIT Process	160
Figure 10.6	Long Leg Measurements for VAL Specimens	161
Figure 10.7	Short Leg Measurements for VAL Specimens.....	161
Figure 10.8	Distribution of Long Leg Measurements for VAL Specimens.....	162
Figure 10.9	Distribution of Short Leg Measurements for VAL Specimens	162
Figure 10.10	Variation of Long Leg Around Mast Arm.....	163
Figure 10.11	Variation of Short Leg around Mast Arm.....	163
Figure 10.12	Global and Local Angle Measurements for the Study Group.....	164
Figure 10.13	Global and Local Angle Measurements for 2" Baseplate Specimens.....	164
Figure 10.14	Influence of Local Angle on Fatigue Life	165
Figure 10.15	Profile View of VALN u GA Showing Smaller Throat Dimension.....	166
Figure 10.16	Ideal Weld Profile Developed in University of Missouri Finite Element Analyses (Alderson, 1999).....	167

LIST OF TABLES

Table 3.1	Standard TxDOT Design Properties	17
Table 3.2	Excerpt from Fatigue Provisions of 2001 AASHTO Highway Signs, Luminaires and Traffic Signal Specifications	20
Table 3.3	Stiffener Designs	23
Table 3.4	Protection Factor	23
Table 3.5	Fatigue Life Improvement Ratio	25
Table 3.6	Phase 1 Test Specimen Matrix	25
Table 3.7	Phase 2 Test Specimen Matrix	35
Table 4.1	Dead Weight of Traffic Signals Used for Mean Stress Calculation	39
Table 5.1	Results of Tensile Tests	46
Table 5.2	Tensile Test Results Compared to Fatigue Testing Limits	47
Table 5.3	Results of Chemistry Analysis	47
Table 5.4	Results of CR9000 Dynamic Strain Monitoring – Part 1	50
Table 5.5	Results of CR9000 Dynamic Strain Monitoring – Part 2	50
Table 6.1	Phase 1 Results	51
Table 6.2	Phase 2 Results	52
Table 6.3	Load and Strain Behavior During UIT Treatment at Dead Load	68
Table 6.4	Load and Strain Behavior During UIT Treatment at Dead Load	69
Table 6.5	Load and Strain Behavior During UIT Treatment at Dead Load	70
Table 7.1	Fatigue Test Results – Phase 1	79
Table 7.2	Fatigue Test Results – Phase 2	80
Table 7.3	Fatigue Constants	81
Table 7.4	Section Properties and Test Data for VALN Col B	82
Table 7.5	Test Results and Calculated A Values for Socket Connection Details	85
Table 7.6	Fatigue Life Coefficients ‘A’ for Stiffened Connection Specimens	87
Table 7.8	Effect of Stiffener Thickness to Pole Wall Ratio, and Angle of Incidence of Stiffener on Fatigue Life	92
Table 7.9	Fatigue Life Coefficients, A, for 6x3/8 Stiffened Connection Based on the Stress Range at the Termination of a Vertical Stiffener	96
Table 7.10	Results Phase 1 – UIT Treated Specimen	98
Table 7.12	Results Phase 1 – LMS UIT Treated Stiffened Specimens	100
Table 7.13	Results Phase 2 – UIT Treated Specimen	102
Table 7.15	Results VALNu PR ul Specimens	104
Table 7.16	Results of Base Plate Thickness Variable	107
Table 7.17	Results of Galvanized Specimens	108
Table 7.18	Results of U-Rib Stiffened Specimens	109

Table 7.19 Results of External Collar Stiffened Specimens	113
Table 7.20 Results of Internal Collar Stiffened Specimens	115
Table 7.21 Results of Full-Penetration Weld Connection Specimens	116
Table 8.1 Section Properties and Test Data for VALN Col B (Reprinted from Chapter 7).....	121
Table 8.2 Phase 1 Results	123
Table 8.3 Phase 2 Results	124
Table 8.4 Average Values for Each Series of Tests.....	126
Table 9.1 Geometric Variables Analyzed.....	131
Table 9.2 Abaqus Material Properties	132
Table 9.3 Comparison of SCF Evaluation Techniques.....	139
Table 9.4 Analyzed Unstiffened Models	143
Table 9.5 SCFs for Unstiffened Models	145
Table 9.6 Analyzed Stiffened Models	150
Table 9.7 Socket Weld and Stiffener SCFs for Stiffened Models	150
Table 10.1 Radius of Curvature at Toe of Weld and UIT Pin Diameter.....	165

SUMMARY

Changes in the AASHTO Specifications and an increasing rate of fatigue related problems have raised awareness of fatigue concerns in traffic signal mast arms. Prior research has indicated that the most commonly used connection details exhibit poor fatigue performance. This study was initiated to confirm the previous research results, as well as to investigate a larger variety of connection details and a weld treatment method. During this study, 55 full-size mast arm connection detail specimens were tested for fatigue resistance. The present specifications were found to overestimate the fatigue life of connections with stiffeners. The results indicate that the Ultrasonic Impact Treatment weld treatment can significantly improve the fatigue life of a fillet-welded socket connection detail. Several other connection details exhibited improved fatigue lives; however, the improvements were not as significant as the UIT treated specimens. An extensive finite element analysis generated stress concentration factors for a variety of connection geometries. These finite element analyses extended the range of geometries beyond those included in the experimental study.

CHAPTER 1: INTRODUCTION

1.1 BACKGROUND INFORMATION

This study investigated the fatigue characteristics of traffic signal mast-arms. Throughout the U.S., there are a variety of traffic signal structures in service; however, these can usually be described based on the types of vertical and horizontal members.

The vertical members are typically referred to as columns, poles, posts, or masts. Traffic signal structures with only one pole are referred to as cantilever structures based on the cantilevered horizontal member. A structure with two or more columns may be referred to as a sign bridge or overhead structure.

The horizontal members of the structures typically consist of either one member or a truss. The single member is called a monotube or mast-arm and usually consists of a tapered tube in order to reduce the dead load of the structure. The truss structure usually has two chords and is called a two-chord truss. Another structure commonly used, which does not easily fit into the above categorization, is a cable structure in which a series of cables are used to support the traffic signal.

The traffic signal shown in Figure 1.1 is a cantilever tapered mast-arm, which is a typical traffic signal structure used by many transportation departments throughout the U.S. This cantilever mast-arm design, as shown, has many advantages over the other structures described above. The single column structure provides fewer collision hazards and vision obstacles for drivers. The cantilever mast-arm is cost efficient and relatively simple to design. The overall structure is more aesthetically pleasing than a cable structure or a truss cantilever structure. The same characteristics that make this traffic signal structure desirable also lead to the largest negative factors of the structure; it is a non-redundant structure and the mast-arm is very flexible.



Figure 1.1 Typical Cantilever Mast-Arm Traffic Signal Support Structure

The flexibility, combined with the lengths of mast-arms utilized today, means that the cantilever mast-arm structure is prone to fatigue problems. The geometry of the two chord truss structures and multicolumn structures eliminates many of the vibrations that lead to the high numbers of stress cycles. For this reason, this study focuses on the cantilevered tapered mast-arm structure.

On a typical cantilever mast-arm structure, the connection details at the mast-arm to column connection and the column to base plate connection are identical, which creates two possible critical locations. However, the column typically has a larger cross section, which reduces the local stresses at the column to base plate connection. The column is also under an axial compressive force, which further reduces the local tensile stresses at the column to base plate connection. These two factors cause the mast-arm to column connection to be the critical connection.

Figure 1.2 shows a close up view of a typical mast-arm to column connection. The column has a built up box detail to which the mast-arm mates. The base plate, which connects to the built-up-box, is connected to the tapered tube with a fillet-welded socket connection.



Figure 1.2 Built-Up-Box Connection Detail

The socket connection detail is shown schematically in Figure 1.3. In this connection, the tapered tube of the mast-arm is socketed into a hole through the base plate. The base plate and tube are then connected by two fillet welds. The primary weld is a multiple pass unequal leg fillet weld located on the outside of the tube. This weld transfers the majority of the forces from the tube to the base plate. The second weld is a small fillet weld connecting the end of the tube to the inside of the base plate hole. This weld is primarily in place to seal the connection to prevent corrosion and entrance of molten zinc during galvanizing and does not transfer a significant amount of load.

The tapered tubes of traffic signal mast-arms are fabricated from coiled steel plates. The steel plates are cut into a trapezoidal shape and the tube is formed around a mandrel. The tapered tube is then burnished on a mandrel so that the tube conforms to the round mandrel. During this process, the steel in the tapered

tube is cold worked. Finally, the longitudinal seam is welded. After the tube is cut to the proper length, the base plate and any attachments are welded to the tube.

The socket connection detail is shown schematically in Figure 1.3. In this connection, the tapered tube of the mast-arm is socketed into a hole through the base plate. The base plate and tube are then connected by two fillet welds. The primary weld is a multiple pass unequal leg fillet weld located on the outside of the tube. This weld transfers the majority of the forces from the tube to the base plate. The second weld is a small fillet weld connecting the end of the tube to the inside of the base plate hole. This weld is primarily in place to seal the connection to prevent corrosion and entrance of molten zinc during galvanizing and does not transfer a significant amount of load.

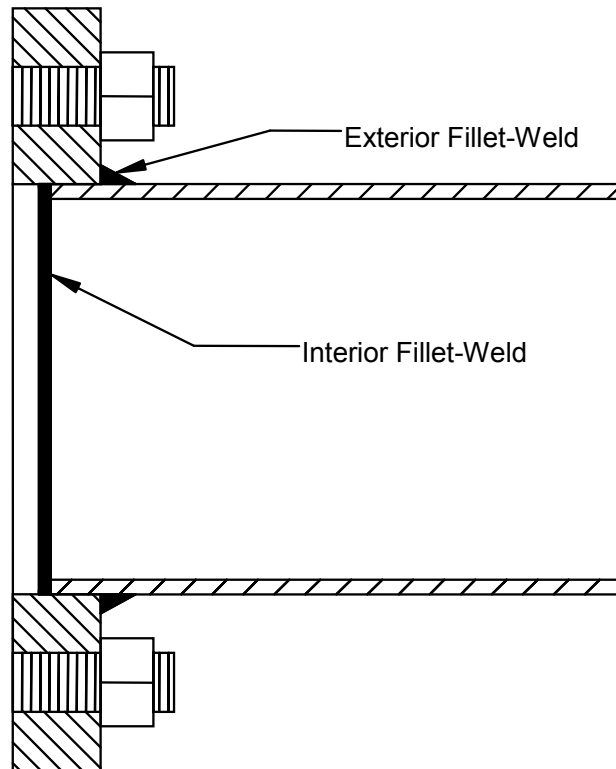


Figure 1.3 Fillet Welded Socket Connection Detail

1.2 WIND PHENOMENA AND RESULTING FATIGUE RELATED CONCERNS

The fatigue problems that were studied in this test program are the result of vibrations of the traffic signal mast-arms under service conditions. The extent of these vibrations was studied and documented by Kaczynski et al. (1998). This report documented vibrations that reached amplitudes of 48" at the tip of the mast-arm. This is a significant amount of deflection, especially when compared with the limit of 8" proposed by Kaczynski. The limit of 8" is approximately the point at which motorists begin have difficulty seeing the traffic signals and begin to be concerned about the safety of the structure (Kaczynski et al., 1998).

The vibrations of traffic signal mast-arms are generally caused by one of four wind phenomena: natural wind gusts, truck induced wind gusts, vortex shedding, or galloping. The wind phenomena have been investigated by researchers at the University of Minnesota, the University of Florida, the University of Wyoming and Texas Tech University. While the study of these phenomena is beyond the scope of this

project, a brief description of each follows. A more thorough discussion of these phenomena can be found in References 5, 6, and 7.

1.2.1 Natural Wind Gusts

Natural wind gusts are caused by the natural variability in the direction and velocity of wind flow. The changes in velocity and direction cause fluctuating pressures on the various components of a traffic signal structure, which may, in turn, lead to vibration of the structure. If vibration occurs due to the natural wind gust loading, the displacements have been observed to be variable and randomly distributed. The cumulative effects of these vibrations over the life of a traffic signal structure may result in fatigue cracking.

The design of traffic signal structures for natural wind gust loading is based on an ultimate strength limit state. In the applicable equations of the AASHTO Highway Signs, Luminaires and Traffic Signal Specifications, a gust factor of 1.3 is applied to the expected wind velocities to create a design wind pressure. This design pressure, when applied statically to the vertically projected surface areas of the structure represents the maximum loading expected under dynamic loading conditions.

1.2.2 Truck Induced Wind Gusts

Truck induced gusts are caused by the passage of semi tractor-trailer rigs underneath traffic signal structures. The passage of these vehicles leads to increased wind pressures on the front and undersides of signs and support structures. An increase in the magnitude of truck induced wind gusts has been attributed to the increased use of wind deflectors on the cabs of semi-tractors (Kaczinski et al., 1998).

The horizontal components of these wind gusts can cause bending and/or torsional moments in cantilever traffic signal supports. However, studies have shown that the stresses due to the gust loading on the vertically projected faces are typically below the fatigue threshold stress (Kaczinski et al., 1998). Therefore, the horizontal effects of truck induced wind loads need not be considered in fatigue design.

On the other hand, the vertical components of the truck-induced gusts create an increased pressure on the underside of the attachments and support structures. For a typical cantilevered mast-arm supporting vertically oriented traffic signals, the projected area of the structures is relatively small and these wind gusts do not lead to a significant increase in loading. The Texas Department of Transportation uses horizontally oriented traffic signals, which result in a larger horizontally projected area. In limited cases, the truck induced wind loads have controlled the fatigue design in Texas due to the larger horizontally projected area.

Similarly, the projected area of variable message signs (VMS) can be fairly large. The truck-induced gusts may cause a significant pressure increase on the underside of these signs resulting in large bending moments in the support structure. The effects of this loading may be more significant than the effect of galloping for variable message signs.

The impact of the truck induced wind gusts has been reduced in the recent editions of the specifications, as the applied wind loading has been reduced by approximately 50%. The impact has been reduced further as the loading has been limited to consider the loading due to only one truck at a time (AASHTO Interim, 2002). These reductions in the applied loading have reduced the cases for which truck induced gusts control the fatigue design of a structure.

1.2.3 Vortex Shedding

Vortex shedding causes vibrations normal to the direction of the wind due to the shedding of vortices on the leeward side of a structure. The vortices are shed in an alternating pattern that is known as a von Karman vortex street. If the frequency of the shedding of the vortices approaches one of the natural

frequencies of the structure, a condition called lock-in may develop. Under lock-in, the displacement of the mast-arm induces a stronger, more regular vortex shedding pattern, which in turn leads to larger displacements. In this manner, if lock-in occurs, the vortex shedding may cause significant displacements at the tips of mast-arms and significant stress ranges at the critical connection details.

The potential for lock-in of a structure may be calculated from the Strouhal relation of fluid mechanics. The Strouhal relation states that the frequency of vortex shedding is dependant on the wind velocity and across-wind dimension of the structure, or the diameter of a mast-arm. In the case of a tapered mast-arm, under a given wind condition, the changing diameter limits the length of lock-in to only a small portion of the overall structure. The loading of the small regions for which lock-in may occur is typically too small to create significant oscillations of the entire structure.

The traffic signal attachments have also been shown to not be susceptible to vortex shedding lock-in, however signs may be susceptible (Kaczinski, 1998). If lock-in occurs on a sign, the loading may be substantial enough to initiate galloping, the fourth wind phenomenon.

1.2.4 Galloping

In an article entitled “Damping of Cantilevered Traffic Signal Structures,” the authors provide a definition of galloping that is attributed to J.W. Smith. Galloping is defined as an “unstable phenomenon caused by aerodynamic forces generated on certain cross-sectional shapes resulting in displacements transverse to the wind” (Cook et al., 2001). This definition implies that the phenomenon of galloping is not fully understood; however, it has been shown that it is caused by variation in the angle of attack of the wind direction. The wind variation causes displacements normal to the direction of the wind, which is similar to the effect of vortex shedding lock-in. Under appropriate conditions, the displacements occur at the natural frequency of the structure causing an amplification of the displacements.

The potential susceptibility of a structure to experience galloping can be calculated based on an equation called the Den Hartog stability criterion (Kaczinski et al., 1998). The Den Hartog stability criterion states that a structure is susceptible to galloping if the summation of the structure’s lift force coefficient and the drag coefficient produces a negative value. The wind velocity acting on a structure must also exceed a minimum onset velocity in order to initiate galloping behavior.

It has been shown that galloping typically occurs in flexible, lightly damped structures, and only in structures that have non-symmetric cross sections (Kaczinski et al., 1998). Based on the requirement that the cross section is non-symmetric, the typical mast-arms under study are not affected by galloping due to the circular cross section. However, research has shown that, under certain conditions, the traffic signal attachments are susceptible to galloping (Kaczinski et al., 1998). Traffic signals without backing plates are not susceptible to galloping. Traffic signals with backing plates are susceptible to galloping, and the effect is increased when the wind is from the rear of the structure.

The Den Hartog stability criterion is most effectively used to determine which structures are not susceptible to galloping. A structure that is potentially susceptible to galloping, according to the stability criterion, may or may not gallop under service conditions. Instead, research and field studies have shown that the initiation of galloping is a highly unpredictable phenomenon. Under wind tunnel testing performed at the Wright Brothers Memorial Wind Tunnel at the Massachusetts Institute of Technology, a structure which was observed to gallop under a specific set of wind conditions did not gallop later in the test program under identical testing conditions (Kaczinski et al., 1998). Researchers have also observed a similar unpredictability in structures in service. A series of identical traffic signal structures were observed in place along a roadway. At a particular wind speed and with the wind hitting the structures from the same direction, only one structure experienced galloping.

In the fatigue provisions of the 2001 AASHTO Highway Signs, Luminaires and Traffic Signal Specifications, the forces due to galloping are applied to the structure as a 21 psf shear force applied vertically to the surface

area of any attachments on the structure. The 21 psf load has been determined through wind tunnel testing on scale models. However, this loading of the frontal areas of all attachments does not seem to account for the susceptibility of attachments with only specific geometries to experience galloping. Instead, this loading is an indirect method of applying loads to simulate the stresses caused by galloping.

Although the causes of and the loads associated with galloping may not be fully understood, it is widely acknowledged that the galloping phenomenon is the most likely wind phenomenon to cause a large number of significant stress ranges at the critical sections of traffic signal mast-arms. For this reason, the oscillations due to this wind phenomenon are of particular importance to this research project.

1.3 FATIGUE FAILURES OF TRAFFIC SIGNAL MAST-ARMS

The issue of fatigue in traffic signal mast-arms was first studied at Lehigh University in 1983, and the effects of fatigue were first documented under service conditions in a survey performed by Kaczinski et al. in 1993. The conclusions of these reports are important and will be summarized in the following paragraphs.

The test program at Lehigh University evaluated the fatigue strength of traffic signal mast-arms (Miki, 1984). The results from the research indicated that the typical socket weld connection in use was worse than a category E' detail with an equal leg fillet weld, and the same connection was a category E detail with an unequal leg fillet weld. The improvement related to the unequal leg fillet weld was attributed to the contact angle of the weld, or the angle of incidence at the weld toe. The study showed significant fatigue improvement from a weld with a contact angle of approximately 30°, compared to the 45° contact angle of an equal leg fillet weld. Based on the results of this testing, the unequal leg fillet weld, with the long leg on the pole, became the standard weld utilized in the socket connection detail.

The significance of fatigue related failures of traffic signal mast-arm connection details was documented by Kaczinski et al. in NCHRP Report #412. The authors reported the results of a survey of fatigue cracking problems experienced by Departments of Transportation throughout the United States (Kaczinski et al., 1998). Thirty-six Departments of Transportation from throughout the U.S. responded to the survey and approximately half of the responding DOT's reported fatigue cracking problems in traffic signal structures. In all, a total of 80 incidences of fatigue cracking in traffic signal structures were reported in the 1993 survey. Although the number of incidences of fatigue cracking seems large, the number of failures is small in comparison with the number of mast-arms in service.

Although the NCHRP #412 report documented a low number of traffic signal failures, a subsequent report by Dexter indicated that the number of failures of traffic signal mast-arms has increased in recent years (Dexter, 2001). This increase can be attributed to the increasing spans of mast-arms, and the inherent flexibility of the structures. The lengths of mast-arms are increasing, as roadways across the U.S. are being widened to add additional turn lanes or greater capacity. The set back distances between the columns and the edge of the roadway are also increasing, which has further lengthened the typical mast-arm. This lengthening of the mast-arms demands that engineers push the limits of the structures in an effort to design a lightweight and efficient structure.

The increased length of these structures combined with the inherent flexibility of the mast-arm has significantly contributed to the fatigue problems under study in this project. The resulting lightweight structures are very flexible and have very low natural frequencies. The low natural frequencies mean that these structures are more susceptible to resonance, which can lead to a large number of relatively high stress cycles.

1.3.1 TxDOT Mast-Arm Failure

The motivation for this research project was provided by a limited number of fatigue failures of traffic signal experienced by TxDOT and the perceived inability of the AASHTO specifications to accurately predict behavior. The Texas Department of Transportation provided a section of a traffic signal structure

that had failed under service conditions. The fatigue cracking in the failed mast-arm was not detected until the critical section failed completely and the mast-arm collapsed.

Pictures of the fracture surface are shown in Figures 1.4-1.7. An overall view of the mast-arm section is shown in Figure 1.4. Although the details of the failure surface cannot be determined from these pictures, the text in Figure 1.4 shows the different regions evident in the failure surface. The fatigue crack initiated at the top of the pole section, or in the area of max tensile stress. The fatigue cracking propagated symmetrically to slightly more than half of the overall depth of the cross section. When the cracking reached this point, the remaining cross section was no longer capable of supporting the loads and the structure collapsed.

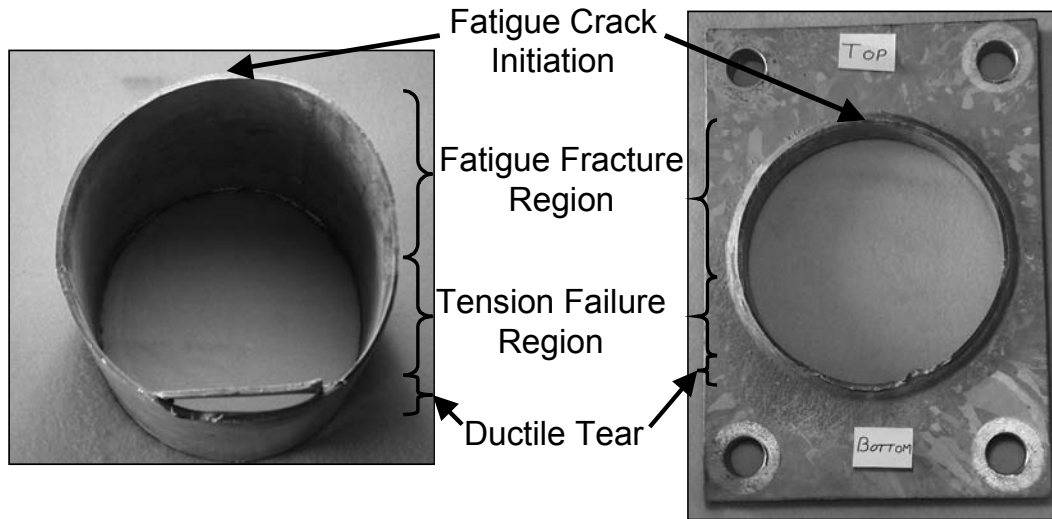


Figure 1.4 Portion of Failed Mast-Arm from TxDOT

Figure 1.5 shows the fracture surface of the pole. No yielding of the steel was observed in this area, which indicates that the cracking was due to fatigue. The arrows indicate locations of beach markings. These markings indicate the general progression of the crack during the fatigue life. The jagged edge of the fracture surface corresponds to the jagged toe of the socket weld, indicating that the fracture surface followed the weld toe.

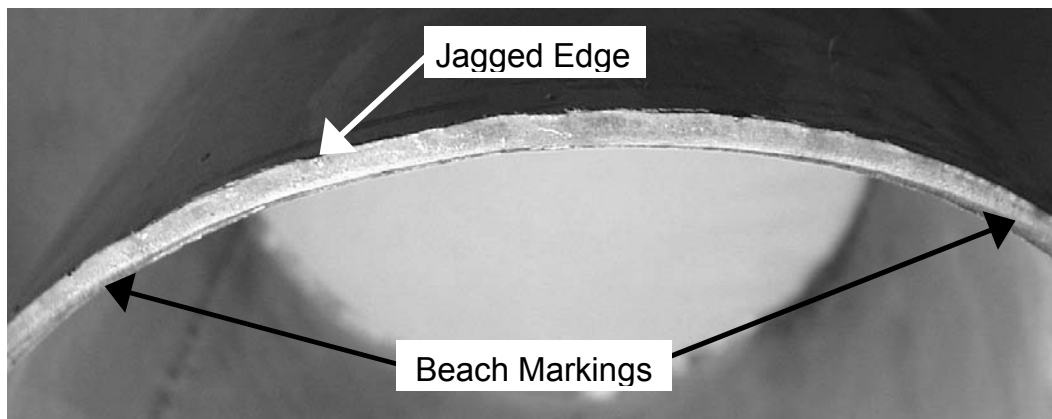


Figure 1.5 Pole Fatigue Fracture Surface of TxDOT Mast-Arm

Figure 1.6 shows the fracture surface of the base plate. In this picture, the same beach markings are evident. The fillet weld of this connection detail was deposited in two passes. The edge of the final pass is evident in Figure 1.6, slightly below the edge of the fracture surface.

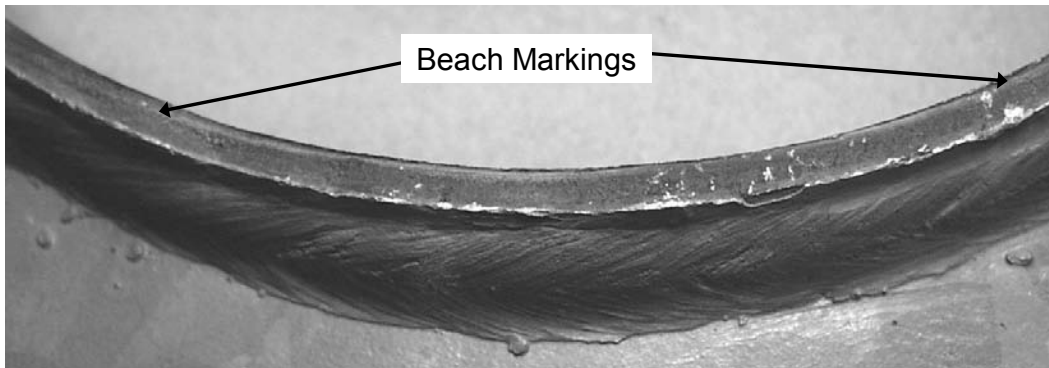


Figure 1.6 Base Plate Fatigue Fracture Surface of TxDOT Mast-Arm

Figure 1.7 shows the transition from the fatigue cracking region to the region of tensile failure. The multiple pass weld is also evident from this picture. The fracture surface clearly follows the toe of the socket weld in the fatigue fracture region on the right side of the picture. Where the fatigue fracture surface reached the tension failure region, the failure surface diverges from the toe of the socket weld into the pole section. The tensile failure region is evident based on the shear lips that developed during tearing of the pole wall.

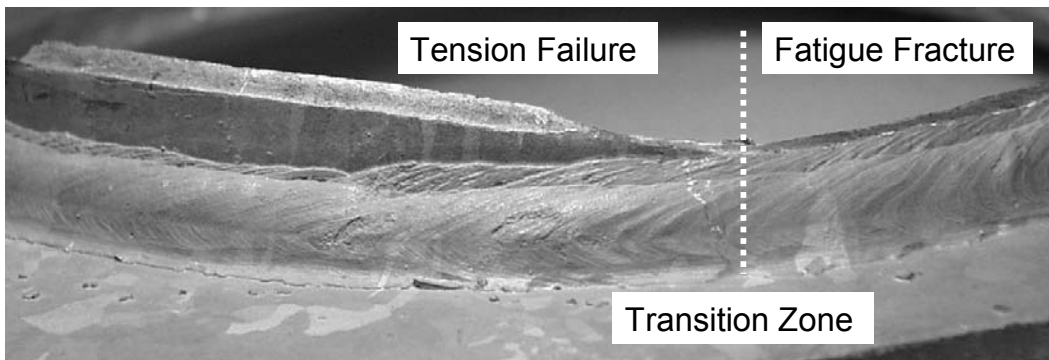


Figure 1.7 Failure Surface Transition Zone of TxDOT Mast-Arm

TxDOT has observed that the number of fatigue related failures and fatigue cracking found have increased in the past few years. This trend follows the nationwide trend noted by Dexter et al. (2001).

1.4 CURRENT AASHTO SPECIFICATIONS

The failures documented in NCHRP Report #412, combined with the increasing rate of fatigue related failures, provided an impetus to create a fatigue based design criterion in the AASHTO Highway Signs, Luminaires and Traffic Signal Specifications. The 2001 edition of this specification included fatigue-based design provisions for the first time.

The provisions of this specification were largely based on the results of the testing performed at Lehigh University (Miki, 1984). While the Lehigh test program tested 4 full-scale mast-arm connection details,

the connection details were limited to socket connections only. Therefore, when the AASHTO specifications were revised, the fatigue categorization of details not covered in the Lehigh University test program was based on AASHTO provisions for welded stiffeners and engineering “judgement” (Kaczinski et al., 1998).

The fatigue provisions also specify an ‘infinite life’ design basis. This means that all structures must be designed such that the stress at the connection detail remains below the applicable Constant Amplitude Fatigue Limit, or CAFL value. While this limit state eliminates the difficulty of attempting to calculate the number of load cycles that a structure must withstand, this may be an overly conservative limit state.

The fatigue provisions of the 2001 edition of the AASHTO Highway Signs, Luminaires and Traffic Signal Specifications have generated complaints and concern among the traffic signal structure design and manufacturing industries. They feel that the provisions are too conservative and difficult to satisfy. The new provisions require much larger and more costly structures. The connections of the mast arm to the mast become very large and difficult to fabricate using the new specification. The owners were concerned that higher cost and ungainly looking structures that result from the application of the specifications may not be necessary to produce reliable signal structures.

As a result of the fatigue sections of the 2001 specifications, the designers are faced with limiting the length of the structures, using an alternative connection detail, or increasing the size of the cross section. In cases of a multi-lane roadway, limiting the length of the mast-arm is not a viable solution. The use of alternative connections is more costly, and the connection details are typically unproven with few, if any, applicable test results available. Increasing the size of the mast-arm cross section is also less than desirable, as the increase in the weight of the mast-arm results in a significant increase in the applied loading, since the dead load is typically the largest portion of the loads applied to the structure. The increased weight results in a series of design iterations in which the size of the cross section must be increased significantly—adding a significant amount to the cost of the structure while only slightly improving the fatigue performance of the structure.

1.5 RESULTS OF RELATED RESEARCH

Aside from the research performed at Lehigh University, three other test programs evaluating the fatigue resistance of mast-arm connection details had been completed prior to or were underway during the testing as reported herein. These three test programs took place at Valmont Industries in Valley, Nebraska, the Tokyo Institute of Technology in Tokyo, Japan, and at the University of Missouri – Columbia in Columbia, Missouri. The results of the testing performed at Lehigh University, Valmont Industries, the Tokyo Institute of Technology, and the University of Missouri - Columbia are provided in tabular form in Appendix A.

The specimens tested at Lehigh University consisted of a mast-arm and column assembly (Miki, 1984). The tip of the mast-arm was loaded to create the desired stress ranges. The tests were performed with an imposed dead load—meaning that the mean stress of the cyclic loading was elevated such that the local stresses of the connection details always remained in either tension or compression. No stress reversal was applied.

The research conducted by Valmont Industries tested a number of full-size mast-arms in a rotating test setup as shown in Figure 1.8 (Macchietto, 2001). In this test setup, two poles were tested back-to-back with weights between the base plates of the poles creating the desired stress ranges. During the testing, the poles were rotated about their longitudinal axis causing a complete reversal of loading for each revolution of the pole. The results of the Valmont testing show a large amount of scatter, with the unstiffened socket connections performing better than the stiffened connections.

The research conducted at the Tokyo Institute of Technology focused on the testing of stiffened connections using typical triangular gussets, internal collars, external collars, and newly developed U-Rib

stiffeners (Miki, 2001). The testing was performed under cyclic loading with a mean load of zero, which causes a complete stress reversal at the critical connection detail. The results of the Tokyo Institute of Technology testing showed a significant fatigue life improvement when specially designed U-Rib stiffeners were used. The other connection details showed typically poor fatigue performance, which is in agreement with other test programs.



Figure 1.8 Test Setup for Tests Performed at Valmont Industries, Valley, NE.

The research program performed at the University of Missouri – Columbia had a much broader scope than the previous three test programs, as they investigated the influence of wind loading under service conditions, as well as the fatigue resistance of several connection details (Alderson, 1999). Based on the broad scope of this test program, only five laboratory fatigue tests were performed. The laboratory testing was performed in a cantilever test setup. The base plate of the mast-arm was fixed, and the tip was loaded cyclicly to create the desired stress range. The tests were performed under a mean stress of 14 ksi.

Of the five tests performed, flaws were detected in two of the specimens prior to testing, so the results of these specimens will not be discussed. The remaining three specimens provided mixed results. Two of the specimens performed at the level of a category E' detail as expected. The final specimen performed very poorly, and the researchers detected a possible lack of fusion defect in the socket weld.

1.6 SCOPE

The design problem described in Section 1.4, coupled with the increasing occurrences of fatigue cracking experienced by TxDOT, provided the impetus for this research project. The objectives of the test program were to evaluate the fatigue categorization of typical connection details, evaluate the design methodology for stiffened connection details and address the validity of the test results discussed in Section 1.5.

The laboratory fatigue testing of the connection details was performed on full-size traffic signal mast-arm specimens. Due to the large number of potential connection detail variations, the testing was separated into two phases. The connection details tested during Phase 1 investigated the connection details commonly utilized by TxDOT. The test specimens tested in Phase 2 addressed questions that arose during the testing of Phase 1 and also investigated a broader variety of possible connection details. In total, the tests investigated the influence of the pole wall thickness and base plate thickness on a common socket connection, as well as the use of connection details with stress reducing attachments. The Ultrasonic Impact Treatment weld treatment process was also investigated.

The following chapters discuss the results of this testing program. The test setup, test specimen design and testing procedure are described in Chapters 2, 3, and 4, respectively. The results of material tensile tests, chemistry analyses, and dynamic strain monitoring are presented in Chapter 5.

The results of the static testing of each series of specimens are discussed in Chapter 6. Along with the results, a general discussion of the specimen behavior, especially cross-sectional distortion, is included.

The results of the fatigue testing are discussed in Chapters 7 and 8. The results are analyzed in Chapter 7 following the typical fatigue life calculations based on the nominal section properties of the critical location. In Chapter 8, the test results are re-evaluated using a value based design method to provide a consistent method of stress calculation so that the test results of the various connection details can be compared directly.

Chapter 9 presents the results of a finite element analysis both unstiffened and stiffened connections. The influence of connection geometry upon the stress at the weld toe is examined using the hot spot stress approach to fatigue prediction used in the offshore industry.

Chapter 10 presents a study of the weld size of selected specimens. The measurements from weld gages and a computer based vision system are compared. The weld geometry is also checked with respect to the specified sizes.

The final chapter, Chapter 11, presents general conclusions from the test results, as well as recommendations for further research.

CHAPTER 2: TEST SETUP

2.1 TEST ASSUMPTIONS AND DESIGN DECISIONS

The moment diagram for the traffic signal structure described in Chapter 1 can be represented as shown in Figure 2.1. In this figure, the mast-arm is simply a cantilevered beam. To transform this service loading into a testing apparatus, the decision was made to test two mast-arms back to back so that the structure could be modeled as a simply supported beam, as shown in Figure 2.2. In this analogy, the critical connection details will be located in the center of the beam and loading will also occur at this point. The simple beam analogy allowed for a very simple test setup and eliminated concerns over fixity at the base plate.



Figure 2.1 Moment Diagram on Cantilever Mast-Arm Traffic Signal

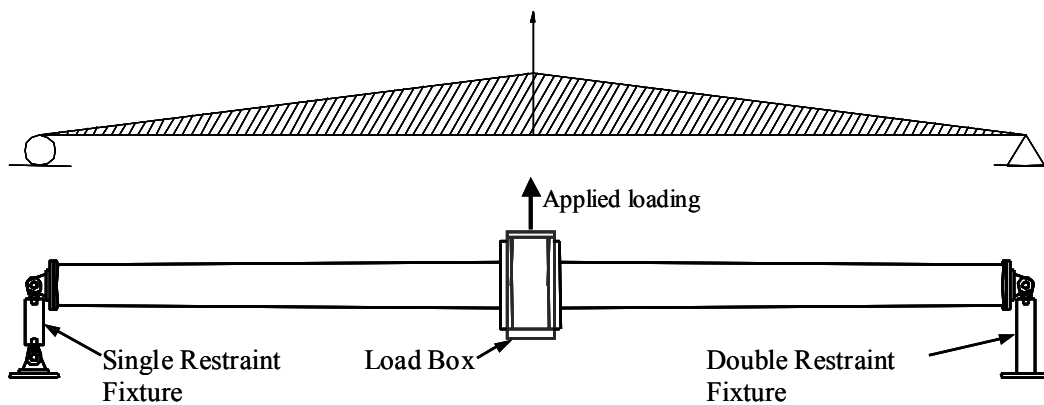


Figure 2.2 Test Setup Design with Simply Supported Beam Analogy

Early in the design process for the test setup, the decision was also made to perform all tests such that the test setup would remain in tension. This decision was based on the need to superimpose a dead load on the test specimen, and the desire to eliminate lateral stability concerns. This decision also simplified the design of the test setup. Lateral braces were not needed as the tensile loading ensured that the test loading occurred in a single vertical plane.

To allow for faster testing, the total length of the test setup was set at 16'. This length resulted in a mast-arm specimen length of approximately 87". The short length of the test setup resulted in typical dynamic displacement amplitudes between 0.35" and 0.40" for a stress range of 12 ksi. The hydraulic system used for loading was able to cycle through the above displacement range at frequencies up to 4.5 Hz. Under this load rate, almost 389,000 cycles could be accumulated per day and the average test lasted approximately one to two days.

2.2 TEST SETUP DESIGN

The test setup used for the testing is shown in Figure 2.3. In this figure, the center box is simply a 'load box' used to connect the base plates of the test specimen to the ram for loading. The ram was connected vertically from the load box to a standard test frame. The connections at both ends of the ram consisted of spherical ball joint clevises to allow for slight alignment imperfections. The ram used in this system was an MTS hydraulic actuator controlled by an MTS 407 Controller. Hydraulic pressure was provided by an external pump supplying 3000 psi constant pressure. This pressure was then tamed by an MTS 290 Hydraulic Service Manifold.

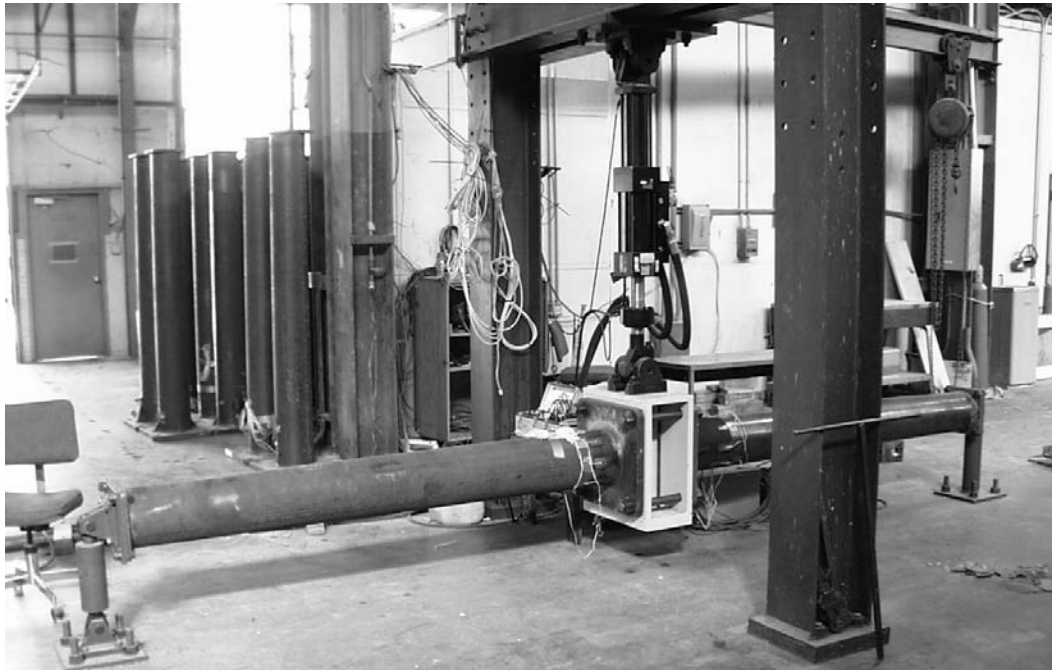


Figure 2.3 Test Setup

The mast-arm specimens were connected to the load box by a threaded rod that passes through the load box. The threaded rod is 1.5" in diameter, which is the same diameter as the bolts typically used by TxDOT. The threaded rod was extended through the load box and used to connect both specimens so that the threaded rod could then be used to pretension the load box. Calculations showed that in order to maintain a compressive force in the threaded rod under the 20 kip capacity of the ram, the threaded rods needed to be tightened to 33 kip prior to testing. The maximum load achieved during the testing program

was 12.5 kip, which is much lower than the 22 kip maximum load of the ram. Due to this low test load, the fatigue of the threaded rods was never a factor.

During the testing of the specimens in Phase 2, the 1.5" threaded rods were exchanged for 1.25" threaded rods due to problems with the boltholes fabricated into the specimen base plates. Many of the holes in the Phase 2 specimens were found to be oval shaped and too small for the original 1.5" threaded rods. In order to minimize the play in the setup due to the smaller threaded rods, inserts were placed in the holes in the load box to center the bolts and fill most of the gap caused by the smaller threaded rods.

In order to eliminate the concern of prying of the base plate from the load box, washers were placed on the threaded rod between the base plate and the load box. Aside from preventing prying, the washers also provided a known load path between the base plate and the load box. With the washers in place, the load was being transferred directly at the bolt holes of the base plate, and not at any other locations around the base plate. This eliminated any rocking of the base plates due to out of flatness of the plates.

The fixtures at each end of the test setup are shown in more detail in Figure 2.4 and Figure 2.5. The fixture in Figure 2.4 replicates a pinned end connection. This fixture consists of a riser section and a spherical rod eye and clevis. The spherical rod eye allows for corrections due to alignment imperfections.

The fixture in Figure 2.5 represents the roller connection of the simple beam analogy. This connection consists of a link between two sets of spherical rod eyes and clevises. Again, the spherical rod eyes allow for corrections due to alignment imperfections. The link allows for displacement along the longitudinal axis of the test specimen, thus eliminating axial loads in the test specimen. During testing, the overall rotation of the link was not noticeable to the eye, which implies that the overall height of the top of this fixture did not change significantly and therefore did not influence the loading in the vertical direction.

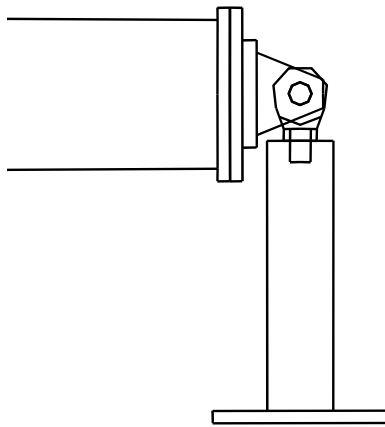


Figure 2.4 Double Restraint Fixture of Test Setup Design

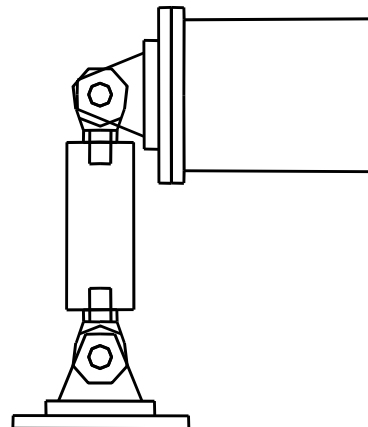


Figure 2.5 Single Restraint Fixture of Test Setup Design

2.3 SETUP LIMITATION - INSTABILITY UNDER COMPRESSIVE LOADING

Although the decision to always maintain a tensile force in the test setup and fixtures simplified the overall design of the test setup, there was one drawback to this design. Due to the two sets of spherical rod eyes and clevises in the roller connection, and the lack of lateral stability, the test setup could not be loaded in compression. This further means that we were not able to perform tests of full cyclic stress reversal similar to those performed at Valmont Industries and the Tokyo Institute of Technology. The impact of this limitation will be discussed in the results section of this report.

CHAPTER 3: TEST SPECIMEN DESIGN

3.1 SPECIMEN DESIGN

The designs of typical traffic signal mast-arms used by TxDOT provided the guidelines for the designs of the test specimens of Phase 1. The test specimens for Phase 2 were designed to further answer questions that arose during Phase 1 and to investigate the possible uses of alternative connection details. Since the specimen for the two phases of this project were developed for different reasons, the descriptions of the designs will be addressed separately.

3.1.1 Phase 1

With very little information available at the beginning of this research project, aside from the limited number of tests performed at Lehigh University, the specimens for Phase 1 were based on mast-arm properties common to TxDOT designs. The connection details were selected to test those details currently in use by TxDOT and those details that TxDOT was planning to utilize in the near future.

The standard plans utilized by TxDOT specify mast-arm section properties as detailed in Table 3.1. Based on this information, a standard mast-arm diameter of 10" was selected, as it was approximately the median diameter. The 10" diameter also allowed the use of a load range for the desired stress range that was well within the limits of the ram selected for the test setup.

As is shown in Table 3.1, the standard tube wall thickness utilized by TxDOT for a 10" mast-arm is 0.239". The manufacturer typically designs mast-arms of the same size and length using a 0.179" tube wall thickness. Due to the difference between the two design solutions, both wall thicknesses were tested during Phase 1.

Table 3.1 Standard TxDOT Design Properties

Arm Length (ft)	Diameter at Base Plate (in)	Wall Thickness (in) [U.S. Gage]
20	8.0	0.179 [7]
24	9.0	0.179 [7]
28	9.5	0.179 [7]
32	9.5	0.239 [3]
36	10.0	0.239 [3]
40	10.5	0.239 [3]
44	11.0	0.239 [3]
48	11.0	0.239 [3]

Two other features of the TxDOT standard mast-arm designs were used to provide correlation between the test results and the expected performance of the TxDOT structures in service. These two features were the base plate thickness and the diameter of the bolts used to connect the mast-arm to the built-up box

connection detail. The base plate thickness for all specimens in both phases of this test was set at 1.5". The threaded rods used to connect the test specimen to the load box were set at a diameter of 1.25".

All test specimens fabricated for testing during Phase 1 were non-galvanized. Other researchers have noted that the galvanization coating tends to bridge over small cracks, meaning that cracks must be larger before they can be observed in a galvanized specimen. For this reason, the specimens in this phase were not coated in order to more easily observe the cracking of the critical location.

As described in Chapter 2, the length of the test specimen was determined based on the length of the test setup in order to facilitate quick testing with a reasonable load range. Removing the lengths of the end fixtures and load box from the overall length of the test setup, the length of the test specimen was set at 86.6" or 7' 2.6". The fabrication drawings for the basic test specimen are provided in Figure 3.1.

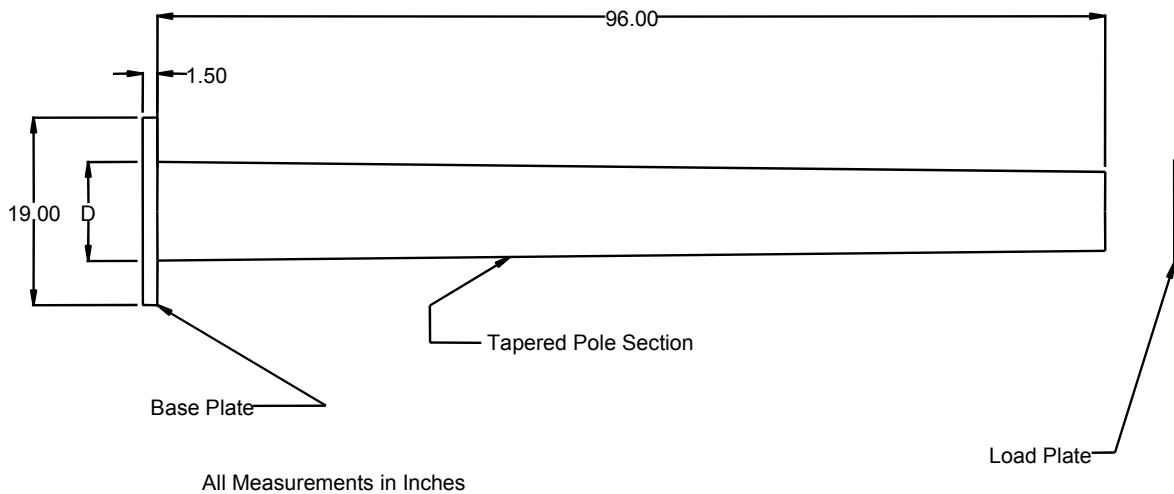


Figure 3.1 Test Specimen Drawing

The drawing in Figure 3.1 shows the base plate and tapered tube, which were fabricated and connected by the pole manufacturer. The figure also shows an additional load plate. The load plate was fabricated by the pole manufacturer, but connected to the pole at the University of Texas laboratory. The load plate allowed connection to the end fixtures.

3.1.1.1 Socket Connection

The fillet welds for the socket connections of Phase 1 were based on the standard designs utilized by Valmont Industries, which are in turn based on the wall thickness of the tube used for the mast-arm. The fillet weld is a standard unequal leg fillet weld with the long leg on the pole. The standard weld sizes are shown in the fillet weld detail in Figure 3.2. In the current AASHTO Specifications, the unequal leg fillet-welded socket connection is a category E' detail. To fulfill the infinite life design requirement of the fatigue provisions, the anticipated stresses at the location of the socket weld must be lower than the 2.6 ksi Constant Amplitude Fatigue Limit of the category E' detail.

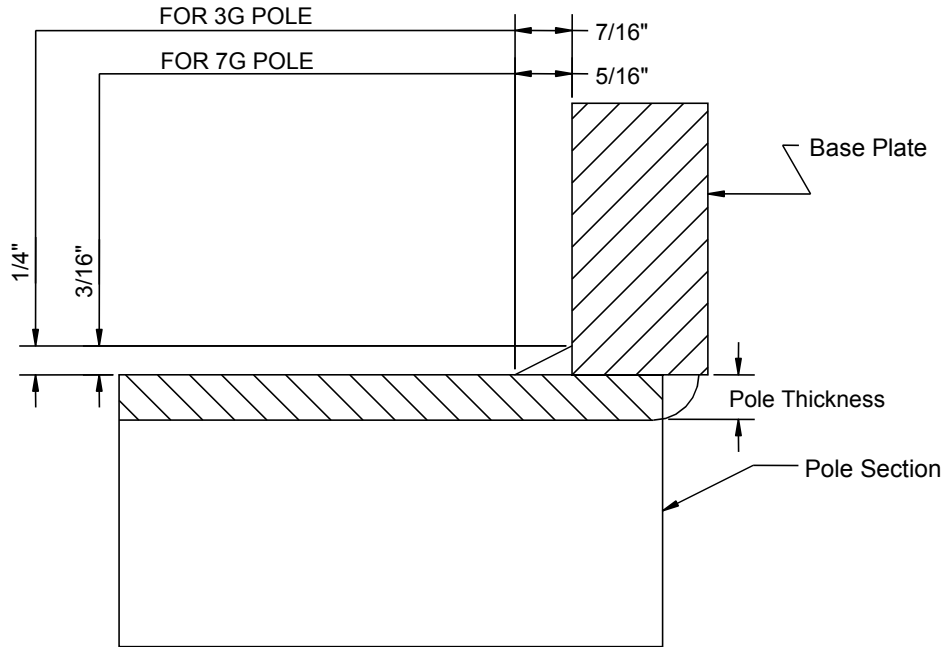


Figure 3.2 Fillet Weld Detail

3.1.1.2 Stiffened Connection

The stiffened connection detail is basically a socket connection with additional gussets, or stiffeners, arranged around the tube of the mast-arm. The weld detail of the socket connection is identical to that of an unstiffened socket connection, shown in Figure 3.2.

The general objectives for testing the stiffened connection details of Phase 1 were to determine the appropriateness of the fatigue categories provided in the AASHTO Specifications and to check the validity of the design equations recommended by Dexter in NCHRP Report #412. With these objectives in mind, the designs for the stiffened connections in Phase 1 were created following the example design procedure provided in NCHRP Report #412. These design examples follow the recommended provisions that were accepted as the fatigue provisions of the 2001 AASHTO Highway Signs, Luminaires and Traffic Signal Specifications.

The fatigue specifications provide fatigue categories for stiffened connections that are based on the overall geometry of the stiffener, the type of weld used, and the length of the stiffener. A portion of the specification is provided in Table 3.2. The stiffeners that are fabricated with a smooth transition and a full penetration weld, indicated as detail #21 in the specification, are more costly and difficult to fabricate. The grinding of the transition of the stiffener also raises concerns of over-grinding resulting in larger initial flaws or gross section reduction. Based on these fabrication concerns, the stiffeners were limited to the triangular stiffeners without a smooth transition and attached with fillet welds.

The general design procedure for the stiffened connection detail involves checking the anticipated stress ranges at three locations. The nominal stress range at each location was calculated assuming linear

behavior and assuming $\sigma = \frac{Mc}{I}$ applies. The calculated stress range is then compared to the Constant

Amplitude Fatigue Limit, or CAFL value, for the appropriate fatigue category. The fatigue category, and therefore the CAFL value, is different for each location.

Table 3.2 Excerpt from Fatigue Provisions of 2001 AASHTO Highway Signs, Luminaires and Traffic Signal Specifications

CONSTRUCTION	DETAIL	STRESS CATEGORY	APPLICATION
Fillet-Welded Connections	16. Fillet-welded tube-to-transverse plate connections.	E'	Column-to-base-plate or mast-arm-to-flange-plate socket connections.
Attachments	20. Non-load bearing Longitudinal attachments with partial- or full-penetration groove welds, or fillet welds, in which the main member is subjected to longitudinal loading:		Weld termination at ends of longitudinal stiffeners. Reinforcement at handholes.
	$L \leq 51$ mm:	C	
	$51\text{mm} < L \leq 12t$ or 102mm :	D	
	$L > 12t$ or 102 mm when $t \leq 25$ mm:	E	
	21. Non-load bearing longitudinal attachments with $L > 102\text{mm}$ and full-penetration groove welds. The main member is subjected to longitudinal loading and the weld termination embodies a transition radius or taper with the weld termination ground smooth:		Weld termination at ends of longitudinal stiffeners.
	$R > 152$ mm or $\alpha \leq 15^\circ$:	C	
	$152 > R > 51$ mm or $15^\circ < \alpha \leq 60^\circ$:	D	
	$R \leq 51$ mm or $\alpha > 60^\circ$:	E	

The three potentially critical locations are identified in Figure 3.3. The first location is the socket weld. The moment of inertia at this location is calculated assuming that the stiffener is fully effective. In other words, the moment of inertia is increased by the addition of the stiffener while the c value, or the distance from the neutral axis, remains equal to the radius of the mast-arm tube. This results in a decrease in the calculated stress range due to the addition of the stiffener, which can be thought of as providing protection to the socket weld. This location is a category E' detail, as it is the same as the socket weld in the unstiffened socket connection specimens.

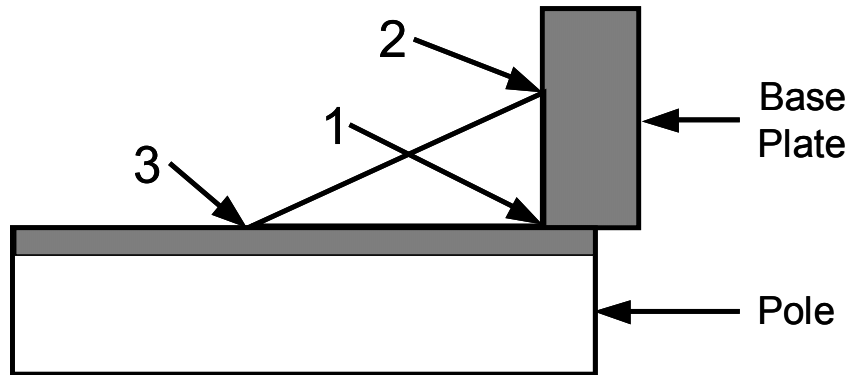


Figure 3.3 Stiffener Diagram with Critical Locations Indicated

The second potential critical location is the stiffener to the base plate weld. The moment of inertia for this calculation is the same as that for the socket weld, however the c value is taken as the distance from the neutral axis to the extreme fiber of the stiffener. This location is a category C detail, and anticipated stresses must be lower than the 10 ksi Constant Amplitude Fatigue Limit of the category C detail to fulfill the infinite life design requirement of the fatigue provisions. Due to the large moment of inertia, the large c value and the high CAFL value, this location most commonly will not control a stiffener design.

The final potential critical location is at the termination of the stiffener. To check this location, the moment of inertia is calculated as the moment of inertia of only the pole at this location. According to the applicable section of the fatigue specification (detail #20), the fatigue category at the termination of the stiffener is based on L , the length of the stiffener along the pole. For short stiffeners, with $L \leq 2"$, the fatigue category is C. For long stiffeners, with $L > 12t$ or $4"$ where t is the thickness of the stiffener, the fatigue category is E. The fatigue category is D for stiffeners of lengths between the two limits above. The thickness of a stiffener is limited to 1 inch.

Following the examples provided by Dexter, the general design of a stiffened connection uses the variables of the length (distance along the pole), width (distance along the base plate) and thickness of the stiffener to adjust the design to, in effect, protect the socket weld. These dimensions are shown diagrammatically in Figure 3.4. Through examination of these variables, and comparison with the specification, the length of the stiffener along the pole is the only variable which influences the fatigue category.

At this point, it is also important to note that the fatigue category of a stiffened connection is not dependent on the thickness of the wall of the pole. Based on this observation, the stiffeners for the two pole wall thicknesses selected for Phase 1 were identical for each pole wall thickness.

A decision was made to use only 4 stiffeners in order to simplify the design and reduce the number of possible failure locations. It must also be noted that the number of stiffeners provided does not influence the fatigue category. The concern behind this omission can more easily be seen by examining the extreme cases. At one extreme, if only two very thick stiffeners are used, the concern of the stiffener punching through the wall of the mast-arm increases. On the other extreme, if the number of stiffeners is increased until there are no unstiffened areas between the stiffeners, the solution approaches that of an external collar stiffener. This extreme reduces the concerns of punching, as the critical location is spread from a small region at the termination of the stiffener to a larger region at the termination of the collar. The use of an external stiffening collar was investigated in Phase 2.

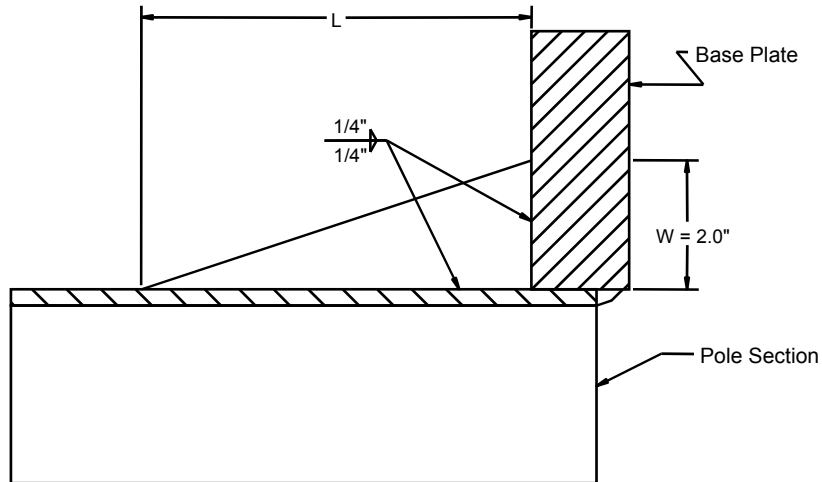


Figure 3.4 Stiffener Detail

The decision was also made to orient the stiffeners vertically from the top and bottom of the mast-arm and horizontally at the neutral axis. The vertical orientation of the stiffeners was selected to place the stiffeners in the location of highest local stresses. This decision placed the termination of the stiffener in the worst possible position for fatigue concerns while also providing the greatest benefit from the stiffener.

With the stiffeners oriented in this arrangement, the stiffeners placed at the horizontal axis do not contribute significantly to the moment of inertia at the face of the base plate. The horizontal stiffeners were only installed on the test specimens to maintain a symmetric specimen. With the four stiffeners, the specimens were symmetric such that each specimen could be tested with any one of the stiffeners positioned on the top of the test specimen. In theory, all four stiffeners could be tested to failure.

The vertical stiffener orientation as selected is contrary to the placement typically used by the TxDOT in which the stiffeners are attached at an angle of 45° to vertical. The 45° orientation of the stiffeners allows the stiffeners to be installed on a smaller base plate. This is especially true in the horizontal direction in which the neutral axis stiffeners result in a wider base than would typically be used. The 45° stiffener orientation was investigated in Phase 2.

While the decision to orient the stiffeners vertically and horizontally was assumed to provide the most dramatic influence in the laboratory, the agreement with the in-service conditions is not as clear. As stated, the typical in-service stiffener placement is at a 45° angle to vertical. Under the wind vibration conditions described in Chapter 1, the predominant motion of most traffic signal mast-arms is in an approximate figure 8 pattern; with the longitudinal axis of the pattern offset approximately 45° from vertical. In this vibration pattern, the significant components of the displacement occur in a plane oriented in the same direction as the longitudinal axis of the figure 8 pattern. Therefore, under the wind loading conditions, the orientation of the stiffeners is approximately along the same plane as the predominant displacement. To correlate the orientation of the stiffeners during the laboratory testing to the location of the stiffeners under the wind loading conditions, the vertical orientation of the stiffeners is the most representative orientation as the displacement of the testing occurred in a vertical plane.

After working through the example design procedure, the decision was made to set the width, or the length along the base plate, of the stiffeners to 2" for all stiffeners. With this variable fixed, the remaining two variables, the length and thickness of the stiffener, could be easily varied to reduce the stress at the socket weld and therefore protect the socket weld by varying amounts. Two lengths and two thicknesses were selected and arranged in three different combinations to create the stiffener designs for testing. The

three combinations are detailed in Table 3.3. The 3" long 3/8" thick stiffener was the base stiffener design. The other designs have either thinner or longer stiffeners.

Table 3.3 Stiffener Designs

Stiffener Label	Stiffener Thickness	Stiffener Length	Design Category
3X1/4	1/4"	3"	D
3X3/8	3/8"	3"	D
6X3/8	3/8"	6"	E

The concept of protecting the socket weld has been mentioned several times during the description of the design procedure. This concept will be further illustrated by examining the three stiffener specimen designs. In order to show quantitatively which location (out of the three potential critical locations) was critical, the protection factor equation was used to calculate the protection provided by the stiffener to the socket weld assuming that the stiffener was fully effective. The protection factor for each stiffener design

was calculated as $Pf = \frac{N_{stiffener}}{N_{socket-weld}}$, where $N = \frac{A}{S_r^3}$, and A is the fatigue constant applicable to each

location as provided in the 2001 AASHTO Highway Signs, Luminaires and Traffic Signal Specifications. The numerator of the protection factor equation was taken as the estimated cyclic fatigue life at the termination of the stiffener, and the denominator was taken as the estimated cyclic fatigue life at the socket weld, assuming that the stiffener was fully effective. The results of these calculations are shown in Table 3.4.

Table 3.4 Protection Factor

Specimen	Protection Factor (termination of stiffener compared to socket weld, stiffener fully effective)
Thin Pole Wall	
3" long x 1/4" thick stiffener	0.60
3" long x 3/8" thick stiffener	0.97
6" long by 3/8" thick stiffener	1.78
6" long by 3/8" thick stiffener offset 45° from vertical	0.62
Thick Pole Wall	
3" long x 1/4" thick stiffener	0.46
3" long x 3/8" thick stiffener	0.69
6" long by 3/8" thick stiffener	1.27

The values presented in Table 3.4 represent the difference in estimated fatigue life between the termination of the stiffener and the socket weld. Values less than one indicate that failure is predicted at

the socket weld, while values greater than 1 indicate that cracking will initiate at the termination of the stiffener.

It is important to note that the 6" long stiffeners are category E details, while the 3" long stiffeners are category D details. The lower fatigue category for the 6" long stiffeners explains the significant difference in the calculated values. This change of the fatigue category seems to be counterintuitive. At the termination of a longer stiffener, the moment will be lower than that for shorter stiffener. However, in a typical traffic signal structure the overall length of the mast-arm is at least an order of magnitude greater than the length of a stiffener. This means that the moment gradient will be fairly low and the decrease of the moment due to the length of the stiffener is most likely negligible. However, for stiffeners of a given width (length along the base plate), the termination of a longer stiffener will have a shallower angle of incidence with the tube of the mast-arm. A shallower angle of incidence is typically regarded as a more desirable fatigue detail as it results in a lower stress concentration. Following this reasoning, it would seem that a longer stiffener would be more desirable, and the specifications seem counter-intuitive. This reasoning provided an impetus to design the 6" long stiffener, which according to the specification was of a lower fatigue category—contrary to intuition.

The values of Table 3.4 for the thin pole wall specimen provide the rationale for selecting the stiffener designs tested in Phase 1. From the calculated values it is clear that the design process predicted that the 3" long by 1/4" thick stiffener design would fail at the socket weld, and the 6" long by 3/8" thick stiffener design would fail at the termination of the stiffener. The 3" long by 3/8" thick stiffener design presented a balanced failure prediction, in that the failure was almost equally likely to initiate at either the socket weld or the termination of the stiffener. Clearly, the three stiffener designs selected for the thin pole wall specimens represented a method to confirm the validity of the design assumptions as the predicted failure location differed for each stiffener design.

Once the stiffener designs were selected for the thin pole wall test specimen, the same designs were utilized on the thick pole wall specimen. As noted earlier, the pole wall thickness is not a factor in determining the design category of a stiffened connection detail. However, the larger pole wall thickness reduced the effect of the stiffeners upon the calculated section properties.

To provide an estimate of the anticipated fatigue life improvement provided by each of the stiffener designs, a fatigue life improvement ratio was calculated for each design. This ratio was calculated as the number of cycles expected under the given loading for the stiffened connection divided by the expected number of cycles expected under the same loading for an unstiffened socket connection. Mathematically,

this equation is written as $FLIR = \frac{N_{critical}}{N_{unstiffened-socket-connection}}$, where $N = \frac{A}{S_r^3}$, and again A is the fatigue

constant applicable to each location as provided in the AASHTO Specification. In the fatigue life improvement ratio equation, the $N_{critical}$ value was taken as the N value calculated for the critical section of the stiffened connection. The critical section was selected from the three potentially critical sections as the location with the lowest estimated fatigue life. This location was either the socket weld or the termination of the stiffener. The stiffener to base plate weld never controlled the fatigue life calculation.

The fatigue life improvement ratios for each of the stiffened connection details are provided in Table 3.5. These values indicate the amount of improvement provided by the stiffeners when compared to an unstiffened socket connection detail. These values are specific to the section properties selected for the test specimen in this test. For example, the fatigue life improvement ratio for the 3" long by 1/4" thick stiffener on the 0.179" thick mast-arm is 3.66. This ratio means the predicted fatigue life of this connection detail is 3.66 times the value for an unstiffened socket connection detail under the same loading. The values in Table 3.5 indicate that every stiffener should provide a greater fatigue life than an unstiffened socket weld connection. Furthermore, the prolonged fatigue life indicates that the base plate weld is protected from failure by the addition of the stiffeners.

Table 3.5 Fatigue Life Improvement Ratio

Specimen	Fatigue Life Improvement Ratio (as compared to unstiffened connection detail)
Thin Pole Wall	
3" long x 1/4" thick stiffener	3.66
3" long x 3/8" thick stiffener	5.94
6" long by 3/8" thick stiffener	3.40
6" long by 3/8" thick stiffener offset 45° from vertical	5.94
Thick Pole Wall	
3" long x 1/4" thick stiffener	2.82
3" long x 3/8" thick stiffener	4.24
6" long by 3/8" thick stiffener	3.40

3.1.1.3 Summary of Phase 1 Specimens

The variables for testing in Phase 1 were pole wall thickness, stiffener length and stiffener thickness. The properties of each specimen are detailed in Table 3.6. The specimen labels are included in this table and will be explained towards the end of this chapter. As is indicated in Table 3.6, at least 3 specimens of each specimen type were ordered.

Two sets of three specimens were ordered for the unstiffened socket connection specimen. The second set was ordered so that the influence of Ultrasonic Impact Treatment (UIT) on the fillet welds could be treated. The UIT procedure will be further discussed in Chapter 7. After the initial sets of testing, the specimens to be treated with the UIT treatment were adjusted so that two unstiffened socket weld specimens and one stiffened specimen from each wall thickness group were treated.

Table 3.6 Phase 1 Test Specimen Matrix

Specimen Label	Wall Thickness	Connection Detail	Specimens Tested
VALu	0.179"	Socket: Unequal leg fillet weld	6
VAL 3x1/4	0.179"	Stiffener: Length = 3", Thickness = 1/4"	3
VAL 3x3/8	0.179"	Stiffener: Length = 3", Thickness = 3/8"	3
VAL 6x3/8	0.179"	Stiffener: Length = 6", Thickness = 3/8"	3
TXu	0.239"	Socket: Unequal leg fillet weld	6
TX 3x1/4	0.239"	Stiffener: Length = 3", Thickness = 1/4"	3
TX 3x3/8	0.239"	Stiffener: Length = 3", Thickness = 3/8"	3
TX 6x3/8	0.239"	Stiffener: Length = 6", Thickness = 3/8"	3

3.1.2.1 Fabrication Location

Due to the variety of new connection details included in Phase 2, it was decided to have the specimens fabricated at the Valmont Industries headquarters plant in Nebraska to allow the engineers at Valmont to supervise the fabrication of specimens.

In order to determine the extent of the fabrication location influence, a set of two test specimens identical to the (thin pole wall) unstiffened socket connection specimens tested in Phase 1 were tested during Phase 2. This set of specimen also allowed for correlation between the results of Phase 1 and Phase 2.

3.1.2.2 Galvanizing

During the Phase 1 testing, the influence of galvanizing was questioned. As almost all traffic signal mast-arms in service are galvanized, any influence of this coating would have a significant impact on the applicability of the test results. To test this variable, a set of two unstiffened socket connection specimens were fabricated and coated prior to testing.

The issue of galvanizing is also included in the UIT weld treatment test matrix. These two test specimens were utilized as control specimens for the UIT study.

3.1.2.3 Base Plate Thickness

In comparing the results of Phase 1 to results from testing performed at other locations, the Phase 1 results were noticeably lower than the results from testing at Valmont Industries and the Tokyo Institute of Technology. More information on the discrepancies between the various test programs is provided in Section 1.5 and Section 7.9. One of the differences between the test specimens from the different test programs was the thickness of the base plate.

In order to test the influence of the thickness of the base plate, a set of two specimens was tested with a 2" thick base plate. The base plate thickness was intentionally exaggerated in an effort to magnify the influence of the thickness.

3.1.2.4 Stiffener Orientation

As discussed previously, the stiffeners of the stiffened connections designed and tested in Phase 1 were oriented vertically and horizontally, which is contrary to the design typically utilized by TxDOT. To further determine the influence of the stiffener orientation and to correlate the results of the laboratory testing to the in-service conditions, a total of four specimens were tested with the stiffeners oriented at 45° angles from vertical.

The 6" long and 3/8" thick stiffeners exhibited the best fatigue performance of any stiffener design during the Phase 1 testing. Based on these results, the same 6"x3/8" stiffeners were placed at 45° angles to vertical. The fabrication drawings for these specimens are shown in Figure 3.6.

The Protection Factor and Fatigue Life Improvement Ratio were calculated for these specimens using the same equations as used for the Phase 1 stiffened specimens. The calculated Protection Factor is included in Table 3.4, and the Fatigue Life Improvement Ratio is included in Table 3.5.

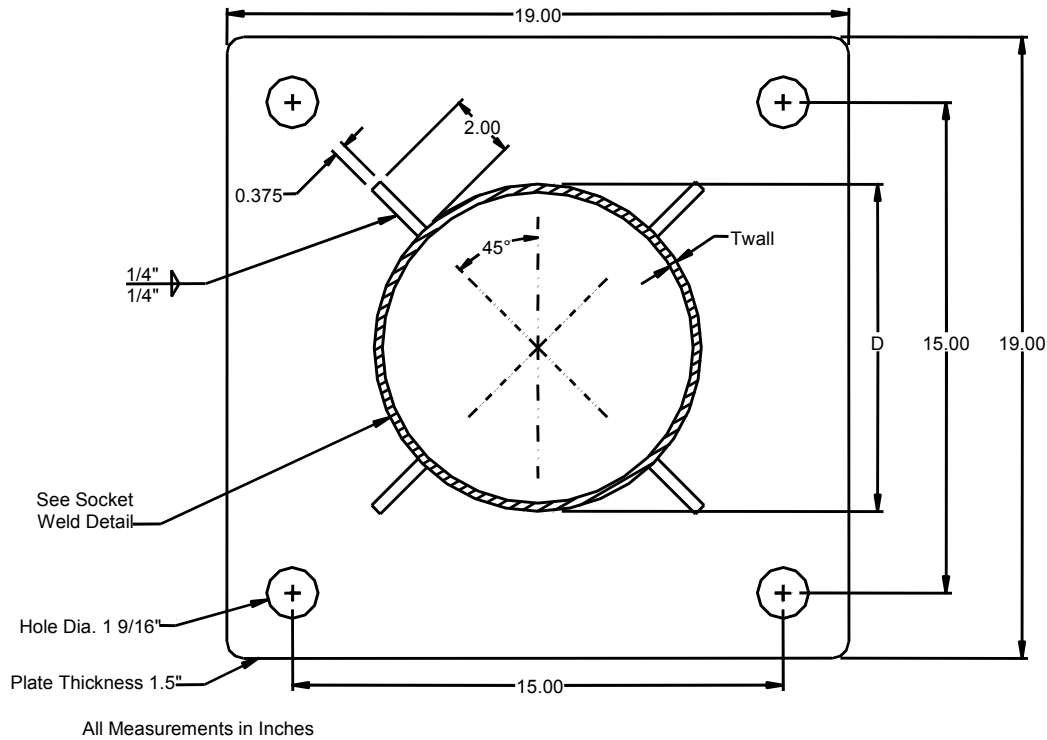


Figure 3.6 Base Plate Fabrication Drawing with Stiffeners Offset at 45° Angles

3.1.2.5 UIT Weld Treatment

During Phase 1 of this test program, one of the UIT treated specimens was tested at a low mean stress. This specimen exhibited a significant fatigue life improvement and performed much better than the specimens tested under a higher mean stress. This particular test result will be more thoroughly discussed in the results section.

Three UIT weld treatment processes were envisioned to apply the low mean stress test condition to an in-service condition in which the dead load results in an elevated mean stress. The three methods include a retrofit procedure, as well as two fabrication procedures in which the UIT weld treatment is performed at different points in the fabrication process.

A set of two unstiffened socket weld connection specimens was fabricated for each of the three UIT weld treatment procedures. For each procedure, the specimens were treated while in the test setup under the minimum test load. On each specimen, the toe of the socket weld in the top half (tension portion) of the cross-section was treated with the UIT weld treatment process. The three testing procedures varied based on the order of the galvanization process relative to the UIT process and the action taken immediately after treatment. These differences are discussed in greater detail in the following sections.

Fabrication Processes

The UIT weld treatment fabrication processes were designed to represent two potential fabrication procedures in which the mast-arms would be loaded to an approximate dead load in the fabricator's shop and then treated with the UIT weld treatment. The UIT weld treatment could be performed in the fabrication process either before or after the mast-arms are galvanized. Even though these procedures insert at least one more step in the fabrication process, a significant fatigue life improvement would easily offset the additional cost.

Valmont Industries, the manufacturer of the test specimens for this test program indicated that they would prefer to perform the UIT weld treatment prior to the galvanizing process. Valmont Industries utilizes separate galvanizing and fabrication facilities. Due to the separate facilities, after fabrication the mast-arms are sent to the galvanizing facility, and the finished mast-arms are typically shipped directly from the galvanizing facility to the client. With the UIT weld treatment inserted into the fabrication process prior to galvanizing, the fabricator can complete the fabrication and weld treatment prior to shipping the mast-arms to the galvanizing facility. This minimizes the touch up of the treated area and the handling cost of the mast-arms since the process eliminates the need for the mast-arms to be returned to the fabrication facility.

Applied Ultrasonics, the company responsible for the UIT weld treatment, was concerned that the heat incurred in the galvanizing process would reduce the effectiveness of the UIT weld treatment. Instead, they preferred to perform the UIT weld treatment after the galvanizing process.

In light of the uncertain effects of the galvanizing process, both potential fabrication procedures were investigated. One set of test specimens was treated with the UIT weld treatment before the galvanizing process, and another set was treated after the galvanizing process.

UIT Prior to Galvanizing

The specimens in this test set were not galvanized upon delivery. After the UIT weld treatment, the specimens were unloaded, removed from the test setup and shipped to United Galvanizing in Houston, Texas for galvanizing. After galvanizing, the specimens were tested to failure.

UIT After Galvanizing

For this test set, the specimens were delivered already galvanized. After the UIT weld treatment, the specimens were unloaded, removed from the test setup, and set aside to be tested at a later date.

UIT Retrofit

The specimens in this test set were tested almost identically to the ‘UIT After Galvanizing’ specimens described in the previous section. The test specimens were delivered already galvanized. The specimens were not unloaded after the UIT weld treatment; instead, the fatigue test was started immediately.

This treatment procedure was designed to represent performance of the UIT weld treatment under in-service dead load conditions. As the procedure name implies, this treatment procedure could be utilized to retrofit existing structures currently in use. As a retrofit procedure, this is a fairly simple way to improve the fatigue life of structures that would otherwise need to be replaced.

The treatment procedure could also be utilized to improve new structures by treating the socket weld immediately after the structure is erected. If utilized in this manner, the treatment procedure would be more difficult than either of the fabrication techniques. While it does remove the need for a fabricator to create a loading setup, the weld treatment must be performed in the field. This means that the treatment equipment must be transported to the location of installation. The treatment must then be performed while the mast-arm is in place, which typically means that the operator would have to be lifted approximately 20' in the air.

3.1.2.6 Alternative Connection Details

A variety of alternative connection details were suggested during the design meeting for Phase 2. Many of these details were tested because little or no test data was available to provide guidance when determining a fatigue category. A brief background and general design discussion are provided for each connection detail tested in the following sections.

External Collar

The concept of an external collar was raised previously during the stiffener discussion for Phase 1 in Section 3.1.1.2. The external collar was proposed as a way to take the ‘large number of stiffeners’ analogy to an extreme. According to this analogy, since the collar would increase the stiffness of the tapered tube an equal amount around the circumference, the collar would therefore create less of a stress concentration than created at the termination of a stiffener.

Carl Macchietto of Valmont Industries designed the external collar. The fabrication drawings for these specimens are shown in Figure 3.7, and a picture of a completed specimen is included in Figure 3.8. The fabrication drawing indicates that the collar to pole weld should be ground concave to produce a better weld profile. A set of two specimens with the external collar connection was fabricated. The ground areas on the test specimens were observed to be roughly ground with the ground area extending beyond the toe of the weld and into the pole in several locations.

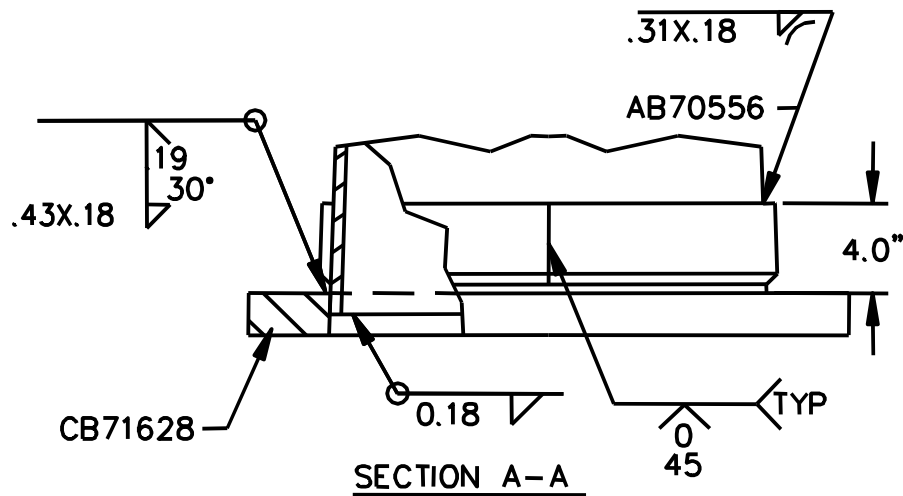


Figure 3.7 External Collar Connection Detail



Figure 3.8 External Collar Stiffened Specimen

Internal Collar

The internal collar was suggested and designed by Carl Macchietto of Valmont Industries. The fabrication drawings for these specimens are shown in Figure 3.9. This figure shows the welded connection at the base of the test specimen. The termination of the inner collar was not welded, but instead the collar was hydraulically pressed into the tapered tube to create a friction fit. The length of the inner collar was specified to be at least 12.25" from the back of the base plate – a more exact dimension was not provided. A set of two specimens with the internal collar connection was fabricated. The fabricated lengths of the internal collars measured from the back of the base plate were 13.4" and 14.1".

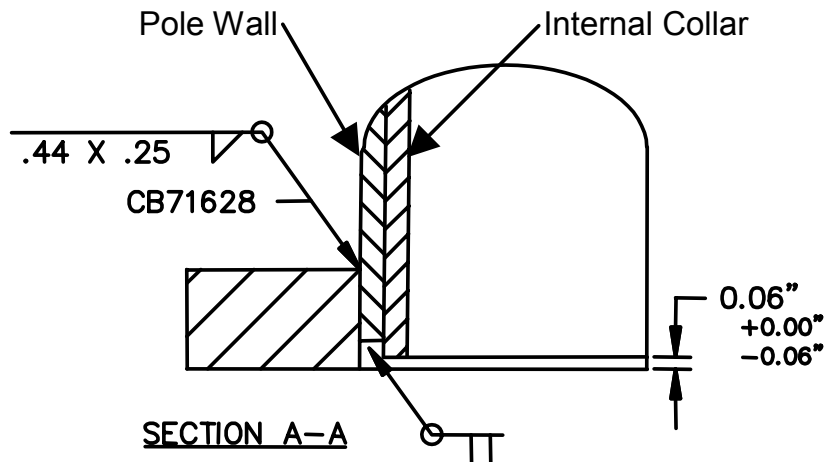


Figure 3.9 Inner Collar Detail

It is important to emphasize the fact that the internal collar was only welded to the base plate due to a lack of accessibility at the termination of the internal collar. As mentioned above, the only mechanism for transferring forces between the internal collar and the mast-arm tube was through friction. As will be discussed in the results section, this resulted in a non-linear load vs. displacement relation.

U-Rib Stiffeners

The U-Rib Stiffeners were first tested by the Tokyo Institute of Technology. During their test program, the U-Rib stiffeners provided a dramatic fatigue life improvement. More information on the results of the testing program at the Tokyo Institute of Technology is provided in Section 1.5.

Based on the impressive results of the U-Rib stiffener testing at the Tokyo Institute of Technology, this connection detail was selected for testing to evaluate the difference between the testing methodologies. As mentioned in Section 1.5, the testing at the Tokyo Institute of Technology was performed under a zero mean stress condition. The testing at the University of Texas was performed under high mean stress conditions, and the concern was that the high mean stress level would eliminate any beneficial residual stresses in the U-Rib stiffener.

Masakazu Sugimoto of Nippon Steel Corporation performed the design of the U-Rib stiffeners. Since this connection detail is a proprietary design, the basic design equations and fabrication procedure will not be discussed. However, it is important to note that the stiffeners were attached to the pole following a very detailed weld procedure that was designed to create residual stress fields in the proper locations along the stiffener. The fabrication drawings for these connection details are provided in Figure 3.10 and Figure 3.11. A set of two specimens was fabricated with U-rib Stiffener connection details. Two pictures of a completed specimen are included in Figure 3.12 and Figure 3.13.

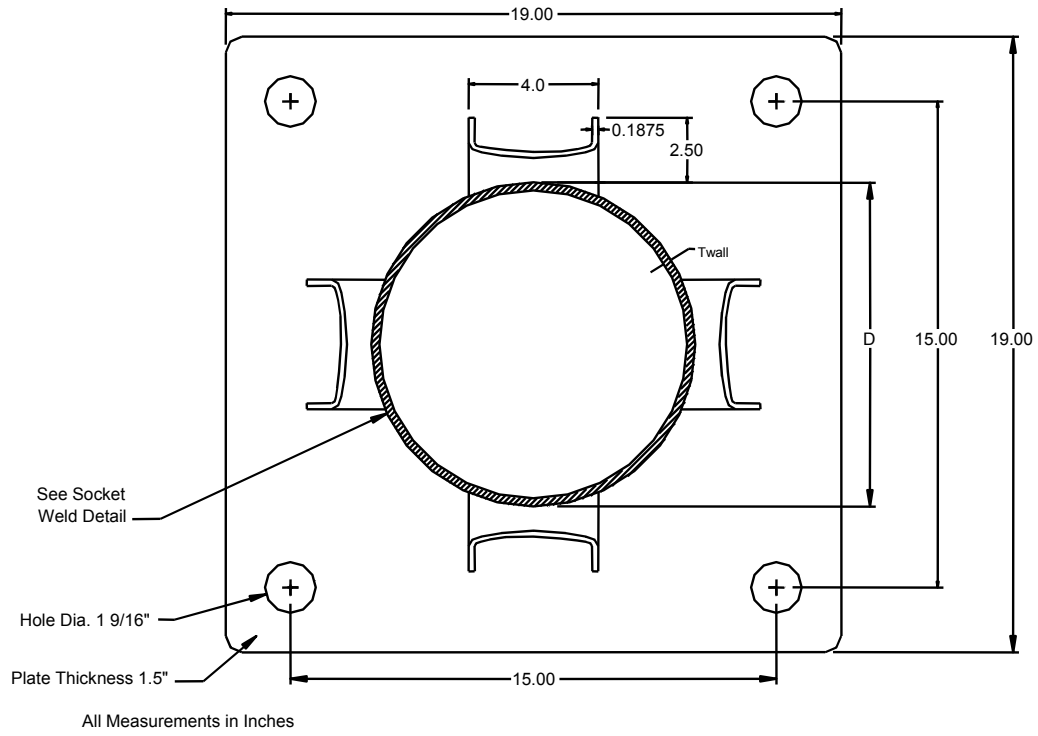


Figure 3.10 U-Rib Stiffener Plan Detail

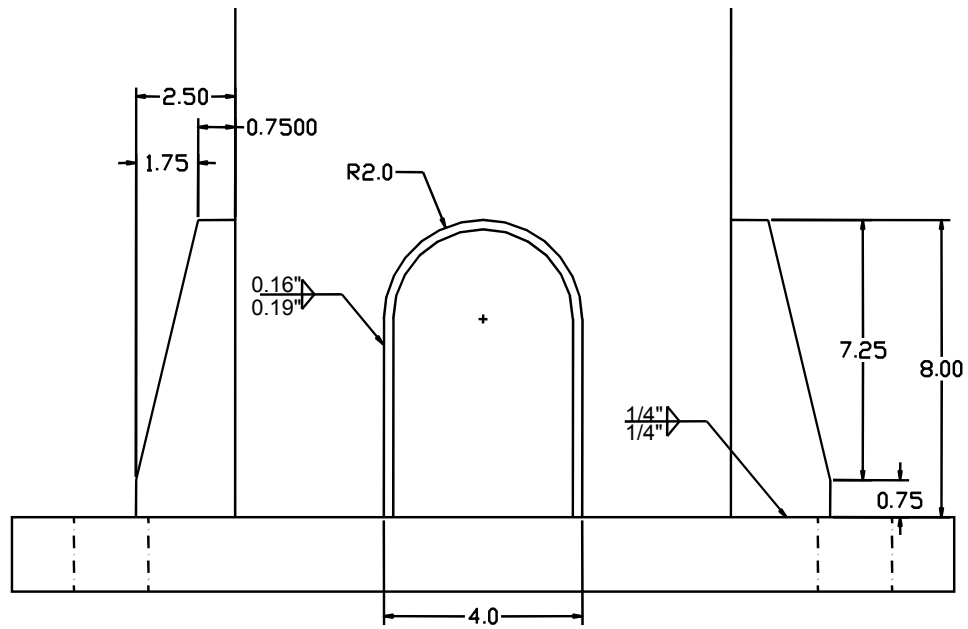


Figure 3.11 U-Rib Stiffener Elevation Detail



Figure 3.12 U-Rib Stiffened Specimen



Figure 3.13 U-Rib Stiffened Specimen

Full Penetration Weld

Carl Macchietto of Valmont Industries suggested testing of a full-penetration-welded connection. This connection detail is typically less desirable than a fillet-welded socket connection due to the increased cost of beveling the tube and placing the full-penetration-weld. The fatigue provisions of the 2001 AASHTO Highway Signs, Luminaires and Traffic Signal Specifications classify this connection detail as a category E' detail, which means that the connection detail will have a fatigue life approximately equal to that of a fillet-welded socket connection. This connection detail was therefore selected to confirm that the extra cost and labor of the full-penetration weld connection detail did not provide a significant fatigue life improvement.

Carl Macchietto performed the design of this connection detail. The backing bar was left intact. The gaps between the backing bar and the base plate or tube were sealed with fillet-welds. The fabrication drawing for this connection detail is provided in Figure 3.14.

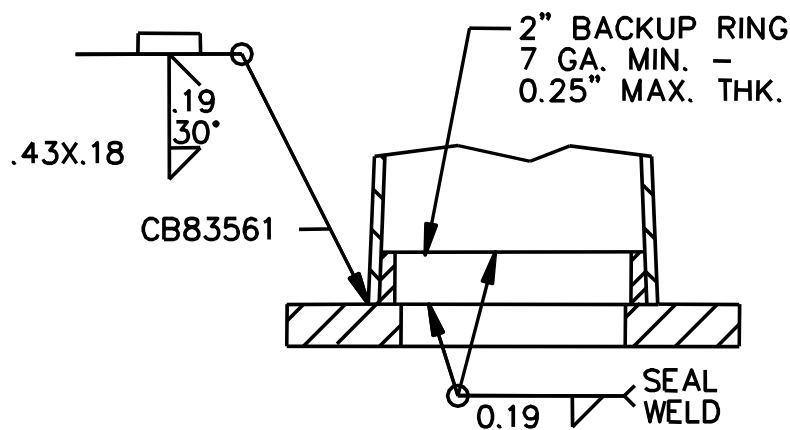


Figure 3.14 Full-Penetration-Weld Connection Detail

3.1.2.7 Quality Control Rejected

As mentioned at the beginning of this section, all test specimens for Phase 2 were fabricated at the Valmont Industries fabrication facility in Valley, Nebraska. During the fabrication of this set of test specimens, four of the unstiffened socket connection specimens were rejected. The internal quality control of Valmont Industries detected the inadequate welds, and the welds were repaired. Although the repaired weld quality was not considered satisfactory by the QC personnel, the specimens were inadvertently shipped to the laboratory for testing. A new set of four unstiffened socket connection specimens were fabricated and shipped at a later date. However, the re-fabricated specimens arrived after several of the original specimens had been tested. Due to the timing of the delivery of the re-fabricated specimens, these specimens were not inserted into the testing program. Instead, the weld profile investigation of this test program will investigate the influence of the inadequate welds on the fatigue life of the test specimens.

One of the re-fabricated specimens was later tested after being treated with UIT weld treatment. The final test specimen of the original specimen order for Phase 2 was left without another specimen to test against. The re-fabricated specimen was used so that the final test specimen could be tested, since the test setup required two specimens for testing. This specimen was not galvanized, and the UIT treatment was performed while the specimen was loaded to the minimum test load. After the UIT treatment, the specimens were unloaded. The specimens were then reloaded and tested to failure.

The properties of each specimen tested in Phase 2 are detailed in Table 3.7. The specimen labels are included in this table and will be explained at the end of this chapter.

Table 3.7 Phase 2 Test Specimen Matrix

Specimen Label	Galvanization	Specimen Details	Specimens Tested
VALNu	None	Socket - Unequal leg fillet weld	2
VALNu G	Galvanized	Socket - Unequal leg fillet weld	2
VALNu 2	None	Socket - Unequal leg fillet weld – 2" thick base plate	2
VALN 6x3/8@45	None	Stiffener – Length = 6", Thickness = 3/8" – Offset at 45° Angles	4
VALN Col	None	External Collar Connection	2
VALN IC	None	Internal Collar Connection	2
VALN W	None	Full-Penetration Welded Connection	2
VALN UR	None	U-Rib Stiffened Connection	2
VALNu PG	Galvanized after UIT Treatment	Fabrication Process - UIT Prior to Galvanization	2
VALNu GP	Galvanized	Fabrication Process - UIT After Galvanization	2
VALNu PR	Galvanized	Retrofit Process	2

3.2 SPECIMEN LABELS

The labeling system used to identify the test specimens of this test program is explained in Figure 3.15. The following paragraphs will provide two examples explanations of the labeling system.

Specimen **VALu CP** is the third specimen from the series of unstiffened socket connections with a wall thickness of 0.179" manufactured in Brenham, Texas. The specimen was treated with UIT treatment.

Specimen **TX 3x3/8 A** is the first specimen from the stiffened series with a 3" long by 3/8" thick stiffener. The pole wall thickness is 0.239" and it was manufactured in Brenham, Texas.

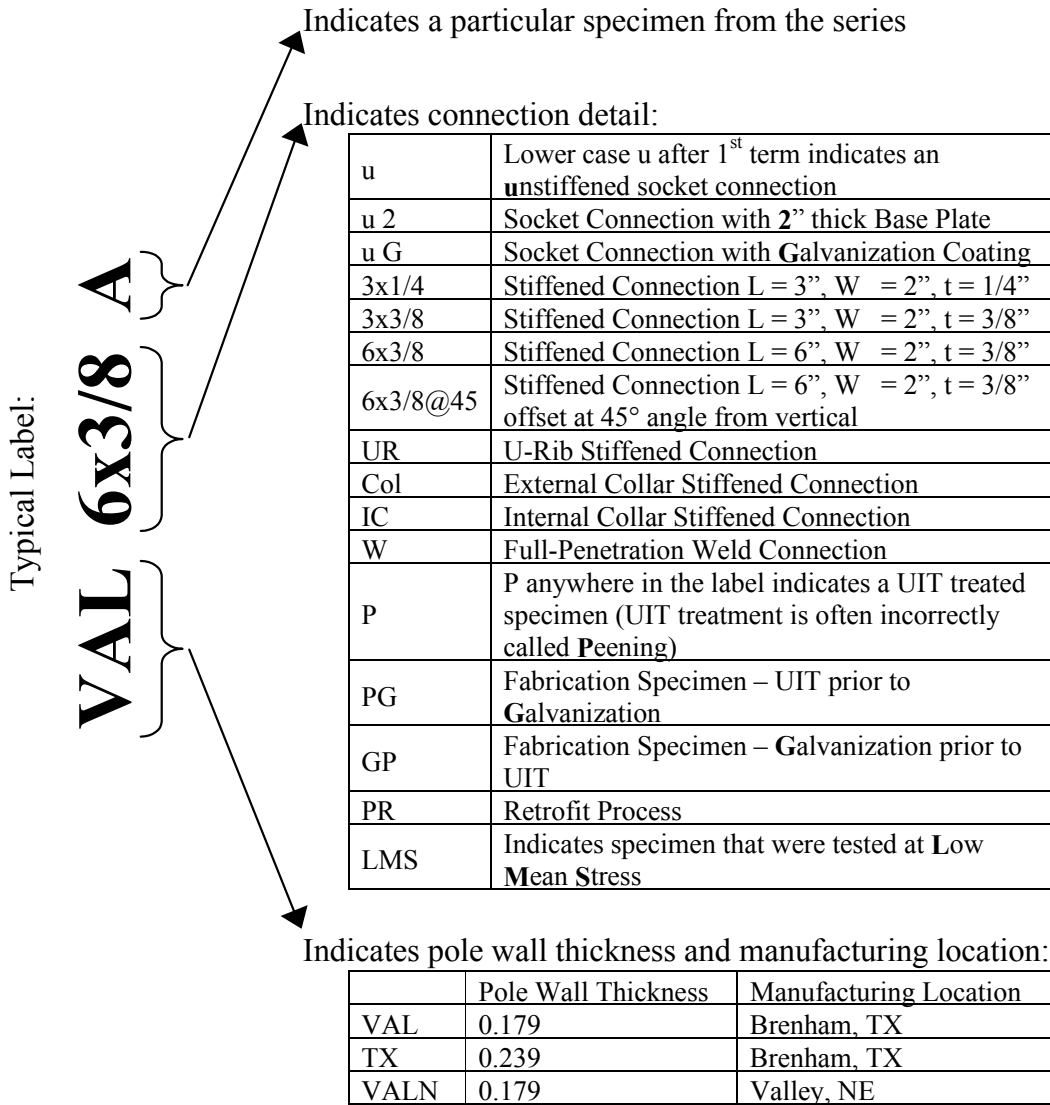


Figure 3.15 Specimen Label Explanation Chart

CHAPTER 4: TESTING PROCEDURE

4.1 GENERAL TEST PROCEDURE

All tests were performed following the test procedures described in this chapter. In a few cases, especially with the UIT treated specimen, the test procedure was modified slightly; all exceptions are noted.

The testing procedure can be divided into areas of specimen preparation, static testing and dynamic testing. Each of these areas will be addressed in separate sections.

4.2 SPECIMEN PREPARATION

4.2.1 *Cutting of Specimens*

As shown in Figure 3.1, the test specimens were fabricated to a length of approximately 8'. The specimens were cut to the appropriate length prior to testing. The excess tapered tube material was used to obtain samples for material properties testing.

To facilitate the cutting process, a jig was constructed to hold the specimen in the proper position and ensure the cut was performed at the proper length. The base of the cutting jig was a wide flange shape turned on its side. The web of the wide flange was deep enough so that the base plate of the test specimen fit between the flanges. Fixtures were constructed to hold the specimen in the proper position and to provide a stop that fixed the length of the cut. The cutting jig is shown in Figure 4.1.

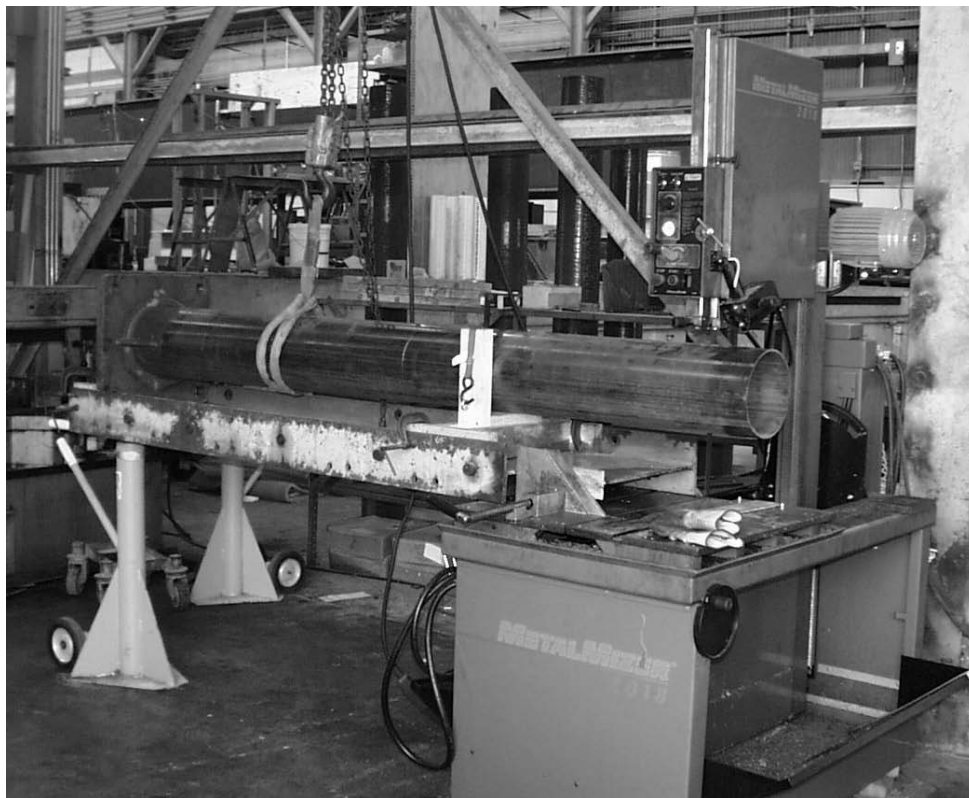


Figure 4.1 Cutting Jig

4.2.2 Attachment of Load Plates

Once each specimen was cut to the proper length, the load plate described in the specimen design section was welded onto the end of the specimen that had been cut. All load plate welding was performed by a certified welder at the Ferguson Structural Engineering Laboratory. The weld attaching the load plate to the test specimen was a single-pass $\frac{1}{4}$ " fillet weld.

To facilitate the welding process, a welding jig was constructed similar to the cutting jig. The base of the welding jig was a wide flange shape of the same size as used for the cutting jig. Again, this wide flange shape was turned on its side so that the base plate of the test specimen rested on the web of the structural shape. Fixtures were constructed to hold the test specimen in a proper position and to hold the load plate in a proper position relative to the cut end of the test specimen.

Once the alignment of the test specimen and load plate was properly adjusted, the connection was tack welded. After tack welding, the test specimen was positioned so that the load plate was resting on a welding table and the axis of the tapered tube was vertical. The fillet weld was then performed downhand.

4.2.3 Measurement and Strain Gauge Instrumentation

Prior to testing, measurements were taken on each specimen. In general, these measurements included: diameter at the base of the tapered tube, tube wall thickness, and measurements of the two legs of the unequal fillet weld. On the more complex connection details, the stiffeners or additional components were measured as thoroughly as possible and the orientation of the stiffeners was noted. The measurements for each test specimen are presented in tabular form in Appendix B.

Each test specimen was also instrumented with strain gauges prior to testing. The strain gauges were installed after the load plate was attached to the test specimen. The strain gauges used for this test program were encapsulated gauges with a 6mm gauge length. On all specimens, strain gauges were placed on the top and bottom of the specimen at a location approximately 3" from the toe of the socket weld or termination of the alternative connection detail. On most specimens strain gauges were also placed on the horizontal axis of the test specimen at the same distance from the toe of the socket weld or termination of the alternative connection detail. Additional strain gauges were applied to a few of the test specimens in order to determine the strain ranges at points of interest.

4.3 MEAN STRESS CALCULATIONS

Prior to the start of Phase 1 of the test program, calculations were performed to determine the approximate mean stress at a typical socket connection due to dead load from the mast-arm and any attached traffic signals.

The assumed dead weights of the traffic signals used for this calculation are shown in Table 4.1. Both metal and the lighter composite traffic signals were considered. To perform the calculations, it was assumed that there was one five-section traffic signal at the end of the mast-arm. Then an additional three-section traffic signal was placed on the mast-arm at each 12' interval, except that no traffic signals were placed within 20' of the column. The calculations were performed for both pole wall thicknesses selected for Phase 1 of this test program. The length of the mast-arm in the calculations was varied from 20' to 60', a range that encompasses the typical limits of a mast-arm with a 10" base diameter.

The results of the calculations are shown in Figure 4.2. The points on the plots where the calculated stress rises sharply correspond with the addition of another traffic signal to the mast-arm. With the knowledge that the TXDOT standard plans utilize a 10" diameter mast-arm for lengths of up to 40', as discussed Chapter 3, the typical mean stress due to dead load can be determined from this figure. The mean stress values for a 40' long mast-arm vary between 14 ksi and 17 ksi based on the traffic signal material and mast-arm wall thickness.

Under typical service conditions, the vibrations due to wind loading will cause the stress at the critical location to oscillate about the imposed dead load value shown in Figure 4.2. In this situation, the stress due to the dead load represents the mean stress value of the cyclic loading.

Table 4.1 Dead Weight of Traffic Signals Used for Mean Stress Calculation

	Dead Weight Metal Signal (lb.)	Dead Weight Composite Signal (lb.)
3-Section Traffic Signals	75	50
5-Section Traffic Signals	125	80

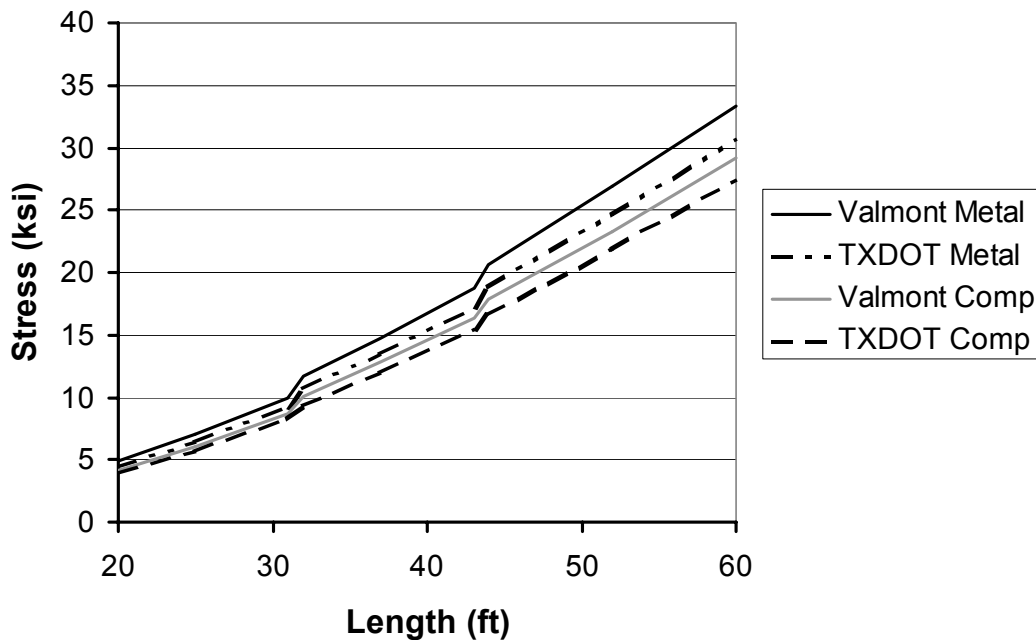


Figure 4.2 Plot of Mean Stress vs. Mast-Arm Length due to Dead Load

In order to simulate the effect of the dead load stress, the target minimum stress for all standard tests was set to be 16 ksi for the thick pole wall specimens and 16.5 ksi for the thin pole wall specimens. The slightly higher value for the thin pole wall specimens was selected as the thin pole wall mast-arms have a slightly higher calculated mean stress value. The minimum stresses selected resulted in mean stresses of 22 ksi and 22.5 ksi, respectively, which are slightly higher than the values shown in Figure 4.2, so that they are worst-case, conservative values. Unless noted as a low mean stress test, all tests were initiated at the minimum stress levels of 16 ksi or 16.5 ksi.

4.4 GENERAL TESTING NOTES

Due to the significant variety of connection details tested in this test program coupled with the two pole wall thicknesses, the relative stiffnesses of each set of test specimens was largely unknown. For example, the stiffened connection details and the collar connection details were expected to have greater stiffness in the connection region than the typical socket connection; however, the difference in stiffness was not quantifiable through calculations alone.

In the case in which two non-identical specimen would be tested in the test setup, the potentially different stiffnesses could lead to a fixity condition in the area of the load box that is different than the assumed fully fixed condition. In this situation, the load box could potentially undergo a small rotation based on the different stiffnesses of the specimen attached to each side of the load box. The simple beam analogy presented in the discussion of the test setup would no longer be valid and the more flexible specimen would experience a larger strain at the critical section.

To minimize the effects of the stiffness issue, the two specimens being tested in the test setup were almost always replicates. In a few cases, replicate test specimens were not available, in which case a specimen of approximately the same stiffness was substituted. In these situations, the strain gauge data from the static test of the unmatched specimens was compared to the results of static test for the original symmetric set of specimens. The loading of the test setup was adjusted until the static test results from the two static tests matched to ensure that the stiffness difference between the two specimens did not significantly alter the expected values.

4.5 STATIC TEST

A static load test was performed prior to the start of the cyclic fatigue testing of each pair of test specimen. The purpose of the static test was to determine the dynamic test displacements and to allow for more accurate readings of the strain gauges at various load increments.

After the test specimens were installed in the test setup but prior to the static test, the test setup was cycled between the maximum and minimum load to seat the specimens in the test fixtures.

Two static tests were then performed on each set of test specimen. The first test was a simple up and down load pattern from a load of 1 kip to the maximum load for the test specimen and back to 1 kip. The second test involved three load cycles between the minimum and maximum loads. In each test, the strain at each strain gauge was recorded at each 1 kip load increment, as well as at the calculated minimum and maximum test loads.

A typical set of static test results are shown in Figure 4.3 and Figure 4.4. These figures plot the measured strain readings vs. load for each typical static test pattern. Figure 4.3 shows the results of a single load and unload static test and Figure 4.4 shows the results of a static test in which the load was cycled between the minimum and maximum load three times. The two plots indicated that there was little difference between the results of the two static test methods. Based on this agreement, only the static test results from the cyclic load pattern will be discussed in the results section of this paper.

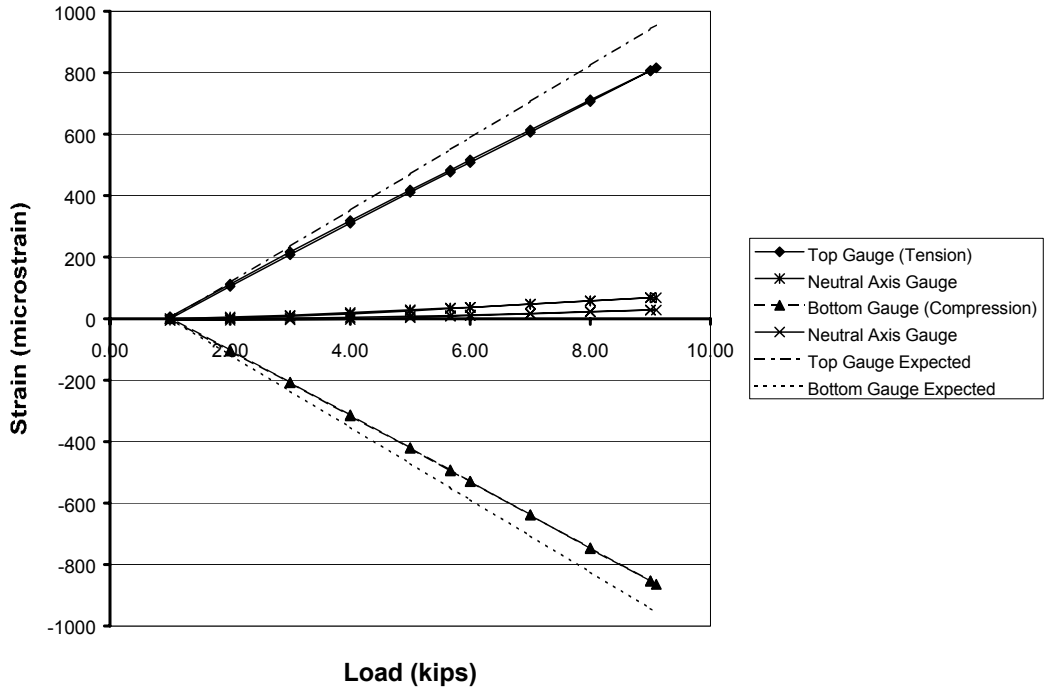


Figure 4.3 Static Test Result – Up-and-Down Test – Typical Results

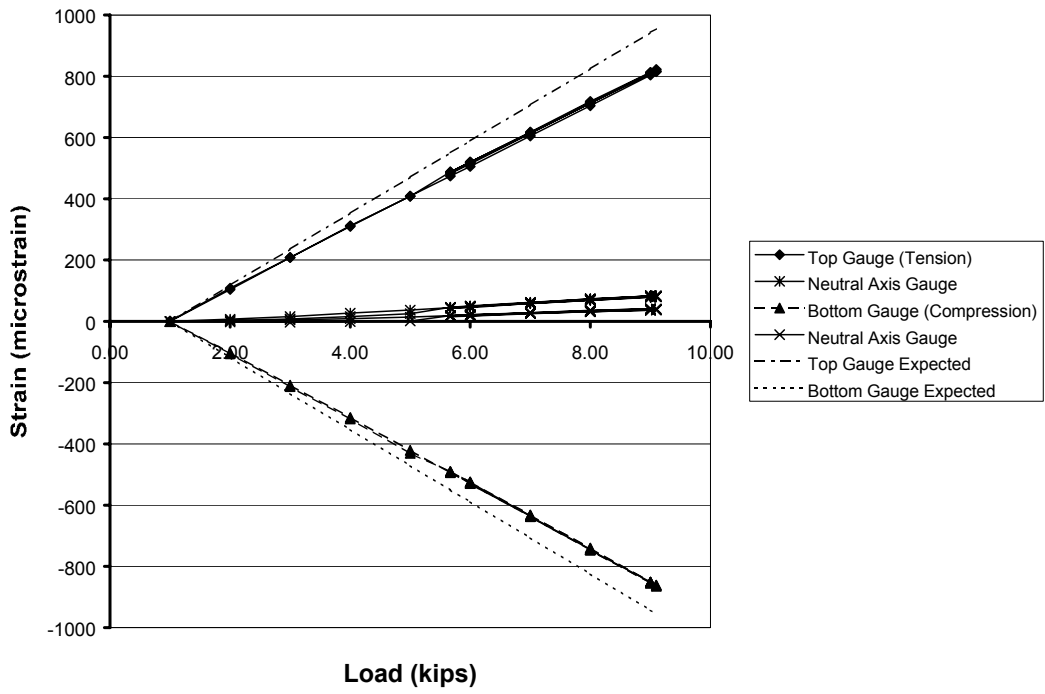


Figure 4.4 Static Test Result – Cyclic Test – Typical Results

From Figure 4.3 and Figure 4.4 it is apparent that the strain vs. load relation is linear at a distance of approximately 3" from the critical section. The figures also show that the measured strain values are slightly lower than the values calculated using the linear strain relation $\epsilon = E \cdot \frac{M \cdot c}{I}$, where E = 29,000 ksi.

4.6 DYNAMIC TEST

The dynamic testing was performed under displacement control at cyclic load frequencies between 3 Hz and 5 Hz. The test frequency for a specific test was selected to allow for rapid testing without a loss in accuracy of the amplitude of the cyclic loading. The displacement limits for the test were determined as described in the following section.

4.6.1 Determination of Loads for Limits of Dynamic Testing

During the initial static test for the first set of test specimen, it was observed that behavior of the test specimen did not conform to all expected behaviors. Namely, the calculated load vs. displacement relation did not match the measured values. The strain measurements from the strain gauge located on the top of the test specimen (in the tension region) and the measurements from the strain gauge on the bottom of the test specimen (the compression region) also did not correlate to the expected values.

A plot of the load vs. displacement for the initial test is shown in Figure 4.5. While the figure shows that the measured load vs. displacement relation is linear, the slope of the relation, or the stiffness of the system, was less than the calculated value. The discrepancy meant that the calculated displacements could not be used to determine the limits of the dynamic testing.

In order to account for the actual system stiffness, the limits of the dynamic testing were determined through the static test. For each set of specimens, the loads that would create the desired stress range were calculated. For example, to impose a 12 ksi stress range, the minimum and maximum loads were 5.7 and 9.1 kips for the unstiffened VALu and VALNu series of specimens, and 7.7 and 12.3 kips for the TXu series of specimens. For the stiffened connection details, the loads listed above resulted in a stress range at the termination of the stiffener slightly smaller than the 12 ksi stress range. This small difference was not significant, so the minimum and maximum test loads were kept constant for these specimens. Slight adjustments were made in the case of the alternative connection details of Phase 2 to provide more appropriate stress ranges.

The loads associated with the desired stress range were then used as the basis for the static test. From the static test results, the displacements related to the desired minimum and maximum loads were determined and the dynamic testing was performed based on these displacements. The 'as tested' stress range was

then calculated based on either $\sigma = \frac{Mc}{I}$ using the section properties specific to each specimen, or based on the strain gauge data from the static test. The difference between these two methods will be discussed in Chapter 6.

Although this process of determining the dynamic test loads resulted in each specimen having a slightly different stress range, the process simplified the dynamic testing as it eliminated the need to fine-tune each test to provide the desired stress range. Typically, the variation between the desired stress ranges and the 'as tested' stress ranges was insignificant.

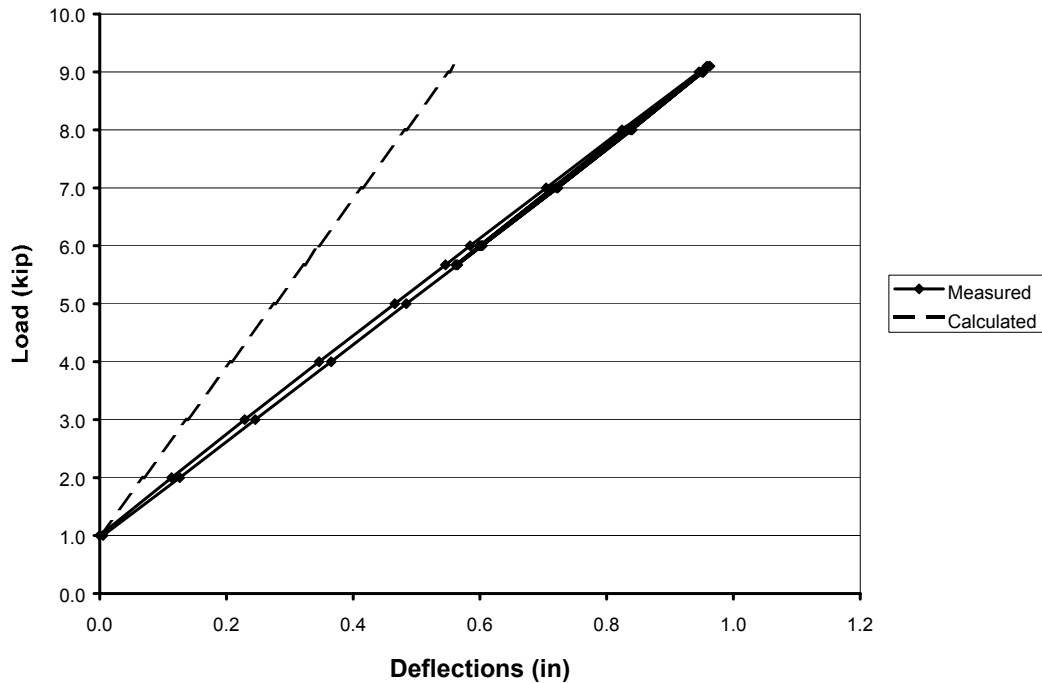


Figure 4.5 Plot of Load vs. Deflection for First Test

4.6.2 Dynamic Test Procedure

The dynamic testing was performed under displacement control, as indicated in Section 4.6. As the testing frequency of each dynamic test was increased to the desired 3 Hz to 5 Hz range, the applied load required to maintain the displacement amplitudes of the static test declined. The decline of the loads indicated that the mass of the load box and the masses of the test specimen base plates, which were concentrated in the center of the test setup, were participating in dynamically loading the system. The observation that the loads associated with the dynamic test did not correspond with the loads from the static test for the same displacements confirmed the decision to operate the dynamic testing under displacement control.

Once started, each dynamic test was allowed to run until one or both specimens reached failure. The specimens were monitored 24 hours a day using a web camera installed in the laboratory. At this point, a static test was performed to check for a failure, and the specimens were visually inspected to identify cracking.

Except in a few rare cases, only one of the two specimens would fail initially. In order to create a failure in the second specimen, the first specimen was either repaired or rotated and the test was resumed until both specimens had failed. To repair the specimen, a groove was ground to a depth of approximately half the wall thickness that followed the crack and extended beyond the visible crack tips. The crack was then re-welded. This option was fairly time consuming, so more often the failed specimen was rotated 180°. As a result of this rotation, the crack was positioned in the zone of local compression and did not influence the stiffness of the specimen.

In a limited number of instances, the first specimen to fail couldn't be repaired or rotated in order to fail the second specimen. In these cases, a specimen of similar stiffness was substituted. A static test was then performed and the results were used to ensure the unfailed specimen was being loaded to the same stress range as the initial test.

After any specimen repair, rotation or change, a static test was performed to ensure the imposed stress ranges had not changed.

During the dynamic testing of a limited number of specimens, a data acquisition system was used to monitor the strain gauge readings. The CR9000 data acquisition system was used for this task. The resulting strain ranges from the CR9000 corresponded with the results from the static testing. Based on this correspondence, the CR9000 was only used to monitor a small number of tests.

4.6.3 Failure Definition

Failure of a specimen in this test program was determined by three factors. The first was a 5% overall reduction in the loads required to meet the minimum and maximum displacements. The 5% load reduction was set as an interlock limit for the cyclic loading controller. The 5% reduction was also checked during the static test performed after each failure.

The second failure limit was defined as a 10%, or greater, reduction in the strain range measured from the strain gauge associated with the location of cracking.

The two numerical limits above were arbitrarily set to ensure that the extent of fatigue cracking present in each specimen at failure was relatively consistent. The extent of visible cracking was the third definition of failure. A failure crack was defined as a crack that had propagated a significant distance around a socket weld connection, or had branched out into the pole on a stiffened connection. Once a crack had reached this point, most of the fatigue life had been expended, and a complete failure would occur in a relatively small number of additional cycles.

CHAPTER 5: RESULTS OF TENSILE TESTS, CHEMISTRY ANALYSES AND DYNAMIC STRAIN MONITORING

5.1 TENSILE TEST RESULTS

5.1.1 Process

A series of tensile tests were completed to confirm the yield strength of the steel from the mast-arm test specimens. Tensile test coupons were manufactured from the drop sections cut off of the ends of the test specimens. A total of four coupons were machined, two from each of the two pole wall thicknesses tested during Phase 1.

The tensile coupons were manufactured in accordance with ASTM A 370. The test region of the tension specimens was machined down to a width of 0.495". This width resulted in cross-sectional areas of 0.112 in² and 0.084 in² in the coupons from the TX and VAL series of specimens, respectively.

The tension coupons were tested in a closed loop MTS machine under displacement control. The strain in the specimen was measured with an extensometer with a 2" gauge length. During the testing, the displacement was stopped at three points to determine the static yield strength. The static loads were not valid yield strength loads since these specimens did not exhibit a yield plateau due to the cold working of the steel during the fabrication process as discussed in Section 1.1. Instead, the yield strength of the coupons was determined based on the 0.2% offset. Two plots showing the typical stress vs. strain behavior are shown in Figure 5.1 and Figure 5.2. The plot in Figure 5.1 shows the total recorded behavior, while Figure 5.2 shows only the initial portion of the behavior in the area of the 0.2% offset calculations.

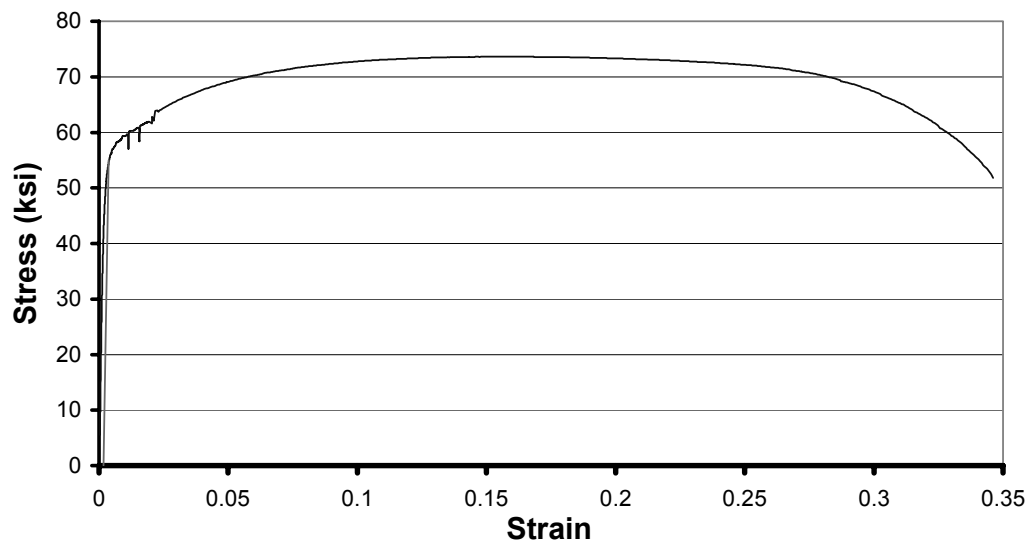


**Figure 5.1 Tensile Test Results for 3g (0.239" thickness)
Steel Coupon – Entire Measured Behavior**

The results of the four tensile tests are shown in Table 5.1. Aside from the strengths and elongation measured in the tensile test, this table also shows the mill test reported strengths, as well as the minimum specified strengths and elongation. Comparing the measured values to the minimum specified values, the

steel fulfills all of the minimum requirements, with specimen TX 3x3/8 A having the lowest yield strength of the samples tested. The measured yield strength for this specimen was 55.1 ksi, which meets the minimum specified value of 55 ksi.

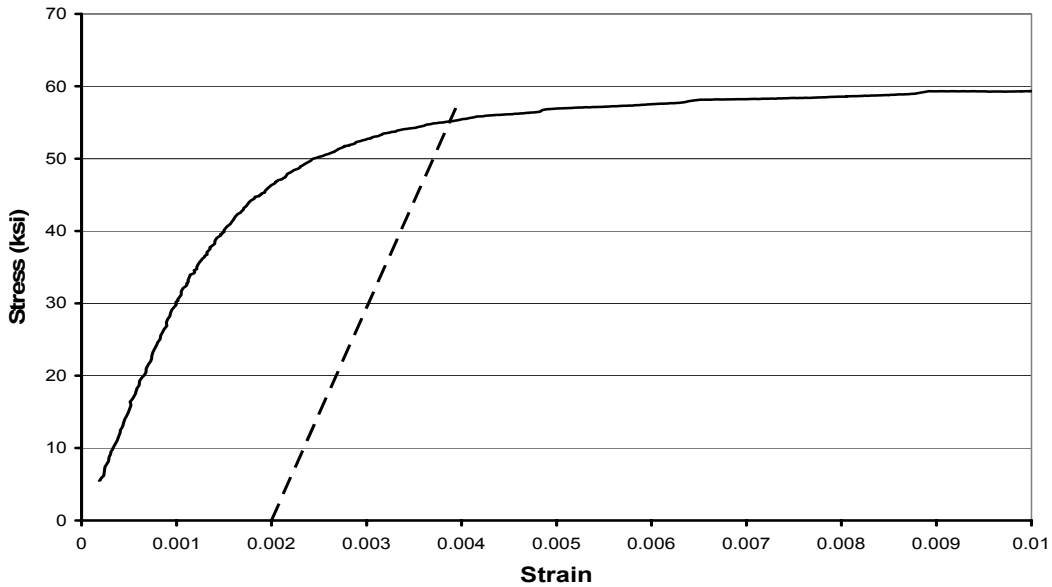


**Figure 5.2 Tensile Test Results for 3g (0.239" thickness)
Steel Coupon – Closeup of Initial Portion of Graph**

Table 5.1 Results of Tensile Tests

Specimen	Laboratory Measured Values			Mill Report Values	
	Yield Strength (ksi)	Ultimate Strength (ksi)	Elongation at Ultimate (in)	Yield Strength (ksi)	Ultimate Strength (ksi)
VAL 3x1/4 A	65.5	79.66	26.2	60.2	75.3
VAL 3x3/8 C	56.9	73.51	30.8	60.2	75.3
TX 3x3/8 A	55.1	75.59	34.6	60.1	72.8
TX 6x3/8 B	57.1	73.64	32.1	60.1	72.8
Specified Minimum Values ASTM A595	55	65	23.0		

The tensile test data is presented again in Table 5.2 along with the stress ranges and maximum stresses of the fatigue tests. The final column of the table shows the ratio of the maximum stress achieved during the fatigue testing versus the yield strength as determined by the 0.2% offset. The highest ratio is just over 0.52, which means that during the fatigue testing the stresses in the test specimen were, at most, just over 50% of the yield strength of the material.

Table 5.2 Tensile Test Results Compared to Fatigue Testing Limits

Specimen	Stress Range (ksi)	Max. Stress (ksi)	Laboratory Yield Strength (ksi)	Max. Stress/ Yield Strength
VAL 3x1/4 A	12	28	65.5	0.43
VAL 3x3/8 C	12	28	56.9	0.49
TX 3x3/8 A	12	28.5	55.1	0.52
TX 6x3/8 B	12	28.5	57.1	0.50

5.2 CHEMISTRY ANALYSIS

As a part of this test program, a set of three chemical analyses was performed by Chicago Spectro Service Laboratory, Inc. in Chicago, IL. The test for carbon was performed in accordance with ASTM E 1019, and the tests for the other requested elements were performed in accordance with ASTM E 1085.

Three test specimens were selected for the chemistry analyses. The specimens were selected at random; however, one sample was taken from each of the three major series of specimens to ensure that a chemistry analysis was performed on each batch of steel used in the fabrication of the test specimens. The three batches of steel consisted of: the 7g (0.179" thick) steel of the VAL series of specimens manufactured in Brenham, TX; the 7g (0.179" thick) steel of the VALN series manufactured in Valley, NE; and the 3g (0.239" thick) steel of the TX series. The three material samples were taken from the drop sections that were cut off of the end of the test specimens during the process of preparing each specimen for the fatigue testing.

Table 5.3 Results of Chemistry Analysis

Elements	Specified Limits		Specimen Tested		
	Minimum	Maximum	TX 6x3/8 B	VAL 3x3/8 C	VALN IC B
C	0.12	0.29	0.22	0.20	0.22
Mn	0.26	0.94	0.73	0.80	0.74
P		0.045	< 0.005	< 0.005	0.008
S		0.045	0.008	0.012	0.010
Si	*	0.04	0.02	0.02	0.02
Ni			< 0.01	< 0.01	< 0.01
Cr			0.04	0.04	0.05
Mo			< 0.01	< 0.01	< 0.01
Cu			0.01	0.01	0.01
V			< 0.005	< 0.005	< 0.005
Nb			< 0.005	< 0.005	< 0.005
Al	*		0.036	0.046	0.048
B			< 0.0005	< 0.0005	< 0.0005
N			0.007	0.010	0.009

* Silicon or silicon combined with aluminum must be sufficient to ensure uniform mechanical properties.

The results of the analyses are presented in Table 5.3. The specified steel for the test specimens was ASTM A595 Grade A steel. The minimum and maximum allowable limits for the specified elements are included in the second and third columns of Table 5.3. The results show that the steel met all of the requirements of ASTM A595 Grade A.

5.3 DYNAMIC CORROBORATION OF STATIC TEST STRAINS

In the course of the dynamic fatigue testing, the strain ranges from the dynamic testing were corroborated with the strain ranges from the static test through the use of the CR 9000 data acquisition system. The CR 9000 was capable of recording the readings from the eight strain gauges of each test at sampling frequencies up to 50Hz. This reading rate was more than 10 times the cyclic loading frequency for all tests that were monitored, and therefore the dynamic monitoring should accurately represent the behavior under the dynamic loading.

Due to the difference between the sampling frequency and the loading frequency, the strain measurements did not always record the peak values of each cycle. To account for this difference, the maximum and minimum strain readings over each period of 10 cycles were used to calculate a strain range. These strain ranges were then plotted as shown by a typical plot shown in Figure 5.3. This figure shows that the strain ranges imposed during the testing were very consistent. A small amount of the variation evident may be attributed to experimental noise.

The plot in Figure 5.4 shows the calculated strain ranges for the dynamic monitoring of another test specimen. This graph exhibits slightly more noise. The significant observation from this plot is the attenuation of the measured strain ranges as the testing progressed. The attenuation indicates that the specimen began cracking, and the strain at the strain gauge location slowly declined as the crack propagated.

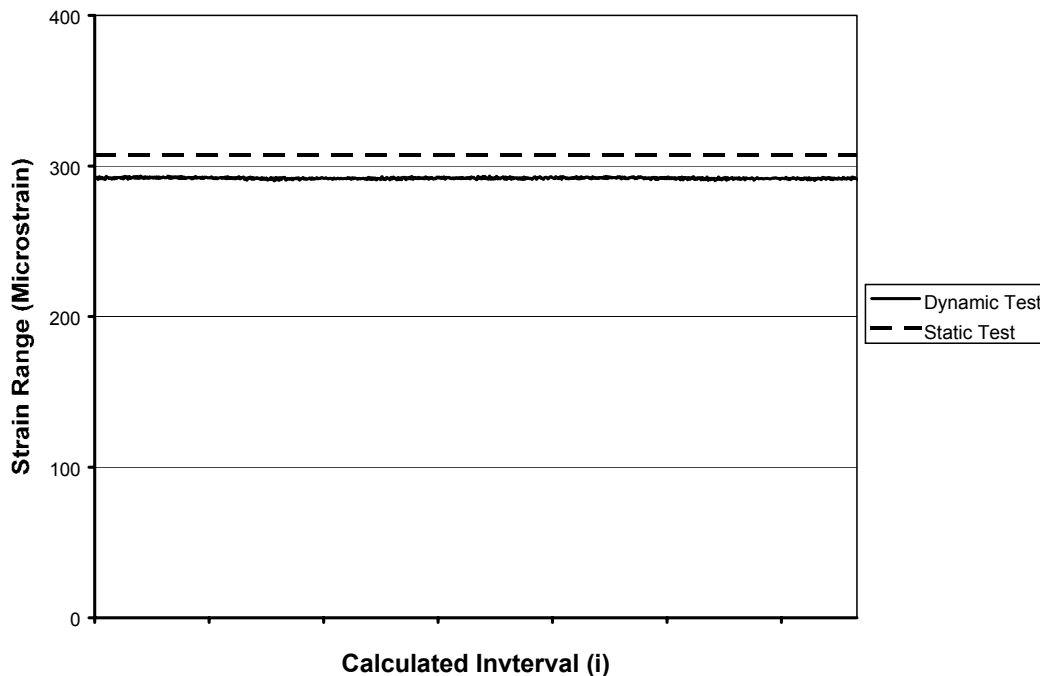


Figure 5.3 Dynamic Strain Monitoring of Top Gauge on Specimen VALN IC A

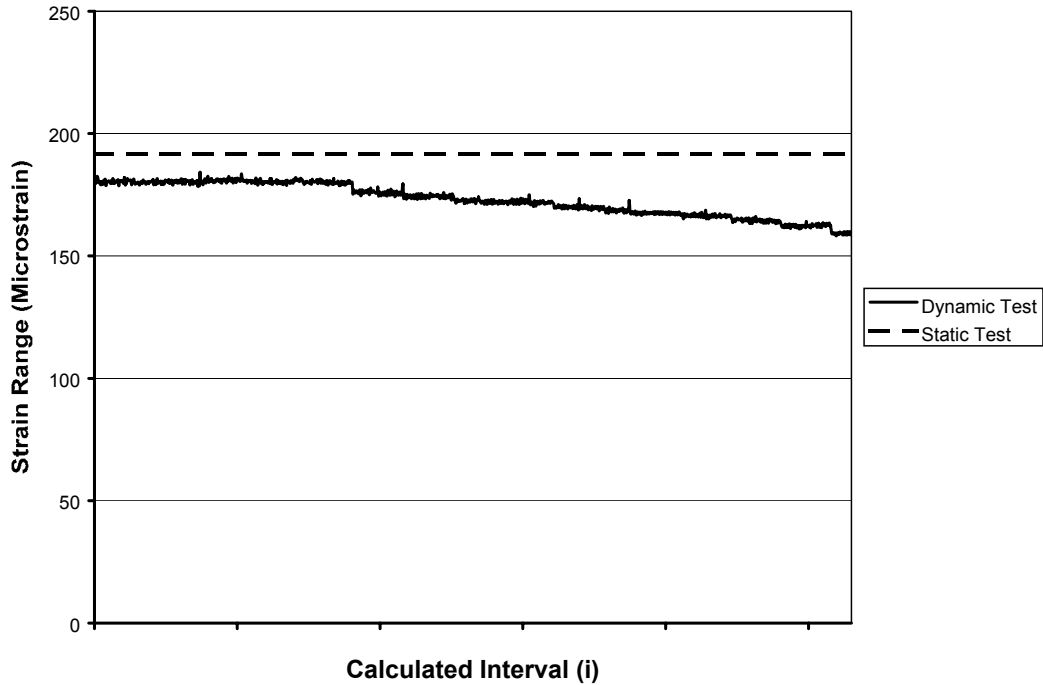


Figure 5.4 Dynamic Strain Monitoring of Top Gauge on Specimen VAL 3x1/4C

The calculated strain ranges from the dynamic monitoring were then averaged over a period approximately equal to one tenth of the entire length of the dynamic monitoring to provide quantitative values to compare with the results from the static test. This calculation smoothed the measured strain ranges. The average values recorded throughout each of the dynamically monitored tests are presented in Table 5.4 and Table 5.5. These tables also include the strain ranges from the static test for each of the specimens monitored, as well as the results of a percent error calculation.

The data in Table 5.4 and Table 5.1 indicates that the strains measured during the dynamic loading were in good agreement with the strains measured during the static testing. The error between the dynamic and static test results was less than 6% for all cases. The correlation between the static strain ranges and those measured dynamically confirmed the ability of the load system to dynamically impose the same desired stress ranges as measured in the static test.

Table 5.4 Results of CR9000 Dynamic Strain Monitoring – Part 1

Specimen	VALNICA	VALNICB		VALNu2A	
Gauge Location	Top	Top	Bottom	Top	Bottom
Average Measurements	292	247	238	362	352
	292	247	238	362	352
	292	245	238	362	351
	292	244	238	362	351
	292	243	238	362	352
	292	247	238	362	352
	292	246	238	362	351
	292	245	238	362	351
	292	244	238	362	351
Average	292	245	238	362	351
Static Test	307	246	253	373	361
% Error	4.9%	0.4%	5.9%	5.3%	4.6%

Table 5.5 Results of CR9000 Dynamic Strain Monitoring – Part 2

Specimen	TXuA	VALNu2A		VALNu2B	
Gauge Location	Top	Top	Bottom	Top	Bottom
Average Measurements	171	362	352	365	348
	171	362	352	364	348
	164	362	351	361	346
		362	351	361	346
		362	352	363	347
		362	352	363	347
		362	351	364	347
		362	351	363	347
		362	351	363	347
		362	351	363	347
Average	169	362	351	363	347
Static Test	169	373	361	365	362
% Error	0.1%	2.9%	2.7%	0.5%	4.1%

CHAPTER 6: STATIC TEST RESULTS

6.1 STATIC TESTING

The specimens tested during this test program are listed in Table 6.1 and Table 6.2. These tables also list the minimum stress, and the stress range. These stresses are the nominal stresses and stress ranges based on the nominal cross-sectional properties of the critical section of the specimens as designed. These values represent the desired limits of the static and dynamic testing. Due to slight variations in the actual dimensions of each specimen as compared to the specimen designs, the stress ranges achieved during both the static and dynamic tests will vary slightly from those in Table 6.1 and Table 6.2.

Table 6.1 Phase 1 Results

Specimen Name	Nominal Stress Values		
	Minimum (ksi)	Mean (ksi)	Range (ksi)
VALu A	16	22	12
VALu B	16	22	12
VALu C	16	19	6
VALu D	16	19	6
VALu EP	16	22	12
VALu FP	16	22	12
TXu A	16.5	19.5	6
TXu B	16.5	19.5	6
TXu C	16.5	22.5	12
TXu D	16.5	22.5	12
TXu EP	16.5	22.5	12
TXu FP	16.5	22.5	12
VAL 3x1/4 A	16	22	12
VAL 3x1/4 B	16	22	12
VAL 3x1/4 C	16	19	6
TX 3x1/4 A	16.5	22.5	12
TX 3x1/4 B	16.5	22.5	12
TX 3x1/4 C LMS	2.5	8.5	12
VAL 3x3/8 A	16	22	12
VAL 3x3/8 B	16	22	12
VAL 3x3/8 CP	16	22	12
VAL 3x3/8 CP(2)	16	22	12
TX 3x3/8 A	16.5	22.5	12
TX 3x3/8 B	16.5	22.5	12
TX 3x3/8 CP LMS	2.5	8.5	12
VAL 6x3/8 A	16	22	12
VAL 6x3/8 B	16	22	12
VAL 6x3/8 C	16	19	6
TX 6x3/8 A	16.5	22.5	12
TX 6x3/8 B	16.5	22.5	12
TX 6x3/8 C	16.5	19.5	6

Table 6.2 Phase 2 Results

Specimen Name	Nominal Stress Values		
	Minimum (ksi)	Mean (ksi)	Range (ksi)
VALNu A	16	22	12
VALNu B	16	22	12
VALNu G A	16	22	12
VALNu G B	16	22	12
VALNu 2 A	16	22	12
VALNu 2 B	16	22	12
VALN 6x3/8@45 A	16	22	12
VALN 6x3/8@45 B	16	22	12
VALN 6x3/8@45 C	16	18.15	4.3
VALN 6x3/8@45 D	16	18.15	4.3
VALN Col A	16	22	12
VALN Col B	16	22	12
VALN IC A	16	19.75	7.5
VALN IC B	16	19.75	7.5
VALN W A	16	20.75	9.5
VALN W B	16	20.75	9.5
VALN UR A (#4)	16	22	12
VALN UR B (#1)	16	22	12
VALN UR B (#2)	16	22	12
VALNu PR A	16	22	12
VALNu PR B	16	22	12
VALNu GP A	16	22	12
VALNu GP B	8	18	20
VALNu PG A	16	22	12
VALNu PG B	16	22	12
VALNu CP	8	18	20
VALNu PR ul A	16	22	12
VALNu PR ul B	16	22	12

Static tests were performed on each test specimen prior to the fatigue testing. The results of the static testing will be presented in the remainder of this chapter. Each test variable will be discussed beginning with the socket connection details, then continuing to the stiffened connection details, the UIT treated specimens and finally proceeding to the alternative connection details.

6.2 UNEQUAL LEG FILLET-WELDED SOCKET CONNECTION SPECIMENS

Since the socket connection detail is the most commonly used connection detail in traffic signal support structures, this detail and specifically the thin pole wall socketed connection specimens were the control specimens for this test program. As the control specimens, the discussion of the results must begin with an understanding of the behavior of these test specimens. The behaviors of the three series of unstiffened socket connection specimens during the static test were similar, so the results will be discussed as one group.

The results of the static tests for the very first set of test specimens were already discussed to a limited extent in Chapter 4. The static test results for the remainder of the socket connection specimens exhibited similar behavior. Since the static test results presented in Chapter 4 represent the typical results, these

same plots will be discussed in greater detail. A graph of the static test results for specimen VALu A is reprinted in Figure 6.1.

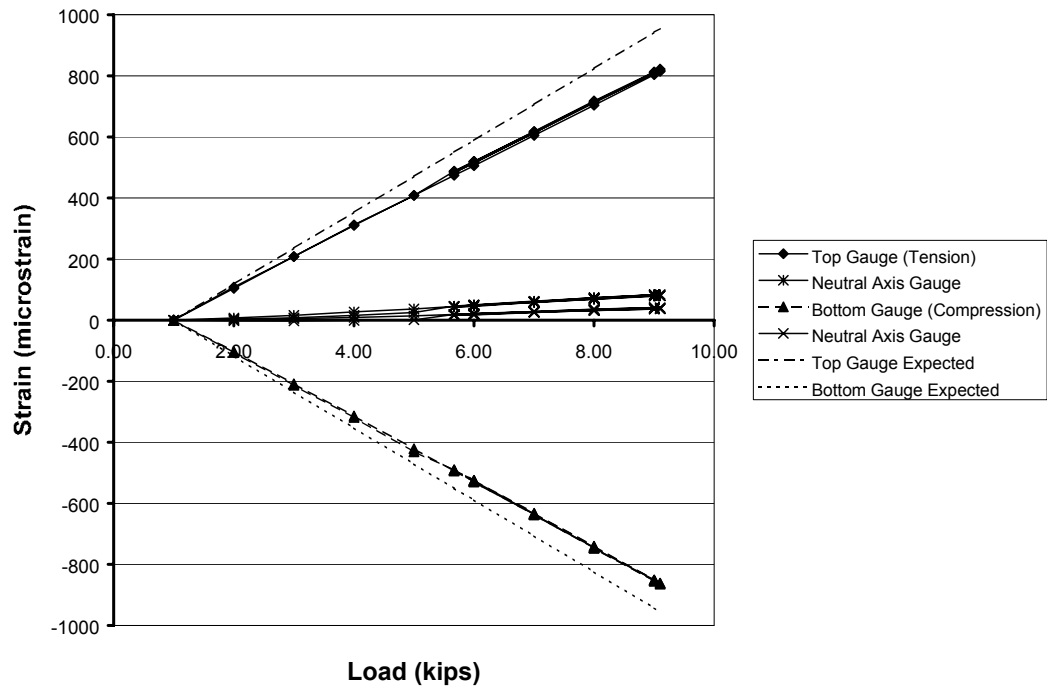


Figure 6.1 Static Test Results for VALu A

The most notable aspects of this plot are that the measured values are less than the predicted values and that the measured values exhibit a linear relation. The linearity of the strain vs. load relation is important in that it indicates that the behavior of the test specimen is linear; no material or geometric non-linearities are evident. This linear strain vs. load behavior was true for all static test results unless otherwise noted in the remaining sections of the discussion.

Preliminary results from a finite element analysis and the static strain gauge data indicate that the assumption that strain varies linearly with height from the neutral axis does not accurately predict the stresses present in the region of the socket weld. Instead, there is a peak stress, as would be expected, at the toe of the socket weld, and a valley in the local stresses just beyond the peak. The strain gauges installed 3" from the toe of the socket weld were placed beyond the valley.

The static test results for specimen VALu A are shown again in Figure 6.2; however, this figure shows the strain ranges measured at each strain gauge versus the distance from the horizontal axis of the cross section. This figure illustrates that the magnitude of the strain ranges measured at the top and bottom strain gauges are lower than those that are calculated from the linear strain equation. In the static test results presented for specimen VALu A, the values are slightly more than 15% less than the expected values. This percent error is slightly higher than the values for the other socket connection specimens, which were typically in the range of 10-15%. The lower than expected strain measurements, when extrapolated to the toe of the socket weld, provide a lower value for the stress, which does not account for the stress concentration present at the toe of the socket weld. The extrapolated stress values will result in a low value for the fatigue categorization of these details.

The static test results shown in Figure 6.2 also indicate that the magnitude of the tension strain ranges is lower than the magnitude of the compressive strain ranges. The magnitude of the tension strain range was

typically 10% less than the value of the compression strain range. This observation is evident in every socket connection test specimen. The assumption that plane sections remain plane would provide that the magnitudes of these two strain ranges would be equal. Along with this unusual behavior, the strain gauges placed along the horizontal axis of the test specimens always indicated non-zero strain ranges. This indicates that the neutral axis was not at the horizontal axis. These two observations combine to indicate that the cross section in this area was distorting.

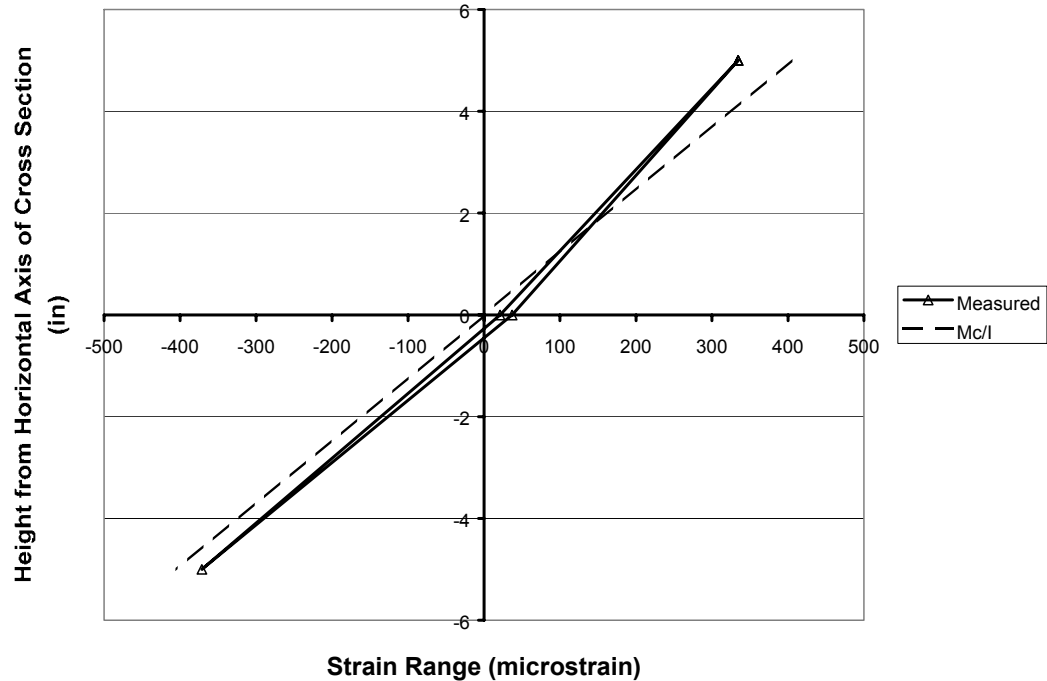


Figure 6.2 Strain Range vs. Height from Horizontal Axis Plot of Static Test Results for VALu A

The static test results for the thicker pole wall series, TXu, exhibited the same behavior as the thin pole wall specimens. In an attempt to understand the behavior of a socket connection test specimens, specimen TXu A was instrumented with a series of 8 strain gauges separated by 45° angles at the standard location 3" from the toe of the socket weld.

The results of the static testing of these strain gauges are shown in Figure 6.3 and Figure 6.4. Figure 6.3 shows that the behavior for all strain gauges was linear with respect to load.

In Figure 6.4, the measured strain ranges are plotted versus height from the horizontal axis. This figure indicates that the expected values as calculated by the linear stress assumption do not match the measured behavior. Instead, the measured behavior indicates a reduction in the local stresses at the top and bottom of the cross section, which is in agreement with the previous strain gauge measurements. Similar to the results of the VALu series of specimens, the difference between the expected and measured strain ranges measured at the top and bottom strain gauges was approximately 10% to 15%.

Another observation from Figure 6.4 is that the strain ranges measured at the 45° strain gauges show much better agreement with the values expected based on the linear strain assumption. The improved agreement in the 45° strain gauges results in a non-linear relation between the strain versus distance from the neutral axis, which further indicates that the plane sections do not remain plane. Although the plot in Figure 6.4 shows that plane sections do not remain plane, the strain gauges positioned at 45° angles from

vertical showed symmetric behavior, which indicates that the distortion of the cross section was symmetric about the vertical axis.

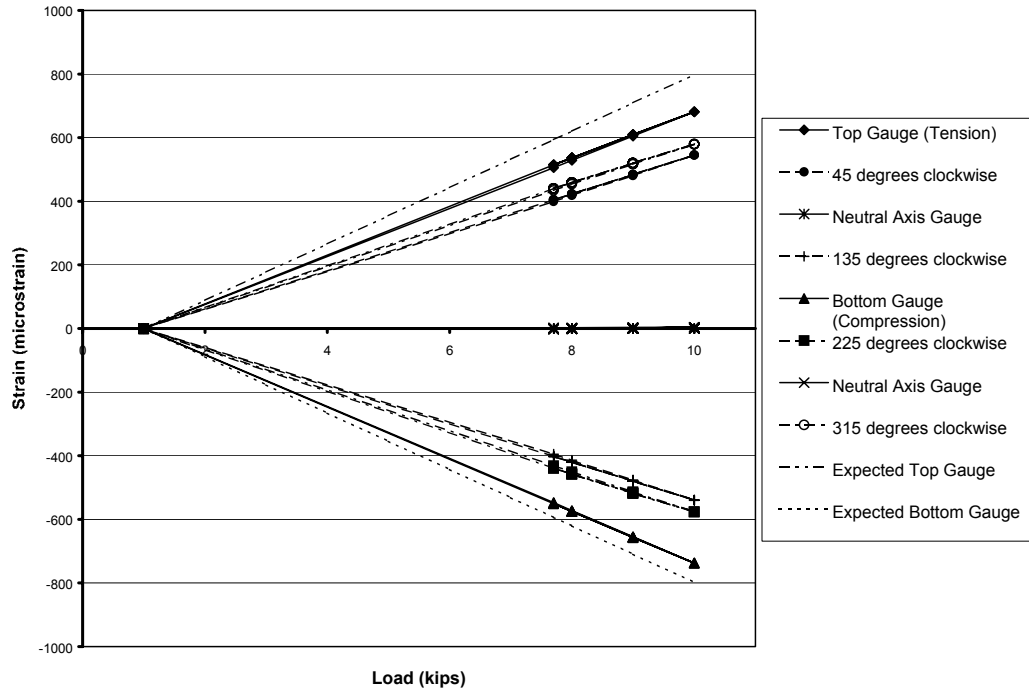


Figure 6.3 Plot of Static Test Results for TxuA

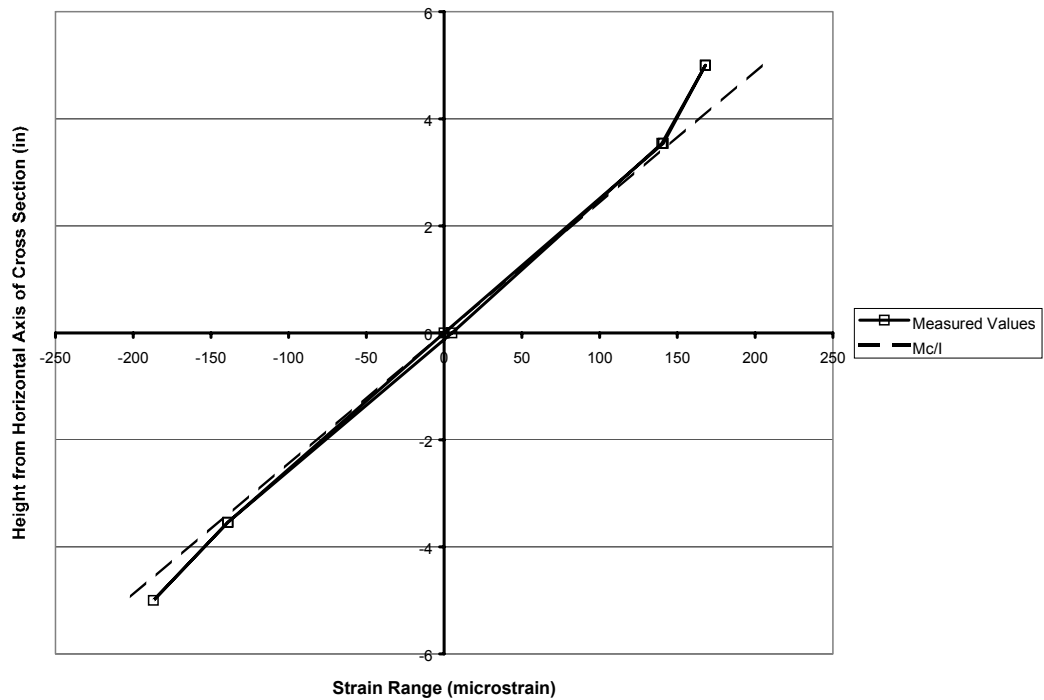


Figure 6.4 Plot of Strain Range vs. Height for TXu A

The static test results of specimen TXu A are presented again in Figure 6.5. This figure shows the results presented in a plot of strain versus height from the horizontal axis; however, instead of graphing the testing strain ranges, as was done in the previous graphs, the strains at the minimum and maximum testing load are graphed in this figure. It is evident that the two sets of data in Figure 6.5 exhibit similar behavior, in that the strain versus height relation has a similar shape, and the amount of variation between the measured and expected values are proportional to the applied load. These consistencies between the two sets of data indicate that the behavior of the test specimen is not dependent on the applied loading, which is further proof that the test specimens do not exhibit material or geometric non-linear behavior.

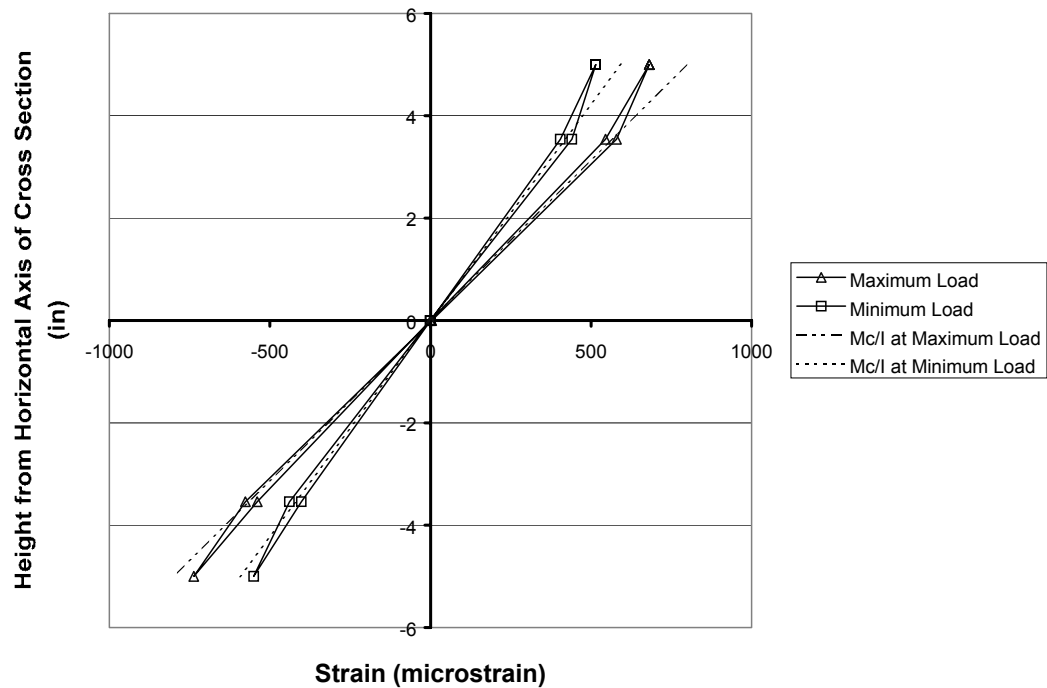


Figure 6.5 Plot of Strain vs. Height for TXu A under the Minimum and Maximum Loads

Two additional strain gauges were installed on specimen TXu A inside the pole along the top chord of the pole. The first gauge was located 3" from a point corresponding with the toe of the exterior socket weld. The second strain gauge was installed as close to the interior fillet weld as possible. The static test results from these strain gauges are presented in Figure 6.6 in a strain versus applied load plot.

Figure 6.6 indicates that the gauge located 3" from the toe of the exterior socket weld exhibited behavior similar to that of the exterior gauge. The gauge located near the interior fillet weld indicated the presence of local compressive stresses. The behavior of the region near the interior fillet weld is not fully understood.

The static test results from the VALNu series exhibited the same trends as the other groups of unstiffened socket welds. Based on this general agreement, these results will not be presented.

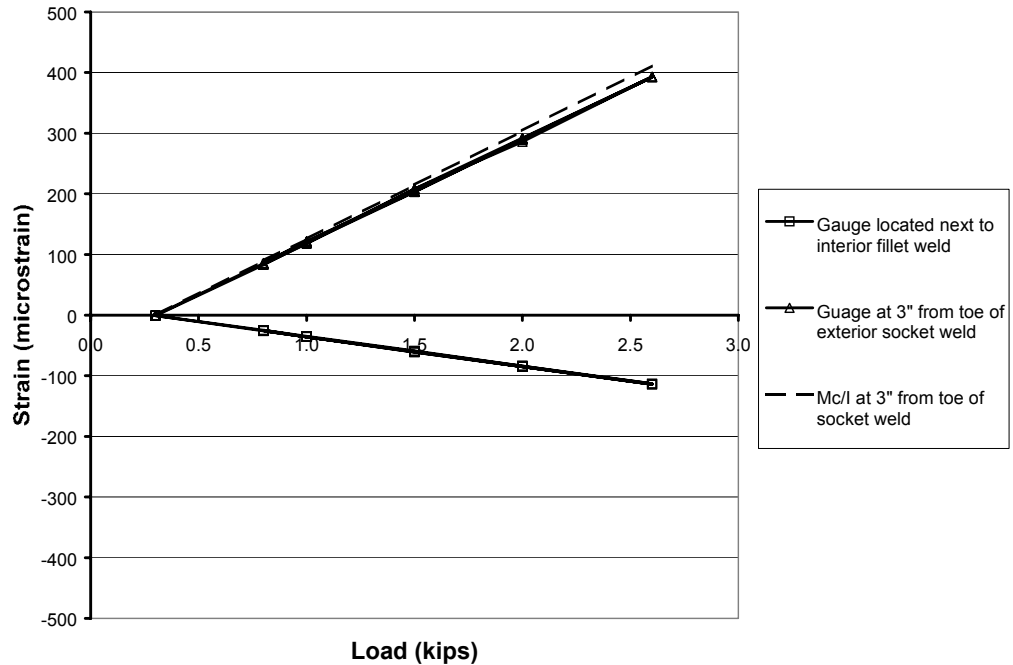


Figure 6.6 Plot of Strain vs. Load for Strain Gauges Located inside the Pole of Specimen TXu A

6.3 STIFFENED SPECIMEN

In this test program, the stiffened connection details consist of socket connections with stiffener attachments of various sizes. As much as possible, the behavior of the stiffened connection specimens will be discussed as a group. The results and behavior of the specimens with the stiffeners oriented at 45° angles were significantly different than the behavior of the specimens with vertically oriented stiffeners. Based on this difference, the discussion of the static testing of the stiffened connection details will be separated based on the orientation of the stiffeners.

6.3.1 Vertical and Horizontally Oriented Stiffeners

Independent of the size of the stiffener, the stiffened connection details with the stiffeners oriented vertically and horizontally exhibited very good agreement between the expected strain ranges and those measured in the static test. The static test results from three of the stiffened specimens are presented in Figure 6.7, Figure 6.8, and Figure 6.9. The three figures show a variety of stiffener size and pole wall thickness combinations, but the general results are similar, so the results are not dependent on these variables.

By comparison with the results from the static testing of the socket connection details, these figures indicate much better agreement between the measured strain values and the expected strain values. In the various stiffened connection specimens, the measured strain ranges at the top and bottom strain gauges range from slightly below to slightly above the expected values. The error was typically less than 5% - 8% in either direction. This level of error is insignificant.

Similar to the instrumentation used to measure the behavior of TXu A, specimen TX 6x3/8 C was instrumented with 8 gauges arrayed around the circumference of the pole at 45° angles, at a location 3" from the termination of the stiffener. The strain ranges measured at each location during the static testing are plotted versus distance from the horizontal axis in Figure 6.10. The resulting plot differs dramatically from the similar plot for specimen TXu A. For specimen TX 6x3/8 C, the strain range at the top of the specimen is slightly less than the expected value, but the error is in the range of 5%. What is more

interesting, however, is that the strain ranges at the 45° strain gauges are significantly lower than the expected values. This indicates a behavior that is opposite the behavior of the TXu A specimen. The discrepancy may show that the stiffener acts to restrain the distortion of the cross section in the vertical and horizontal axes, but allows distortion in the regions between the stiffeners.

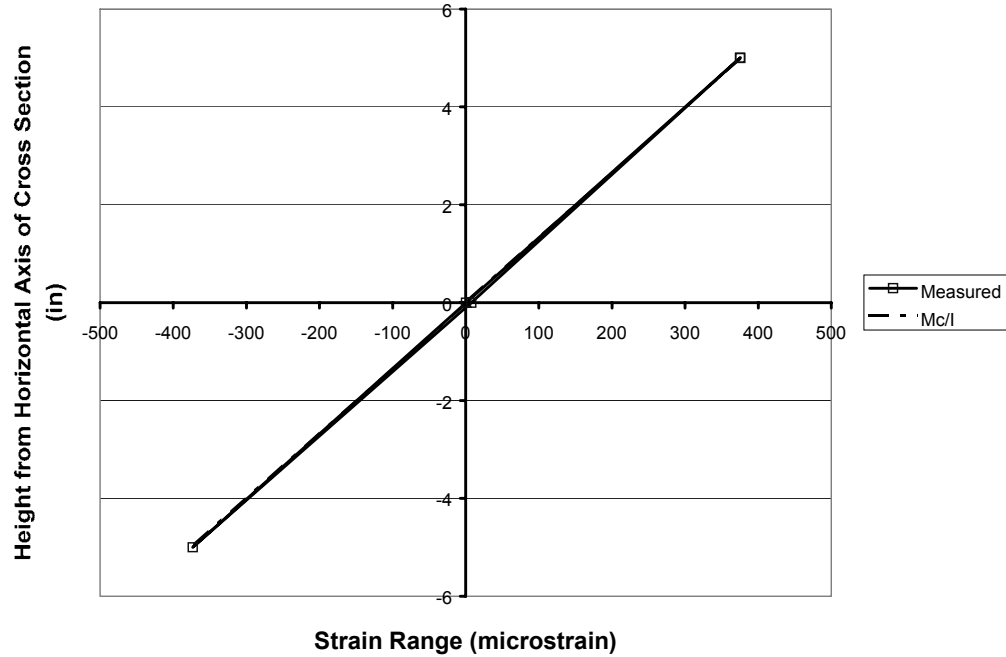


Figure 6.7 Plot of Static Test Results for VAL 3x1/4 A

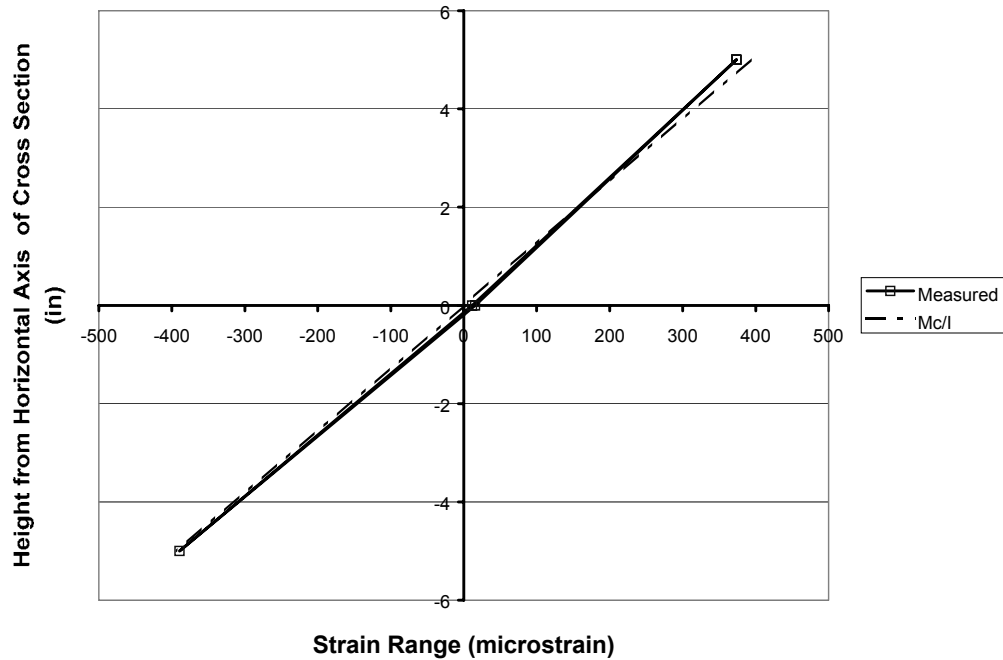


Figure 6.8 Plot of Static Test Results for VAL 6x3/8A

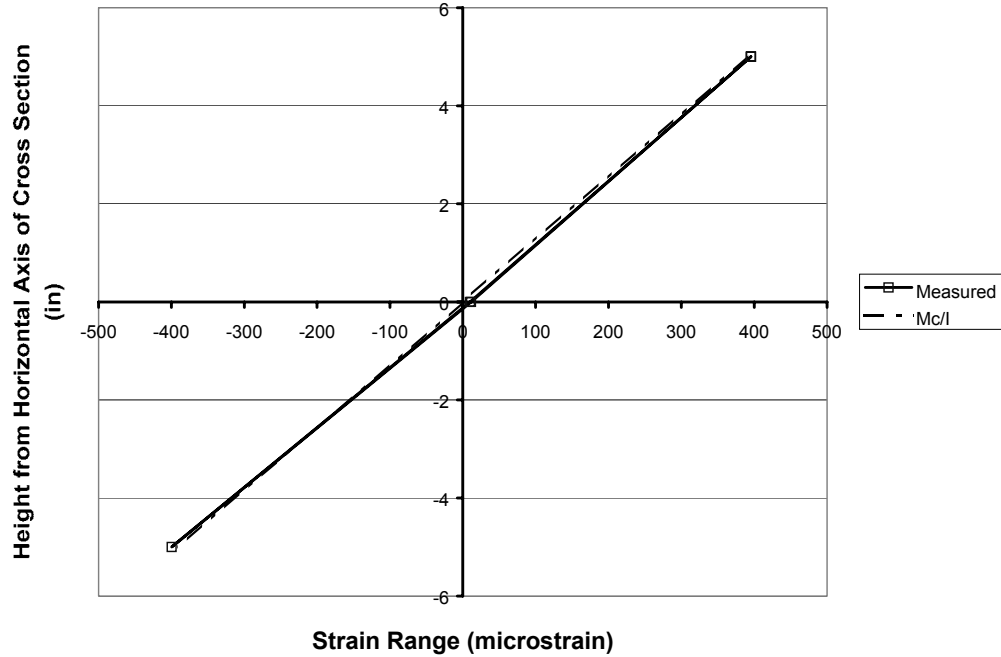


Figure 6.9 Plot of Static Test Results for TX 3x3/8 A

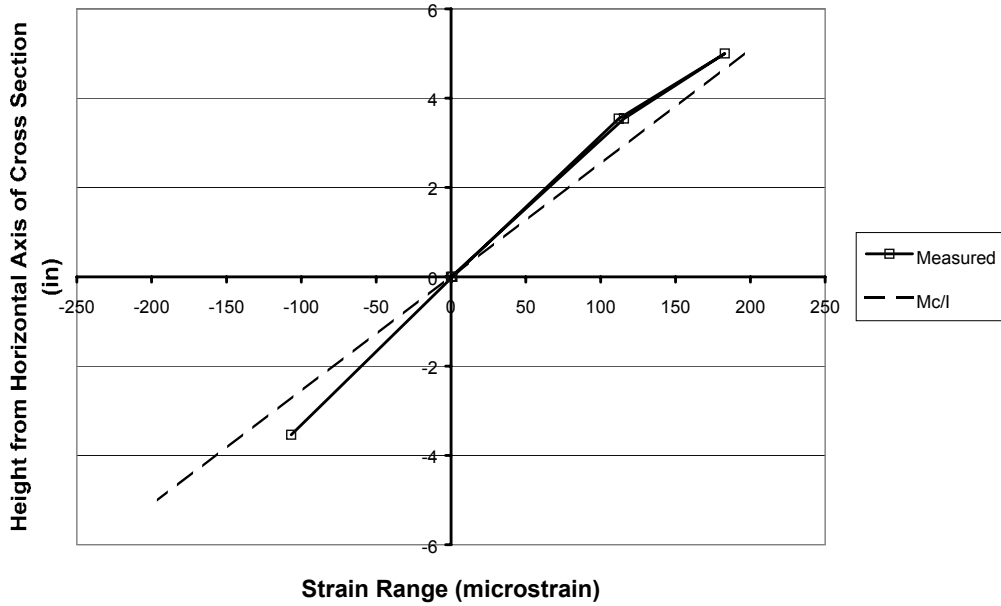


Figure 6.10 Plot of Strain vs. Height for TX 3x3/8 C

6.3.2 Stiffeners Oriented 45° from Vertical.

The test specimens with the stiffeners oriented at 45° angles from vertical behaved significantly different than the specimens with the vertically oriented stiffeners. The results of the static testing for specimen VALN 6x3/8@45 A are presented in Figure 6.11. Six strain gauges were installed on this specimen at a distance of 3 inches from the termination of the stiffener, with four of the gauges arranged in the typical

fashion, with one each at the top and bottom and two on the horizontal axis. The remaining two gauges were installed in line with the top two stiffeners, or in other words, the stiffeners in the tension region.

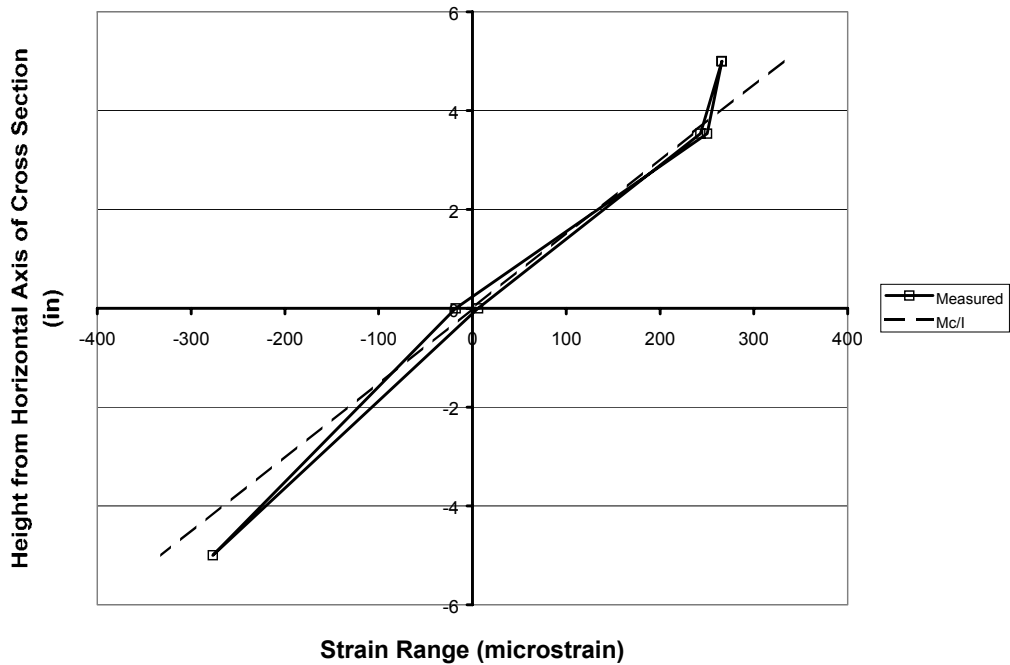


Figure 6.11 Plot of Static Test Results for VALN 6x3/8@45 A

From Figure 6.11, it is evident that the behavior of the poles in the unstiffened section of the tube behaved more like an unstiffened connection detail than as a stiffened connection detail. The strain readings are less than the expected values by approximately 20% of the expected value. This magnitude of error is much closer to the range of errors observed in the socket connection specimen than in the stiffened specimens.

The results of the two strain gauges in line with the stiffeners, or at a height of 3.5" from the horizontal axis, indicate very good agreement with the expected values. The discrepancy is approximately 5-7%. The different levels of agreement observed between the top strain gauge and the strain gauges in line with the stiffeners indicates that the stiffeners restrain the distortion of the cross section in the area of the stiffeners, but allow for distortion in the areas between the stiffeners.

One of the other specimens in this series was instrumented with strain gauges 3" from the socket connection on the top and bottom of the test specimen. The results of this static test are presented in Figure 6.12. Only the results from these two gauges are included in this plot. Along with the measured readings, the figure shows the expected strain values for the case in which the stiffener is fully effective at reducing the stress in the connection detail, and for the case in which the stiffener is not effective at reducing the stress. This latter condition is identical to that of an unstiffened socket connection. The plot shows that the measured values are less than the expected values calculated by either method. The values are approximately 35% less than the expected values for the fully effective condition. This indicates that the stiffeners reduce the stress in the critical socket connection area by more than just the effect of the addition of the stiffener to the moment of inertia calculation.

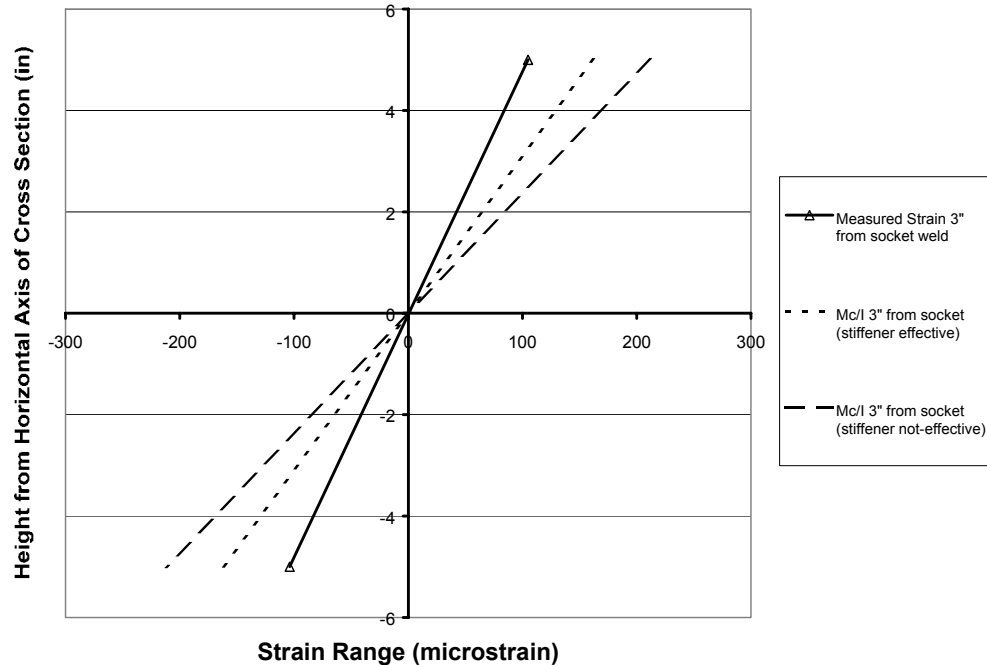


Figure 6.12 Plot of Static Test Results for VALN 6x3/8@45 D

6.4 UIT WELD TREATMENT PROCESS

The Ultrasonic Impact Treatment (UIT), which has been mentioned in previous sections, is a weld improvement method that was developed in Russia. The technology has been tested and shown to be effective at improving the fatigue life of plate girders for bridge applications. The UIT weld treatment is a proprietary treatment marketed by Applied Ultrasonics.

The equipment used to perform the UIT weld treatment is shown in Figure 6.13. The equipment is relatively compact, making it easy to transport in two large suitcase-sized boxes. The key component of the equipment is the treatment tool shown in Figure 6.14. During the treatment process, the rounded pins in the head of the tool are pressed against the area to be treated. The head of the treatment tool, which is shown in Figure 6.15, oscillates at ultrasonic frequencies causing the rounded pins to impact the area being treated. The impact of the pins causes plastic deformation of the material in the treatment area. A treated area is easily identified as the mill scale or other coating is knocked off, revealing shiny material. Typically the treated area is the toe of a weld; however, larger areas may be treated if heat affected zones are a concern. Figure 6.16 shows equipment being used to treat the weld of a specimen.

Although there are some complexities that arise in determining the areas to be treated and the treatment method to be used, the actual UIT weld treatment process is simple and fairly easy to learn. A representative of Applied Ultrasonics treated all of the specimens treated in this test program, except for one. The remaining specimen was treated by someone with very little experience in using the equipment. The treatment performed by the untrained personnel was as effective as the treatment performed by the representative of Applied Ultrasonics.

The benefits of UIT weld treatment are primarily due to imposed compressive stresses and improved weld profile. During the treatment process, the plastic deformation caused by the oscillating pins results in a smoother weld profile. The toe of the treated weld is rounded. The shape of the weld toe is transformed from a sharp transition to a rounded area with a radius equal to the radius of the pins in the treatment tool. The rounding of the weld toe is shown in Figure 6.17. The plastic deformation imparts residual compressive stresses in an area that due to the welding process would typically be under residual tensile stresses.

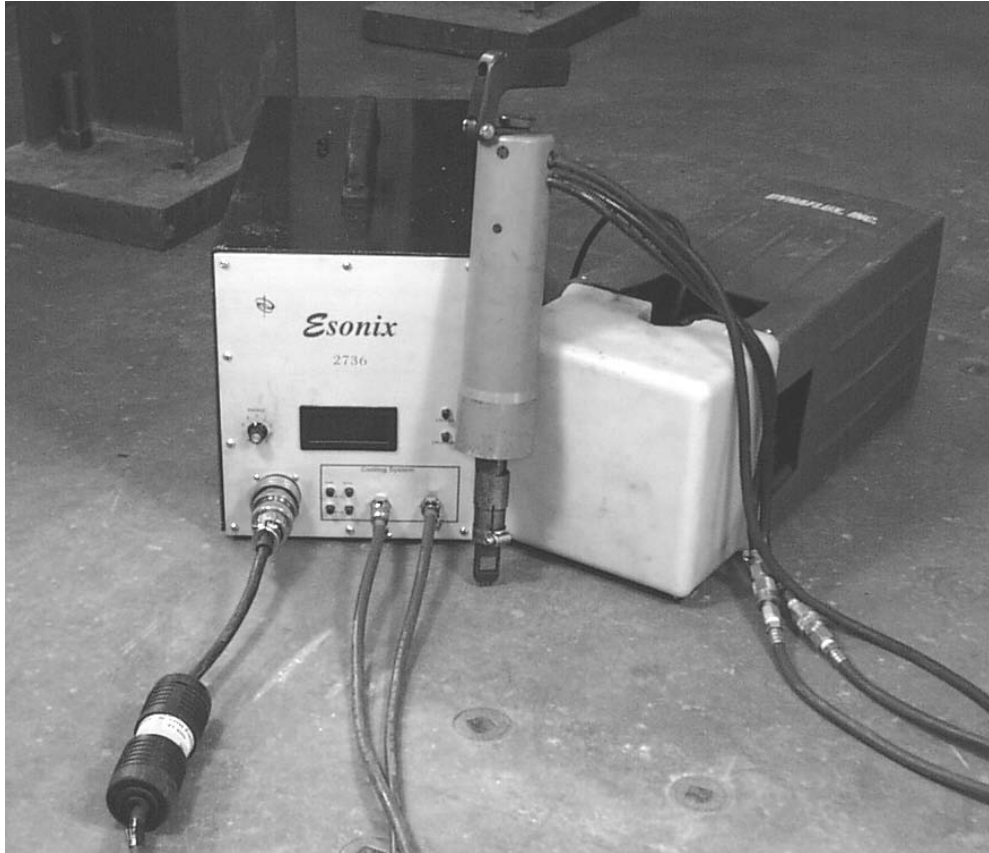


Figure 6.13 UIT Equipment



Figure 6.14 UIT Treatment Tool



Figure 6.15 UIT Treatment Tool Head



Figure 6.16 UIT Treatment in Progress



Figure 6.17 UIT Treated Socket Connection Specimen prior to testing.

6.5 UIT TREATED SPECIMENS

The discussion of the results of testing of the UIT treated specimens will be separated based on the two phases of the testing program.

6.5.1 Phase 1

During Phase 1 of the test program, a total of six specimens, four socket connection specimens and two stiffened connection specimens, were treated with the UIT weld treatment. These specimens were not treated in the test setup, but were instead treated in an unloaded condition. For the four socket connection details treated, the entire circumference of the socket weld toe was treated with the weld treatment. On the two stiffened specimens treated, the toe of the stiffener to mast-arm weld was treated on each of the four stiffeners. The weld treatment was extended back from the termination of the stiffener approximately 2" into a lower stress area that was thought to correspond with a significant reduction in the stress due to the effectiveness of the stiffener. The extent of treatment is shown by the dashed line in Figure 6.18.

In all treated areas on the Phase 1 test specimens, the treatment was performed in two passes. During the first pass, the head on the treatment tool contained pins that were 3mm in diameter. This resulted in a small treatment area along the toe of the weld. The second pass was performed with a head on the treatment tool that contained 5mm diameter pins, resulting in a slightly larger treatment area. The double pass procedure was thought to be the best possible treatment method for this particular application.

In general, the static tests of the treated specimens corresponded with the static tests of the untreated specimens. The static test results of VALu EP, a treated socket weld detail, are presented in Figure 6.19. The results in this figure exhibit behavior similar to that of an untreated socket connection detail; specifically that the strain vs. height from the horizontal axis relation was not linear, and that the strain ranges measured at the top and bottom strain gauges were slightly less than the expected values. The strain values for each of the treated socket connection specimens were approximately 10% to 15% below the expected values. These percentages are similar to those of the non-treated socket connection specimens.

The results of the static test of VAL 3x3/8 CP, a UIT treated stiffened specimen are presented in Figure 6.20. These results agree with the static test results of a non-treated VAL 3x3/8 specimen. For this particular specimen, the measured strain readings were slightly higher than the expected values.

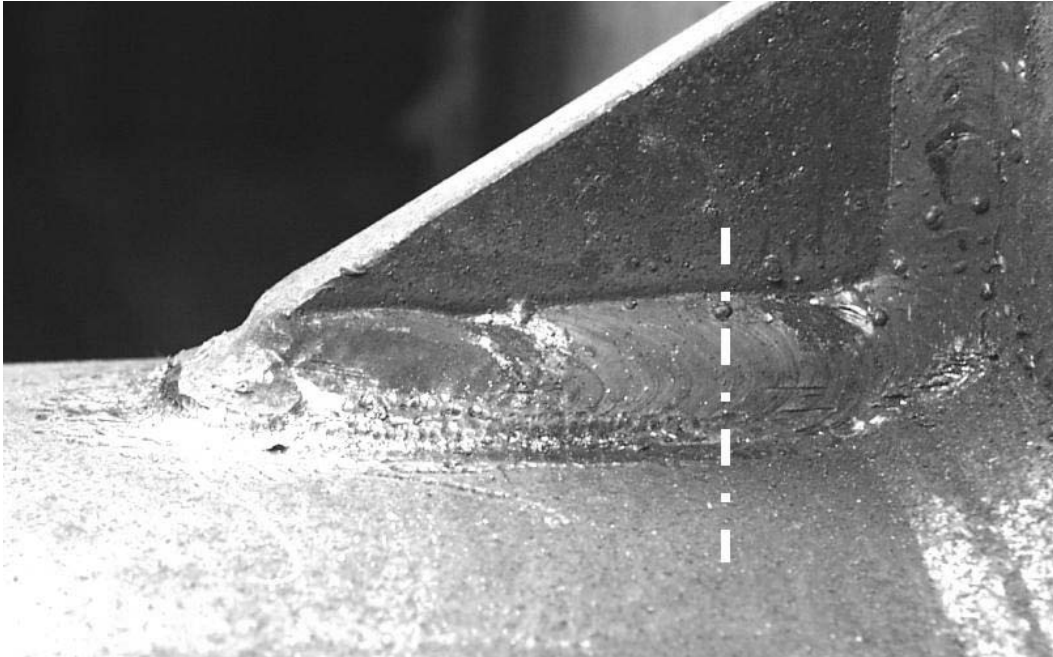


Figure 6.18 UIT Treated Stiffened Connection Specimen Prior to Testing (dashed line indicates the termination of the treated area)

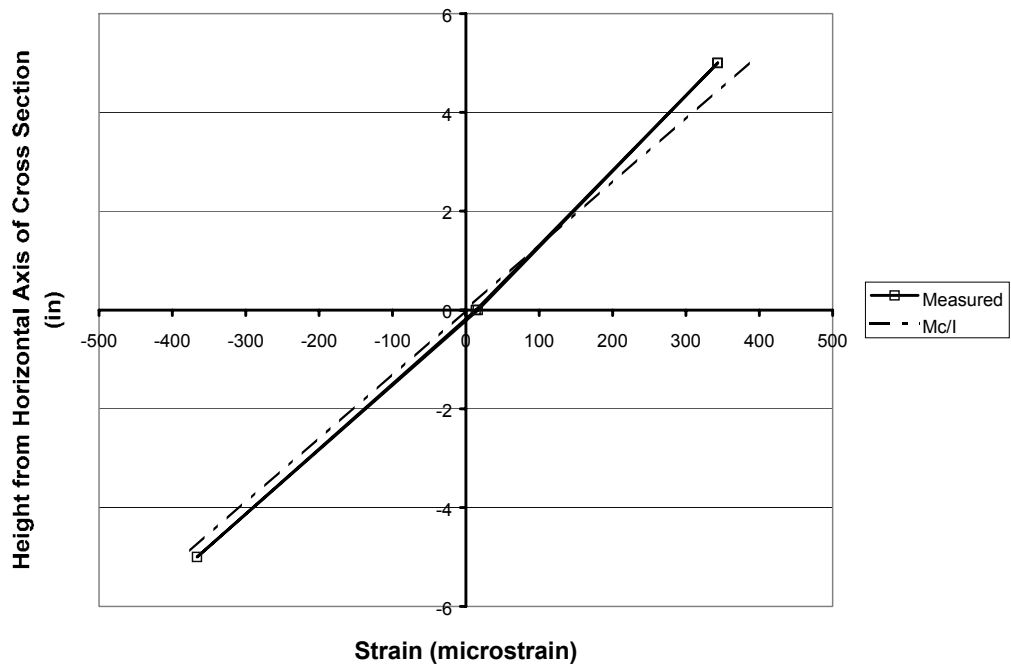


Figure 6.19 Plot of Static Test Results for VALu EP

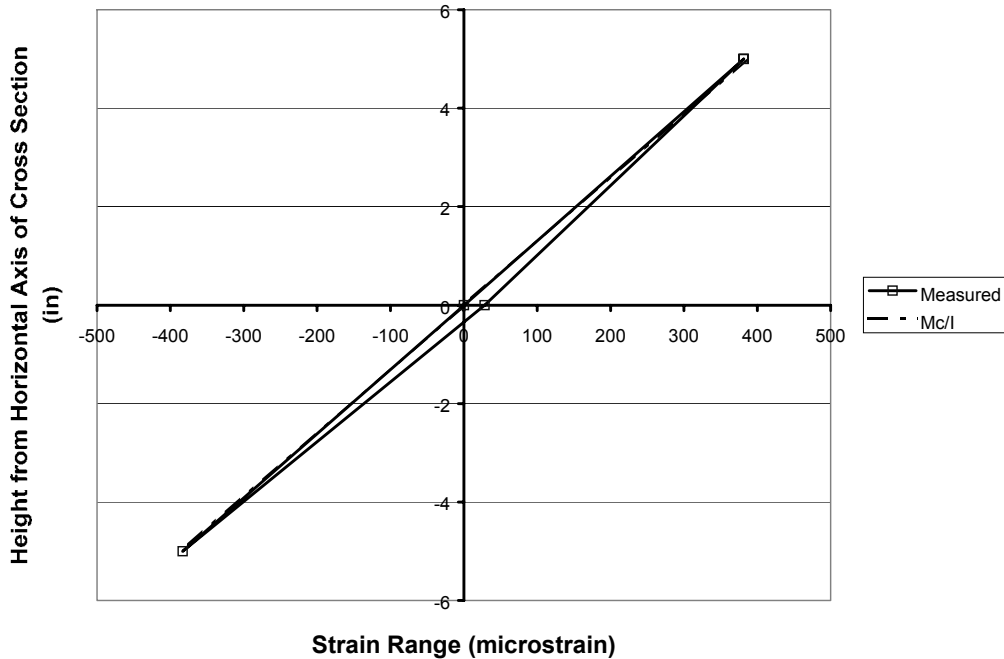


Figure 6.20 Plot of Static Test Results for VAL 3x3/8 CP

6.5.2 Phase 2

Based on the positive result of the UIT treated specimen under the low mean stress test conditions of Phase 1, the Phase 2 UIT treatment specimens were designed and treated as described in Chapter 3. In the treatment process utilized in Phase 2, the connection details were treated while the test specimen was loaded to a dead load condition. The results of each set of test specimens will be addressed separately.

6.5.2.1 UIT Retrofit – VALNu PR Series

Since the Retrofit specimens were treated under dead load conditions, and then immediately tested for fatigue without unloading, the static test for these specimens was performed prior to the UIT weld treatment. At this point, the test specimens were non-UIT treated galvanized socket connection specimens. The static test results were similar to the static test of a typical socket weld connection specimen. The minimum and maximum testing loads were determined from this initial static test.

After the static test, the test setup was loaded to the minimum load and the UIT weld treatment was performed. On these specimens, since the area of local tension stresses were clearly defined, only these regions were treated. In other words, only the toe of the socket weld on the top half of each test specimen was treated. The UIT treatment procedure was performed on each specimen separately – the first specimen was completely treated before the treatment of the second specimen began.

For all of the UIT treated specimens in Phase 2, the treatment was performed with the 3mm diameter pins in the treatment tool. Unlike the specimens in Phase 1 that were then treated with the 5mm diameter pins in the treatment tool, this second step was not performed on the specimens in this series. The altered weld profile due to the UIT treatment process is shown in Figure 6.21.



Figure 6.21 UIT Treated Region of a VALNu PR Specimen

The total treatment time for each test specimen was between 15 to 30 minutes. The treatment time was slowed slightly due to the awkward treatment position required since the test specimens were treated in the test setup; portions of the test setup did not allow for the most favorable access to the treatment area.

The representatives from Applied Ultrasonics anticipated that the UIT weld treatment procedure would result in an overall stress relaxation at the connection detail. Due to this anticipated behavior, the treatment process was performed while the test setup was held in position under displacement control. The representatives felt that if performed under load control, the deflection of the test setup and the strain at the weld toe would continue to increase during the treatment procedure, and this behavior would then influence the effectiveness of the UIT treatment process.

During the treatment process, the load did indeed decrease as predicted. The behavior of the test setup throughout the treatment procedure is provided in Table 6.3. The information in this table shows that during the UIT treatment, the load required to hold the test setup at the desired displacement declined by approximately 5% during the treatment of each of the two test specimens. The table also shows the strain gauge readings taken before and after each treatment. This data indicates that the magnitudes of the strains measured in the top and bottom gauges also decreased during the UIT treatment process. In both specimens, the decline in the magnitude of the strain readings was 6.5% and 6.3% of the initial measured value.

Table 6.3 Load and Strain Behavior During UIT Treatment at Dead Load

	Load (kip)	Displacement (in)	VALNu PR A		VALNu PR B	
			Strain		Strain	
			Gage 1	Gage 3	Gage 5	Gage 7
Initial State	5.711	2.4564	496	-480	496	-487
After Treatment of VALNu PR B	5.426	2.4564	468	-450	475	-504
Final	5.171	2.4564	464	-446	465	-466
Percent Change (from initial)						
After 1 st Treatment	-5.0%	0%	-5.6%	-6.3%	-4.2%	3.5%
Final	-9.5%	0%	-6.5%	-7.1%	-6.3%	-4.3%

6.5.2.2 Fabrication Method – Galvanized Prior to UIT – VALNu GP series

The test specimens of the VALNu GP series were delivered already galvanized. The specimens were then treated with the UIT process under a dead load condition prior to testing. This method was selected to represent a potential fabrication method as has been described previously in Chapter 3.

Prior to the weld treatment process, a short static test was performed on the two test specimens for this set in order to determine the minimum and maximum displacements. The UIT process was then performed at the minimum displacement as determined from the static test. The weld treatment performed on the VALNu GP specimens was identical to the treatment performed on the retrofit specimens. The treatment was performed using the 3mm diameter pins along the toe of the socket weld in the tension region of the test specimen.

The weld treatment of the VALNu GP specimens was again performed under displacement control, and a reduction in the load and strain readings similar to that observed during the treatment of the VALNu PR specimens was observed during the treatment process. A summary of the load and strain readings taken during the UIT process is presented in Table 6.4. The values in Table 6.4 show similar trends as observed during the treatment of the retrofit specimens, in that the load declined about 5% during the treatment of each specimen, and the strain gauge readings decreased between 7.5% and 12.2% during the entire treatment process.

After the weld treatment process, the specimens were unloaded, removed from the test setup and tested under fatigue loading at a later date. A full static test was performed immediately prior to the start of the fatigue testing. The results of this static test were similar to those of the UIT treated specimens and the untreated socket connection specimens of Phase 1.

Table 6.4 Load and Strain Behavior During UIT Treatment at Dead Load

	Load (kip)	Displacement (in)	VALNu GPA		VALNu GP B	
			Strain		Strain	
			Gage 1	Gage 3	Gage 5	Gage 7
Initial State	5.805	2.0014	494	-500	499	-497
After Treatment of VALNu GP B	5.515	2.0014	467	-472	463	-507
Final	5.244	2.0014	457	-485	438	-480
Percent Change (from initial)						
After 1 st Treatment	-5.0%	0%	-5.5%	-5.6%	-7.2%	2.0%
Final	-9.7%	0%	-7.5%	-3.0%	-12.2%	-3.4%

6.5.2.3 Fabrication Method – UIT Prior to Galvanizing – VALNu PG series

The VALNu PG series was treated with the UIT process under a dead load condition prior to being galvanized. This method was selected to represent a potential fabrication method as has been described previously in Chapter 3.

Similar to the VALNu PG series specimen, a short static test was performed on the two test specimens for this set prior to the weld treatment process, in order to determine the minimum and maximum displacements. The UIT process was then performed at the minimum displacement as determined from the static test.

The representatives from Applied Ultrasonics were concerned about the influence of the heat incurred during the galvanization process on the behavior of the UIT weld treated areas. In an attempt to compensate for this heat influence, a heat affected area treatment was performed on these test specimens. After the standard treatment was performed using the 3 mm diameter pins along the toe of the socket weld, the same head in the treatment tool was used to treat an area around the socket weld. The resulting condition of the socket weld after the heat affected area treatment is shown in Figure 6.22.



Figure 6.22 UIT Treatment of Heat Affected Region on VALNu PG Series

The weld treatment of the VALNu PG specimens was again performed under displacement control, and a reduction in the load and strain readings was observed during the treatment process. A summary of the load and strain readings taken during the UIT process is presented in Table 6.5.

The values in Table 6.5 show a trend that is different than the trend of the VALNu PR series or the VALNu GP series. After the treatment of the first test specimen, the strain measured in that specimen decreased, while the strain in the other specimen increased. This indicates a redistribution of the strain. When the second specimen was treated with the UIT weld treatment process, a similar behavior was observed in that the strain in the treated specimen declined, and the measured strain increased in the specimen that was treated first. In this manner, the change in the strain of each specimen was not a continuous decrease, but instead the change had different directions of change. Overall, the total strain decrease in each specimen was approximately 5% of the initial strain readings.

Table 6.5 Load and Strain Behavior During UIT Treatment at Dead Load

	Load (kip)	Displacement (in)	VALNu PGA		VALNu PG B	
			Strain		Strain	
			Gage 1	Gage 3	Gage 5	Gage 7
Initial State	5.714	2.1336	501	-540	499	-540
After Treatment of VALNu PG B	5.327	2.1336	462	-500	521	-550
Final	4.949	2.1343	480	-506	483	-514
Percent Change (from initial)						
After 1 st Treatment	-6.8%	0%	-7.8%	-7.4%	4.4%	1.9%
Final	-13.4%	0%	-4.2%	-6.3%	-3.2%	-4.8%

In contrast to the strain behavior, the load required to maintain the test setup at the treatment displacement decreased during the treatment of each test specimen. The decrease in the measured load was approximately 7% during each treatment step.

After the UIT weld treatment process, the specimens were unloaded, removed from the test setup and tested for fatigue at a later date. A full static test was performed immediately prior to the fatigue testing. The results were similar to the static test results of the UIT treated specimens and untreated socket connection specimens in Phase 1.

6.5.2.4 Specimen VALNu CP

Based on the initial fatigue test results of the Phase 2 UIT treated specimens, the VALNu GP B specimen was tested at a high stress range of 20 ksi. At the time of testing, VALNu GP B was the last specimen to be tested, and there was not a specimen to test in the test setup against this specimen. To provide a matched testing set, an additional test specimen was treated with the UIT weld treatment.

VALNu CP was one of the test specimens that were refabricated by the pole manufacturer due to unacceptable welds in the test specimens delivered for Phase 2. This specimen was not galvanized. The specimen was treated with the UIT weld treatment process at an imposed deadload similar to the rest of the UIT treated specimens in Phase 2.

Prior to the UIT treatment, a short static test was performed to determine the displacements associated with the minimum and maximum testing loads, as well as the load associated with the calculated 16.5 ksi stress. The other UIT treated specimens of Phase 2 were treated at the minimum load, which corresponds with a

stress of 16.5 ksi. The UIT weld treatment of VALNu CP was performed at the displacement corresponding with the 16.5 ksi stress so that the treatment conditions were as similar as possible.

Since this test specimen was treated separately from other specimens with the UIT weld treatment in Phase 2, the representatives from Applied Ultrasonics were not available to perform the UIT treatment. Instead, the UIT weld treatment was performed by Mark Koenigs, with only a limited amount of training prior to performing the treatment.

Similar to the treatment of the VALNu GP series of specimens, the weld treatment was performed using the 3mm diameter pins in the treatment tool head, and the treatment was performed along the toe of the socket weld in the area of tensile stresses. After the treatment, the specimens were unloaded. Prior to testing, a short static test was performed to determine the displacement that corresponded with the minimum and maximum loads.

6.6 MISCELLANEOUS CONNECTION DETAILS AND VARIABLES

The remainder of the tests performed during the testing of Phase 2 encompassed a large variety of variables and alternative connection details. Since these tests do not conveniently fit into the categories discussed in the previous chapters, they will be discussed in this chapter. Each variable or alternative connection detail will be discussed in a separate section.

6.6.1 Base Plate Thickness: VALNu 2 Series

The static test results for specimen VALNu 2A are shown in Figure 6.23. In this figure it is clear that the static results follow the same trends as the socket connection specimens with the thinner base plate, but with a slight difference. The 2" thick base plates had measured strain values ranging from 5% to 10% less than the expected values. This shows considerably better agreement than the 15% to 20% typical in the socket connection specimens with the thinner 1.5" base plate.

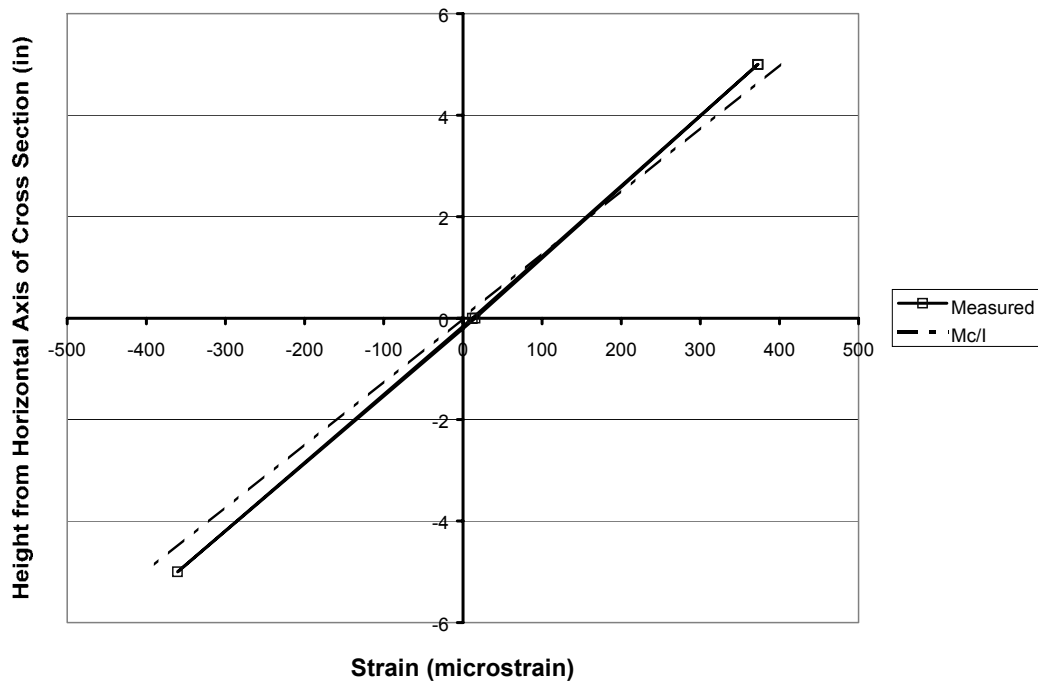


Figure 6.23 Static Test Results for VALNu 2 A

6.6.2 Galvanizing: VALNu G Series

The static test results for the VALNu G series of test specimens were very similar to those of a typical socket connection specimen. These results are thoroughly discussed in Section 6.2 so they will not be discussed here.

6.6.3 U-Rib Stiffener Connection – VALN UR Series

In order to get a better understanding of the behavior of the U-Rib stiffener connection details, additional strain gauges were placed around the U-Rib stiffener. Strain gauges were placed at the typical location, 3" from the termination of the stiffener. The geometry of the U-Rib stiffeners allowed for a strain gauge to be placed inside the U-Rib itself. This strain gauge was installed 3" from the socket weld. Additionally, on one of the specimens, strain gauges were installed 3" from the socket weld at angles of 45° from vertical. The results from the various sets of strain gauges will be discussed separately.

The static test results from the strain gauges located 3" from the termination of the stiffener of specimen VALN UR A are shown in Figure 6.24. In this plot, the strain gauges at the top and bottom of the test specimen exhibit very good agreement with the predicted strain values. The measured strain values agree with the predicted strain values within 5% of the expected values. This agreement is similar to the agreement observed in the specimens with the typical stiffener details.

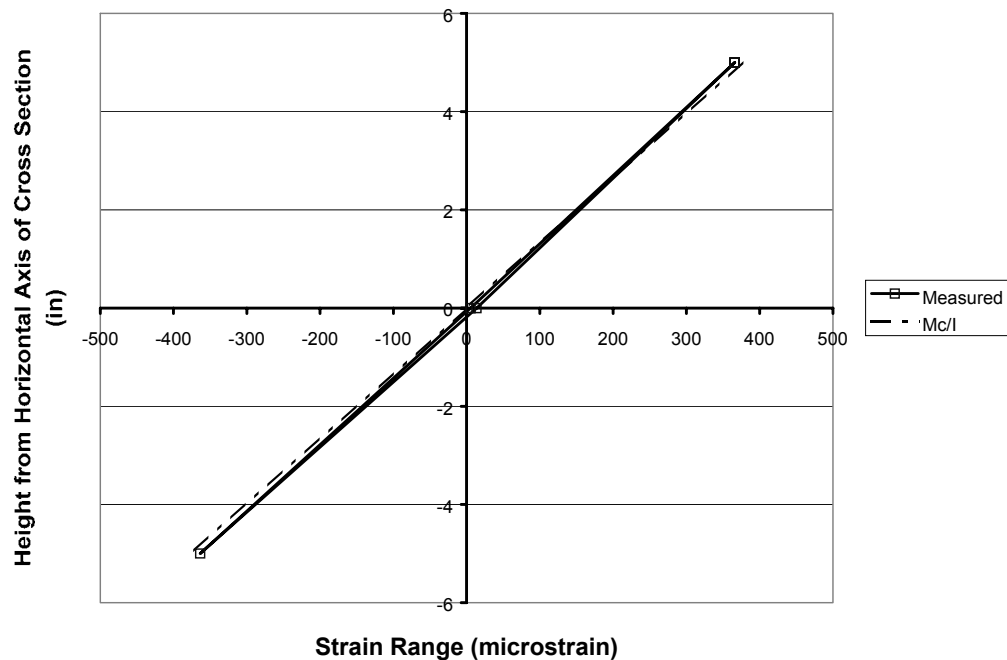


Figure 6.24 Static Test Results for Strain Gauges Located 3" from Termination of Stiffener on Specimen VALN UR A

The static test results from the strain gauges installed 3" from the socket weld, both inside the U-Rib stiffener and at 45° angles from vertical, on specimen VALN UR B are presented in Figure 6.25. This graph also shows the calculated upper and lower expected values. The expected value line with the steeper slope was calculated assuming that the U-Rib stiffener is fully effective, or that the entire area of the U-Rib stiffener adds to the moment of inertia calculation at the location of the strain gauge. The second expected value line was calculated assuming that the stiffener is not effective; the stiffener is not included in the section property calculation. These two conditions should provide boundaries for the measured behavior.

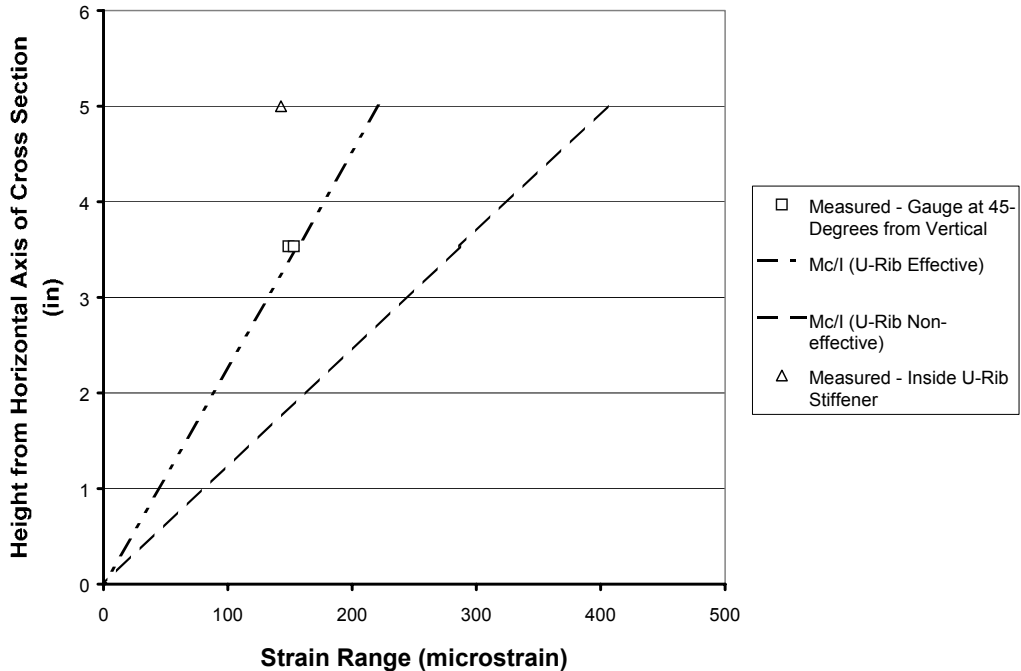


Figure 6.25 Static Test Results of Strain Gauges located 3" from Socket Weld on Specimen VALN UR B, Includes Strain Gauge Located Inside the Stiffener and at 45°Angles from Vertical

It is evident from the plot in Figure 6.25 that for the strain gauge installed inside the U-Rib Stiffener, or at a height of 5" from the horizontal axis of the cross section, the measured strain range is significantly less than the expected strain range as calculated assuming that the stiffener is fully effective. The only explanation for this behavior is that the stiffener restrains the area inside the stiffener from deforming, therefore producing less strain than expected.

From the plot in Figure 6.25, it is clear that the strain ranges measured at the strain gauges oriented at 45° angles from vertical show very good agreement with the set of expected values, which assume that the stiffener is fully effective. This means that in order to calculate the stress in areas away from the stiffener, the entire cross-sectional area of the stiffener should be included in the moment of inertia calculations.

6.6.4 External Collar Connection Detail – VALN Col Series

The strain gauges on the external collar specimens were installed 3" from the termination of the collar. On one of the specimens, an additional set of strain gauges was installed on the collar, at the top and bottom of the cross section and at a distance of 1.5" from the toe of the collar to base plate weld.

The results measured with the strain gauges installed 3" from the end of the collar on specimen VALN Col A are shown in Figure 6.26. In this figure, the measured strain gauge values show reasonable agreement with the expected values. The measured strain gauge readings range from 5% to 10% less than the expected values. This discrepancy is relatively low compared with the discrepancy in the socket connection specimens.

The strain gauges installed on the collar were installed on specimen VALN Col B. The results of the static testing for these two gauges are shown in Figure 6.27. The figure also shows the expected strain values that were calculated assuming that the collar stiffener was fully effective at this location. The figure shows that the strain measures are more than 30% lower than the expected values. The lower measured values mean that the collar stiffener is not fully effective at this section. In other words, the stress does not 'flow' into the collar and the tube material is still carrying most of the load.

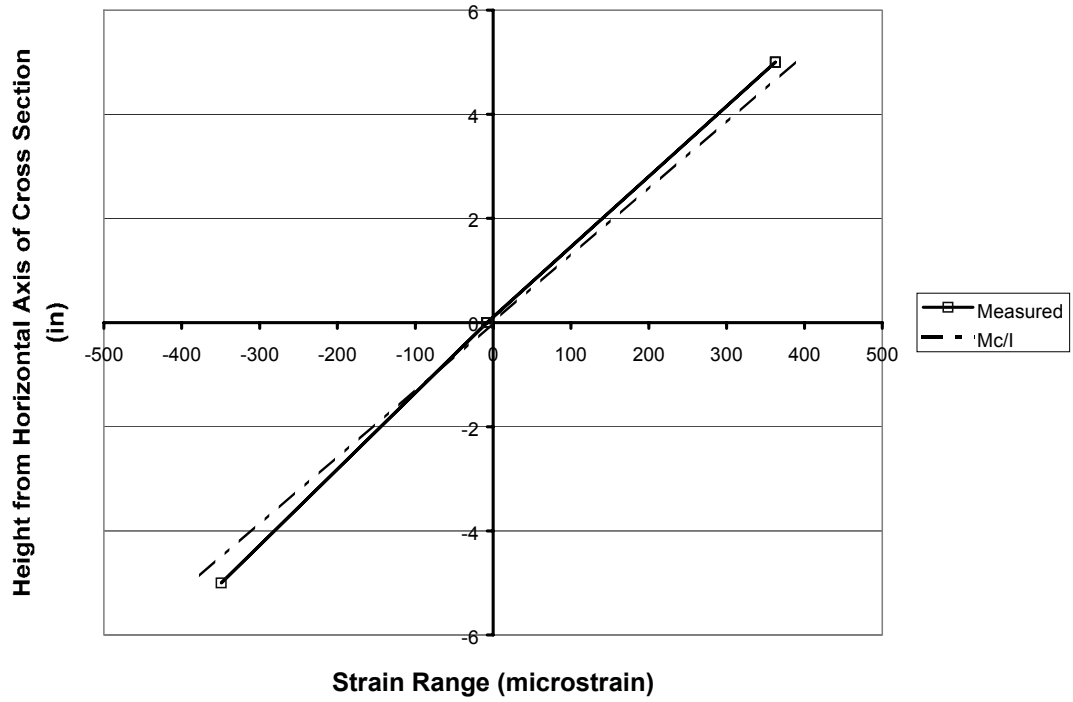


Figure 6.26 Static Test Results for VALN Col A

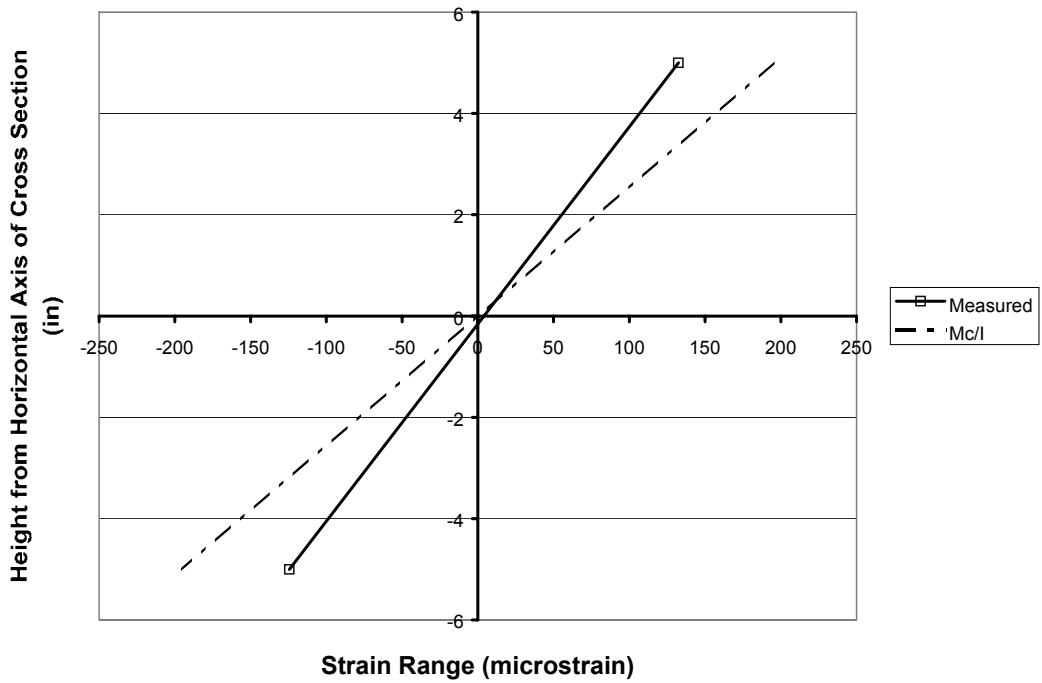


Figure 6.27 Static Test Results for Strain Gauge on the Collar of Specimen VALN Col B

6.6.5 Internal Collar Connection Detail: VALN IC Series

Prior to the start of the static test for this series of specimens, the behavior of the specimens was largely unknown. The strain gauges were installed 3" from the toe of the full-penetration weld between the tube and base plate. An additional strain gauge was installed 3" beyond the termination of the internal collar.

The static test results for the strain gauges installed 3" from the base plate weld are shown in a strain versus applied load plot in Figure 6.28. Since these strain gauges were installed within the length of the internal collar, the expected values for the top and bottom gauges were calculated for the case of the fully effective internal collar, and for the case of the ineffective internal collar. This later case is the same as having no collar. The test results show several important behavior characteristics.

First, the strain measurements fall in between the two sets of expected values. Neither set of expected values seems to provide a closer fit to the measured data.

Secondly, the strain vs. applied load relation is not linear. Instead, the behavior indicates that slip occurs between the internal collar and tube due to the lack of a weld at the termination of the collar in the tube. Since the collar is only welded at the base plate, the only forces between the collar and the tube are friction. Slip initially occurs between the tube and collar prior to the point at which friction develops and engages the collar to reduce the stress at the critical section.

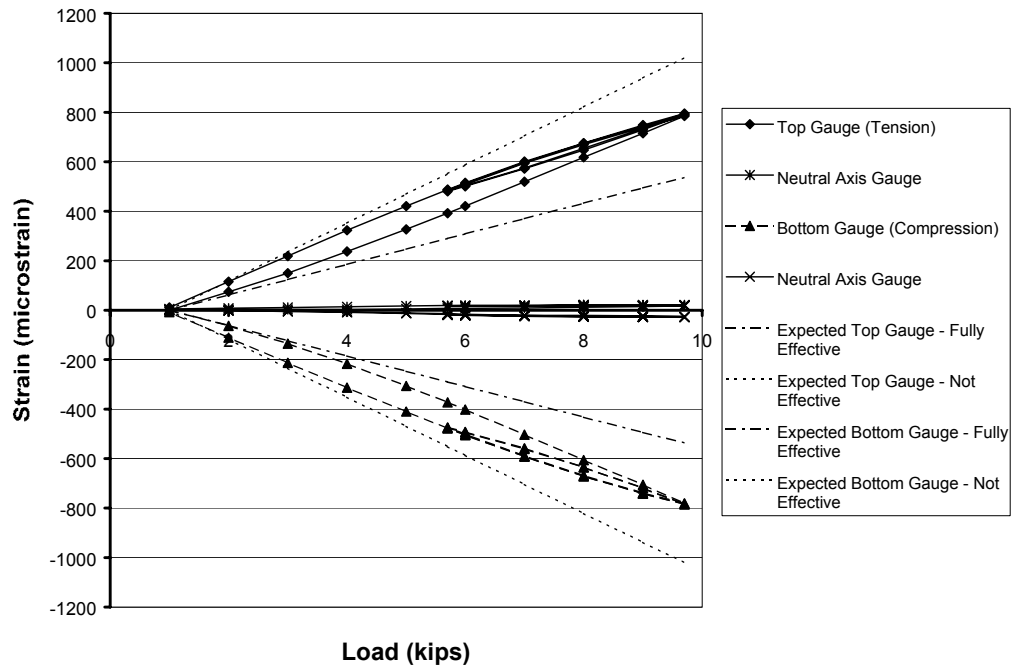


Figure 6.28 Static Test Results for VALN IC A

Although the behavior is non-linear, it is important to note that the behavior is stable. Upon unloading, the strain vs. load plot returns to the same initial point, which results in consistent strain range values for each load cycle. The stable cyclic behavior is an important observation, as it means that during the cyclic fatigue loading, the stress range at the critical location will have a constant amplitude. The constant amplitude loading means that the test results may be analyzed following the same methods as the other specimens.

The strain ranges measured with the strain gauges 3" from the toe of the pole to base plate weld are plotted in a strain versus height from the horizontal axis plot in Figure 6.29, in order to provide comparison with previous static test results. Similar to the previous strain versus applied load plot, this

figure shows that the strain ranges are between the two sets of expected values. This further illustrates the point that the internal collar is not fully effective.

The strain gauge that was installed beyond the termination of the stiffener exhibited more typical results. The results of the static test for this strain gauge are presented in Figure 6.30. This figure shows that the strain versus load relationship is linear with the measured values being 5% to 10% less than the expected values.

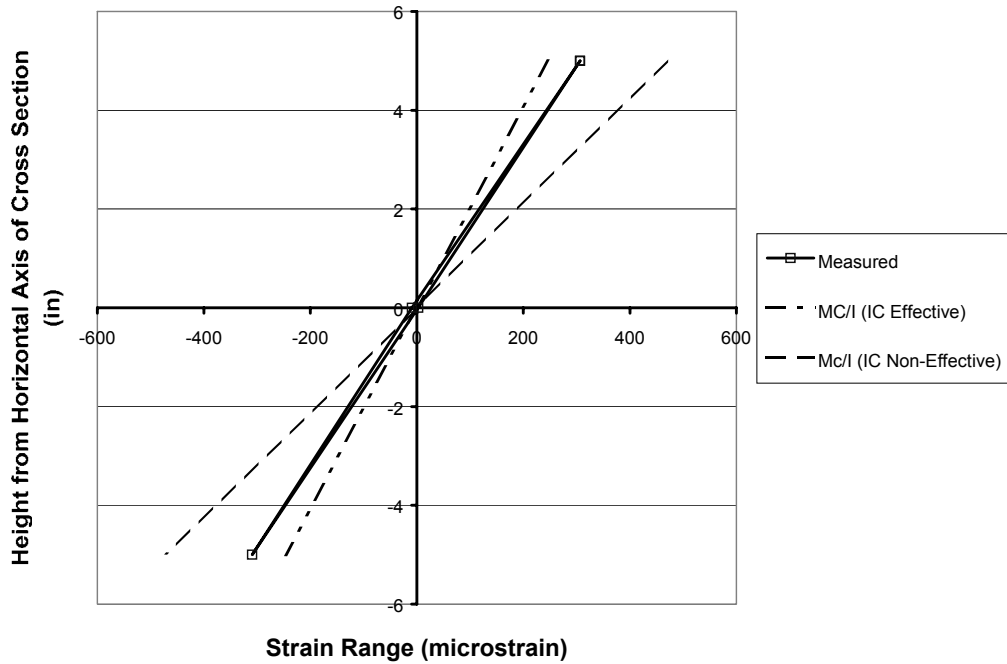


Figure 6.29 Static Test Results for VALN IC A presented in a Strain Versus Height Plot

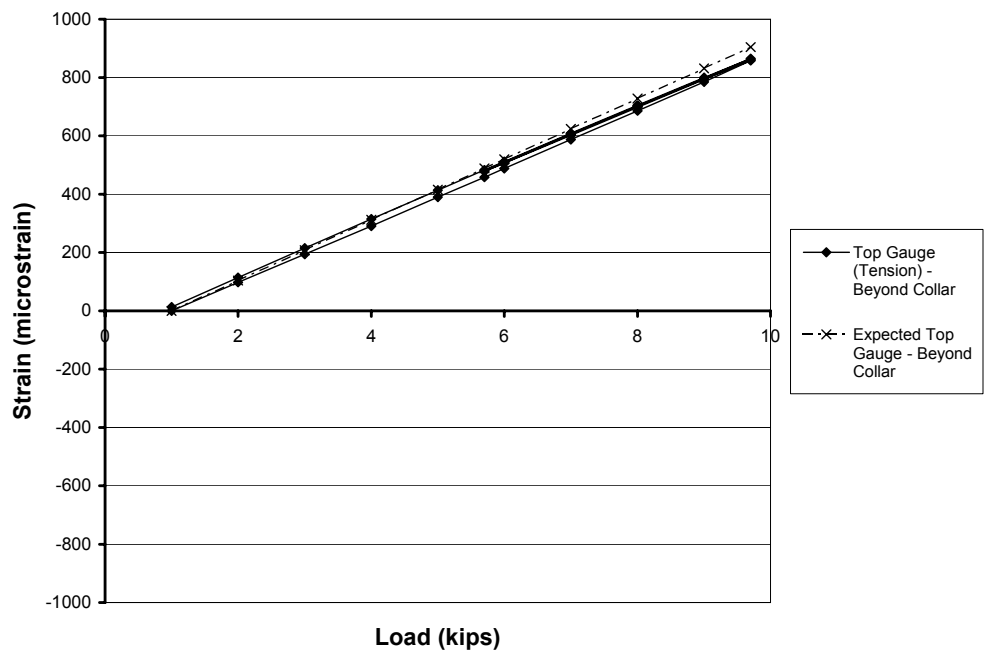


Figure 6.30 Static Test Results for VALN IC A SG beyond Collar

6.6.6 Full-Penetration Weld Detail – VALN W Series

A visible weld heat affected band was evident on the outer surface of the pole of the two specimens in this series from the fillet weld used to seal the end of the backing bar to the pole. To ensure that the weld affected area and backing bar did not influence the strain readings during the static test, the typical strain gauges for these specimens were installed 3" from the end of the backing bar. An additional strain gauge was installed on the top of the specimen between the toe of the full-penetration weld and the end of the backing bar.

The static test results for strain gauges beyond the end of the backing bar are shown in Figure 6.31. From this figure, it is evident that the measured strain values exhibited good agreement with the expected values. The measured values were typically 5% to 10% less than the expected values.

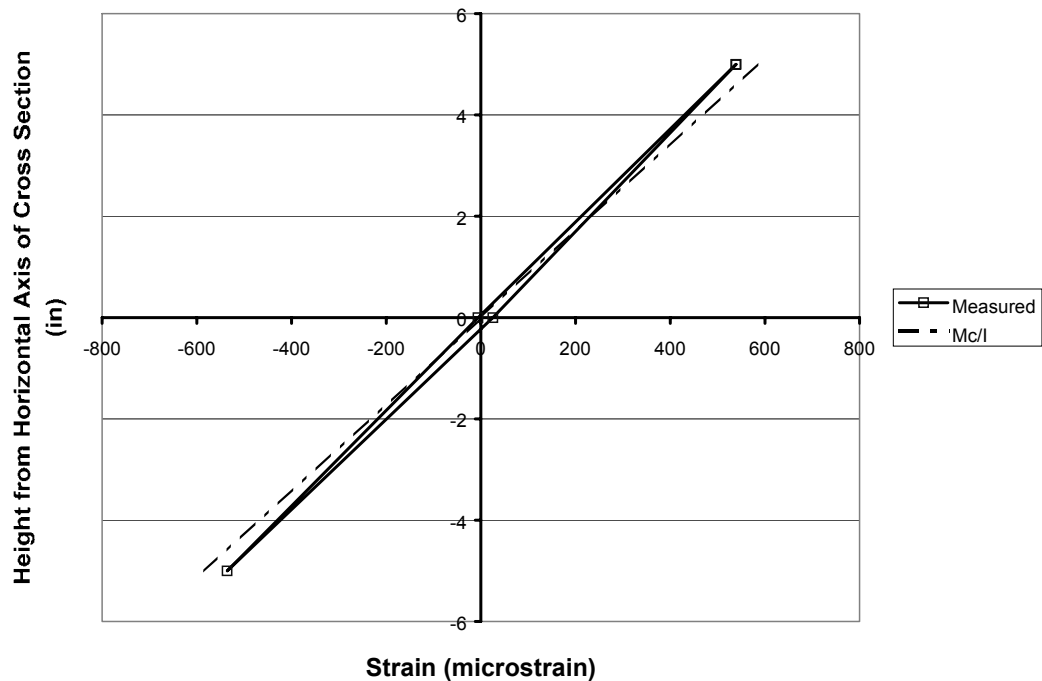


Figure 6.31 Static Test Results for the Strain Gauges Located Beyond the Backing Bar of Specimen VALN W B

The static test results for one of the strain gauges installed within the length of the backing bar are shown in a strain versus applied load plot in Figure 6.32. The two sets of expected values shown in this figure represent the case in which the backing bar is not effective, and the case in which the backing bar is effective. The results clearly show that the backing bar is effective, and reduces the stress in the area of the full-penetration weld.

The observation that the long fillet-welded backing bar is effective in reducing the stress at the weld toe is unusual. Most backing bars are too short to provide significant reduction in stress. The length of the bar and fillet welding at the end of the backing bar were felt to produce this stress reduction.

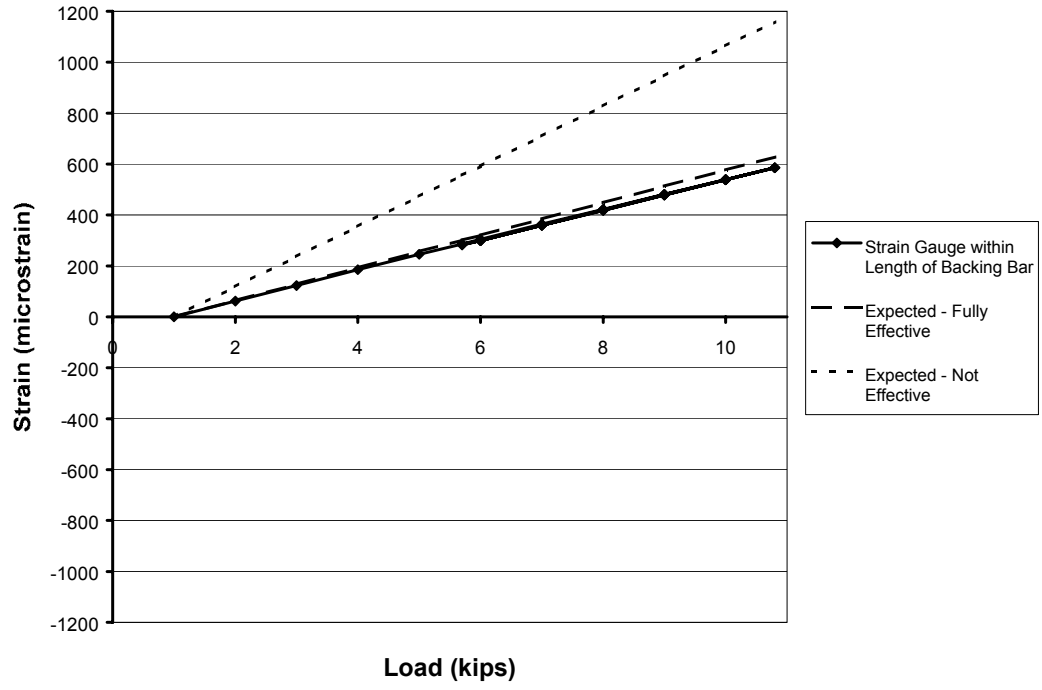


Figure 6.32 Static Test Results for Strain Gauge Located within the Length of the Backing Bar on Specimen VALN W B

CHAPTER 7: FATIGUE TEST RESULTS

7.1 TESTING PROGRAM

In the course of this test program, 55 specimens were tested. All but one of these specimens failed under fatigue loading. The specimens tested are listed in Table 7.1 and Table 7.2. These tables also list the controlling stress range, the number of cycles at failure and the location of failure.

Table 7.1 Fatigue Test Results – Phase 1

Specimen Name	Controlling Stress Range (ksi)	Cycles at Failure	Crack Location(s)
VALu A	11.90	249,446	Toe of socket weld
VALu B	11.90	453,948	Toe of socket weld
VALu C	6.29	2,072,592	Toe of socket weld
VALu D*	6.20	6,856,881	Run Out - no cracking
VALu EP	11.40	393,767	Toe of socket weld
VALu FP	11.50	353,103	Toe of socket weld
TXu A	6.00	2,199,343	Toe of socket weld
TXu B	6.10	2,816,706	Toe of socket weld
TXu C	11.80	177,596	Toe of socket weld
TXu D	12.00	194,694	Toe of socket weld
TXu EP	11.80	320,915	Toe of socket weld
TXu FP	11.70	141,155	Toe of socket weld
VAL 3x1/4 A	11.10	476,269	Toe of socket weld & Termination of stiffener
VAL 3x1/4 B	11.40	696,326	Toe of socket weld & Termination of stiffener
VAL 3x1/4 C	6.10	3,592,372	Termination of stiffener
TX 3x1/4 A	11.70	616,136	Toe of socket weld & Termination of stiffener
TX 3x1/4 B	11.80	416,146	Toe of socket weld & Termination of stiffener
TX 3x1/4 C LMS	11.90	523,397	Termination of stiffener
VAL 3x3/8 A	11.70	386,253	Termination of stiffener
VAL 3x3/8 B	11.60	410,410	Termination of stiffener
VAL 3x3/8 CP	11.50	393,767	Termination of stiffener
VAL 3x3/8 CP(2)	11.50	353,103	Termination of stiffener
TX 3x3/8 A	11.70	473,735	Toe of socket weld & Termination of stiffener
TX 3x3/8 B	11.60	657,716	Termination of stiffener
TX 3x3/8 CP LMS	12.10	1,707,128	Toe of socket weld & Termination of stiffener
VAL 6x3/8 A	11.20	242,728	Stiffener to Base Plate (lack of fusion defect)
VAL 6x3/8 B	11.30	653,392	Termination of stiffener
VAL 6x3/8 C	5.90	3,592,372	Termination of stiffener
TX 6x3/8 A	11.20	783,857	Termination of stiffener
TX 6x3/8 B	11.30	783,857	Termination of stiffener
TX 6x3/8 C	5.76	7,503,037	Termination of stiffener

*Testing Stopped – Run-Out

The stress ranges listed in Table 7.1 and Table 7.2 vary slightly from those provided in the previous chapter due to slight variations in the actual dimensions of the specimens compared to the specimen designs. The method used to calculate the stress ranges at the failure location, and therefore to evaluate the fatigue life of each specimen, will be discussed further in Section 7.3.

Table 7.2 Fatigue Test Results – Phase 2

Specimen Name	Controlling Stress Range (ksi)	Cycles at Failure	Crack Location(s)
VALNu A	11.90	389,428	Toe of socket weld
VALNu B	11.80	265,540	Toe of socket weld
VALNu G A	11.60	183,132	Toe of socket weld
VALNu G B	11.50	151,679	Toe of socket weld
VALNu 2 A	11.90	5,144,528	Toe of socket weld
VALNu 2 B	11.80	1,683,127	Toe of socket weld
VALN 6x3/8@45 A	11.96	238,515	Toe of socket weld & Termination of stiffener
VALN 6x3/8@45 B	11.98	161,843	Toe of socket weld & Termination of stiffener
VALN 6x3/8@45 C	4.30	6,066,817	Termination of stiffener
VALN 6x3/8@45 D	4.30	6,066,817	Termination of stiffener
VALN Col A	5.49	4,245,460	Toe of collar to base plate weld
VALN Col B	5.73	2,363,152	Toe of collar to base plate weld
VALN IC A	10.75	227,030	Toe of socket weld
VALN IC B	10.68	227,030	Toe of socket weld
VALN W A	17.71	422,400	Toe of full-penetration weld
VALN W B	17.56	422,400	Toe of full-penetration weld
VALN UR A (#4)	7.62	1,776,724	Stiffener to Base Plate
VALN UR B (#1)	7.60	950,670	Stiffener to Base Plate
VALN UR B (#2)	12.57	339,152	Stiffener to Base Plate
VALNu PR A*	11.60	4,557,126	Run Out - no cracking
VALNu PR B*	11.50	4,557,126	Run Out - no cracking
VALNu GP A	11.60	4,545,952	Toe of socket weld
VALNu GP B	19.91	224,240	Toe of socket weld
VALNu PG A	11.60	277,634	Toe of socket weld
VALNu PG B	11.50	313,727	Toe of socket weld
VALNu CP	19.95	1,301,077	Toe of socket weld
VALNu PR ul A	11.60	5,004,729	Toe of socket weld
VALNu PR ul B	11.50	5,440,165	Toe of socket weld

* Testing Stopped – Run-Out

In two cases, the same stiffened specimens were tested twice. This was possible by rotating the specimen after the first stiffener failed to place the failure location in a compression zone. The specimen was then tested again resulting in a second data point. In these cases, the specimen is listed twice with two different sets of results.

7.2 FATIGUE LIFE COEFFICIENT, A, CALCULATION

Throughout the course of this test program, the various connection details were tested at a variety of stress ranges. At times the variety of stress ranges was intentional in order to demonstrate that a detail corresponded to a particular fatigue category independent of the stress range. On other occasions, the variety arose due to stiffeners, collars, or other attachments that were not fully effective in reducing the stress at the critical section.

To account for the variety of stress ranges and facilitate the comparison of results, a fatigue life coefficient, A , was calculated for each detail. This coefficient was calculated as $A = \frac{N \cdot S_R^3}{10^8}$ and is similar to the A constant used to define fatigue category curves on the standard S-N plot. To simplify the discussion of the fatigue life coefficient, A , the 10^8 factor was included in the denominator of the equation, which eliminates the need to include the 10^8 factor in all discussions. For comparison sake, the fatigue life coefficients, A , for the fatigue categories are presented in Table 7.3.

Table 7.3 Fatigue Constants

Category	Fatigue Life Coefficient A (10 ⁸)
A	250
B	120
B'	61
C	44
C'	44
D	22
E	11
E'	3.9

7.3 CALCULATION OF REPORTED STRESS

The results of the fatigue tests are presented in this chapter following the standard fatigue life analysis method, which is based on the nominal stresses at the failure location. In this method, the stresses at the failure location are based on the applied loading and the nominal section properties at the critical section, assuming a linear relation of $\sigma = \frac{Mc}{I}$. The moment of inertia used in this calculation is based on the geometry of the critical section, assuming that any attachments added to the connection detail for the purpose of reducing the stress at the critical location are fully effective and fully contribute to the moment of inertia calculation. The stresses in Table 6.1 and Table 6.2 were calculated following this method; however the section dimensions were based on the design geometry. The stress values used for other comparisons will be based on the measured geometry of each individual specimen.

During the analysis phase of this test program, it was evident that the fatigue life analysis method based on the nominal stress ranges does not convey all of the important implications of this research. To account for this shortcoming, a second method of analysis, the Value Based Design Method, was developed. Each of the two methods is useful in presenting a portion of the results, but no one method completely conveys the intricacies observed during the testing. Since neither method is acceptable for all specimens, both methods of analysis will be presented. The Value Based Design Method will be described and applied to the results in Chapter 8.

The assumption of the linear stress verses distance from the neutral axis assumed in the fatigue life calculation was shown in Chapter 6 to be inaccurate. In many specimens the cross section near the critical section distorts and plane sections do not remain plane. In the calculation of the fatigue life coefficient, the A value includes the influence of any variation of the local stress pattern, including any stress concentration. Similarly, the fatigue life coefficient will also account for the inaccuracy of the stress calculation.

To more clearly illustrate the stress calculation method, example calculations are provided in the following paragraphs for specimen VALN Col B, which is a thin pole wall external collar stiffened specimen fabricated in Valley, Nebraska. The example shows the calculations used to calculate the stress at the toe of the base plate to collar weld.

In order to calculate the stress range using this calculation method, the loads utilized during the fatigue testing, the effective loading length and the outer and inner diameters of the connection detail must be known. These details are provided for specimen VALN Col B in Table 7.4.

Table 7.4 Section Properties and Test Data for VALN Col B

Variable	Description	Value
P_{\max}	Maximum Test Load	5.7 kip
P_{\min}	Minimum Test Load	9.1 kip
L	Effective Length (distance from critical section to tip of cantilever)	88.67 in.
OD_{Collar}	Outer diameter of collar at crack location	10.344 in.
OD_{Tube}	Outer diameter of tapered tube at crack location (neglecting collar thickness)	9.992 in.
ID	Inner diameter at crack location	9.651 in.
N	Number of Cycles to Failure	2,363,152 cycles

Based on the values from Table 7.4, the stress range for the fatigue life – design method is calculated as:

$$S_R = \frac{M_R \cdot c}{I}$$

Where:

$$M_R = 1/2 \cdot (P_{\max} - P_{\min}) \cdot L = 0.5 \cdot (9.1 - 5.7) \cdot 88.67 = 150.74 \text{kip-in}$$

$$c = \frac{OD_{\text{Collar}}}{2} = 5.172 \text{in.}$$

$$I = \frac{1}{4} \cdot \pi \cdot \left[\left(\frac{OD_{\text{Collar}}}{2} \right)^4 - \left(\frac{ID}{2} \right)^4 \right] = 136.1 \text{in}^4,$$

Then

$$S_R = \frac{M_R \cdot c}{I} = 5.73 \text{ksi}$$

With the fatigue life noted in Table 7.4 for this specimen of 2,363,152 cycles, this stress value can then be used to calculate an A constant of 4.45.

Through this example it is clear that in this analysis method, the entire additional moment of inertia due to the addition of an attachment is assumed to be effective in reducing the stress in the critical location. For the specific case of the external collar stiffened specimen used in this example, the static test results indicate that the collar is not fully effective. The non-fully effective condition illustrates one of the drawbacks of this analysis method.

In this analysis method, the stress concentration at the toe of a weld, and any non-fully effective conditions are reflected in the fatigue life coefficient, A. For a connection detail for which the behavior is well documented, the A coefficient simplifies the design as the effectiveness of any attachments and the magnitude of the stress concentration need not be considered. However, if the geometry of an attachment is modified, the effectiveness of the attachment may vary. In this situation, the A coefficient may no longer accurately represent the effectiveness of the attachment and may result in an inaccurate fatigue life estimation. Based on this reasoning, the A coefficients determined in this test program are only applicable for section and attachment geometries similar to those studied.

Even though the results of the fatigue life calculations presented in this test program may only be applicable to the specific geometries tested, this method is the most commonly used method to analyze and design these connection details. Since this method is the most commonly utilized method, the calculations of the fatigue life analysis method provide a fatigue life coefficient that can more readily be compared to other research results.

7.4 FATIGUE TEST RESULTS

The results of the fatigue testing will be presented in the remainder of this chapter. Similar to the order of the previous chapter, each test variable will be discussed beginning with the socket connection details, then continuing to the stiffened connection details, the UIT treated specimens and finally proceeding to the alternative connection details.

7.5 UNEQUAL LEG FILLET-WELDED SOCKET CONNECTION SPECIMENS

As mentioned in Chapter 6, the thin pole wall socket connection specimens were the control specimens for this test program. As the control specimens, the discussion of the results must begin with the results of these test specimens. The three series of unstiffened socket weld connections will be discussed as one group.

The typical failure of a fillet-welded socket connection detail was a crack through the wall of the pole, which followed the toe of the socket weld. This cracking initiated at the top of the test specimen, or at the extreme tension fiber. Pictures of a typical failure are shown in Figure 7.1 and Figure 7.2. The failure locations and crack surfaces agreed with the failures experienced by TxDOT under service conditions. Typically when a specimen was declared failed, the crack had extended to an approximate length of 5 to 8 inches and the crack had extended through an angle of approximately 50° to 90°. At this point, the majority of the fatigue life had been exhausted and the crack propagated quickly.

One of the primary objectives of this research program was to verify the results of the testing performed at Lehigh University. The results of the Lehigh University testing showed that an unequal leg fillet-welded socket connection would be categorized as a category E' detail.

As is evident from the S-N plot of Figure 7.3, the unstiffened socket connection details tested as a part of this program performed at or below the level of an E' detail. This confirms that the socket connection details are as poor in fatigue as Lehigh University had originally reported. The results of the fatigue testing are presented in Table 7.5 and a mean fatigue life coefficient, A_{average} , has been calculated for each series of test specimens.



Figure 7.1 Failure of Socket Weld Connection Specimen

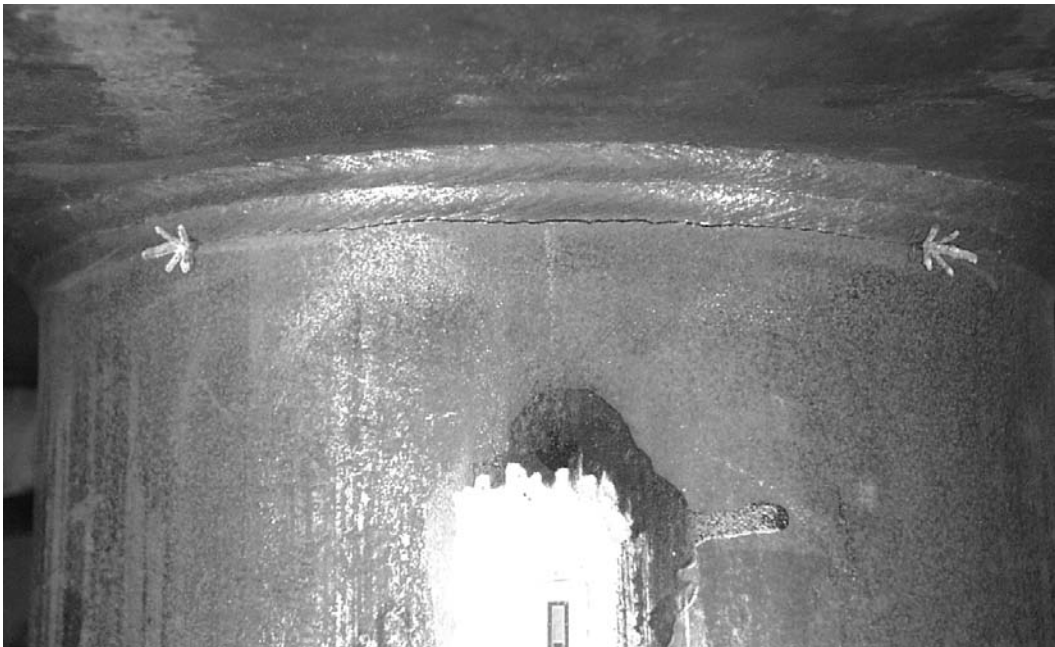


Figure 7.2 Failure of Socket Connection Specimen – Painted arrows indicate extents of visible cracking

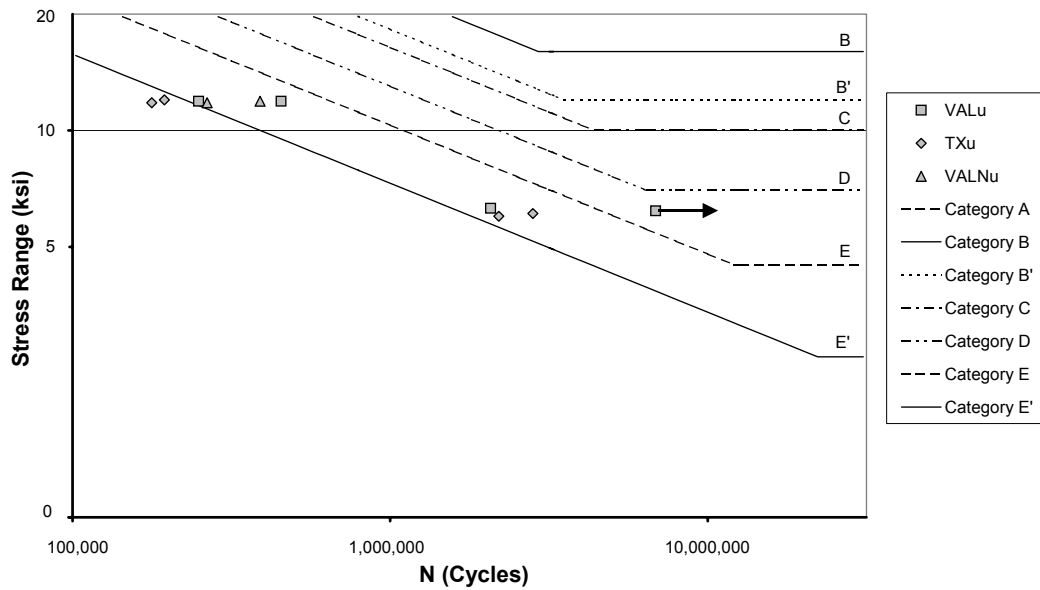


Figure 7.3 S-N Plot of Unstiffened Socket Connection Results

Table 7.5 Test Results and Calculated A Values for Socket Connection Details

Specimen Name	Number of Cycles	Stress Range (ksi)	A	A _{average}
VALu A	249,446	11.9	4.20	5.67
VALu B	453,948	11.9	7.65	
VALu C	2,072,592	6.3	5.17	
VALu D*	6,856,881	6.2	16.32	
VALNu A	389,428	11.9	6.56	4.36
VALNu B	265,540	11.8	4.36	
TXu A	2,199,343	6.0	4.75	5.46
TXu B	2,816,706	6.1	6.39	
TXu C	177,596	11.8	2.92	
TXu D	194,694	12.0	3.36	

* Testing Stopped – Run-Out

The testing of VALu D was stopped after reaching 6 million cycles as the specimen had reached a run-out condition. As the data for this test specimen does not represent a failure condition, the result has been excluded from the average A value calculation.

The three types of socket connection specimens tested illustrate two of the possible variables outlined in Chapter 3, Specimen Design. These two variables include the pole wall thickness and the influence of manufacturing location.

By comparison of the average A values in Table 7.5, it is apparent that an increase in the pole wall thickness reduces the anticipated fatigue life, as the average A coefficient was 5.67 for the VALu series and 4.36 for the TXu series of specimens. However, the difference between the coefficients is small, and due to the scatter of the test data, the influence of pole wall thickness cannot be classified as a significant factor.

When compared using the average A coefficient values, the second variable, manufacturing location, shows no effect on the fatigue life. The average A coefficient was 5.67 for the VALu series and 5.46 for the VALNu series of specimens. The agreement between the two series of tests also provides a method to correlate the results from Phase 1 of the test program with the results of Phase 2 of the test program. The overall agreement indicates that the results of the two phases can be compared directly, even though the test specimens from the two phases were fabricated at different facilities.

7.6 STIFFENED SPECIMENS

As much as possible, the results of the stiffened connection specimens will be discussed as a group. The results and behavior of the VALN 6x3/8@45 series specimens were dramatically different than the behavior of the remainder of the specimens. Based on this difference, the discussion of the fatigue testing of the stiffened connection details will be separated based on the orientation of the stiffeners.

The fatigue test results of the stiffened connection details are presented in Table 7.6. The average A coefficients for the socket connection specimens are also provided for comparison.

7.6.1 Vertical Stiffeners

From the values in Table 7.6, it is evident that all of the stiffener designs in which the stiffeners were oriented vertically provided increased fatigue life compared with the socket connection specimens. In other words, the stiffeners protected the socket weld.

The first observation of the fatigue testing was the location of the fatigue cracks in the test specimen. All stiffened test specimens experienced cracking at the termination of the stiffener. In a majority of the stiffened specimen, this was the only location of cracking at failure. However, in a few cases, cracks were visible at the toe of the socket weld, as well as at the termination of the stiffener.

In the specimens in which the cracking only occurred at the termination of the stiffener, the cracking initiated at the toe of the weld that wraps around the termination of the stiffener. This cracking then either followed the toe of the weld along the stiffener, or it branched out into the pole. Once the crack branched out into the pole, the crack propagation rate increased and the remaining fatigue life of the specimen was relatively short. The branching of the weld into the pole was taken as an indication of failure. The pictures in Figure 7.4 and Figure 7.5 show typical cracks observed at the termination of the stiffener. Figure 7.6 shows similar cracking, however the extent of the visible cracking is indicated by the painted lines. The picture in Figure 7.6 also shows that no cracking was evident at the toe of the socket weld in this specimen.

As previously mentioned, in a limited number of specimens, the cracking at the termination of the stiffener was accompanied by cracking at the toe of the socket weld. The cracking evident at the termination of the stiffener was similar to that described above. The cracking present at the toe of the socket weld was similar to that of a socket connection specimen, however due to the location of the stiffeners at the top of the connection detail, cracking did not initiate at the top of the tube section. Instead, the cracking initiated at the toe of the socket weld approximately 45° from vertical. The cracking then extended symmetrically in both directions, but the cracks did not propagate from the socket weld into the stiffener. Figure 7.7 and Figure 7.8 show typical crack patterns in stiffened connection details in which the cracking initiated at the toe of the socket weld and at the termination of the stiffener. The location of first crack initiation—the socket weld or the termination of the stiffener—was not observed during the testing.

Table 7.6 Fatigue Life Coefficients ‘A’ for Stiffened Connection Specimens

Specimen Name	Number of Cycles	Stress Range (ksi)	A	A_{average}
VAL _{u average}				5.67
VAL 3x1/4 A	476,269	11.1	6.51	8.33
VAL 3x1/4 B	696,326	11.4	10.32	
VAL 3x1/4 C	3,592,372	6.1	8.15	
VAL 3x3/8 A	386,253	11.7	6.19	6.30
VAL 3x3/8 B	410,410	11.6	6.41	
VAL 6x3/8 A**	242,728	11.2	3.41	8.40
VAL 6x3/8 B	653,392	11.3	9.43	
VAL 6x3/8 C	3,592,372	5.9	7.38	
VAL _{Nu average}				4.36
VALN 6x3/8@45 A	238,515	12.0	4.08	4.13
VALN 6x3/8@45 B	161,843	12.0	2.78	
VALN 6x3/8@45 C	6,066,817	4.3	4.82	
VALN 6x3/8@45 D	6,066,817	4.3	4.82	
TX _{u average}				5.46
TX 3x1/4 A	616,136	11.7	9.87	8.35
TX 3x1/4 B	416,146	11.8	6.84	
TX 3x1/4 C LMS	523,397	11.9	8.82	8.82
TX 3x3/8 A	473,735	11.7	7.59	8.93
TX 3x3/8 B	657,716	11.6	10.27	
TX 6x3/8 A	783,857	11.2	11.01	12.22
TX 6x3/8 B	783,857	11.3	11.31	
TX 6x3/8 C	7,503,037	5.8	14.32	

** Denotes failure due to lack of fusion weld defect.

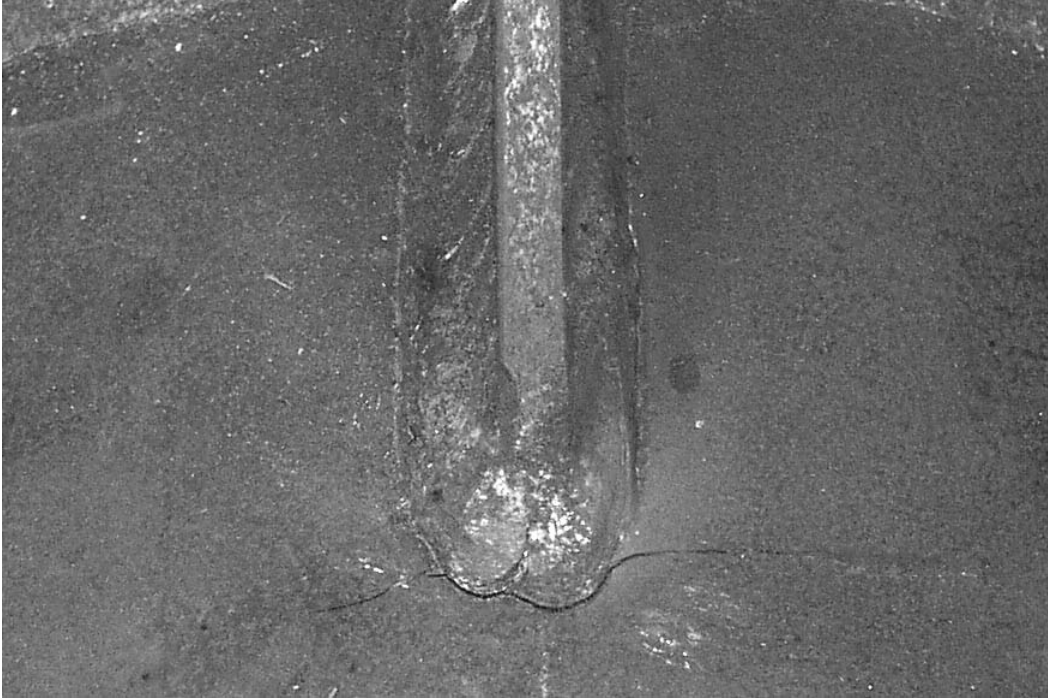


Figure 7.4 Failure of VAL 3x1/4 Specimen



Figure 7.5 Failure of VAL 6x3/8 Specimen



Figure 7.6 Failure of TX 3x3/8 Specimen – Note: Paint line represents extent of visible cracking

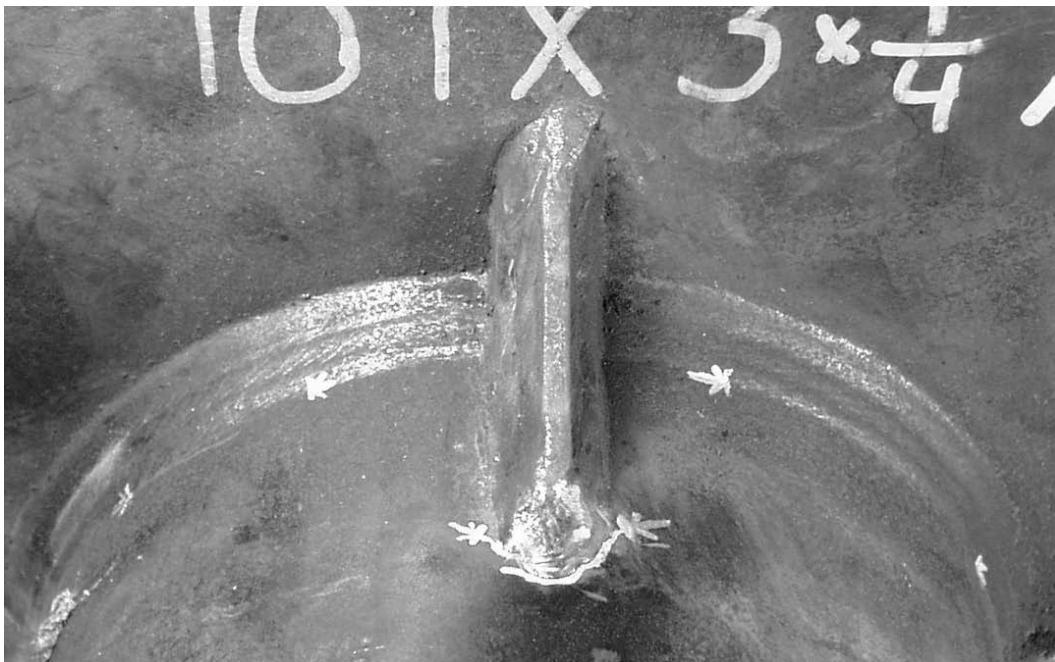


Figure 7.7 Failure of TX 3x1/4 Specimen – Note: Paint line at termination of stiffener represents extent of visible cracking, and painted arrows indicate visible crack tips in socket weld toe



Figure 7.8 Failure of VAL 3x1/4 Specimen – Note: Paint line at termination of stiffener represents extent of visible cracking, and painted arrows indicate visible crack tips in socket weld toe

The only specimen in this series not to fail due to cracking at the termination of the stiffener or socket weld was specimen VAL 6x3/8 A. This specimen failed due to lack of fusion in the stiffener to base plate weld. Upon investigation, the stiffener that failed was shown to have almost no fusion along the width of the stiffener. The number of cycles to failure is presented for this specimen; however, the results will not be used for any calculation or comparison.

In Chapter 3, the design process used to design the test specimen predicted that the failure location could potentially be different in each series of specimens. In the VAL series, the 3x3/8 stiffener was predicted to perform the best, with the design equations predicting a balanced failure condition in that the failure was as equally likely to occur at the socket weld as it was at the termination of the stiffener. The thinner stiffeners and longer stiffeners were predicted to provide an increased fatigue life, but yet not as much protection as the 3x3/8 stiffeners. The 3x1/4 stiffened specimens were expected to fail at the socket weld, and the 6x3/8 stiffeners were expected to fail at the termination of the stiffener.

The two common types of crack patterns evident in the vertically oriented stiffener specimens confirm, to a certain extent, the validity of the design process for this connection detail. As mentioned in the previous paragraphs, the 3x1/4 stiffened specimens were predicted to fail at the toe of the socket weld. While four out of the six of these specimens did experience cracking at the socket weld as is indicated in Table 7.1, cracking was also present at the termination of the stiffener at failure. The protection factor for these specimens, as reported in Chapter 3, are 0.60 for the VAL 3x1/4 series, 0.46 for the TX 3x1/4 series, and 0.69 for the TX 3x3/8 series.

From the lack of a consistent crack pattern trend, it is apparent that the significance of the protection factors was not entirely correct. The discussion above suggests that the protection factor must be significantly less than one, possibly on the order of 0.7, in order for cracking to occur at the toe of the socket weld. Values below this do not indicate that the toe of the socket weld will be the only location of cracking, and therefore the location of failure, but instead indicate that cracking may occur at the toe of

the socket weld, as well as at the termination of the stiffener. The low occurrence of cracking at the socket weld toe indicates that the stiffeners added to the socket connection detail do protect the socket weld better than predicted.

The protection factor concept did not work for all specimens in each series, as at least one specimen in each series with a protection factor less than 0.70 did not exhibit cracking at the socket weld. These specimens indicate an amount of scatter in the validity of the protection factor concept.

Even though the protection factors discussed in Chapter 3 did somewhat accurately indicate whether cracking would develop along the toe of the socket weld, the design equations did not accurately predict the location of crack initiation along the socket weld toe. In the design equations used to determine the protection factors, the potential for cracking is evaluated at the toe of the socket weld on the top chord of the pole, at the same location as the stiffener. However, the cracking along the toe of the socket weld in the stiffened specimens occurred at locations approximately 45° from the vertical axis of the pole. The design equations indicate that the stress at the location 45° from vertical is less than the stress along the top chord of the pole, so cracking initiation is not predicted in the region in which cracking did initiate. This inaccuracy is a further indication that the design equations do not accurately represent the behavior of the stiffened connection details.

Although the protection of the socket weld was to a limited extent confirmed, the predicted fatigue behavior of the stiffened connection details was shown to be inaccurate. Through comparison of the A constants for the VAL series of stiffeners, it is apparent that the 6x3/8 and 3x1/4 stiffeners exhibited the best fatigue life. These stiffeners provided an increase in the fatigue constant of just less than 50% of the socket connection values. As the fatigue life of a connection detail is directly proportional to the fatigue constant, the stiffeners provide a potential increase in the fatigue life of 50%. The 3x3/8 stiffeners provided a slight increase in the fatigue life compared with the socket connection details, however with the scatter in the data, the increase in fatigue life is negligible. The improvement due to the 6x3/8 stiffeners and the 3x1/4 stiffeners could be due to either the thickness of the stiffeners or the angle of incidence of the termination of the stiffener.

The average A constants for the TX series of stiffened specimens indicate a different trend compared to the VAL series of stiffeners. In the TX series, all stiffeners provided an improvement in the fatigue life of the connection detail. Specifically, the 3x3/8 stiffener details show a dramatic improvement in the fatigue life as compared with the same stiffener design in the VAL series of test specimens. The TX 6x3/8 stiffener series also shows a dramatic improvement in the fatigue life as compared with the similar stiffener design in the VAL series. The impact of the individual variables will be more thoroughly discussed in the following paragraphs.

In order to more clearly illustrate the importance of the thickness of the stiffeners, a ratio of the stiffener thickness to pole wall thickness was calculated for each set of stiffened specimens. The results of these calculations are presented in Table 7.7 along with the average calculated A value for each set of specimens. From comparing the results of only the 3" long stiffeners, it is clear that the stiffener thickness to pole wall ratio does influence the fatigue life of a connection detail. The data shows that fatigue life is greatly improved for stiffener designs with ratios less than or equal to approximately 1.5.

The improvement in the fatigue life due to the thinner stiffeners, or details with a stiffener to wall thickness ratio of 1.5 and lower, indicates that the fatigue life may be improved with a stiffener thickness that is closer to the thickness of the pole wall. In this situation, the stiffener is less likely to punch into or pull away from the pole wall causing a higher stress at the termination of the stiffener. To illustrate this point, in the case of a very thick stiffener, the stiffener would not deform as the pole wall deformed. This difference in stiffness would result in the stiffener punching into the pole wall. In the tension area of the connection detail, this effect would be visualized as the pole wall tearing away from the stiffener.

Table 7.7 Effect of Stiffener Thickness to Pole Wall Ratio, and Angle of Incidence of Stiffener on Fatigue Life

Specimen Series	Average A Constant	Stiffener Thickness to Pole Wall Thickness Ratio	Angle of Incidence of Termination of Stiffener (degrees)
VALu	5.67		
VALNu	5.46		
VAL 3x1/4	8.33	1.47	33.7
VAL 3x3/8	6.30	2.09	33.7
VAL 6x3/8	8.40	2.09	18.4
VALN 6x3/8@45	4.13	2.09	18.4
Txu	4.36		
TX 3x1/4	8.35	1.05	33.7
TX 3x3/8	8.93	1.57	33.7
TX 6x3/8	12.22	1.57	18.4

The improvement in the fatigue life that is provided by the longer stiffeners of this test program can be attributed to either the reduced angle of incidence at the termination of the stiffener, or the reduction of moment at the termination of the longer stiffeners. These two influences will be discussed separately in the following paragraphs.

The influence of the length of the stiffeners can be illustrated by comparing the angle of incidence of each of the stiffener designs. Table 7.7 shows the calculated angle of incidence at the termination of the stiffener of each specimen set. This angle of incidence is calculated as:

$$\alpha = \text{Tan}^{-1}\left(\frac{W}{L}\right)$$

Where L is the length of the stiffener along the pole, and W is the length of the stiffener along the base plate, which was a constant 2" for all stiffened specimens in this test program.

The results of the 3/8" thick stiffeners of both lengths indicate that the angle of incidence has a significant impact on the fatigue life of a connection detail. In both the VAL and TX series of specimens, the stiffeners with the lower angle of incidence exhibit a significant improvement in the fatigue life of the connection detail. This influence is independent of the stiffener thickness to pole wall thickness ratio, as even the VAL 6x3/8 specimens indicate an improved fatigue life when compared with the VAL 3x3/8 specimens. As discussed above, both of these stiffener designs have stiffener thickness to pole wall thickness ratios greater than 1.5, above which the stiffeners were shown to be less effective at increasing the fatigue life of the connection detail.

The improvement due to the reduced angle of incidence is in agreement with traditional concepts of fatigue design. Typically, a lower angle of contact between a stiffener and the main member will result in a lower stress concentration, and a favorable fatigue condition. The improvement of the 6x3/8 stiffeners appears to confirm this concept.

Along with the reduced angle of incidence, the length of the stiffener results in a reduction of the moment, and therefore the stress, at the termination of the stiffener. However, the impact of this reduction is relatively small as will be shown by evaluating the change in moment, or the shear, along the length of the pole.

The moment gradient range, or shear range, was 1.7 kip for the VAL series of specimens and 2.6 kip for the TX series of specimens. Based on these shear ranges, the change in stress range due to a 3" change in stiffener length is 0.4 ksi for both series of specimens. The 0.4 ksi stress range change is insignificant in the fatigue life equations. In an actual traffic signal mast-arm, the length of the arm is much longer and the shear, or moment gradient, is much lower, so the reduced stress due to a longer stiffener would be even less significant.

The fatigue results of the stiffened connection details are shown in S-N plots in Figure 7.9 and Figure 7.10. From these plots, it is clear that the stiffened specimens do improve the fatigue life, to a certain extent. However, the 3" long stiffened connection details are less than a category C detail as assumed in the specifications.

Also from the plots in Figure 7.9 and Figure 7.10, the 6x3/8 stiffeners appear to perform best. This is contrary to the specifications, which predict a shorter fatigue life. The plots indicate that the 6x3/8 stiffeners may be properly categorized, but the 3" long stiffeners are improperly categorized.

Based on the limited number of test results available, the best stiffener design appears to have a low ratio of the stiffener thickness to the pole wall thickness, and a small angle of incidence at the termination of the stiffener. These recommendations are not represented in the current specification. The thickness of the stiffener is addressed by limiting the length of the stiffener to 12 times the thickness of the stiffener, which is a limit based upon buckling of the stiffener. This limit, however, does not consider the impact of the ratio of the stiffener thickness to the pole wall thickness.

The current specifications also penalize longer stiffeners with a lower fatigue category. The test results show that the longer stiffeners perform better under fatigue loading, and therefore this penalty is not appropriate.

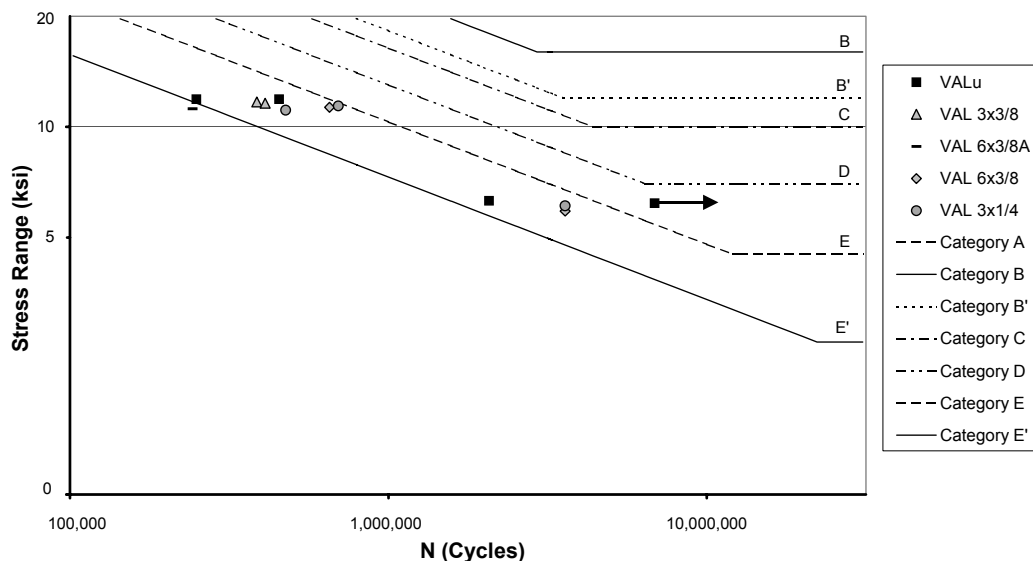


Figure 7.9 S-N Plot of Stiffened VAL (thin pole wall) Connection Results

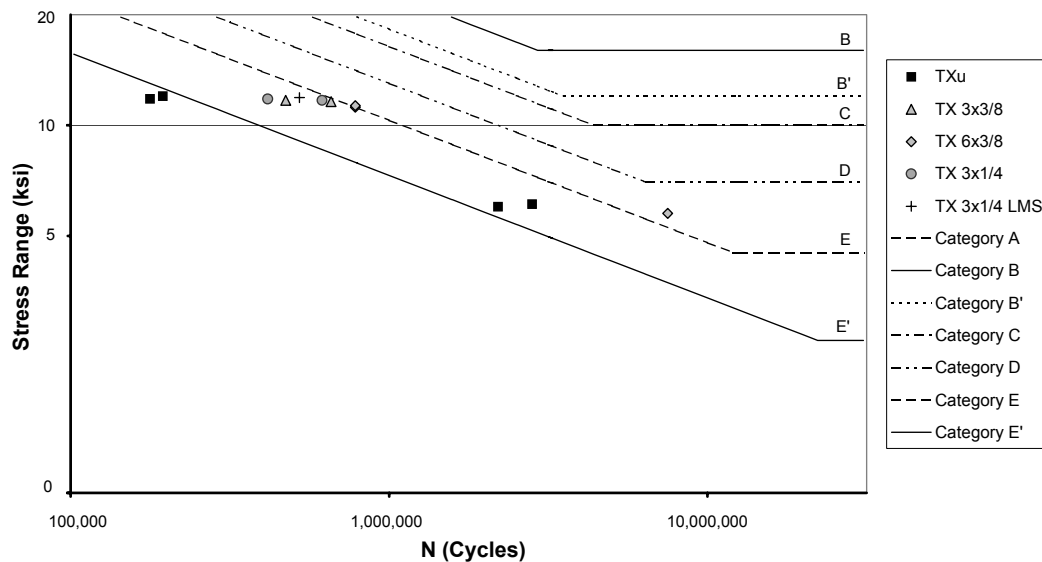


Figure 7.10 S-N Plot of Stiffened TX (thick pole wall) Connection Results

7.6.2 VALN 6x3/8@45 specimens

As stated at the beginning of Section 7.6, the connection details with the stiffeners offset by 45° from vertical behaved significantly different than the specimens with the stiffeners oriented vertically. Along with the difference in observed behavior, the results must also be carefully compared to the initial results so that the geometric properties do not lead to erroneous conclusions.

The cracking behavior of the 6x3/8@45 specimens was different in the two sets of test specimens. In the two specimens tested at a low nominal stress range of 6 ksi, the cracking initiated at the termination of the stiffener. This behavior was similar to the behavior of the vertically oriented stiffeners. The cracking at the termination of the stiffeners is shown in Figure 7.11. There was no visible cracking at the toe of the socket weld.

On the specimens tested at a nominal 12 ksi stress range, cracking was observed at the termination of the stiffeners, as well as at the toe of the socket weld. This cracking is shown in Figure 7.12. The location of first crack initiation was not observed during the fatigue test.

The protection factors presented in the specimen design chapter indicated that the failure of the offset stiffeners should have initiated at the socket weld. The specimens tested at the low stress range performed contrary to this prediction, and the specimens tested at the higher stress range did not completely fulfill this prediction as they exhibited cracking in both locations at relatively the same time.

The results of the VALN 6x3/8@45 series of specimens have already been presented in Table 7.6. However, the direct comparison of these results with the other results must be qualified with a brief discussion. Since the stiffeners are offset at 45° angles from vertical, the stress ranges at the termination of the stiffeners are lower than the stress ranges at the termination of the vertically oriented specimens. However, due to the failure observations, this was still a critical location. During the testing, the test load range was increased slightly for the VALN 6x3/8@45 specimens in an effort to create a stress range of 12 ksi at the termination of the stiffener. This increase in loading means that the testing conditions for the specimens of different stiffener orientations were not identical.



Figure 7.11 Failure of VALN 6x3/8@45 Specimen – Painted line indicates extent of visible cracking, specimen tested at 6 ksi stress range



Figure 7.12 Failure of VALN 6x3/8@45 Specimen – Paint lines at termination of stiffeners represent extents of visible cracking, and painted arrows indicate visible crack tips in socket weld toe, specimen tested at 12 ksi stress range

The reduced stress at the termination of the stiffener brings up a dilemma in the method of reporting the fatigue results. In the traditional manner of presenting fatigue results, the stress range at the critical location is used to determine the fatigue life. The results presented in Table 7.6 show the fatigue life as calculated following the standard method. The A coefficients presented in this table are much lower than the stiffeners with the vertical orientation. The offset stiffeners have an average fatigue constant of 4.13, which is less than the average fatigue constant for the unstiffened socket weld connection details. This indicates that the stiffened specimens performed worse than the unstiffened specimens, and did not protect the socket weld.

However, as mentioned above, there are several methods with which to look at the fatigue performance of the offset stiffeners. In order to compare the results with the results from the VAL 6x3/8 vertical stiffeners, the stress range calculated at the top of the test specimen, in the same location as the termination of a vertically oriented stiffener, must be used. Following this method, the fatigue life coefficients of the specimens improve dramatically. The resulting values are shown in Table 7.8. In this table, the average fatigue life coefficient for the offset stiffeners is shown to be 11.68, which is higher than that of the VAL 6x3/8 series (with vertically oriented stiffeners).

Table 7.8 Fatigue Life Coefficients, A, for 6x3/8 Stiffened Connection Based on the Stress Range at the Termination of a Vertical Stiffener

Specimen Name	Number of Cycles	Stress Range (ksi)	A	A_{average}
VAL 6x3/8 B	653,392	11.3	9.43	8.40
VAL 6x3/8 C	3,592,372	5.9	7.38	
VALN 6x3/8@45 A	238,515	17.1	11.86	11.68
VALN 6x3/8@45 B	161,843	17.1	8.08	
VALN 6x3/8@45 C	6,066,817	6.1	13.47	
VALN 6x3/8@45 D	6,066,817	6.0	13.32	

While the data in Table 7.6 and Table 7.8 can be manipulated to show either better or poorer fatigue performance, the value of using an offset stiffener connection detail will be discussed further in Chapter 8.

7.6.3 Protection of Socket Weld due to Addition of Stiffeners

In an effort to more fully convey the protection afforded to a socket weld by the addition of stiffeners, the fatigue results of specimen VAL 6x3/8 B are analyzed in the S-N plot of Figure 7.13. In this figure, the solid triangle represents the stress range at the termination of the stiffener, the solid square represents the calculated stress range at the socket weld assuming that the stiffener is fully effective, and the open square represents the calculated socket connection stress range without the addition of stiffeners.

The points in this plot show that the addition of the stiffeners reduces the calculated stress range at the socket weld from the open square to the solid square. Due to this reduction in stress, the solid square point falls below the E' curve, the fatigue life of a connection without stiffeners. Without the stiffeners the specimen would have failed at the E' line and would never have reached to the location on the plot which show it producing a fatigue life comparable to a category E detail.

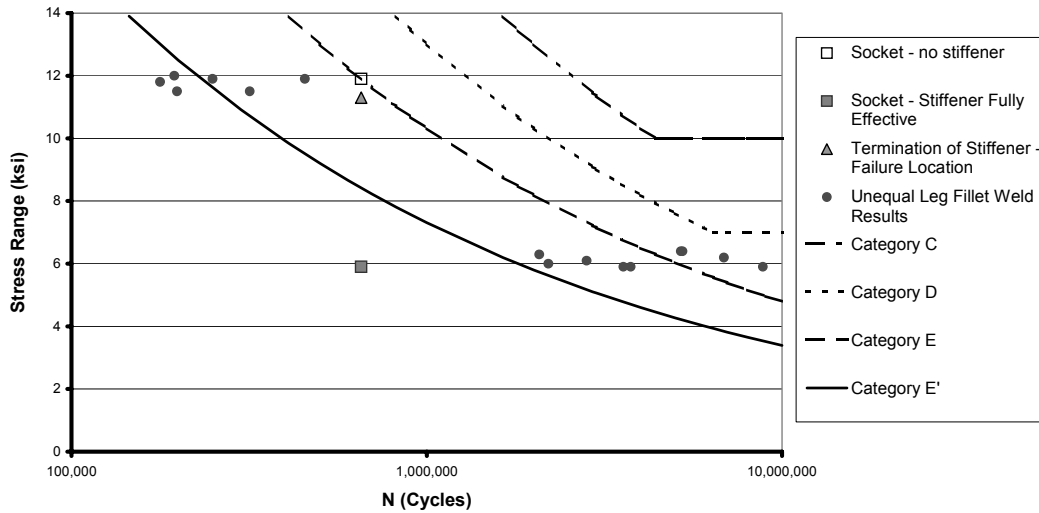


Figure 7.13 S-N Plot of Protection Provided by TX 6x3/8 Stiffeners – Plotted on a Semi-Log Plot

7.7 UIT WELD TREATED SPECIMENS

The discussion of the fatigue test results of the UIT treated specimens will be separated based on the two phases of the testing program.

7.7.1 Phase 1

As stated in Section 6.5.1, a total of six specimens were treated with the UIT weld treatment during Phase 1 of the test program. Two socket connection specimens and one stiffened specimen from each of the two pole wall thickness series, VAL and TX, were treated. These specimens were treated in an unloaded condition.

The fatigue test results of the Phase 1 UIT treated specimens are presented in Table 7.9. The average A values for the non-treated socket weld specimens are also included in this table for comparison. From this table it is clear that the UIT treatment did not have the desired effect of improving the fatigue life. In the unstiffened VALuP series, the specimens with the UIT treatment showed the same performance as the non-treated specimens and in the unstiffened TXuP series, the specimens with the UIT weld treatment exhibited slightly lower fatigue life performance than the non-treated specimens.

The performance of the VAL 3x3/8 CP specimen was also approximately equal to the non-treated VAL 3x3/8 specimens.

The UIT treated specimens failed in the same manner as a non-treated specimen – the visible cracks followed the toe of the socket weld. Two pictures of typical failures of UIT treated specimens are shown in Figure 7.14 and Figure 7.15. The failure occurred in the UIT treated region. Prior to the testing, the failure was expected to occur at another location, as the UIT weld treatment should have improved the weld toe region and forced the failure to the next critical location. The failure of the specimen in the UIT treated region was another indication that the UIT treatment was ineffective.

Table 7.9 Results Phase 1 – UIT Treated Specimen

Specimen Name	Number of Cycles	Stress Range (ksi)	A	A_{average}
VALu _{average}				5.67
VALNu _{average}				5.46
VALu EP	393,767	11.4	5.83	5.60
VALu FP	353,103	11.5	5.37	
TXu _{average}				4.36
TXu EP	320,915	11.8	5.27	3.77
TXu FP	141,155	11.7	2.26	
VAL 3x3/8				6.30
VAL 3x3/8 CP	393,767	11.5	5.99	5.68
VAL 3x3/8 CP(2)	353,103	11.5	5.37	
TX 3x3/8				8.93
TX 3x3/8 CP LMS	1,707,128	12.1	30.24	30.24

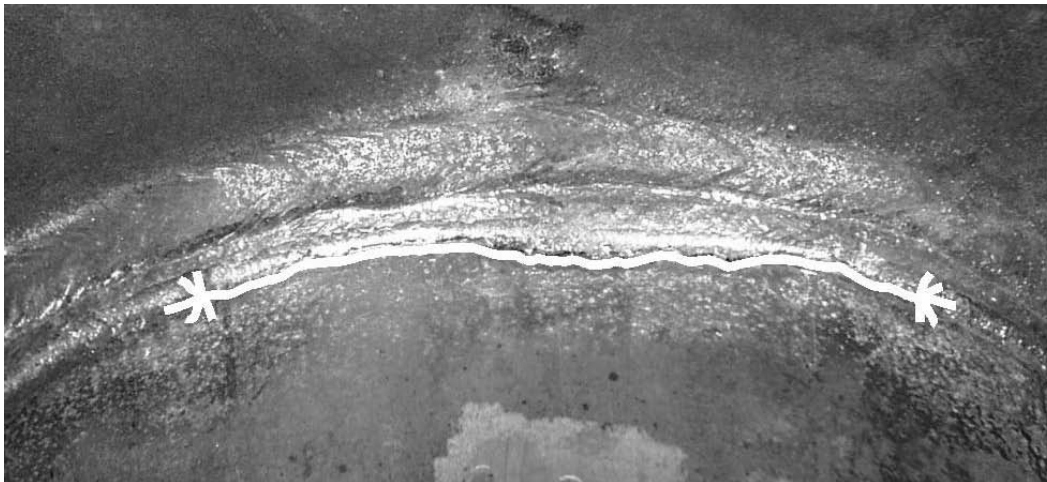


Figure 7.14 Failure of UIT Treated Socket Connection Specimen – Painted line indicates extent of visible cracking



Figure 7.15 Failure of UIT Treated Socket Connection Specimen

The lower or equal levels of fatigue life performance were contrary to the expected improvement in the fatigue life. The representatives from Applied Ultrasonics felt that the high mean stress of our testing procedure was eliminating the local residual compressive stresses and therefore making the UIT treatment ineffective. In an attempt to confirm this concept, the final UIT treated stiffened specimen, TX 3x3/8 CP, was tested at a low mean stress.

As mentioned previously in the test setup design chapter, the test setup could not be used in compression as the setup lacked lateral stability. Ideally, the TX 3x3/8 CP specimen would have been tested at a zero mean stress. Due to the limitations of the testing setup, the test was performed at the lowest reasonable mean stress of 8 ksi. At this mean stress, the testing ranged from 2 ksi to 14 ksi.

The specimen tested with specimen TX 3x3/8 CP was specimen TX 3x1/4 C. To distinguish the low mean stress testing method used for these specimens, the specimen labels were extended to include LMS, which stands for Low Mean Stress. The use of TX 3x1/4 C LMS allowed for comparison of the low mean stress testing method with a non-treated stiffened connection specimen.

The results of these two test specimens are presented in Table 7.10. From this table, it is evident that the fatigue life of the TX 3x1/4 C specimen was not significantly influenced by the low mean stress test method. Although the table shows that the calculated fatigue constant is slightly higher for this specimen as compared with the average of the remaining TX 3x1/4 specimens, the increase is insignificant with regard to fatigue design.

Table 7.10 Results Phase 1 – LMS UIT Treated Stiffened Specimens

Specimen Name	Number of Cycles	Stress Range (ksi)	A	A _{average}
TX 3x3/8				8.93
TX 3x3/8 CP LMS	1,707,128	12.1	30.24	30.24
TX 3x1/4				6.81
TX 3x1/4 C LMS	523,397	11.7	8.39	8.39

Contrary to the lack of influence on the non-treated stiffened test specimen, the low mean stress had a significant influence on the fatigue performance of the UIT treated specimen. The fatigue life coefficient values in Table 7.10 show that the calculated A coefficient for the TX 3x3/8 CP specimen was approximately 30, which means that the detail would be classified as a category D detail. This represents a significant improvement in the fatigue life of a structure. The category D fatigue categorization of this specimen and the significant fatigue life improvement are evident in the S-N plot in Figure 7.16.

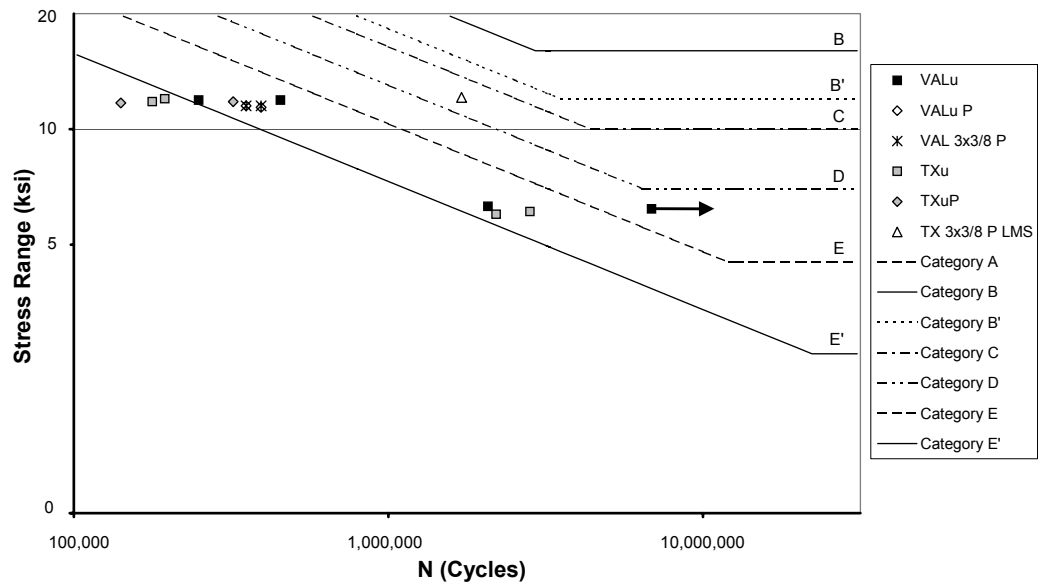


Figure 7.16 S-N Plot of Results of UIT Treated Specimens - Phase 1

The cracking of the TX 3x3/8 CP specimen initiated at the toe of the socket weld, which was not treated with the UIT treatment. This initial crack location indicates that the UIT weld treatment improved the fatigue performance of the treated area around the stiffener, such that the critical location was changed from the termination of the stiffener to the toe of the socket weld. After further testing, cracking initiated in the treated region at the termination of the stiffener. The specimen was declared failed once the cracking at the termination of the stiffener had propagated to the typical distance. Figure 7.17 shows the visible cracking of specimen TX 3x3/8 CP.

The results of TX 3x3/8 CP were the most positive indication of fatigue life improvement of all of the specimens tested during Phase 1. Based on the very positive result, the Phase 2 testing of UIT treated specimens was designed to take advantage of the improvement at zero mean stress.



Figure 7.17 Failure of TX 3x3/8 CP Specimen – Note: Paint lines represent extent of visible cracking at termination of stiffener and socket weld toe

7.7.2 Phase 2

Based on the positive results of the low mean stress test, the Phase 2 UIT treatment specimens were designed and treated as described in Chapter 3. The difference between the maximum stress and treatment stress of the positive test result from Phase 1 was much lower than for the other UIT treated specimens tested during Phase 1. Quantitatively, the maximum stress for the improved fatigue life specimen was 14 ksi, and since the treatment was performed under zero load, the difference between the maximum stress and the treatment stress was 14 ksi. For the other UIT treated specimens of Phase 1, this difference was 28 ksi or 28.5 ksi.

In order to duplicate the low difference between the maximum stress and treatment stress of the successful UIT treated specimen, without lowering the maximum stress, the treatment stress was elevated. For the UIT treated specimens of Phase 2, the treatment was performed under an imposed dead load that resulted in a stress of 16.5 ksi in the treatment region. The stress at the maximum test load for this series of specimens was 28.5 ksi, resulting in a difference between the maximum stress and the treatment stress of 12 ksi. The treatment of the Phase 2 specimens at dead load reduced the difference between the maximum stress and treatment stress such that the specimen performed as though tested at low mean stress.

Although all of the Phase 2 UIT treated specimens were treated at the same minimum load, the treatment conditions and fatigue life improvement of each set of specimens were dramatically different. Based on these differences, the results of each set of test specimens will be addressed separately.

7.7.2.1 UIT Retrofit

After the UIT weld treatment process was completed on both test specimens, the specimens were cycled through a short static test to reconfirm the loads and displacements that were to be the limits of the dynamic testing. Due to the reduction of the loads during the UIT process, the displacements determined during the post-treatment static test did not exactly correspond with the displacements determined during the initial static test for the same desired loads. To eliminate any inconsistencies which might arise due to this discrepancy, the fatigue testing was performed under the displacements determined during the initial static test. Therefore, the loads used in the fatigue testing were slightly lower than the desired loads from the initial static test.

The testing of both of the VALNu PR specimens was stopped after reaching 4.5 million cycles, and the specimens were declared to have experienced run out. The results of the UIT Retrofit specimens are presented in Table 7.11 along with the average A coefficient values of the non-treated socket weld connection details. The values for the fatigue life coefficient, A, presented in this table must be accepted with the qualification that these A values do not represent a failure condition, but instead represent the limit of the run out condition. In other words, the true A value may be higher for these specimens, as the tests were stopped prior to failure due to testing limitations. Even with this qualification, the results demonstrate a remarkable improvement in the fatigue life of a typical socket connection detail. The improvement is evident in the S-N plot of Figure 7.18.

After the testing was stopped at run out, these test specimens were later reinstalled into the test setup to be tested against another test specimen. At this point, the specimens had been unloaded and did not necessarily represent the same retrofit condition. Both specimens failed after approximately a half million additional cycles. In order to distinguish that these specimens had been unloaded, the specimen names were extended to VALNu PR ul A and VALNu PR ul B, where the ul indicates that the test specimens had been unloaded.

The VALNu PR ul specimens both failed due to cracking at the toe of the socket weld. The cracking occurred in the area of the UIT weld treatment. A typical crack in a VALNu PR ul specimen is shown in Figure 7.19.

Table 7.11 Results Phase 2 – UIT Treated Specimen

Specimen Name	Number of Cycles	Stress Range (ksi)	A	A_{average}
VALu _{average}				5.67
VALNu _{average}				5.46
VALNu PR A*	4,557,126	11.6	71.13	70.22
VALNu PR B*	4,557,126	11.5	69.31	
VALNu PR ul A	5,004,729	11.6	78.12	80.43
VALNu PR ul B	5,440,165	11.5	82.74	
VALNu GP A	4,545,952	11.6	70.96	44.33
VALNu GP B	224,240	19.9	17.70	
VALNu PG A	277,634	11.6	4.33	4.55
VALNu PG B	313,727	11.5	4.77	
VALNu CP	1,301,077	19.9	103.29	103.29

*Testing Stopped – Run Out

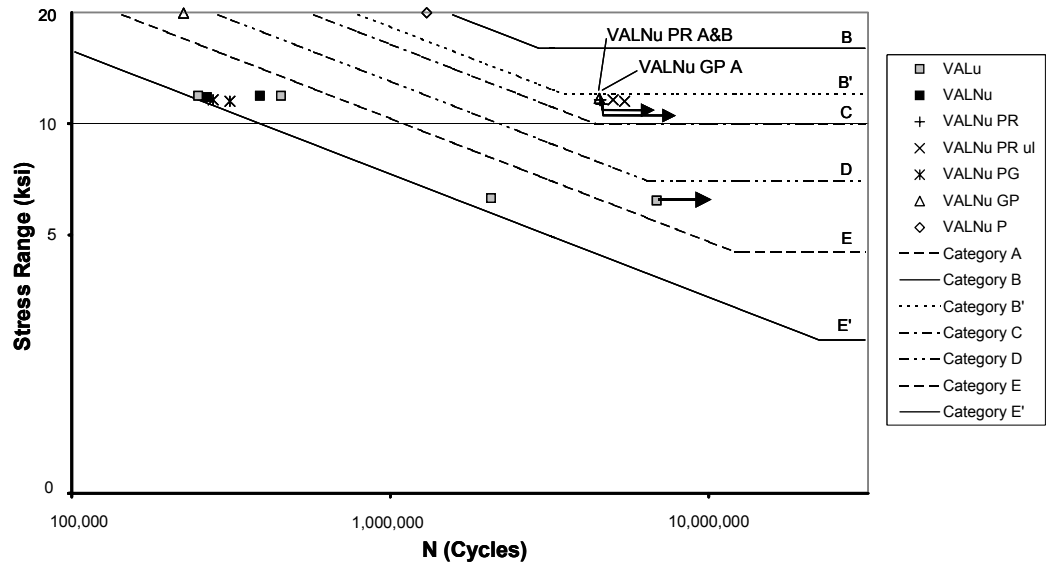


Figure 7.18 S-N Plot of UIT Specimen Phase 2



Figure 7.19 Failure of UIT Retrofit Specimen after Unloading and Retesting – VALNu PR ul Specimen

The results for these specimens after they had been unloaded and retested are presented in Table 7.12. The A value in this table does represent a failure location, and the results still indicate a significant fatigue life performance over the typical socket connection detail as is shown in the S-N plot of Figure 7.18.

The effect on the fatigue life of unloading these two specimens prior to failure is not clear. In the test cycles accumulated after unloading, the residual stress in the UIT treated region may be different than the residual stresses prior to unloading. It is not clear whether the cycles accumulated prior to the unloading should be used in the fatigue life coefficient calculation. The results of the fatigue life coefficient calculation including and excluding the cycles accumulated prior to unloading are presented in Table 7.12. From this table, it is clear that whether the cycles accumulated prior to unloading are included or not, the results show an improved fatigue life due to the UIT treatment.

Table 7.12 Results VALNu PR ul Specimens

Specimen Name	Number of Cycles	Stress Range (ksi)	A	A_{average}
VALu _{average}				5.67
VALNu _{average}				5.46
Results – Including Cycles Accumulated Prior to Unloading				
VALNu PR ul A	5,004,729	11.6	78.12	80.43
VALNu PR ul B	5,440,165	11.5	82.74	
Results – Excluding Cycles Accumulated Prior to Unloading				
VALNu PR ul A	447,600	11.6	6.99	10.21
VALNu PR ul B	883,039	11.5	13.43	

7.7.2.2 Fabrication Method – Galvanized Prior to UIT – VALNu GP series

Based on the significant fatigue life improvement observed in the VALNu PR series specimens, the two specimens of the VALNu GP series were not tested together. Instead, specimen VALNu GP A was tested at the standard 12 ksi stress range, and the second specimen, VALNu GP B was tested at a higher 20 ksi stress range. This higher stress range was selected to provide a shorter testing time period in case the first specimen reached a run out condition. See Section 7.7.2.4 for a more thorough discussion of the 20 ksi stress range test conditions.

The failure of these specimens was due to a crack that formed in the UIT treated area at the toe of the socket weld. The picture in Figure 7.19 shows the crack location that was typical for both specimens in this set.

The results of the fatigue testing for these specimens are shown in Table 7.11. Although specimen VALNu GP A exceeded 4.5 million cycles, which was taken as the run out limit for the retrofit specimens, a fatigue failure occurred in the specimen. The number of cycles at the failure of this specimen was just below the number of cycles at which the retrofit test was stopped. This test result indicates that the UIT treatment after galvanizing improved the fatigue life at the connection detail from a category E' detail to a category B' detail. This represents a significant improvement in the fatigue life of a connection detail.



Figure 7.20 Failure of Specimen VALNu GP B - Arrow points to weld start/stop in critical location

The results of the testing of VALNu GP B indicate a lower level of fatigue life improvement. The low fatigue life may be due to a poor start/stop weld geometry located at the toe of the socket weld in the location of the highest tensile stress. A picture of the weld is shown in Figure 7.20. The fatigue life of this specimen without the UIT treatment would probably have been much less than the other socketed specimens. Even with the poor start/stop weld geometry, the fatigue life of this connection detail was improved to a category D detail under a very high stress range loading condition.

Together, the test results show that the fatigue category of a typical socket connection detail can be improved from a category E' detail to either a category D or category B' detail. In either case, the use of the UIT treatment significantly improved the fatigue life of the connection detail. This improvement is further illustrated in Figure 7.18, which shows an S-N plot of the results of the UIT treated specimens compared with the untreated socket connection specimens. Although these specimens lie below the Constant Amplitude Fatigue Limit for the B' category, if the line is extended downward, the data point for VALNu GP A is beyond the extended line.

7.7.2.3 Fabrication Method – UIT prior to galvanization. VALNu PG series

Both of the VALNu PG specimens failed due to cracking through the UIT treated area at the toe of the socket weld. A picture of the typical cracking of these specimens is included in Figure 7.21.

The results of the fatigue testing are shown in Table 7.11. The results show that this method of weld treatment prior to the galvanizing process was not effective in improving the fatigue life of the socket connection detail. The calculated A values for these two specimens were lower than the values calculated for the untreated socket connection detail; however, the results are slightly higher than those of the VALNu G series, which will be discussed in Section 7.8.2. The difference between the average A constant for the VALNu PG series and the VALNu series is not significant in terms of the fatigue life of the structure. This indicates that performing the UIT process prior to galvanizing is not an effective method of improving fatigue life.

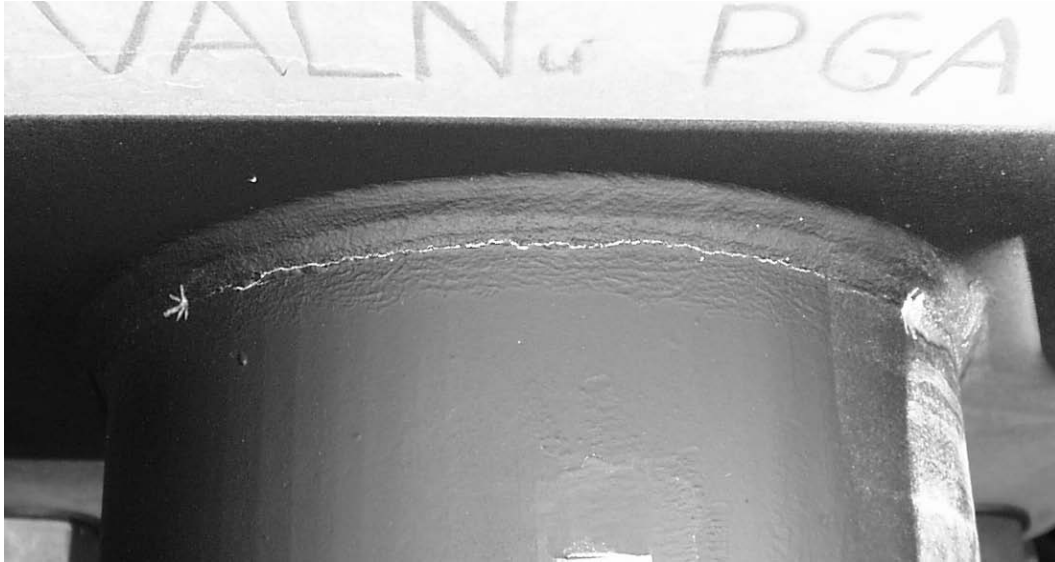


Figure 7.21 Failure of UIT Prior to Galvanization Specimen

7.7.2.4 Specimen VALNu CP

The desired stress range for the testing of VALNu CP and VALNu GP B was set at 20 ksi nominal. In previous tests in which the stress range was reduced, the minimum test load was held constant and the maximum test load was reduced to the appropriate level. However, if this same precedent were followed in the case of the 20 ksi stress range, the maximum stress at the critical connection would be approximately 36 ksi. While this is still well below the yield strength of that material, it was deemed to be too high for this testing. Instead of adjusting the maximum load, it was decided to keep the maximum load constant and reduce the minimum load to create the desired stress range. Based on this decision, the test range for these test specimens was from 8.5 ksi to 28.5 ksi, and the mean stress was 18.5 ksi.

The result of the fatigue test of this specimen is presented in Table 7.14. From this table, it is apparent that the UIT weld treatment of this specimen significantly increased the fatigue life of the socket connection detail. The improvement can also be observed in the S-N plot of the Phase 2 UIT treated connection details presented in Figure 7.18. The UIT weld treatment improved the connection detail from a category E' detail to a category B' detail, which indicates a significant improvement in fatigue life.

Although this particular specimen does not demonstrate the direct application to a fabrication or retrofit procedure that the remaining UIT treated specimens of Phase 2 exhibited, there are several important observations from this specimen.

First, the improvement of the fatigue category to category B' indicates that the test result of VALNu GP B may have been significantly influenced by the start/stop weld geometry in the critical location.

Secondly, the improvement exhibited by the UIT treatment process, which was performed by someone with very little training, indicates that the UIT process is not very sensitive to operator skill. The simplicity of the UIT process increases the value of this treatment procedure.

7.8 MISCELLANEOUS CONNECTION DETAILS AND VARIABLES

During the testing of Phase 2, a large variety of variables and alternative connection details were tested. The test results that did not fit into the previous discussions will be discussed in this section. Each variable or alternative connection detail will be discussed in a separate sub-section.

7.8.1 Base Plate Thickness: VALNu 2 Series

The two specimens with the 2" thick base plate exhibited a dramatic improvement in the fatigue life as compared with the socket connection specimens with the 1.5" thick base plate. Both of these specimens failed at the toe of the socket weld, which is the same failure location as the socket connection specimens with the 1.5" thick base plate.

The results of these tests are presented in Table 7.13 and shown in an S-N plot in Figure 7.22. The results of the two specimens exhibit a large amount of scatter, with the calculated fatigue constants ranging between 28 and 87. However, both of these exhibit an improvement in the fatigue categorization from an E' detail to a category D or B' detail, respectively. If the mean average A value is used, the connection detail is a category C detail.

Table 7.13 Results of Base Plate Thickness Variable

Specimen Name	Number of Cycles	Stress Range (ksi)	A	A _{average}
VALu _{average}				5.67
VALNu _{average}				5.46
VALNu 2 A	5,144,528	11.9	86.69	57.17
VALNu 2 B	1,683,127	11.8	27.65	

The results of the fatigue tests were very surprising. The current AASHTO specification does not include the thickness of the base plate as one of the factors that determines the fatigue categorization of the detail. Based on the specification, the test specimens with the 1.5" thick base plates and the 2" thick base plates should have exhibited the same performance. The factors that lead to an improved fatigue life due to the thickness of the base plate are not fully understood.

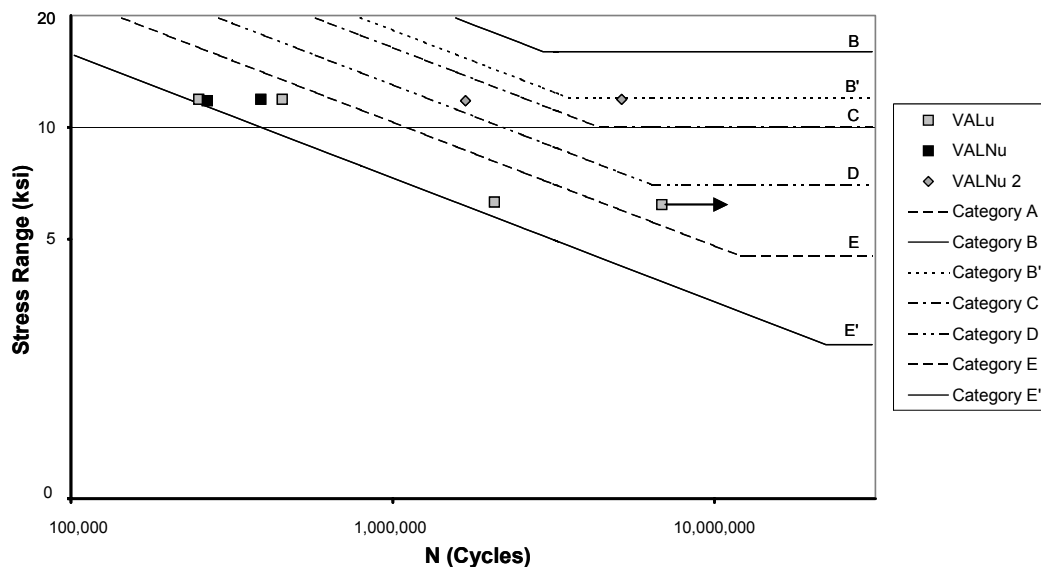


Figure 7.22 S-N Plot of Base Plate Thickness Variable

7.8.2 Galvanizing: VALNu G Series

The results of the fatigue testing indicate that the galvanization has a negative influence on the fatigue life of a socket connection detail. The VALNu G specimens failed in the same manner as the ungalvanized socket connection specimens – cracking initiated in the toe of the socket weld. The results of this testing are presented in Table 7.14 and shown in an S-N plot in Figure 7.23. From Table 7.14, the average calculated A value is 2.58. This value is approximately half of the value of the ungalvanized socket connection specimens tested and indicates that the estimated fatigue life would be approximately half the life of an ungalvanized socket connection detail.

These test results are disconcerting, as they indicate that the galvanizing will reduce the fatigue life of a traffic signal mast-arm structure. As almost all traffic signal structures in use are galvanized, this would imply that the expected fatigue life of any connection detail used in service would be less than the fatigue life predicted according to the results of this test. This is a non-conservative adjustment to the test results.

This test result also indicates that the UIT treatment schemes tested in Phase 2 provide an even greater fatigue life improvement when compared to the results from the VALNu G series, which were lower than the non-coated socket connection results used for comparison in Section 7.7.2.

Table 7.14 Results of Galvanized Specimens

Specimen Name	Number of Cycles	Stress Range (ksi)	A	A _{average}
VAL _u average				5.67
VALNu average				5.46
VALNu G A	183,132	11.6	2.86	2.58
VALNu G B	151,679	11.5	2.31	

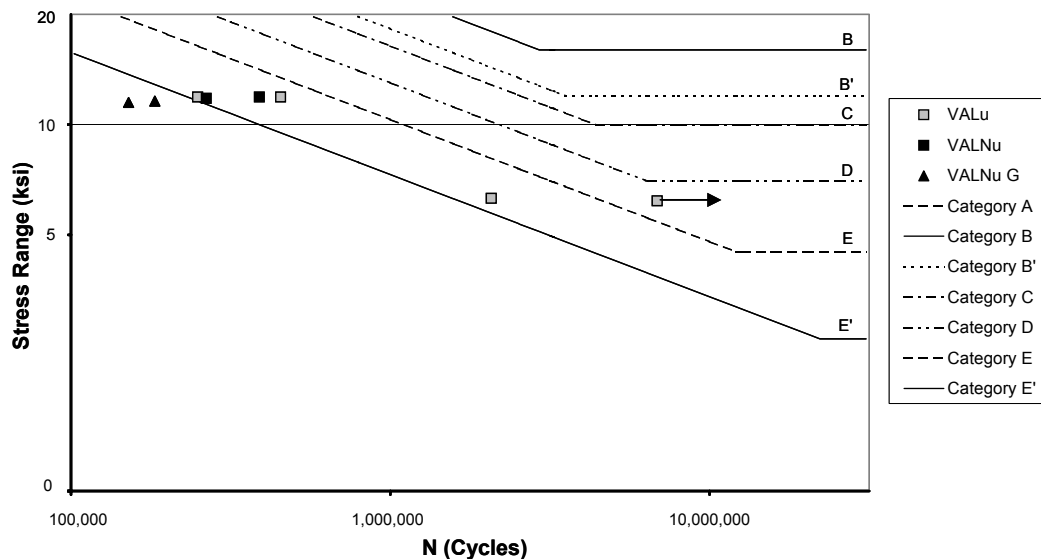


Figure 7.23 S-N Plot of Influence of Galvanizing

7.8.3 U-Rib Stiffener Connection – VALN UR Series

Although only two U-Rib stiffened specimens were fabricated for this testing program, three fatigue tests were performed on these two specimens by rotating a specimen after one stiffener failed. The results from these three tests are presented in Table 7.15.

Table 7.15 Results of U-Rib Stiffened Specimens

Specimen Name	Number of Cycles	Stress Range (ksi)	A	A _{average}
VALu _{average}				5.67
VALNu _{average}				5.46
VALN UR A (#4)	1,776,724	7.6	7.85	6.25
VALN UR B (#1)	950,670	7.6	4.17	
VALN UR B (#2)	339,152	12.6	6.73	

The failures in the U-Rib stiffeners occurred in the stiffener to base plate weld. A picture of a typical failure is shown in Figure 7.24, and a close-up of the crack is shown in Figure 7.25. As is evident from the pictures, the U-Rib stiffeners are very thin, which makes the weld in this location very susceptible to failure.

During the propagation of the fatigue cracking, the location of the crack initiation provided an important observation in that the cracking did not occur at the termination of the stiffener. In a typical stiffener design, the cracking initiated at the termination of the stiffener, and quickly propagated through the wall of the pole. In the U-Rib stiffeners, since the crack initiated between the stiffener and the base plate, it did not lead to a quick failure. Instead, the stiffener provided a type of redundancy, as once one leg of the stiffener cracked; the cracking did not propagate far before the other leg of the stiffener cracked as well. The cracking also tended to propagate fairly slowly after the initiation of visible cracking. A true failure did not occur until the cracking had propagated the entire length of the leg of the stiffener and had entered the socket weld. Until this point, the connection detail performed very well.

The results from Table 7.15 indicate that the U-Rib specimen does not provide a significant improvement to the fatigue life over an unstiffened socket connection detail. From the S-N plot in Figure 7.26, it is clear that the U-Rib specimen would be classified as a category E' detail. The value of the U-Rib stiffeners will be re-evaluated in Chapter 8 by using the value based design analysis method.



Figure 7.24 Failure of U-Rib Stiffened Specimen – Note: Painted lines represent extent of visible cracking



Figure 7.25 Failure of U-Rib Stiffened Specimen

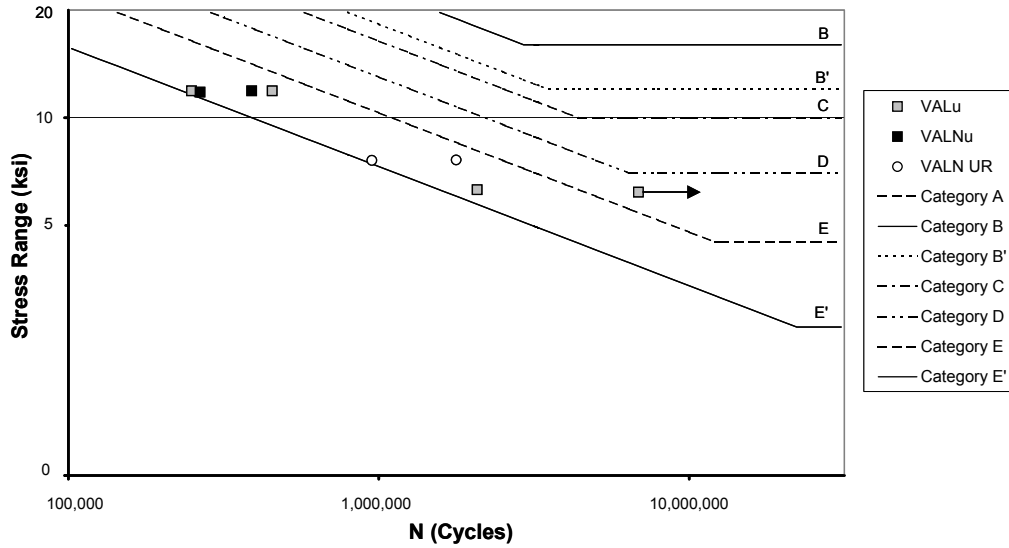


Figure 7.26 S-N Plot of Results of U-Rib Stiffened Specimens

7.8.4 External Collar Connection Detail – VALN Col Series

Prior to the start of the fatigue testing, the critical location, or the location of failure, for these test specimens was not clearly known. Each specimen may fail at the toe of the collar to pole weld, or at the toe of the collar to base plate weld. The collar to base plate weld proved to be the critical location as cracking developed in this region, as shown in Figure 7.27. After removing the specimen from the test setup, another crack was observed through the fillet weld on the inside of the base plate that connects the end of the tube to the base plate. This cracking is shown in Figure 7.28. The externally stiffened specimens were the only specimens to exhibit cracking in this location.



Figure 7.27 Failure of Externally Stiffened Collar Specimen



Figure 7.28 Crack Observed in Interior Weld of External Collar Stiffened Specimen

The fatigue test results of the external collar stiffened specimens are presented in Table 7.16. From this table, the average fatigue life coefficient for this connection detail is 5.7, which means that this connection detail is a category E' detail. The results of these tests are plotted in an S-N plot in Figure 7.29. The S-N plot of Figure 7.29 indicates that this connection detail does not appear to provide any benefit to the connection detail. The larger section properties, however will provide an increased fatigue life over an unstiffened socket connection for the same moment range, as will be illustrated through the value based design analysis method in Chapter 8.

The static tests for these specimens indicated that the collar is not fully effective, as was assumed in the stress range calculations. In the fatigue life analysis method, the effectiveness of the collar, as well as any stress concentrations, are accounted for in the A coefficient. The shortcoming of this method is that the determined A coefficient is only valid for collars of similar geometries. For example, a shorter collar will be less effective, and a longer collar will be more effective. In either of these cases, the accuracy of a solution using the same fatigue life coefficient in the analysis method is not guaranteed.

Table 7.16 Results of External Collar Stiffened Specimens

Specimen Name	Number of Cycles	Stress Range (ksi)	A	A_{average}
VALu _{average}				5.67
VALNu _{average}				5.46
VALN Col A	4,245,460	5.5	7.01	5.73
VALN Col B	2,363,152	5.7	4.45	

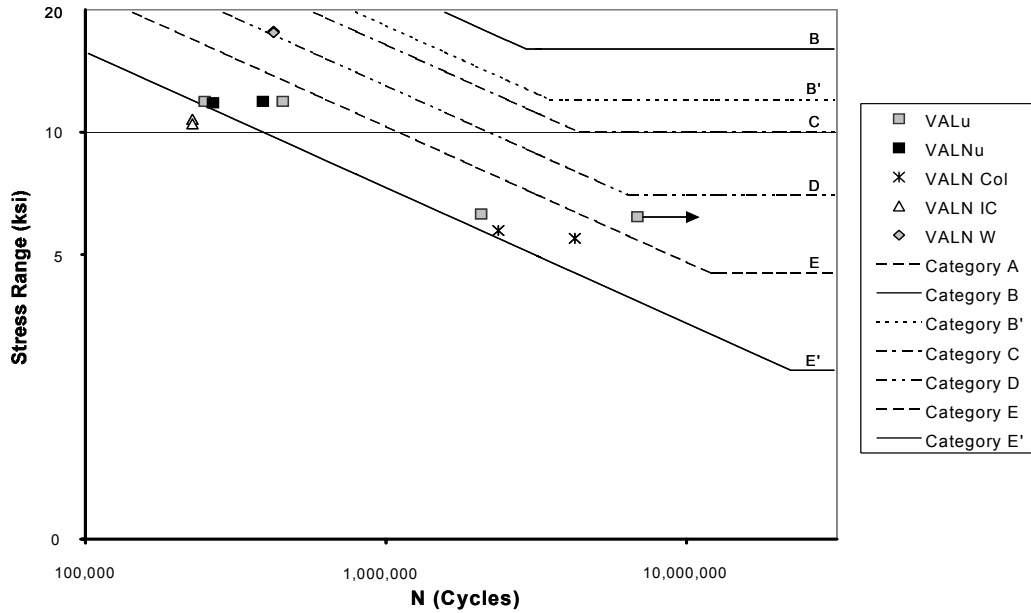


Figure 7.29 S-N Plot of Results of Alternative Connection Specimens

7.8.5 Internal Collar Connection Detail – VALN IC Series

During the fatigue testing of these two specimens, the specimens failed from cracking along the toe of the full-penetration weld between the tube and the base plate. A typical crack for this specimen is shown in Figure 7.30.

The non-linearity of the strain vs. load relation, which was discussed in Section 6.6.5, presented difficulties in determining the proper stress range for the analysis of the results of these specimens. The static test indicated that the internal collar was effective, but was not fully effective. This means that a stress calculation based on the nominal section properties, which assumes that the collar is fully effective, will underestimate the stress at the critical weld location. This will result in a higher value for the fatigue life coefficient.

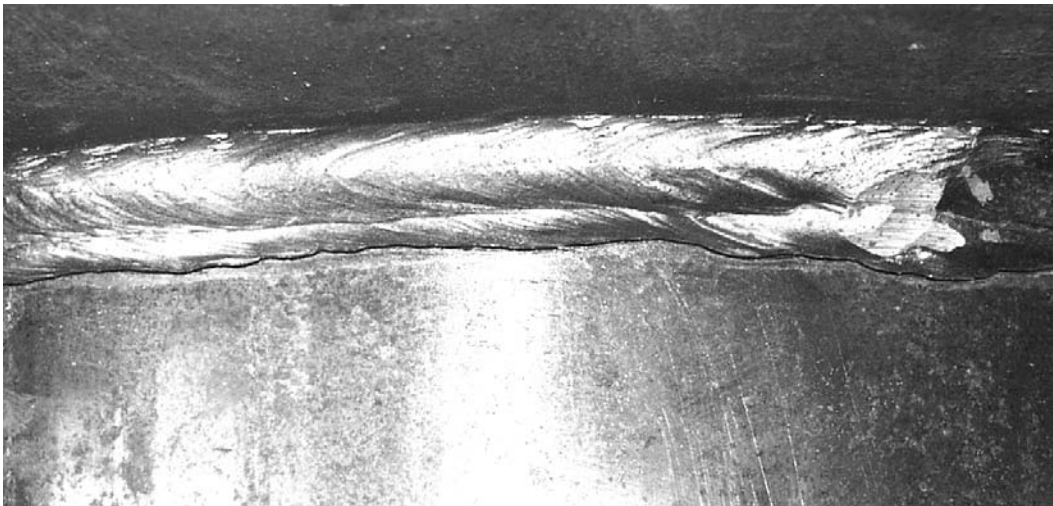


Figure 7.30 Failure of Internal Collar Stiffened Specimen

The results of the fatigue testing are presented in Table 7.1. This table shows that the performance of the internal collar detail was very poor. With an average calculated fatigue life coefficient, A , value of 2.8, this connection detail would be classified as less than a category E' detail. The possible benefits of using this connection detail will be further evaluated in Chapter 8.

Table 7.17 Results of Internal Collar Stiffened Specimens

Specimen Name	Number of Cycles	Stress Range (ksi)	A	A_{average}
VALu _{average}				5.67
VALNu _{average}				5.46
VALN IC A	227,030	10.8	2.82	2.80
VALN IC B	227,030	10.7	2.77	

7.8.6 Full-Penetration Weld Detail – VALN W Series

The VALN W series specimens failed due to a crack at the toe of the full-penetration weld. Two pictures of typical failures are shown in Figure 7.31 and Figure 7.32.



Figure 7.31 Failure of Full-Penetration Welded Connection Detail Specimen – Paint arrows indicate extent of visible cracking

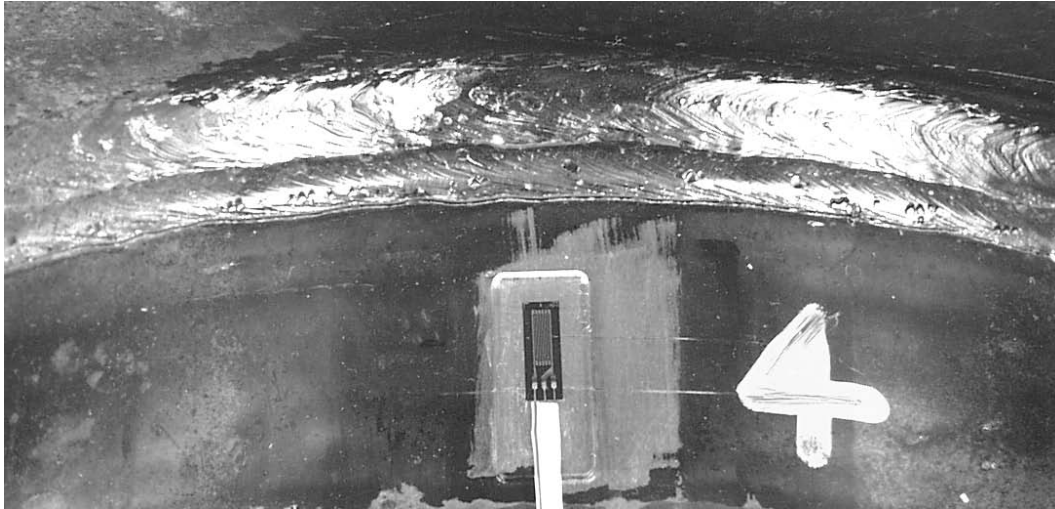


Figure 7.32 Failure of Full-Penetration Welded Connection Detail Specimen

The results of the fatigue testing of these specimens are presented in Table 7.18. The stress ranges at the toe of the full penetration weld calculated assuming that the backing bar effectively reduces the stress in the critical region are presented in the third column of Table 7.18. The strain ranges presented in the fourth column of this table were calculated based on the nominal section properties at the critical location assuming that the backing bar does not reduce the stress in this region. This latter method, neglecting the effect of the backing bar in the calculation of the stress range, is the customary analysis method for this type of connection detail. The fatigue life coefficient, A , in Table 7.21 was calculated based on the nominal stress range neglecting any effects of the backing bar.

From the average fatigue constant value shown in Table 7.21, it is clear that this connection detail would be classified as a category D detail. This classification is confirmed by graphing the results on an S-N plot, as is shown in Figure 7.29. This classification demonstrates an improved fatigue life as compared to a fillet-welded socket connection detail.

Table 7.18 Results of Full-Penetration Weld Connection Specimens

Specimen Name	Number of Cycles	S_R Backing Bar Effective (ksi)	S_R Nominal (ksi)	A	$A_{average}$
VAL _u average					5.67
VAL _{Nu} average					5.46
VALN W A	422,400	9.3	17.7	23.46	23.17
VALN W B	422,400	9.5	17.6	22.88	

As was discussed during the static test discussion of this series of specimens, the strain gauge results indicated that the backing bar was effective at reducing the stress in the critical region. In this way, the backing bar is behaving similar to an internal collar that is welded to the pole at both ends of the collar. Based on the observation that the backing bar was effectively reducing the stress, the stress range at the critical location during the cyclic loading was much less than the nominal stress range utilized in the

fatigue life coefficient calculation. The effect of this lower stress could be accounted for by including the effects of the backing bar in the stress calculations, however this inclusion would be contrary to the standard practice for full penetration welds.

The use of the higher stress range in the fatigue life coefficient calculation results in a higher A value. For connection details with the same geometries and backing bar effectiveness, the higher A coefficient does not influence the results of a fatigue life calculation. However, for a connection detail with a different geometry, or a less effective backing bar, the assumption is unconservative, as it will lead to overestimation of the fatigue life in a design process. Based on this reasoning, the results of the full-penetration weld connection details tested in this test program are only applicable to connection details with similar geometries.

7.9 INFLUENCE OF MEAN STRESS

When the results from the testing at Lehigh University, Valmont Industries, Tokyo Institute of Technology, the University of Missouri – Columbia and the current testing at the University of Texas at Austin are displayed on the same S-N plot, as shown in Figure 7.33, the scatter in the results is almost overwhelming. Due to the large number of test variables and testing laboratories, it is impossible to accurately represent the testing location and connection detail in the graph. To reduce the number of variables included in the graph, the results have been plotted based on the connection detail and the mean stress of the test. The tests performed by Valmont Industries and the Tokyo Institute of Technology were conducted at zero mean stress and the data points from these tests are shown as open symbols. With a few exceptions, the tests from Lehigh University, the University of Missouri-Columbia, and the University of Texas were performed at an elevated mean stress, and these data points are shown as solid symbols.

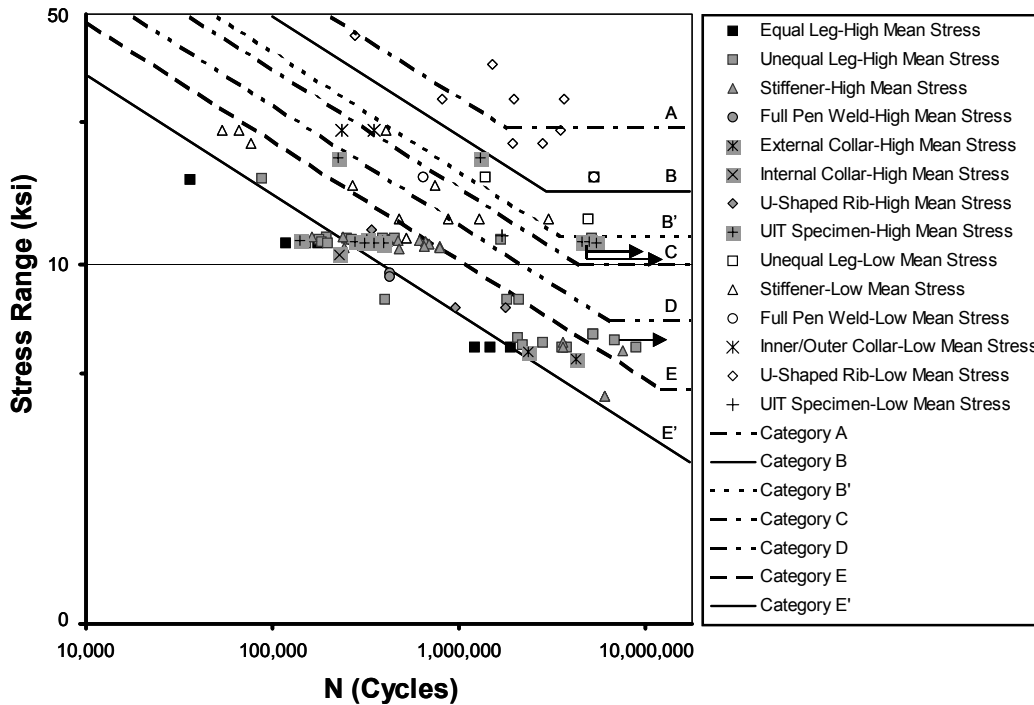


Figure 7.33 S-N Plot of All Available Test Results

It is difficult to discern much from the plot in Figure 7.33, since there is so much scatter in the data. The graph does illustrate one clear trend, as the open symbols, or low mean stress tests, had longer fatigue lives. The scatter in the data and effect of the mean stress on the fatigue life will be discussed separately.

To more properly illustrate the scatter in the data, the results of the triangular gusset stiffened connection specimens are isolated and plotted in Figure 7.34. The results of the U-Rib stiffeners are not included in this plot, so that all of the stiffeners represented are of the same type. From this plot it is evident that the majority of the stiffened specimens tested under a high mean stress condition fall between the E' and E Category limits. Only three data points do not fit within this band. In contrast, the results of the stiffened connection details tested under a low mean stress condition exhibited a range of fatigue categories, from less than an E category to slightly better than a C category. The scatter of the low mean stress test results is much more significant than the scatter of the high mean stress test results.

Along with a large amount of scatter, the plot in Figure 7.33 indicates that the test mean stress influences the fatigue life of the specimen. This influence is more clearly evident in Figure 7.35, in which some of the clutter has been removed by only including the result for the stiffened and unstiffened socket connection details. From this plot, it is apparent that the tests performed under low mean stress conditions produced longer fatigue lives. The test results from Lehigh University and the University of Texas, as indicated by the solid symbols, appear to represent a worst-case loading scenario, and therefore provide the worst-case fatigue category for each connection detail. When applied to a design situation, this results in a conservative estimation of the fatigue life of a connection detail. The high mean stress levels also reflect the actual loading conditions of the cantilever.

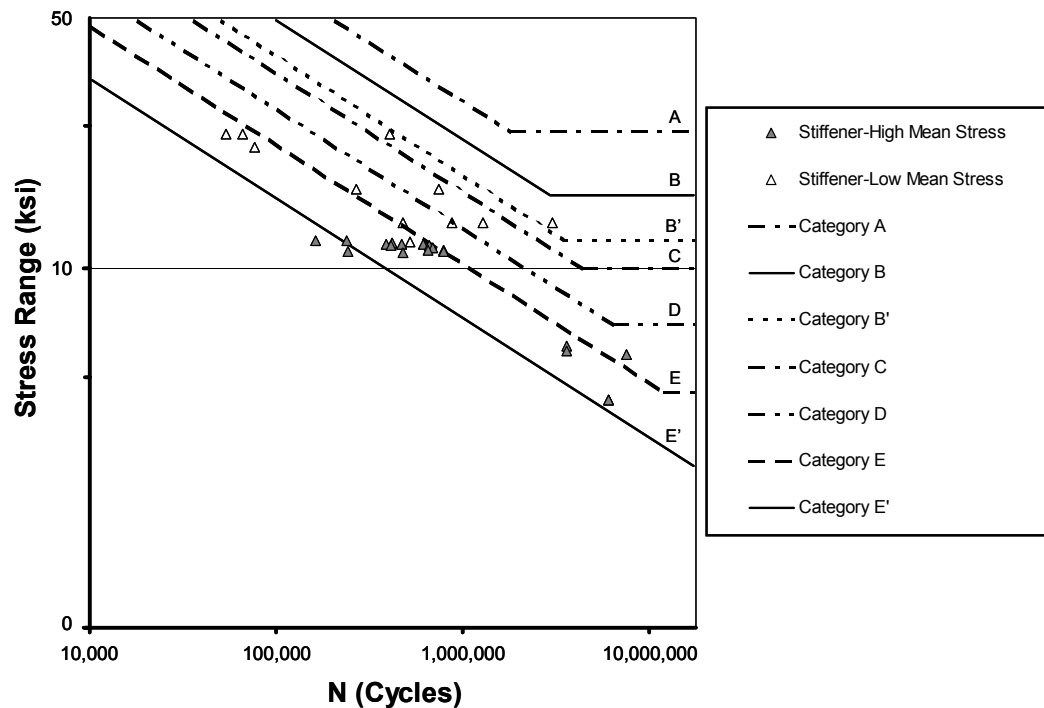


Figure 7.34 S-N Plot of All Available Stiffened Connection Detail Test Results

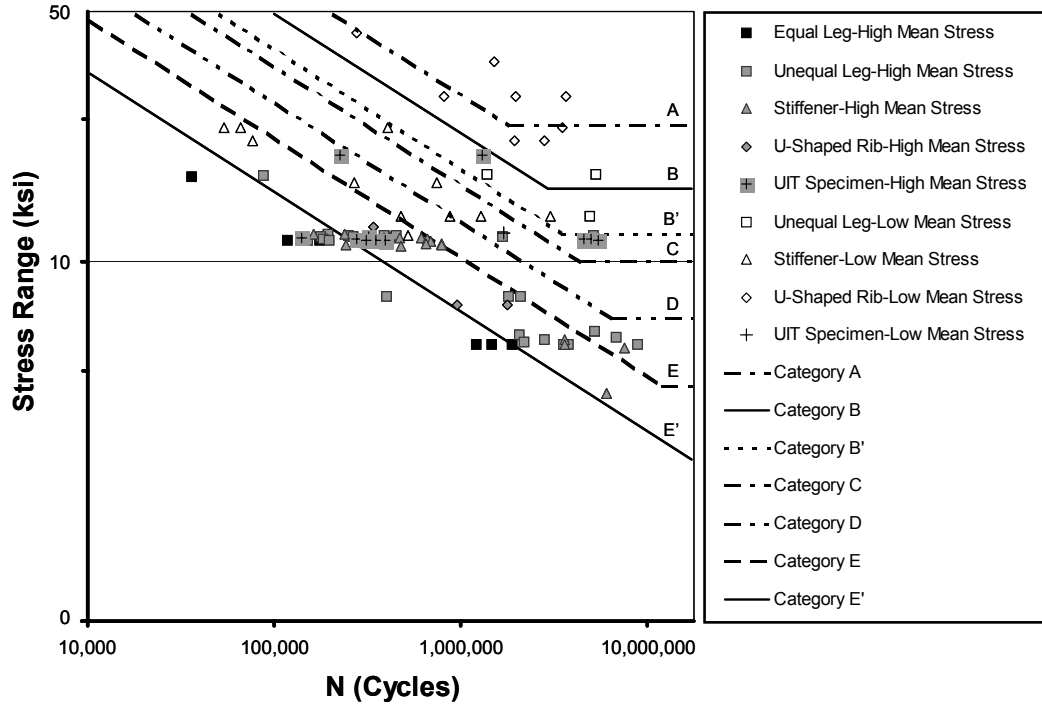


Figure 7.35 S-N Plot of All Available Test Results for Stiffened and Unstiffened Socket Connection Details

CHAPTER 8: RESULTS – VALUE BASED DESIGN ANALYSIS METHOD

8.1 VALUE BASED DESIGN APPROACH

The results of the external collar, U-Rib and internal collar specimens brought to light a problem with the manner in which the test results for these connection details were being presented. The typical fatigue life approach and the calculation of the fatigue coefficient do not seem to fully indicate the value or the potential improvement that can be achieved through the use of an alternative connection detail.

In order to more accurately convey the benefit of the alternative connection details or the weld treatment process studied, the results will be presented using a value based design approach. In this method, the fatigue life of each detail is compared to an unstiffened fillet-welded socket detail of the same pole dimensions and under the same loading conditions.

In the typical fatigue life analysis method, the fatigue life is represented based on the stress at a critical location. This critical location will vary based on the connection detail under investigation. In the case of connection details that use attachments to effectively reduce the stress at the critical location, the fatigue life calculated following this method cannot be directly compared between connection details, unless the stress ranges are somehow correlated.

The value based design method is an attempt to correlate the stress ranges so that a direct comparison can be made. In this analysis method, the stress range that is used for the fatigue life calculation is the stress range of an unstiffened socket connection with the same tube section properties and under the same loading conditions. In this way the fatigue lives of all connection details are related to a similar base stress range.

In the design of a traffic structure, this base stress range will be related to the size of the mast-arm cross section and the loading on the structure. The base stress range will effectively be a constant, as these factors are independent of the type of connection detail selected. The benefit of using this analysis method is that, for a specific load condition and general structure geometry, a designer can directly compare the value of selecting one particular connection detail or weld treatment.

This method is illustrated through example calculations for the VALN Col B specimen. The information required for this calculation is provided in Table 8.1.

Table 8.1 Section Properties and Test Data for VALN Col B (Reprinted from Chapter 7)

Variable	Description	Value
P_{max}	Maximum Test Load	5.7 kip
P_{min}	Minimum Test Load	9.1 kip
L	Effective Length (distance from critical section to tip of cantilever)	88.67 in.
OD _{Collar}	Outer diameter of collar at crack location	10.344 in.
OD _{Tube}	Outer diameter of tapered tube at crack location (neglecting collar thickness)	9.992 in.
ID	Inner diameter at crack location	9.651 in.
N	Number of Cycles to Failure	2,363,152 cycles

Based on the geometry of the mast-arm section, the moment of inertia of only the tapered tube would be calculated as:

$$I_{unstiffened-socket} = \frac{1}{4} \cdot \pi \cdot \left[\left(\frac{OD_{Tube}}{2} \right)^4 - \left(\frac{ID}{2} \right)^4 \right] = 63.4in^4$$

The moment range for the loading was calculated in Section 7.3 to be

$$M_R = 150.74kip - in$$

This results in a stress range for an unstiffened socket connection of:

$$S_{R-unstiffened-socket} = \frac{M_R \cdot c}{I_{unstiffened-socket}} = 11.9ksi$$

Where c is taken as:

$$c = \frac{OD_{Tube}}{2} = 4.996in.$$

The calculated fatigue coefficient, A_{VBDM} , is 39.9.

8.1.1 Comparison with Previous Analysis Methods

The results of the value based design approach calculations are shown for each specimen in Table 8.2 and Table 8.3. These results are summarized by calculating a mean value for each series of test specimens, which are presented in Table 8.4. The calculated average A_{VBDM} values from the value based design method are graphed in Figure 8.1 along with the average A values for the other two test methods utilized in the previous chapters.

For the case of the unstiffened socket connection details, whether UIT treated or not, Figure 8.1 shows that the fatigue life constant calculated by this method is not significantly different from that calculated by the nominal stress fatigue life design method. This is as expected, as the stress range used for the calculation of both methods will be that of an unstiffened socket connection in these situations.

However, for several of the alternative connection details tested during Phase 2 of this test program, the graph of Figure 8.1 indicates a significant increase in the representation of the fatigue life. The benefit of selecting each of the alternative connection details will be discussed in the following sections.

8.2 ANALYSIS OF RESULTS USING VALUE BASED DESIGN APPROACH

To further facilitate comparison of the results, the average A_{VBDM} values have been divided by the fatigue constant for a category E' detail, or 3.9×10^8 . The results of this calculation are presented in the third column of Table 8.4. This calculation was performed to normalize the data with regard to an unstiffened socket connection detail. For values of the $A_{VBDM}/A_{E'}$ ratio less than 1, the connection detail is worse than a category E' detail. On the other hand, values of the $A_{VBDM}/A_{E'}$ ratio greater than one indicate the general level of benefit provided by that detail. The $A_{VBDM}/A_{E'}$ ratios for each series of test specimens are plotted in Figure 8.2.

Table 8.2 Phase 1 Results

Specimen Name	Number of Cycles	Stress Range of Equivalent Unstiffened Socket Connection (ksi)	A_{vBDM}
VALu A	249,446	11.9	4.25
VALu B	453,948	12.0	7.81
VALu C	2,072,592	6.3	5.25
VALu D*	6,856,881	6.2	16.60
VALu EP	393,767	11.5	6.00
VALu FP	353,103	11.6	5.46
TXu A	2,199,343	6.1	4.96
TXu B	2,816,706	6.1	6.44
TXu C	177,596	12.0	3.05
TXu D	194,694	12.1	3.42
TXu EP	320,915	11.9	5.37
TXu FP	141,155	11.8	2.29
VAL 3x1/4 A	476,269	11.5	7.31
VAL 3x1/4 B	696,326	11.7	11.19
VAL 3x1/4 C	3,592,372	6.3	8.81
TX 3x1/4 A	616,136	12.1	10.83
TX 3x1/4 B	416,146	12.2	7.56
TX 3x1/4 C LMS	523,397	12.3	9.66
VAL 3x3/8 A	386,253	12.0	6.76
VAL 3x3/8 B	410,410	12.0	7.09
VAL 3x3/8 CP	393,767	11.8	6.51
VAL 3x3/8 CP(2)	353,103	11.8	5.83
TX 3x3/8 A	473,735	12.1	8.37
TX 3x3/8 B	657,716	12.0	11.33
TX 3x3/8 CP LMS	1,707,128	12.5	33.04
VAL 6x3/8 A	242,728	12.0	4.18
VAL 6x3/8 B	653,392	12.0	11.37
VAL 6x3/8 C	3,592,372	6.3	9.09
TX 6x3/8 A	783,857	11.9	13.12
TX 6x3/8 B	783,857	11.9	13.36
TX 6x3/8 C	7,503,037	6.1	17.20

* Test Stopped – Run-Out

Table 8.3 Phase 2 Results

Specimen Name	Number of Cycles	Stress Range of Equivalent Unstiffened Socket Connection (ksi)	A_{vBDM}
VALNu A	389,428	11.9	6.63
VALNu B	265,540	11.9	4.52
VALNu G A	183,132	11.7	2.91
VALNu G B	151,679	11.6	2.35
VALNu 2 A	5,144,528	11.9	87.23
VALNu 2 B	1,683,127	11.9	28.09
VALN 6x3/8@45 A	238,515	18.0	13.91
VALN 6x3/8@45 B	161,843	18.0	9.48
VALN 6x3/8@45 C	6,066,817	6.4	15.75
VALN 6x3/8@45 D	6,066,817	6.4	15.73
VALN Col A	4,245,460	11.9	71.49
VALN Col B	2,363,152	11.9	39.85
VALN IC A	227,030	14.1	6.38
VALN IC B	227,030	14.0	6.27
VALN W A	422,400	17.7	23.35
VALN W B	422,400	17.6	22.97
VALN UR A (#4)	1,776,724	12.1	31.67
VALN UR B (#1)	950,670	12.1	16.90
VALN UR B (#2)	339,152	12.1	6.03
VALNu PR A*	4,557,126	11.7	72.22
VALNu PR B*	4,557,126	11.6	71.69
VALNu GP A	4,545,952	11.7	72.38
VALNu GP B	224,240	20.1	18.23
VALNu PG A	277,634	11.6	4.35
VALNu PG B	313,727	11.6	4.84
VALNu CP	1,301,077	20.0	104.83
VALNu PR ul A	5,004,729	11.7	79.31
VALNu PR ul B	5,440,165	11.6	85.59

* Test Stopped – Run-Out

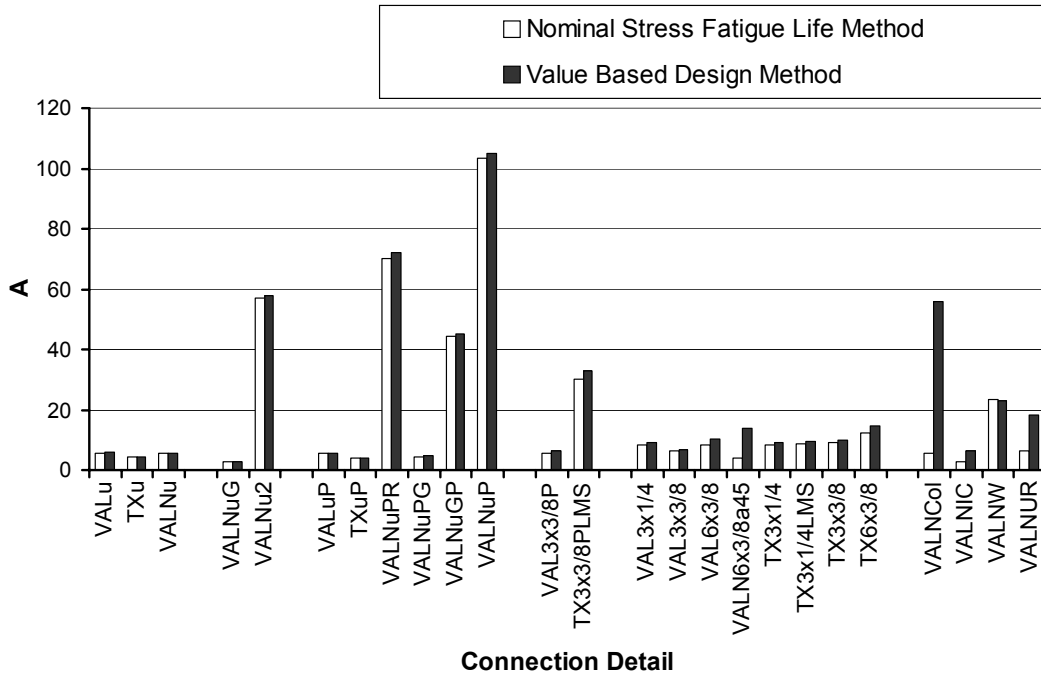


Figure 8.1 Graph of A as Calculated by the Nominal Stress Fatigue Life Method and the Value Based Design Method for All Series of Specimens Tested

8.2.1 UIT Treated Specimens

From the results in Table 8.4 and from the graph of Figure 8.2, it is clear that the UIT weld treatment in the UIT Retrofit and the Galvanizing Prior to UIT Fabrication processes, in which the galvanizing is performed prior to the UIT treatment process, provide the greatest improvement in the fatigue life. For example, the retrofit process can increase the estimated fatigue life of a connection detail by up to 18 times. The conclusion that the UIT weld treatment process was very effective is the same as the conclusion reached through the fatigue life analysis method.

8.3 ANALYSIS OF ALTERNATIVE CONNECTION DETAILS USING VALUE BASED DESIGN APPROACH

Figure 8.3 shows the $A_{VBDM}/A_{E'}$ ratio for all of the test series except for the UIT treated series. From this plot it is clear that many of the connection details provide a beneficial improvement to the fatigue life of the connection, which was not evident using the nominal stress fatigue life analysis method in Chapter 7. Although these connection details do not provide the fatigue life improvement of the UIT treated series, several of the alternative connection details provide enough of an increase in the fatigue life to make the use of the connection detail valuable to a designer.

Table 8.4 Average Values for Each Series of Tests

Specimen Name	$A_{VBDM-Average}$	$\frac{A_{VBDM-Average}}{A_{E'}}$
VALu	5.77	1.48
TXu	4.47	1.15
VALNu	5.57	1.43
VALNuG	2.63	0.68
VALNu2	57.66	14.78
VALuP	5.73	1.47
TXuP	3.83	0.98
VALNuPR	71.96	18.45
VALNuPG	4.60	1.18
VALNuGP	45.31	11.62
VALNuP	104.83	26.88
VAL3x3/8P	6.17	1.58
TX3x3/8PLMS	33.04	8.47
VAL3x1/4	9.11	2.33
VAL3x3/8	6.92	1.78
VAL6x3/8	10.23	2.62
VALN6x3/8a45	13.72	3.52
TX3x1/4	9.20	2.36
TX3x1/4LMS	9.66	2.48
TX3x3/8	9.85	2.53
TX6x3/8	14.56	3.73
VALNCoI	55.67	14.27
VALNIC	6.32	1.62
VALNW	23.16	5.94
VALNUR	18.20	4.67

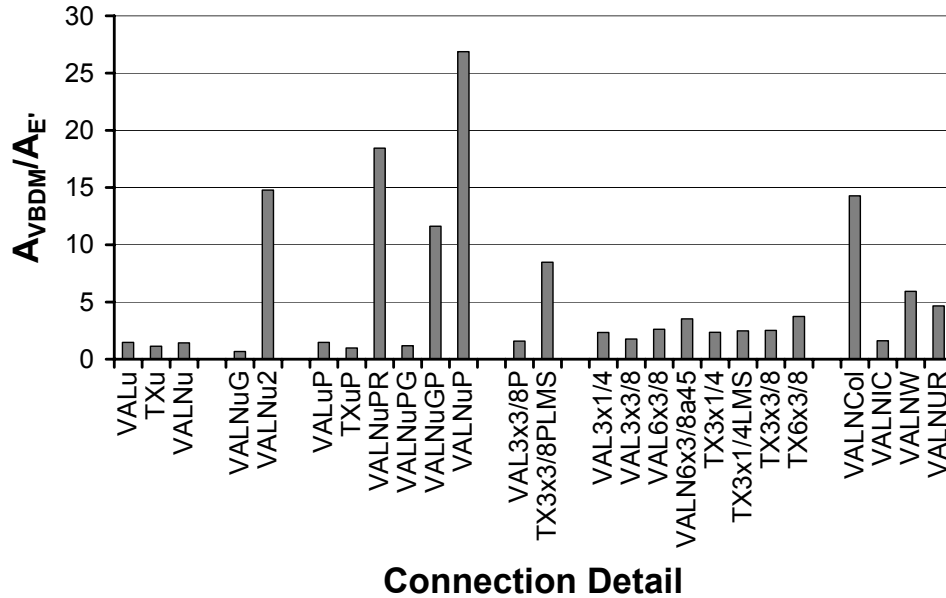


Figure 8.2 Graph of $A_{VBDM}/A_{E'}$ for All Series of Specimens Tested

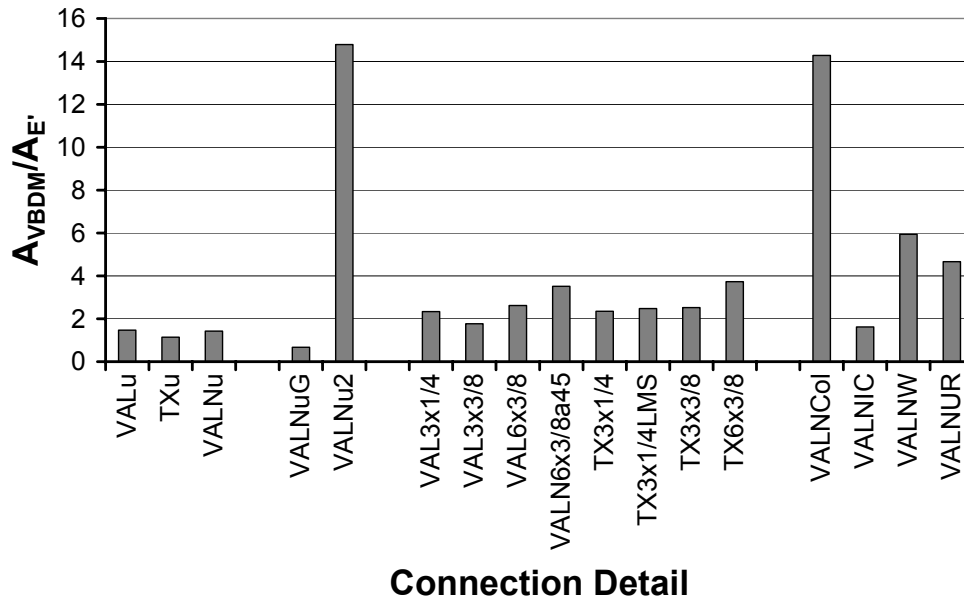


Figure 8.3 Graph of $A_{VBDM}/A_{E'}$ for Each Series of Specimens Tested Excluding UIT Treated Series

8.3.1 Socket Connection Details

Prior to discussing the results of the alternative connection details, it should be noted that the values from the value based design analysis method presented in Table 8.6 show that the socket connection details can sustain between 1.1 and 1.5 times the number of loading cycles as a pure category E' detail prior to a fatigue induced failure. Average $A_{VBDM}/A_{E'}$ values slightly greater than 1.0 are expected as the fatigue life coefficients represent a lower bound. Average $A_{VBDM}/A_{E'}$ values from 1.1 to 1.5 indicates that the socket connection detail is properly classified as a E' category detail.

8.3.2 Stiffeners Oriented 45° From Vertical - VALN 6x3/8@45 Series

The graph in Figure 8.1 indicates that the value based design method provides a significantly different representation of the benefit of this connection detail than does the fatigue life analysis method. For this particular series of specimens, the fatigue life analysis method provides a low value for the fatigue constant because the termination of the stiffener is in an area of lower local stresses due to the orientation of the stiffeners at a 45° offset from vertical.

While the fatigue life analysis method shows that this connection detail is just barely a category E' detail at the termination of the stiffener, due to the lower stresses present at the termination of the stiffener, the connection detail can actually provide a fatigue life that is 3.5 times as many load cycles as a category E' detail. Through this evaluation method, the offset stiffeners provide a better fatigue life than any of the other stiffened connection details tested except for the TX 6x3/8 stiffened specimen.

8.3.3 External Collar Stiffeners - VALN Col Series

The graph in Figure 8.1 shows that the external collar provides the drastic change in improvement at a connection detail as compared with the fatigue life analysis method. Using the Value Based Design method, the collar connection detail is shown to provide over 14 times the number of fatigue cycles as a category E' detail. This shows that the external collar provides almost the same benefit of the VALNu PR and VALNu GP series of specimens.

8.3.4 Internal Collar Stiffeners - VALN IC Series

As is evident from Figure 8.1, the value based design method does show an increased benefit over the fatigue life analysis methods, however the improvement is small. From the data of Table 8.4, it is clear that this connection detail provides only 1.6 times the number of fatigue cycles as a category E' detail. This small benefit is not worth the extra labor and material required to fabricate the internal collar connection details.

8.3.5 U-Rib Stiffeners - VALN UR Series

The U-Rib stiffened specimens exhibit a significant benefit to the fatigue life of a connection detail when evaluated using this method. This is evidenced from the graph in Figure 8.3. From the data in Table 8.4, it is clear that the U-Rib stiffeners provide more than 4.5 times the fatigue life of a category E' detail. While it is unclear whether the labor and material costs associated with the fabrication of the U-Rib stiffener are justified by this increased fatigue life, this method clearly shows that the U-Rib stiffeners are beneficial as compared with an unstiffened socket connection.

8.3.6 Full-Penetration Weld Connections - VALN W Series

The calculated fatigue life coefficient, A, values calculated in Chapter 7 for the VALN W series of specimens are identical to the A_{VBDM} coefficient values calculated using the value based design method. The assumption that the backing bar does not contribute to the moment of inertia of the critical section in the VALN W series results in the same moment of inertia as calculated for an unstiffened socket connection. The static tests of these specimens indicated that the long backing bar, which was fillet welded to the pole and the base plate inside the tube, effectively reduced the stress at the toe of the full-penetration weld. The improved fatigue life of the full-penetration weld specimens may have been due to the stress reduction at the weld toe. For a full-penetration connection detail in which the stress reduction due to the backing bar is not as significant, the use of the A coefficients determined from these tests in a design process would be unconservative.

8.4 BENEFITS OF USING VALUE BASED DESIGN APPROACH

The use of the value based design analysis method shows that many of the alternative connection details are more beneficial or provide a greater value than is indicated by solely comparing the fatigue life or fatigue coefficients calculated through the traditional method. In the fatigue life analysis method, the advantages of using stress reducing attachments in the connection detail are not readily apparent since the calculated stress ranges are not calculated in the same manner or at the same location in each of the various connection details. The value based design analysis method utilizes a consistent method of calculating the stress range so that the fatigue life coefficients of various connection details may be compared directly. While the fatigue life analysis method shows that the external collar stiffeners, the U-Rib stiffeners and the stiffeners oriented at 45° from vertical do not improve the fatigue life of a connection detail, the value based design analysis method shows that these connection details do in fact improve the fatigue life of a connection detail.

The value based design analysis method provides a way to compare and select between different connection details during the design process. At the connection design stage in a design process, the loads and general properties of a structure will be set and the moment that must be resisted at the connection detail is independent of the connection detail. Using the value based design method, the appropriate connection detail may be selected based on the predetermined moment and the design may proceed using the A_{VBDM} coefficients presented in this chapter.

CHAPTER 9: FINITE ELEMENT ANALYSIS OF CONNECTIONS

9.1 INTRODUCTION

This section of the report presents and discusses the results from finite element analyses done on the mast arm connections. The effect of the geometric variables, listed in Table 9.1, on the results was determined. This section also summarizes the analysis tools and techniques used in creating, analyzing, and evaluating the finite element models and results.

9.1.1 Geometric Variables Analyzed

The analyses evaluated the influence of the following geometric variables upon the stress at the toe of the connection welds:

Table 9.1 Geometric Variables Analyzed

Unstiffend Models	Stiffened Models
Pole length	Pole wall thickness
Pole wall thickness	Stiffener thickness
Solid baseplate	Ratio of stiffener thickness to wall thickness
Baseplate thickness	Baseplate thickness
Bolt pattern	45° stiffener offset from vertical
	Netrual axis stiffeners
	Eight equally-spaced stiffeners

A total of 21 finite element models were constructed and analyzed. Combinations of the variables listed in Table 9.1 were evaluated to determine the influence of the variables upon the results. The model nomenclature is defined below.

Sample Names:
TxDOT VAL u2

J	Unstiffened pole
2	Baseplate thickness
6x3/8	6 inch-long, 3/8 in. thick stiffener
@ 45	Offset from vertical by 45°

VAL	0.179 in. wall thickness
TX	0.239 in. wall thickness

TxDOT	TxDOT baseplate from specs
8-Hole	Eight hole baseplate based on As tested baseplate
Long	196.00 inch-long pole
Solid	Solid baseplate

VAL 2 6x3/8 indicates a 0.179 inch-thick wall, 2.00 inch-thick As Tested baseplate, a 6.00 inch-long, 0.375 inch-thick stiffener.

Note: If no baseplate name appears, the As Tested baseplate hole geometry is implied. If no baseplate thickness appears, 1.50 in. is implied.

9.1.2 Purpose

The purpose of the finite element analyses was to determine a stress concentration factor (SCF) at critical locations for mast arms. The intent of determining these SCFs is that they can be used to estimate the fatigue life of the connections. The approach of estimating fatigue life using the SCF at weld toes is employed in the design of tubular joints in offshore structures. The application of this approach to the prediction of fatigue strength of mast arms was examined.

9.2 ANALYSIS TOOLS AND TECHNIQUES

Abaqus Standard v. 6.2 was used to analyze the mast arms on a Windows XP workstation with dual 1.80 GHz Intel Xeon processors, 2.0 GB of RAM, and 16 GB of hard disk space.

9.2.1 Analysis Techniques

All analyses are performed statically. The finite element models were created by drawing solid symmetric models of test specimens using AutoCAD 2002. These models were then exported from AutoCAD and imported into Abaqus as parts. In Abaqus, the parts were meshed, material properties were assigned, and boundary conditions and loads applied.

9.2.1.1 Part List and Material Properties

Each imported model has two parts: a loading plate and a mast arm. They are imported as deformable parts and assigned material properties; the loading plate is assigned a 'rigid' material, while the mast arm is assigned steel. Table 9.2 shows the elastic properties of the materials. Appendix D describes how the models were created in AutoCAD and exported for use in Abaqus.

Table 9.2 Abaqus Material Properties

Material	Elastic Modulus (ksi)	Poisson's Ratio	Assigned To
Steel	29,000	0.3	Mast Arm
Rigid	90,000,000,000	0.3	Loading Plate

9.2.1.2 Assembly and Interaction Definitions

The assembly is defined in the Assembly module by adding one instance of each of the two parts. In the Interaction module, a tie – a surface interaction that preserves compatibility between the master and slave surface – is created on the surface between the loading plate and the mast arm with the loading plate serving as the master surface and the mast arm as the slave.

9.2.1.3 Step Definitions and Output Requests

In the Step module, the load steps and field outputs are defined. The non-linear geometry option was disabled in each load step for the majority of the analyses performed. The impact of non-linear geometry was examined and found to be negligible. The typical output requests for each step were: stress, displacements and rotations, nodal coordinates, and integration point coordinates. No history outputs were requested.

9.2.1.4 Boundary Conditions

In the Load module, symmetric boundary conditions were applied to restrict displacement in the 1 direction. Displacement constraints were applied around the rim of the bolt holes on the bottom of the baseplate to restrict movement in all directions. A point load representing the difference between the maximum and minimum loads – the load range – is applied at the center of the loading plate in the negative 2 direction. For example, for a mast arm with a wall thickness of 0.239 in., the maximum applied test load is 3.075 kips and the minimum test load is 1.925 kips. Therefore, since the materials are linear, a single load of 1.15 kips is applied instead.

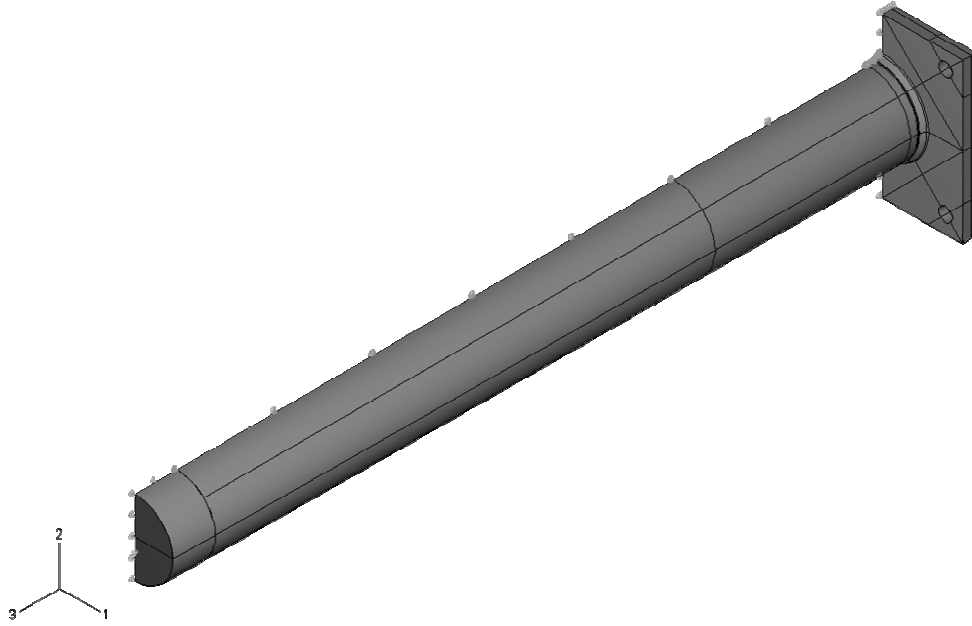


Figure 9.1 Coordinate System and Symmetric Model

9.2.1.5 Meshing

In the mesh, the only element type used is a 20-node, second order brick with 27 Gaussian integration points per element (C3D20 in Abaqus). The refinement of the mesh depends on the SCF quantification approach being used. For the stiffened and unstiffened models, the ABS and DNV approach is followed explicitly except that the first element after the toe is replaced with two elements each $t/2$ long. Figure 9.2 shows a typical meshing scheme using the ABS and DNV approach for an unstiffened model. Figure 9.3 shows a typical meshing scheme using the ABS and DNV approach for a stiffened model.

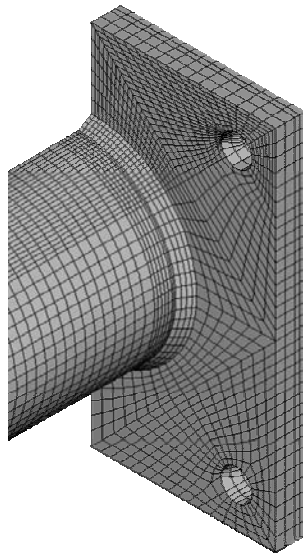


Figure 9.2 Typical ABS and DNV Meshing Scheme for Unstiffened Models

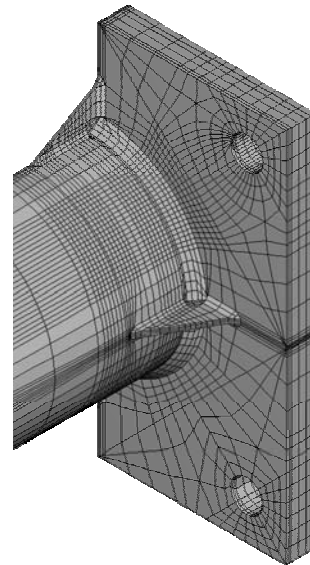


Figure 9.3 Typical ABS and DNV Meshing Scheme for Stiffened Models

Figure 9.4 shows a typical meshing scheme using a refined mesh approach for an unstiffened model. Figure 9.5 shows a typical meshing scheme for the global and subsequent submodels using the submodeling approach for a stiffened model.

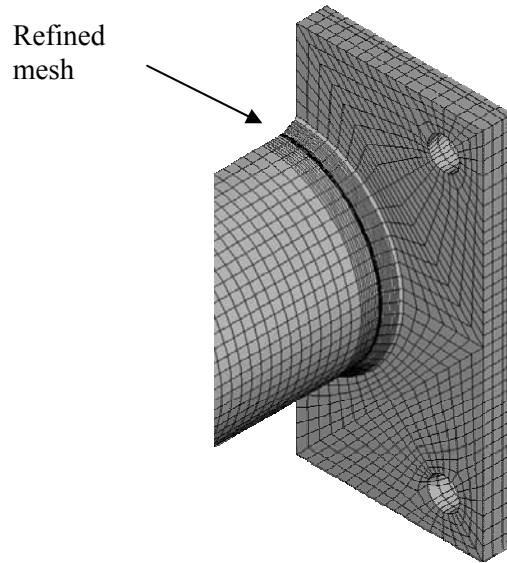


Figure 9.4 Typical Refined Meshing Scheme for an Unstiffened Model

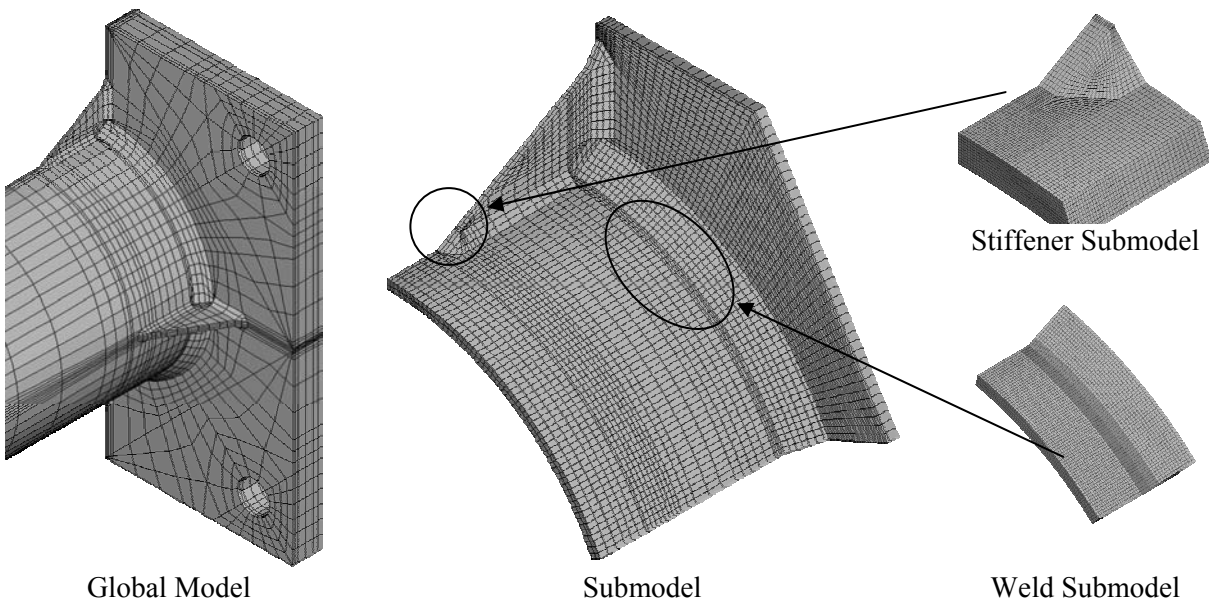


Figure 9.5 Typical Submodeling Meshing Scheme for Stiffened Models

9.3 STRESS CONCENTRATION FACTOR CALCULATION

From the analysis results, a maximum SCF was calculated. The maximum SCF is found by dividing the local maximum principal stress range at a weld toe by the bending stress range at the top-most tension fiber of an unstiffened mast arm (Equation 9.1).

$$SCF = \frac{\text{Maximum Principal Stress Range at Weld Toe}}{\text{Maximum Bending Stress Range}} \quad (\text{Eq. 9.1})$$

For example, in Figure 9.6, the maximum principal stress range is 33.9 ksi. The bending stress range on the top of the mast arm at the face of the baseplate is 11.4 ksi. The SCF therefore is 2.97.

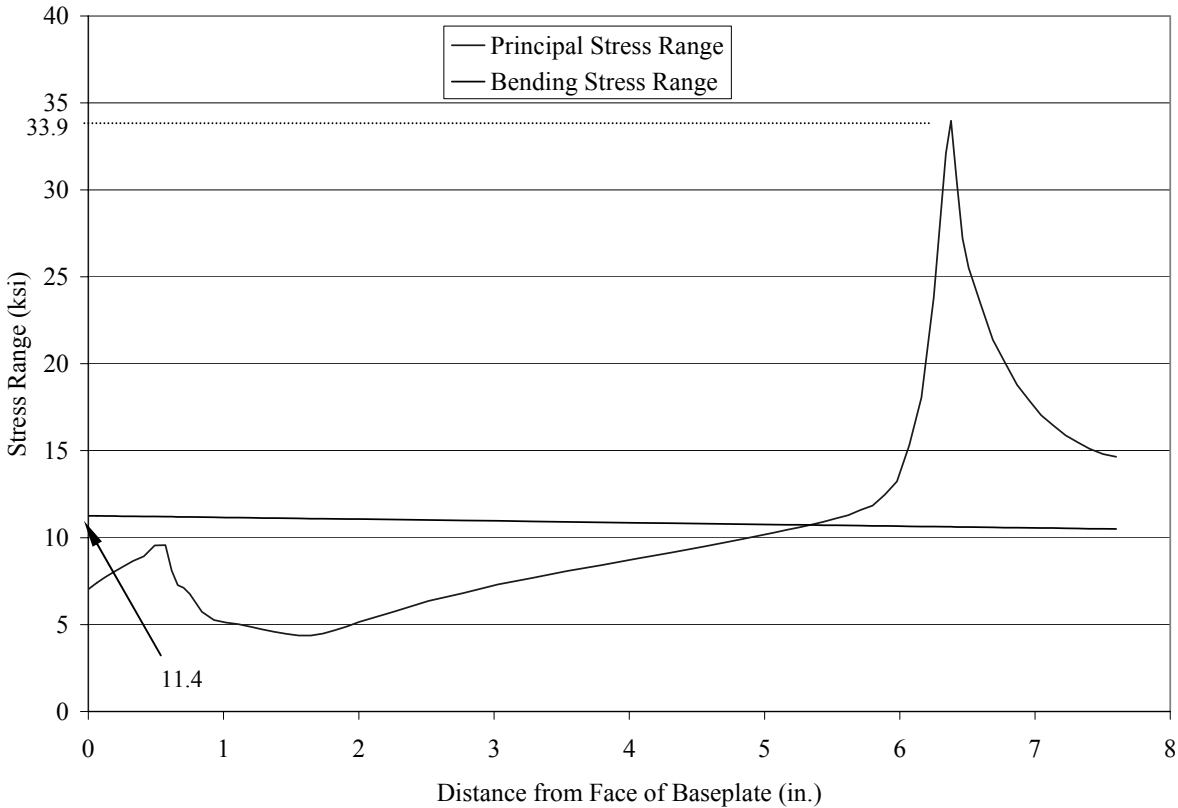


Figure 9.6 Example of SCF Calculation

9.4 GRAPHICAL EXPLANATION OF SCFs

Figure 9.7 shows a concentration of curvature at the toe of the socket welds which causes the stress concentration.

The curvature concentration implies that locally, there are high bending stresses in the mast arm wall. Figure 9.8 shows these bending stresses on the outside and inside of the top tension fiber of the mast arm. Note the sharp peaks in the stresses at about 0.6 in. from the face of the baseplate, the toe of the socket weld, and that at 4-5 in. from the face of the baseplate onward, the longitudinal stresses match the predicted bending stress.

The deviation from the predicted bending stress range can further be shown in stress versus height plots of three cross sections shown in Figures 9.9 and 9.10. The dashed straight line in the figures is calculated assuming plane sections remain plane. The stress at the top and bottom of the mast arm is much larger than the calculated values. The maximum deviation occurs at the socket weld toe, shown in Figure 9.9.

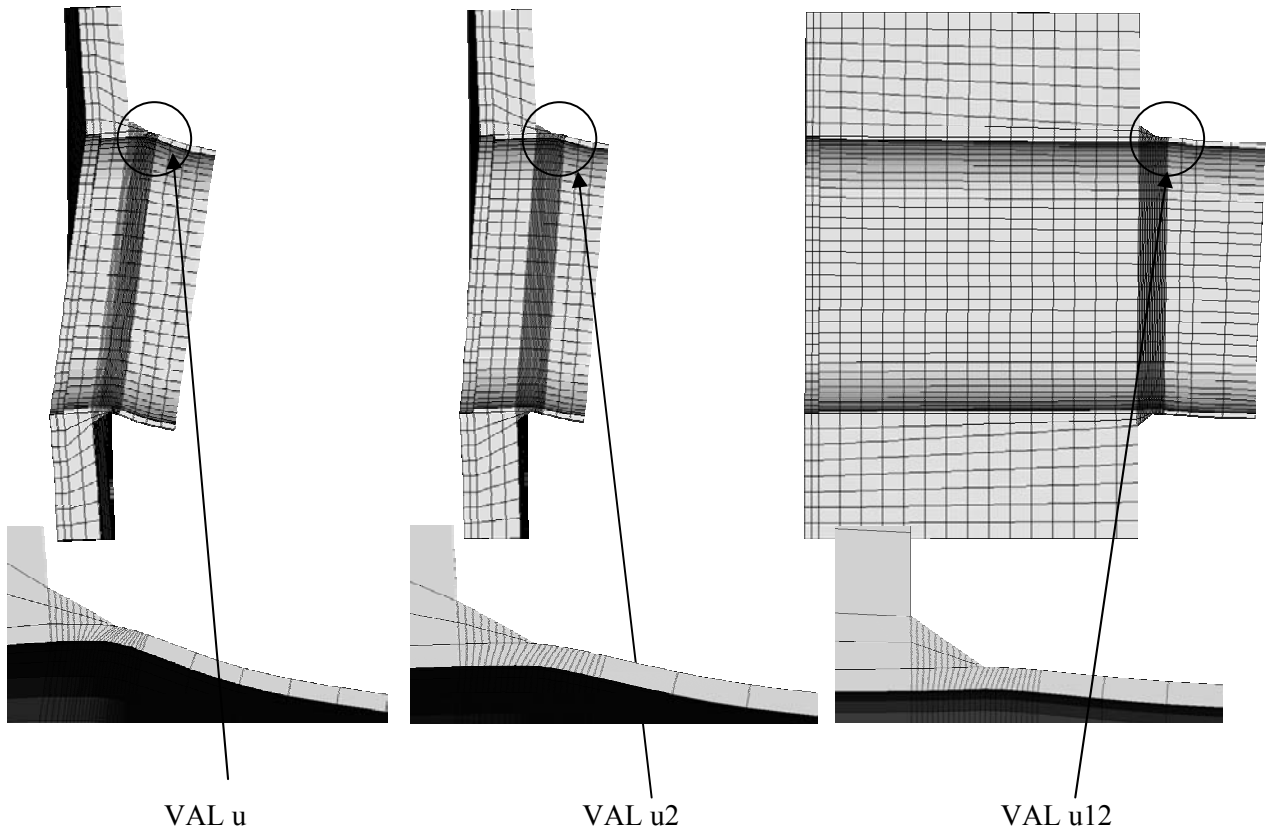


Figure 9.7 Mast Arm Deformations and Local Curvature (100x Deformation using Mesh Refinement Approach)

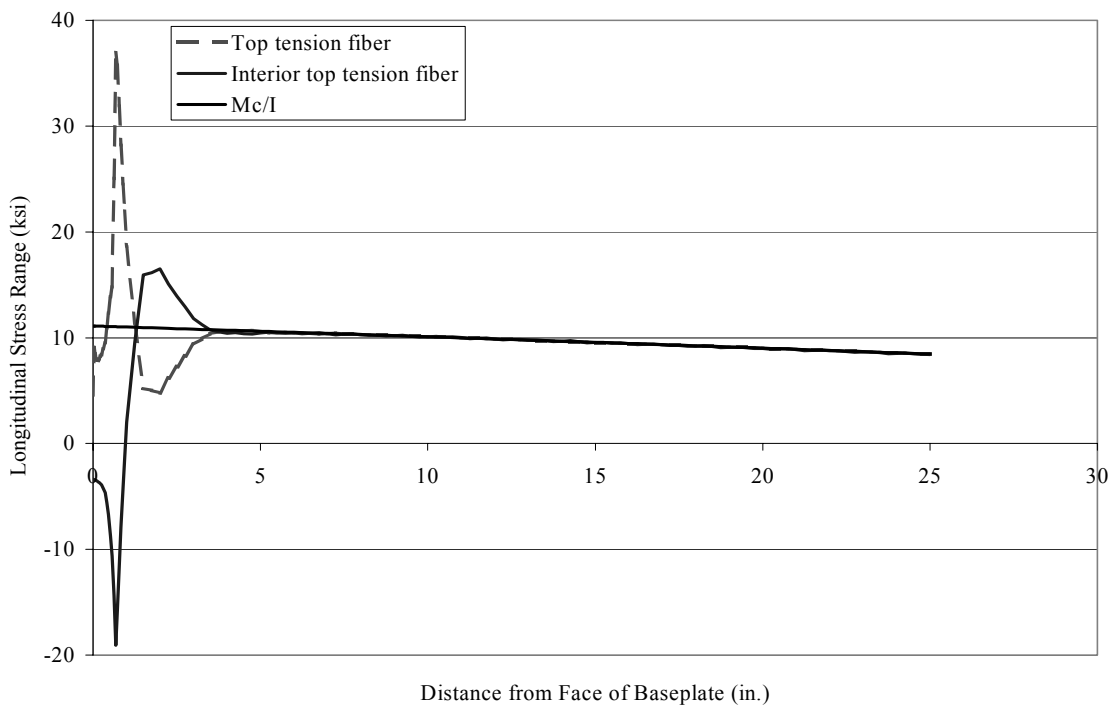


Figure 9.8 Longitudinal Stress Range Along Top of Mast Arm

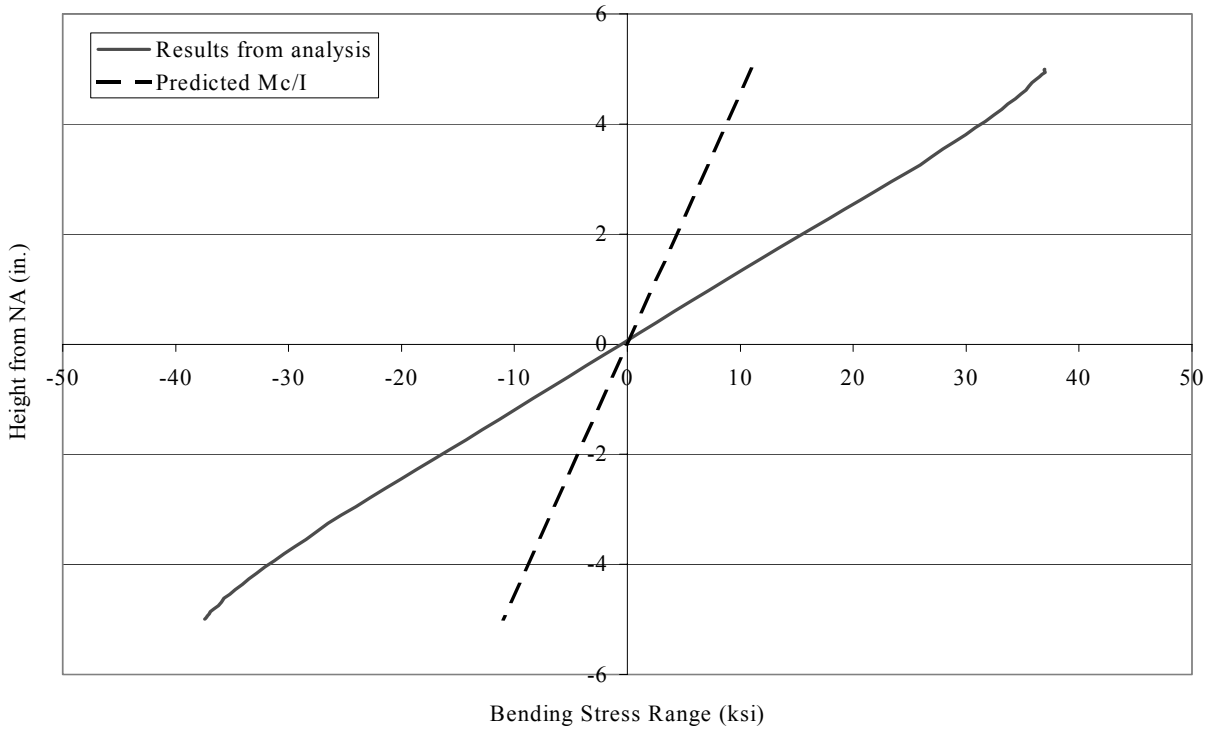


Figure 9.9 Stress vs. Height at Socket Weld Toe

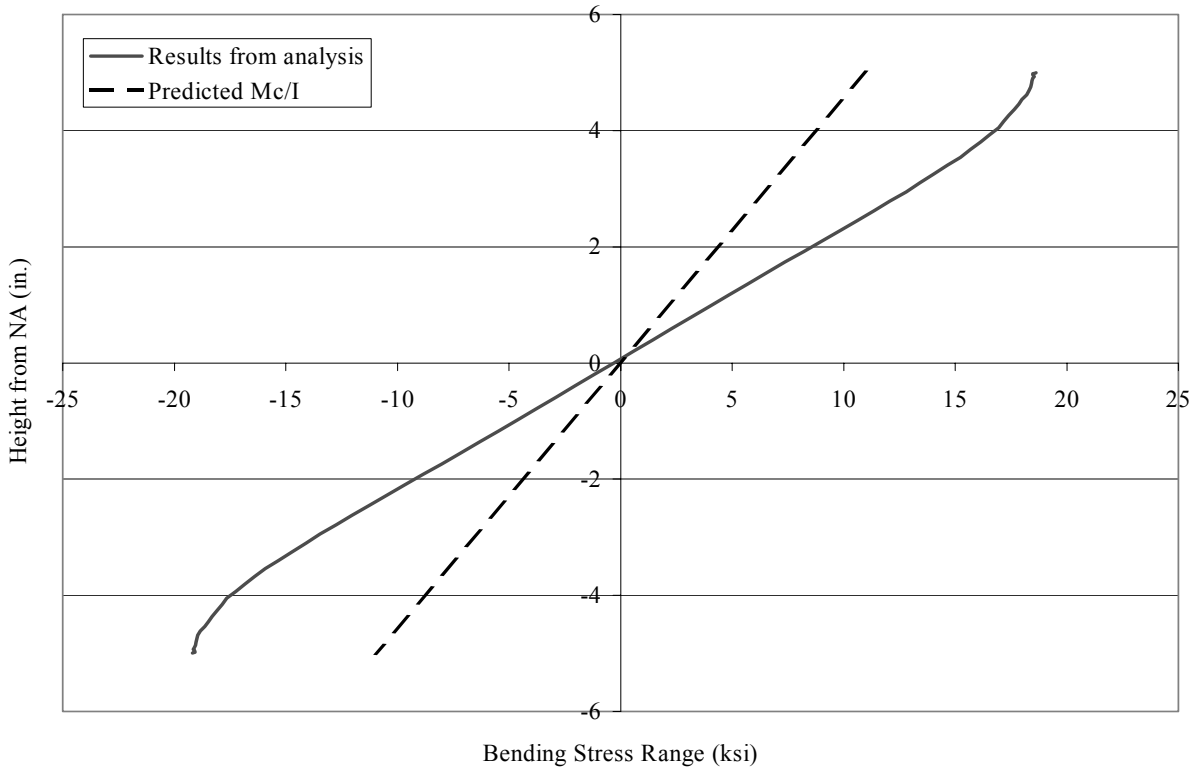


Figure 9.10 Stress vs. Height at 1.00 in. from Face of Baseplate

9.5 STRESS CONCENTRATION FACTOR EVALUATION TECHNIQUES

The plot in Figure 9.11 shows that the weld toe causes a stress singularity. The singularity causes the solution obtained from a finite element model to be mesh-dependent. Figure 9.11 shows how submodeling affects the principal stress range – and thus the SCF – near the singularity. As the size of the elements decreases in each submodel, the stress at the discontinuity will approach infinity. Thus, the calculated stress at the weld toe is not a single value and a method for determining a detail-dependant stress is needed.

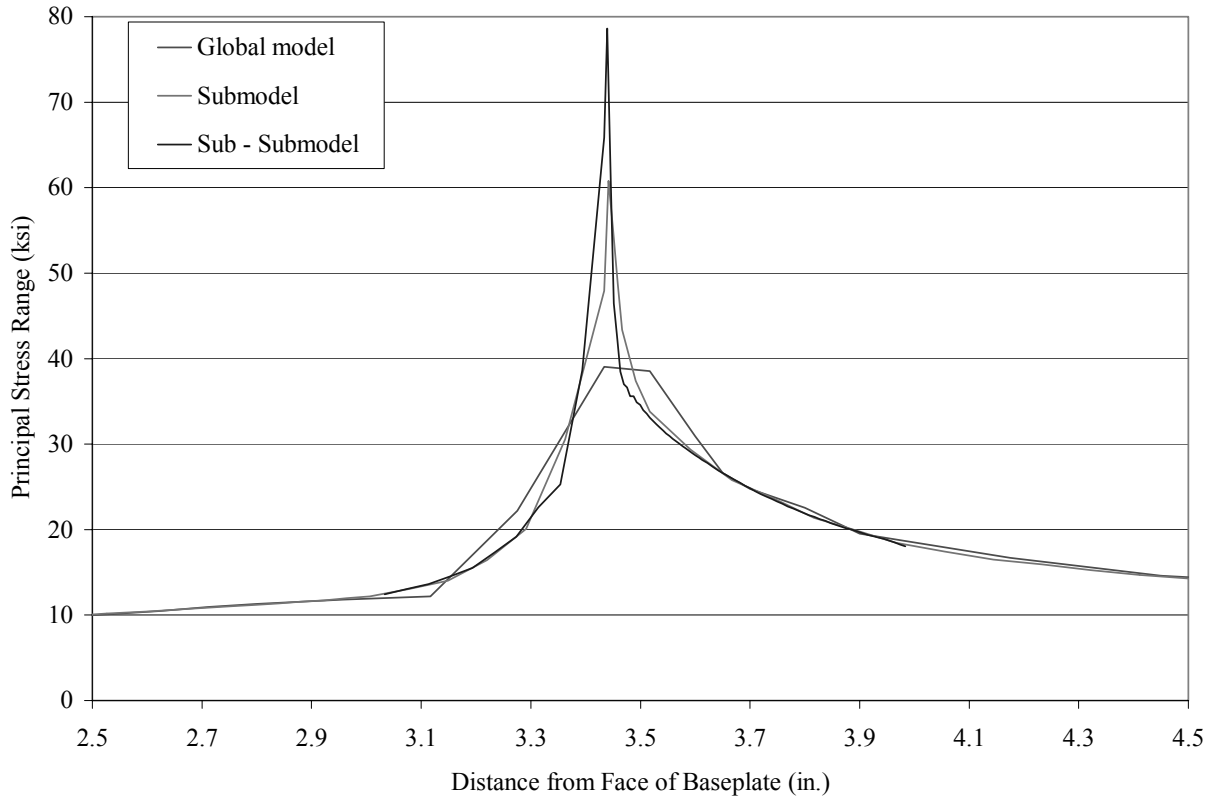


Figure 9.11 Affect of Mesh Size on Stress Singularity

The evaluation of the stress singularity is similar to the problem encountered in the offshore industry when trying to evaluate the fatigue life of welded tubular joints. The recommendations of two organizations were examined: The American Bureau of Shipping (ABS) and Det Norske Veritas (DNV).

To evaluate the SCFs on the mast arms 3 approaches were taken. The first was to use the approach used by ABS, and the second is the approach recommended by DNV. The third approach is to refine the mesh until solution convergence is reached away from the singularity. The purpose of the third approach was to investigate the influence of the mesh size on the DNV results. All three methods have one thing in common: they use the stresses at $t/2$ and $3t/2$, where ‘ t ’ is the mast arm wall thickness, away from the weld toe to linearly extrapolate to the stress at the weld toe. The difference between the techniques lies in how stresses at $t/2$ and $3t/2$ are obtained. The reason for taking these three approaches was to lend confidence to the results obtained from the analyses.

9.5.1 ABS Technique

This method comes from the ABS report, *Rules for Building and Classing – Steel Vessels 2002, Part 5, Specific Vessel Types* and can be found in Appendix E – ABS Technique. The specification requires that

element widths around the weld toe be approximately t . After the analysis is run, the values at the centroids of four neighboring finite elements are used in a Lagrange interpolation to estimate the stresses at $t/2$ and $3t/2$ from the weld toe. The values at $t/2$ and $3t/2$ are used to linearly extrapolate to the stress at the weld toe using Equation 9.2:

$$S_0 = \frac{3S_1 - S_2}{2} \quad (\text{Eq. 9.2})$$

Where S_0 is the stress at the weld toe, S_1 is the stress at $t/2$, and S_2 is the stress at $3t/2$.

The ABS specification is ambiguous in defining the location of the stresses used for the Lagrange interpolation. Section 13.7 of the specification implies that the surface component stresses are used while the notes in 13.7.4 imply that the element centroidal values are used. It is possible that the surface centroidal values, i.e. nodal values, instead of element centroidal values, should be used. In this case, the ABS and DNV approaches are essentially the same. The only differences are element lengths and the interpolation methods summarized in Table 9.3.

9.5.2 DNV Technique

This method comes from the DNV report *DNV-RP-C203*. It requires that the elements' widths around the weld be exactly t . The nodal stress values at $t/2$ and $3t/2$ are extracted and the stress at the weld found using Equation 9.2.

9.5.3 Mesh Refinement / Submodeling Technique

This method is similar to the DNV approach in that it uses nodal stresses to estimate the stress at the weld toe. The difference between this approach and the DNV approach is that by refining the mesh, the displacements and stresses will converge at $t/2$ and $3t/2$ away from the discontinuity (Table 9.3). Once these values are obtained, Equation 9.2 is used to find the stress at the weld toe.

Table 9.3 Comparison of SCF Evaluation Techniques

	ABS		DNV		Refined	Submodeled
	Unstiffened	Stiffened	Unstiffened	Stiffened	Unstiffened	Stiffened
Stress	Centroidal	Centroidal	Nodal	Nodal	Nodal	Nodal
Location for linear extrapolation	$t/2, 3t/2$					
Lagrange extrapolation	Yes	Yes	No	No	No	No
Stress type	Principal	Principal	Principal	Principal	Principal	Principal
Mesh size at discontinuity	$\sim t$	$\sim t$	t	t	0.03 in.	0.02 in.

9.5.3.1 Mesh Refinement

For the unstiffened models, solution convergence is accomplished by refining the global model mesh around the weld. The element lengths around the socket weld toe were approximately 0.03 in. The refined mesh extends approximately 1.5 to 2 inches past the weld toe.

9.5.3.2 Submodeling

As shown in Figure 9.11 using a sufficiently refined mesh gives solution convergence near the stress singularity. However, refining the mesh in the global model would create problems too large to be handled by the available computers, and so a submodeling technique – available in Abaqus – was used. Thus, the stiffener and socket weld toes in stiffened models were submodeled to get solution convergence. To do this, a global model was drawn and analyzed. From this, a submodel with a finer mesh was created and analyzed by imposing the displacements from the global model as the submodel boundary conditions. From this submodel, two smaller submodels were created – of the stiffener and socket weld toes – and analyzed using the displacements from the submodels as their boundary conditions. Element lengths used in these submodels were approximately 0.02 in.

9.5.4 Example of Stress Extrapolation

Figure 9.12 provides an example of how stress extrapolation is done and how it avoids the effect of the singularity. The singularity in this case is located at approximately 0.6 in. The two points used for extrapolation are located at $t/2$ and $3t/2$ away (approximately 0.65 and 0.84 in., respectively). Depending on the method used, the stresses at these points will be different. In the case of the mesh refinement approach the stresses are 31.8 and 22.5 ksi, respectively. Using Equation 9.2, the extrapolated stress is 36.5 ksi.

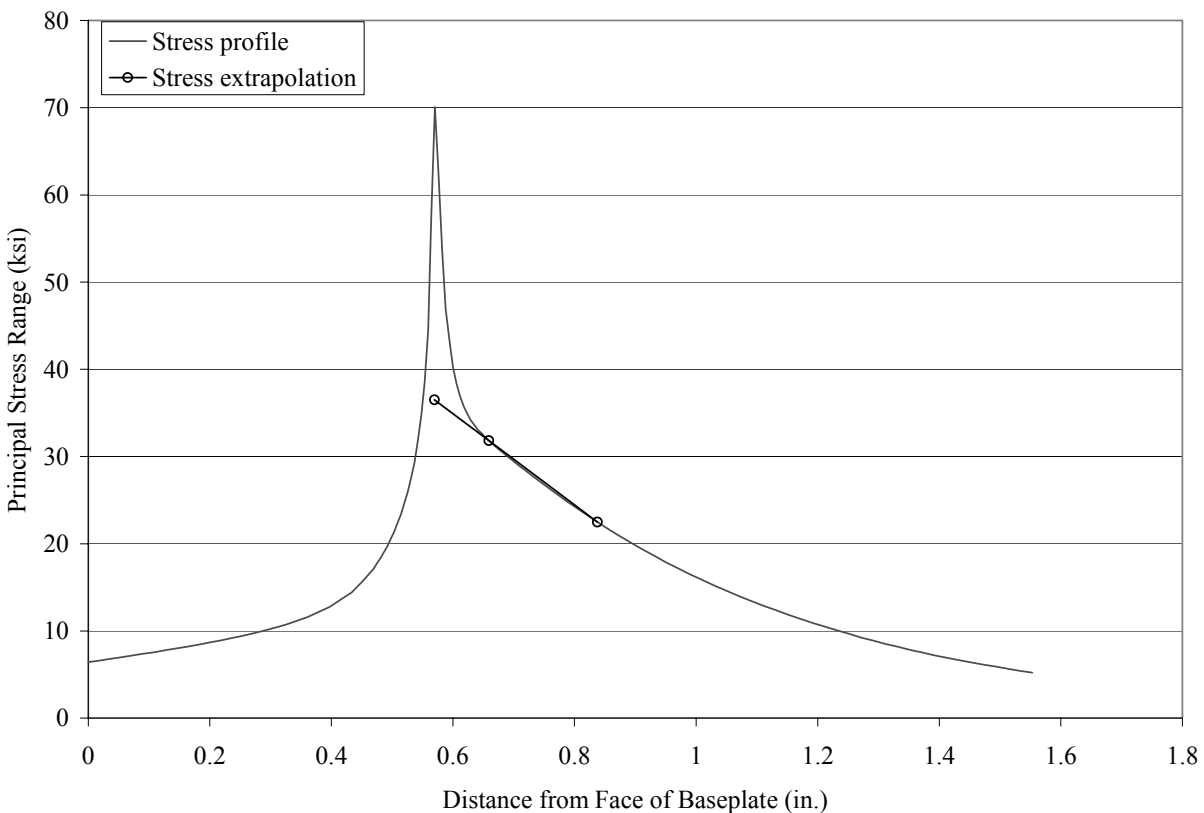


Figure 9.12 Example of Stress Extrapolation

9.5.5 Comparison of Stress Solutions

Figure 9.13 shows how the solutions from the three approaches compare at the toe of a stiffener. All of the stress profiles follow the same trends, but the singularity in the ABS approach is less pronounced than in the DNV or submodeling approaches.

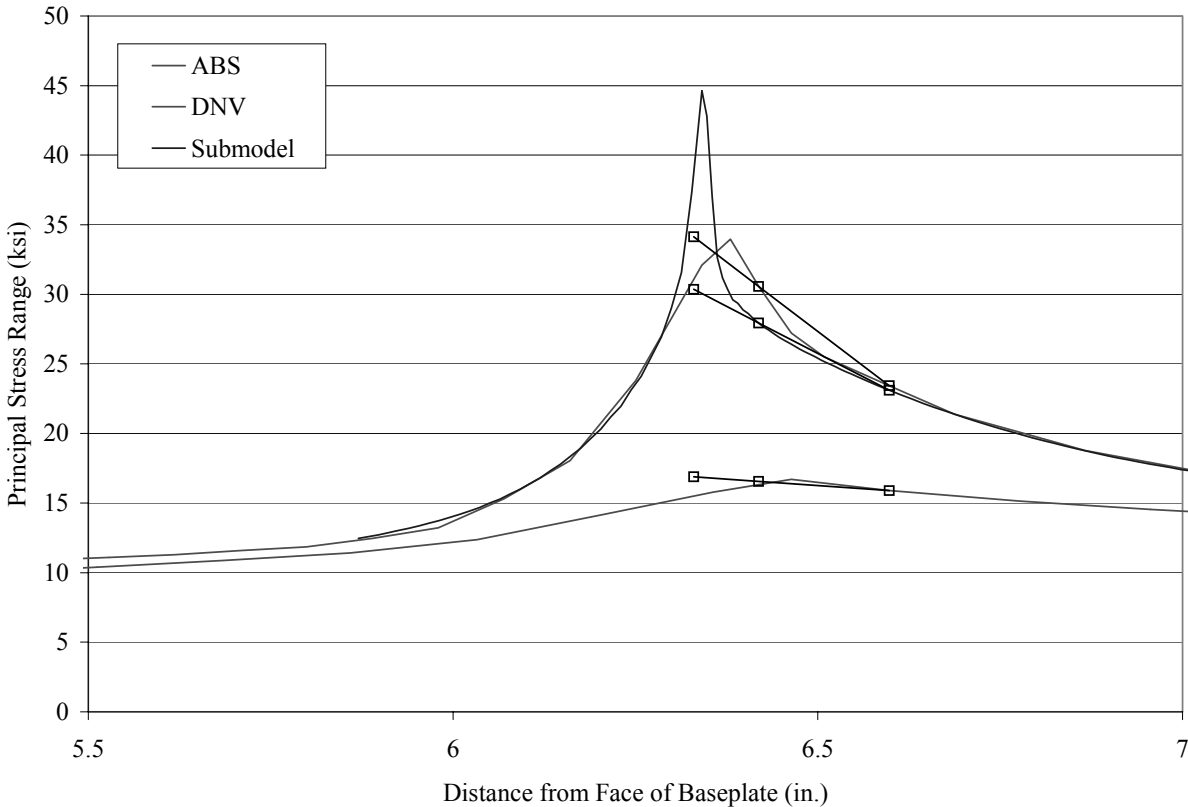


Figure 9.13 Comparison of ABS, DNV, and Mesh Refinement Solutions around Stiffener

The DNV and the submodeling approach track each other well. They diverge near the stiffener toe since the mesh in the submodel is finer than in the mesh in the DNV model.

9.5.5.1 Comparison of Bending and Principal Stress Ranges

To check that the maximum stress range was being used for SCF calculations, the bending and principal stress ranges on a model were compared. Figure 9.14 compares the bending and principal stress ranges at a socket weld. The bending stress range is, as expected, slightly smaller than the principal stress range and at a small distance from the discontinuity, the stress ranges are almost identical.

9.5.5.2 Comparison of SCF Solutions

The solutions from the ABS approach are approximately 40% of those from the DNV and refined mesh approaches. The reason for this is that the ABS approach uses centroidal stresses rather than nodal stresses. In Abaqus, the centroidal stresses are functions of the integration point stresses. An approximation of the centroidal stress is the average of the integration points within the element. The actual computation of the centroidal stresses involves using interpolation functions to find the displacement at the centroid of the element from which the principal stress can be derived. Therefore, if a high bending stress gradient is present in the mast arm walls, using centroidal stresses preserves the SCF solution trend but will suppress the magnitude of the SCFs.

The solutions from the DNV and refined mesh approaches track each other well. The smaller mesh consistently gave smaller values of the SCF. In fact, the ratio between the refined mesh and DNV SCFs for unstiffened models is, on average, 0.94. For stiffened models, this ratio is 0.86. Two points should be concluded from these numbers. The first is that when comparing the average SCF ratios between the stiffened and unstiffened models, the stiffened model SCFs average lower than the unstiffened model

SCFs. This difference may be a fabrication of the submodeling technique rather than a real-world difference. A potential source of the error is the transfer of the solution between a global model and its submodel or a submodel and its local submodel. Here, global displacements are imposed as submodel boundary conditions and a solution in the submodel is calculated. If the calculated global displacements are appreciably smaller than the real displacements, then the solution in the submodel will also be biased towards displacements smaller than the real displacements. This bias will influence the stress range and thus the SCFs. The second point is in regards to ease of modeling. The time involved in creating and running a model using the DNV approach is considerably less – approximately $\frac{1}{4}$ of the time, if not less – than the time required to create submodels and local submodels for each global model.

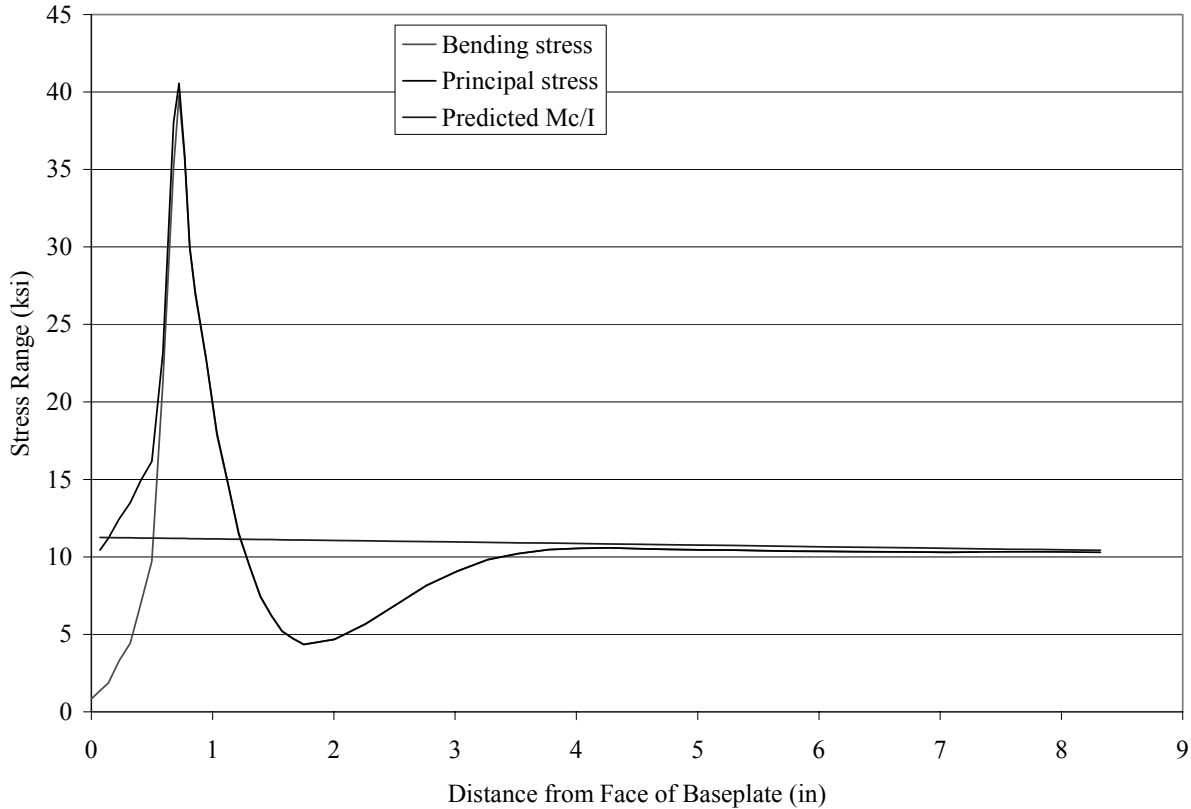


Figure 9.14 Bending vs. Principal Stress Range

Based on the fact that the ABS values underestimate the SCFs, ABS values will be presented in tables, but will not be discussed in results. Since the DNV and refined mesh / submodeled SCFs track each other well and the DNV approach is much easier to use, both values will be presented in tables, but the DNV results will be used to discuss the results.

9.6 UNSTIFFENED MODELS

Table 9.4 is a list of all the unstiffened models analyzed and the dimensions of the bolt patterns. The baseplate height refers to the dimension parallel to the symmetry plane and the baseplate width refers to the dimension normal to the symmetry plane. The bolt hole offset is the distance from the corner of the baseplate in the width and height directions to the center of the bolt hole.

The variables considered in these models were: the baseplate thickness – 1.50 in. versus 2.00 in., the mast arm thickness – 0.179 in. versus 0.239 in., the bolt patterns – As Tested, TxDOT, and 8 Hole, and a solid baseplate – a baseplate with the hole in the center filled in.

In Table 9.4 the first heavy line separates the 2.00 inch-thick baseplates from the 1.50 inch-thick ones. The second heavy line separates the more ‘academic’ models from more realistic ones. The only purpose of these models is to show an extreme effect of a specific variable.

Table 9.4 Analyzed Unstiffened Models

Model	Baseplate Thickness (in.)	Bolt Pattern	Baseplate Height (in.)	Baseplate Width (in.)	Bolt Hole Diameter (in.)	Bolt Hole Offset from Corner (in.)	Mast Arm Wall Thickness (in.)	Mast Arm Length (in.)
VAL u	1.50	As Tested	9.50	9.50	1.625	2.00	0.179	89.35
TxDOT VAL u	1.50	TxDOT	9.00	6.00	1.750	1.50	0.179	89.35
8 Hole VAL u	1.50	8 Hole	9.50	9.50	1.625	2.00	0.179	89.35
TX u	1.50	As Tested	9.50	9.50	1.625	2.00	0.239	89.35
VAL u2	2.00	As Tested	9.50	9.50	1.625	2.00	0.179	89.35
TxDOT VAL u2	2.00	TxDOT	9.00	6.00	1.750	1.50	0.179	89.35
8 Hole VAL u2	2.00	8 Hole	9.50	9.50	1.625	2.00	0.179	89.35
TX u2	2.00	As Tested	9.50	9.50	1.625	2.00	0.239	89.35
Long VAL u	1.50	As Tested	9.50	9.50	1.625	2.00	0.179	196
Solid VAL u	1.50	As Tested	9.50	9.50	1.625	2.00	0.179	89.35
Solid TX u	1.50	As Tested	9.50	9.50	1.625	2.00	0.239	89.35
VAL u12	12.00	As Tested	9.50	9.50	1.625	2.00	0.179	78.85

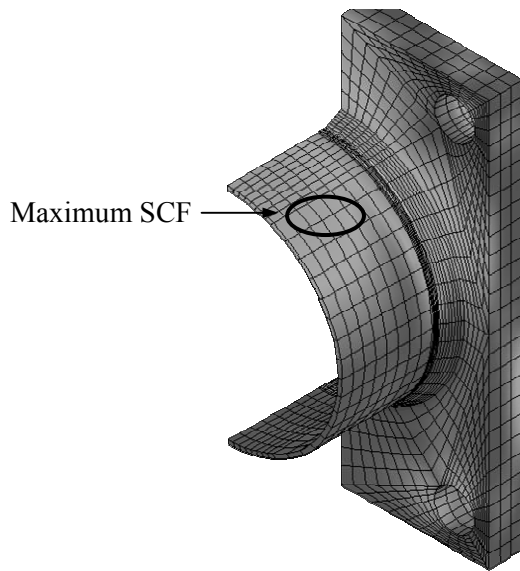


Figure 9.15 Location of Maximum SCF

For each model, stresses along the top cord of the mast arm were analyzed to determine the SCF. The location of the maximum SCF was expected and is shown in Figure 9.15.

9.6.1 Effect of Nonlinear Geometry

The effect of nonlinear geometry on the stress range at weld toes was investigated on the TX 3x1/4 stiffened model. A solution was found around the socket weld and the stiffener for the following combinations of applied load and geometry:

1. Maximum and minimum test load & non-linear geometry
2. Maximum and minimum test load & linear geometry
3. Test load range & nonlinear geometry
4. Test load range & linear geometry

The test load refers to the actual load applied to the specimen during the fatigue tests. Figure 9.16 shows how these combinations affected the stress range at the stiffener toe. Figure 9.17 shows how these combinations affected the stress range at the socket weld toe.

The plots in Figures 9.16 and 9.17 show no significant difference between the calculated stress ranges, especially at the highest stress region at the weld toe. Therefore, all the analyses were performed using the applied test load range and linear geometry.

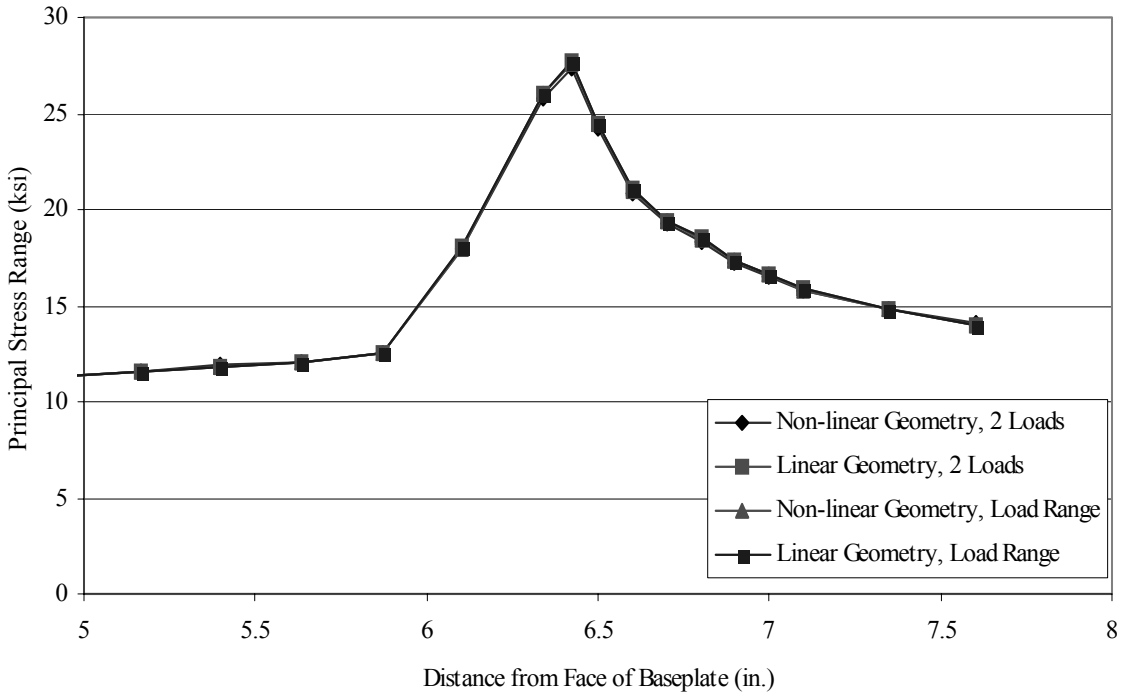


Figure 9.16 Effect of Non-linear Geometry on Stress Range at Stiffener Toe

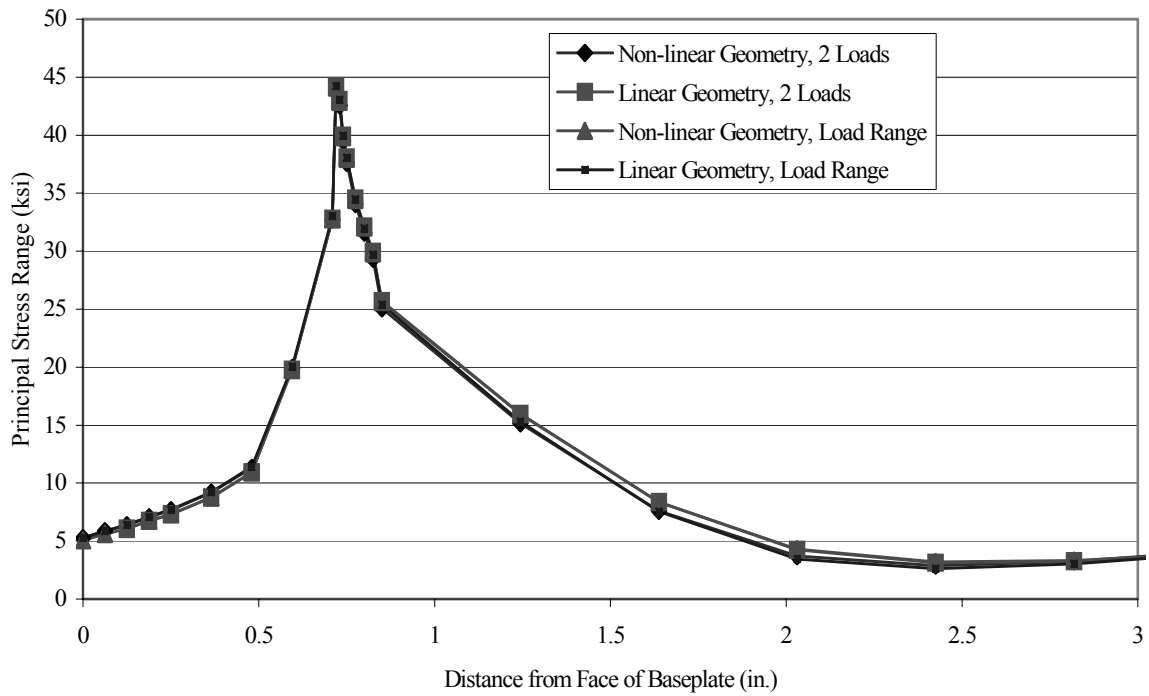


Figure 9.17 Effect of Non-linear Geometry on Stress Range at Socket Weld Toe

9.6.2 Unstiffened Model Results and Discussion

Table 9.5 summarizes the SCFs for the models in Table 4 using the ABS, DNV, and mesh refinement approaches. Based on the discussion in the previous section, all SCF values will be presented in Table 9.4 and Figure 9.18, but only the results of the DNV approach will be discussed in the results.

The plot in Figure 9.18 shows the SCFs for the analyzed models for all three methods. Note that the SCFs from all three methods track each other for most of the models.

Table 9.5 SCFs for Unstiffened Models

Model Name	ABS SCF	DNV SCF	Refined SCF
VAL u	1.56	4.09	3.76
TXDOT VAL u	1.35	3.90	3.56
8 Hole VAL u	1.04	3.36	3.16
TX u	1.72	4.04	3.76
VAL u2	1.12	3.11	2.97
TXDOT VAL u2	1.00	3.09	2.96
8 Hole VAL u2	0.99	2.70	2.56
TX u2	1.21	3.02	2.85
Long VAL u	1.56	4.07	3.74
Solid VAL u	0.83	2.38	2.22
Solid TX u	0.85	2.35	2.21
VAL u12	0.93	2.15	2.02

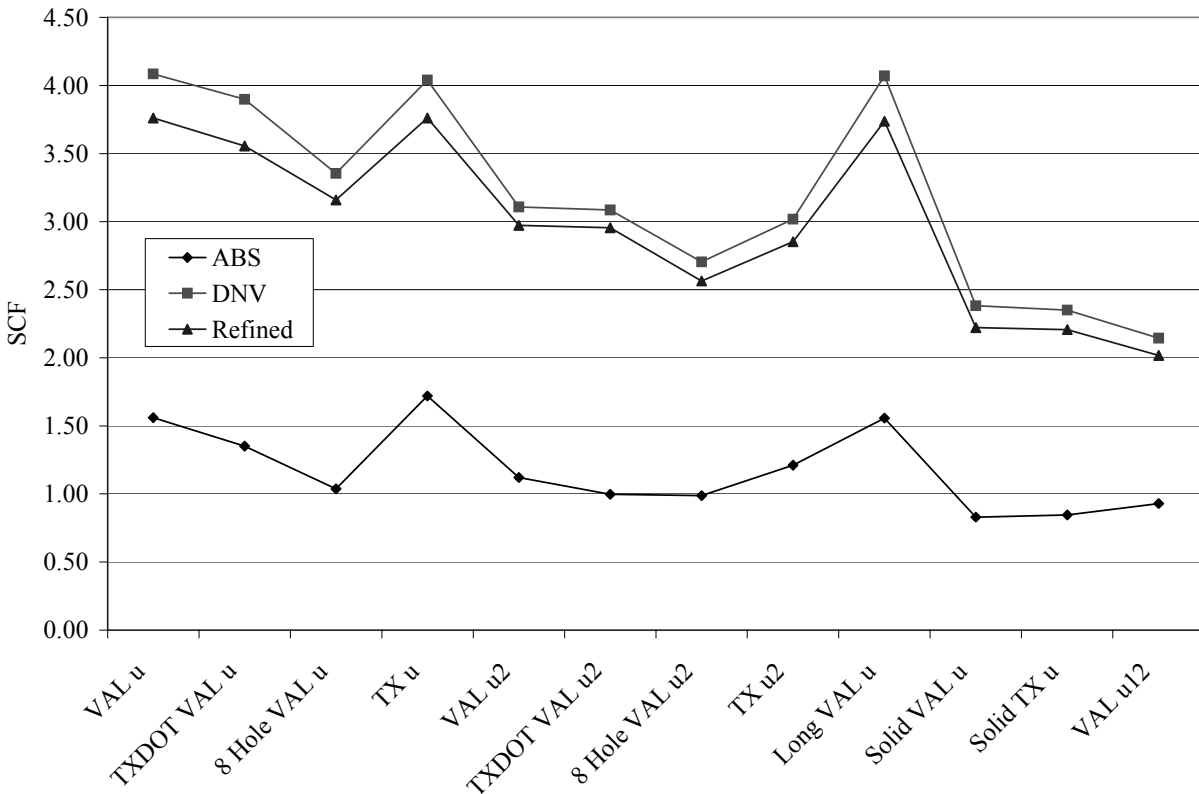


Figure 9.18 SCFs for Analyzed Models

9.6.3 Effect of mast arm thickness and length on socket weld SCF

To determine the effect of shear on the tested specimens, an 89.35 in. mast arm and a 196.00 in. mast arm were analyzed. Figure 9.19 plots the SCFs and shows no influence of mast arm length on the socket weld SCF.

Two wall thicknesses were modeled: 0.179 in. and 0.239 in. The impact of the mast arm wall thickness on the socket weld SCF is shown in Figure 9.19. This figure shows that the mast arm wall thickness does not influence the socket weld SCFs. Thus in this section, the effect of the wall thickness will be ignored and not considered as a variable the remaining graphs.

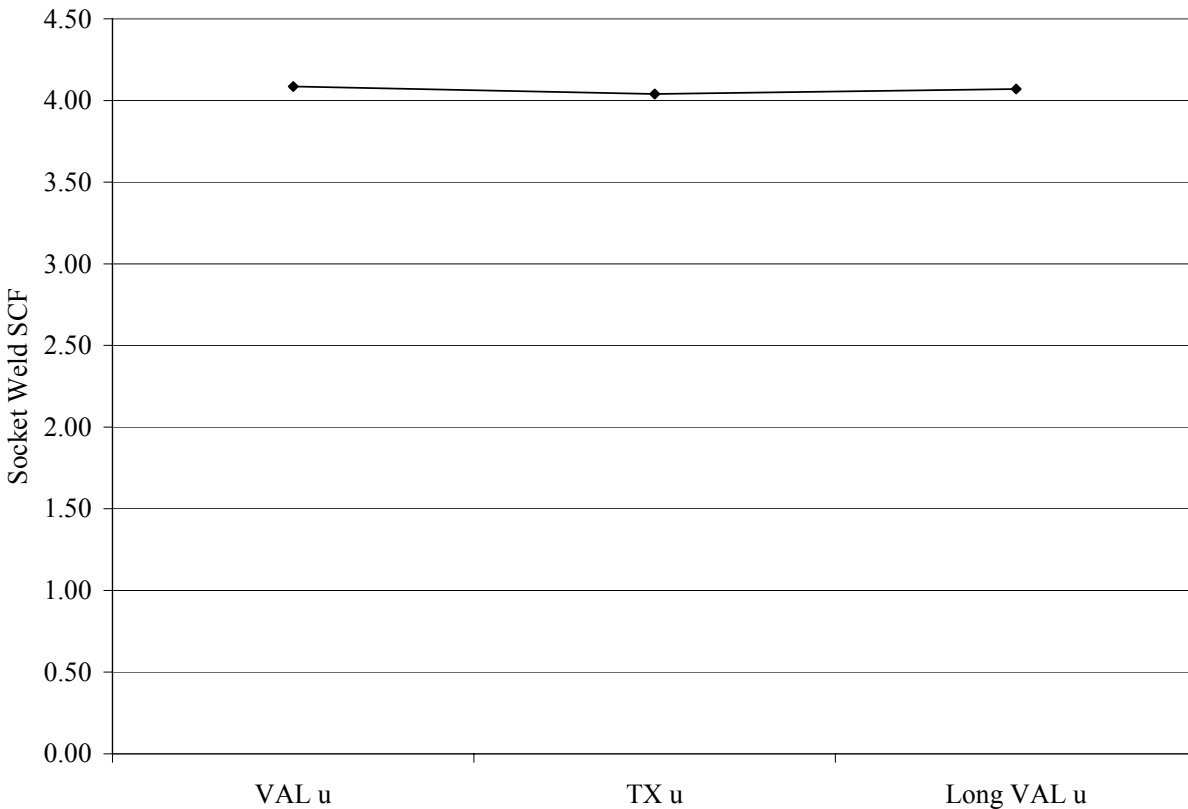


Figure 9.19 Effect of Shear and Mast Arm Thickness on Socket Weld SCF

9.6.4 Effect of Solid Baseplate on Socket Weld SCF

The effect of the solid baseplate – a baseplate with the hole in the center filled in – was investigated to determine how the bending in the wall was transferred into the baseplate. Figure 9.20 shows that the solid baseplate reduces the socket weld SCF by 40%. This result implies that the baseplate geometries have important impacts on the SCF. This issue is discussed further in the next sections.

9.6.5 Effect of Baseplate Thickness on Socket Weld SCF

Three baseplate thicknesses were analyzed: 1.50 in., 2.00 in., and 12.00 in. The impact of the baseplate thickness on the socket weld SCF is shown in Figure 9.21 which plots the SCF versus baseplate thickness. The results show that increasing the thickness of a relatively thin baseplate is the most effective; the SCF is reduced by 24% by increasing the baseplate thickness from 1.50 in. to 2.00 in. while increasing the baseplate thickness from 1.50 in. to 12.00 in. reduces the SCF by 48%.

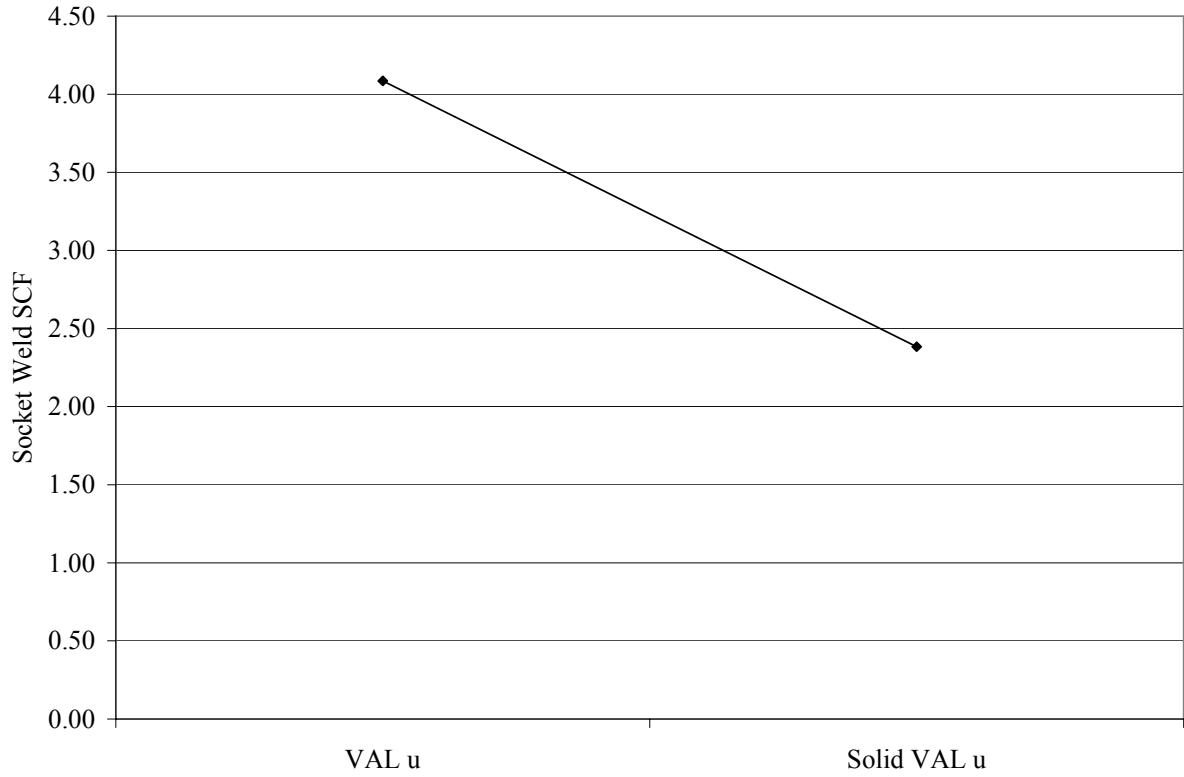


Figure 9.20 Influence of Solid Baseplate on Socket Weld SCF

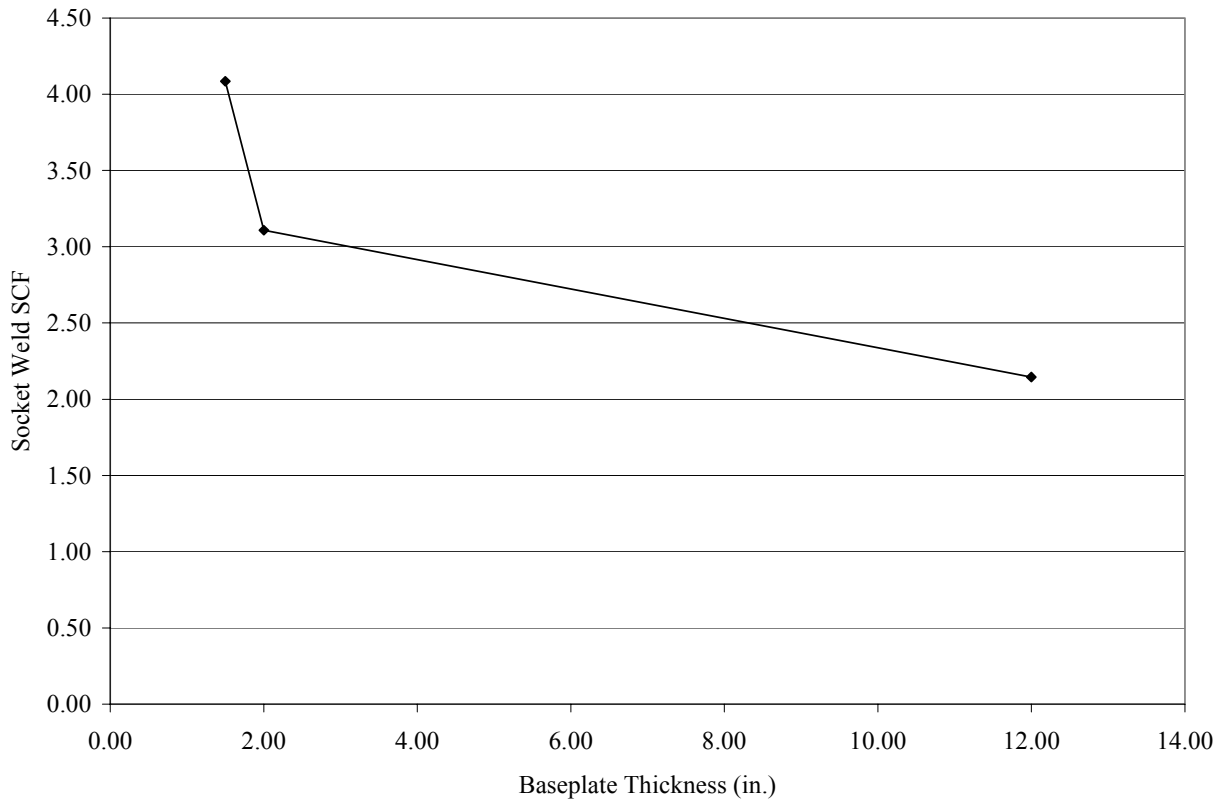


Figure 9.21 Influence of Baseplate Thickness on Socket Weld SCF

9.6.6 Effect of Bolt Pattern on Socket Weld SCF

The three different bolt patterns used in the analyses are: As tested, TxDOT, and 8-Hole. The dimensions of the bolt patterns can be found in Table 9.4. The As tested bolt pattern is the one used on the test specimens. The TxDOT bolt pattern is the one used by TxDOT in their connection details, and the 8-hole bolt pattern is similar to the As tested bolt pattern, but with holes along the vertical and horizontal directions as well. The influence of the bolt patterns on the SCF is shown in Figures 9.22.

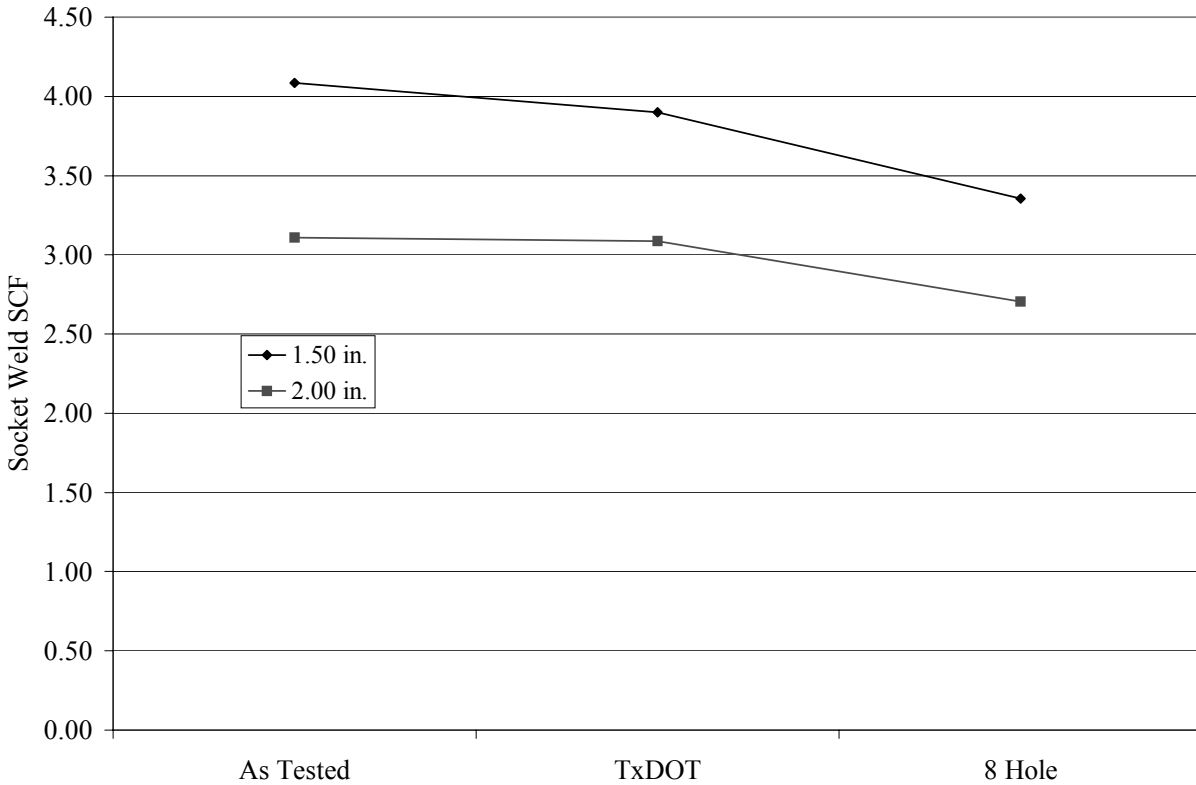
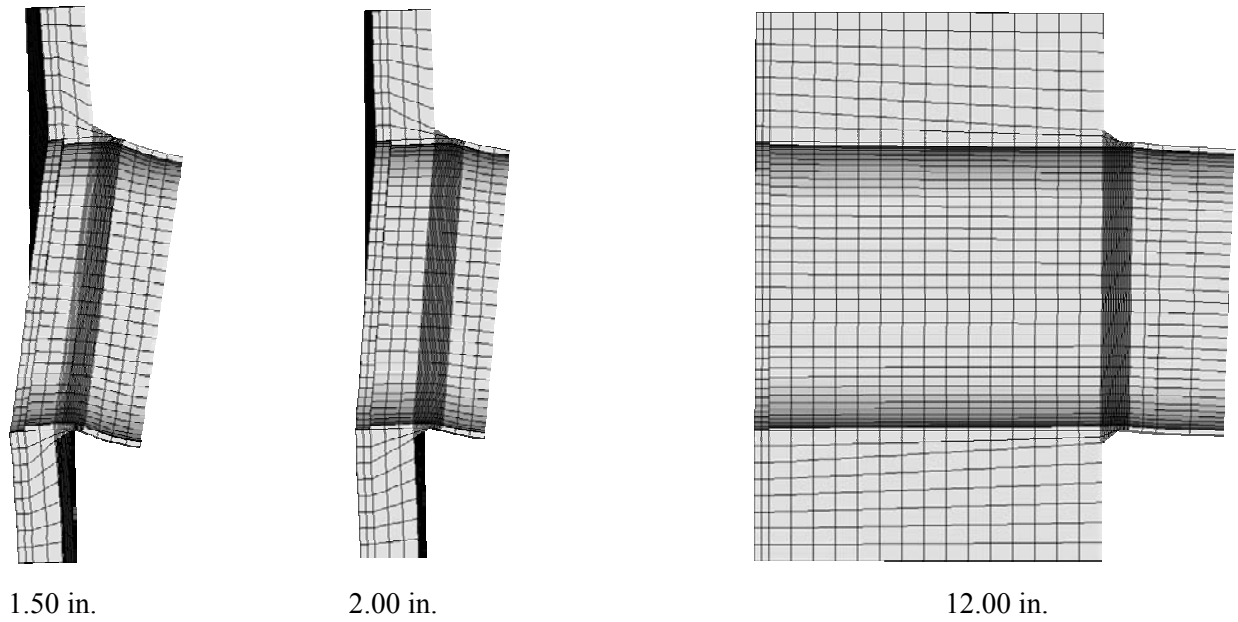


Figure 9.22 Influence of Bolt Pattern on Socket Weld SCF

Figure 9.22 shows a trend of decreasing socket weld SCF with increasing fixity from the bolt pattern. The bolt pattern has less impact upon the 2.00 in. baseplate than the 1.50 in. baseplate, where the bolt pattern produces a more significant change in the SCF. The additional stiffness of the 2.00 in. baseplate minimized the influence of the additional stiffness provided by the TxDOT and 8-hole bolt patterns.

From the results presented, the variables that influenced the socket weld SCF for the unstiffened models were the baseplate geometries. The reason the thicker baseplates lower the SCF, and the reason that the solid baseplate and the TxDOT and 8-hole bolt patterns lower the SCF, is that they provide more rotational restraint. Figure 9.23 compares the deformation in the baseplate for varying thickness baseplates.

The degree to which the baseplate deforms affects the amount of deformation in the mast arm wall which determines the SCFs. Figure 9.24 compares these deformations.



**Figure 9.23 Influence of Baseplate Thickness on Baseplate Deformation
(100x Deformation using Mesh Refinement Approach)**

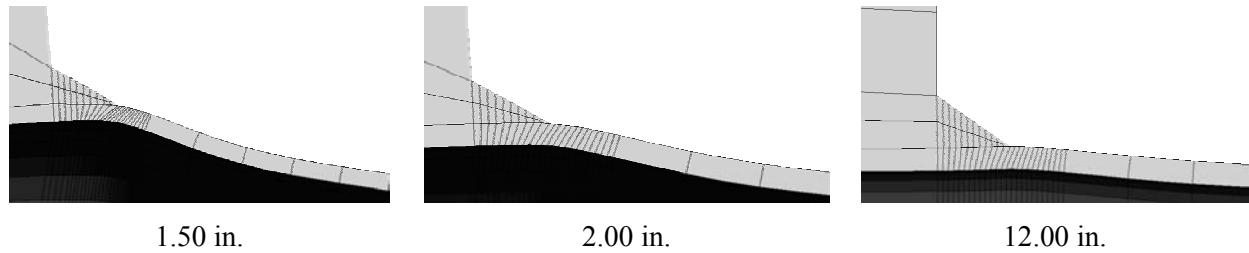


**Figure 9.24 Influence of Baseplate Thickness on Mast Arm Wall Deformation
(100x Deformation using Mesh Refinement Approach)**

9.7 STIFFENED MODELS

All stiffened models were created by adding stiffeners to existing unstiffened models. The models were analyzed with the bolt pattern used in the test specimens. All models have a mast arm length equal to that of the test specimens, 89.35 in. Table 9.6 provides a list of all the stiffened models analyzed and the stiffener dimension. All stiffeners have a height of 2.0 in. at the baseplate and are welded with 0.25 in. equal-leg fillet welds.

Table 9.6 Analyzed Stiffened Models

Model	Baseplate Thickness (in.)	Mast Arm Wall Thickness (in.)	Stiffener Length (in.)	Stiffener Thickness (in.)	Stiffener Location on Mast Arm
TX 6x3/8	1.50	0.239	6.4	0.375	Horizontal & vertical
TX 3x1/4	1.50	0.239	3.5	0.25	Horizontal & vertical
VAL 6x3/8	1.50	0.179	6.4	0.375	Horizontal & vertical
VAL 3x1/4	1.50	0.179	3.5	0.25	Horizontal & vertical
VAL 3x3/8	1.50	0.179	3.5	0.375	Horizontal & vertical
VAL 6x3/8 @ 45	1.50	0.179	6.4	0.375	45° offset from vertical
VAL 6x3/8 @ 180	1.50	0.179	6.4	0.375	Vertical only
VAL 6x3/8 @ 90 & 45	1.50	0.179	6.4	0.375	Horiz. & vert. & 45° offset
VAL 2 3x1/4	2.00	0.179	6.4	0.375	Horizontal & vertical

The first heavy line separates models of the test specimen with different mast arm wall thickness. The second heavy line separates additional models analyzed to extend the analyzed geometries beyond the tested geometries. The third heavy line separates models with different baseplate thicknesses.

9.7.1 Stiffened Model Results and Discussion

For the stiffened models, two SCFs were found: the SCF at the toe of the socket weld and the SCF at the end of the stiffeners. Table 9.7 summarizes the SCF values obtained for the models. Note the location of the SCF on the baseplate weld as shown in Figure 9.25. The SCFs are calculated as the maximum local principal stress ranges at the stiffener and socket weld toes divided by the maximum bending stress range at the top tension fiber of an unstiffened mast arm. Figures 9.26 and 9.27 plot all the socket weld and stiffener SCFs for all models, respectively.

Table 9.7 Socket Weld and Stiffener SCFs for Stiffened Models

Model Name	ABS Approach		DNV		Submodeling Approach	
	SCF _{weld}	SCF _{stiffener}	SCF _{weld}	SCF _{stiffener}	SCF _{weld}	SCF _{stiffener}
TX 6x3/8	1.15	1.37	3.30	2.52	2.75	2.19
TX 3x1/4	1.32	1.55	3.74	3.08	3.16	2.67
VAL 6x3/8	1.09	1.48	3.31	2.99	2.84	2.66
VAL 3x1/4	1.28	1.59	3.81	3.78	3.20	3.24
VAL 3x3/8	1.27	1.60	3.80	4.02	3.18	3.36
VAL 6x3/8 @ 45	1.38	1.14	4.11	2.30	3.54	2.05
VAL 6x3/8 @ 180	1.09	1.48	3.33	3.01	2.80	2.60
VAL 6x3/8 @ 90 & 45	0.66	1.09	1.78	1.92	1.53	1.65
VAL 2 3x1/4	1.00	1.47	2.48	3.30	2.31	2.81

The typical locations of the SCFs are shown in Figure 9.25.

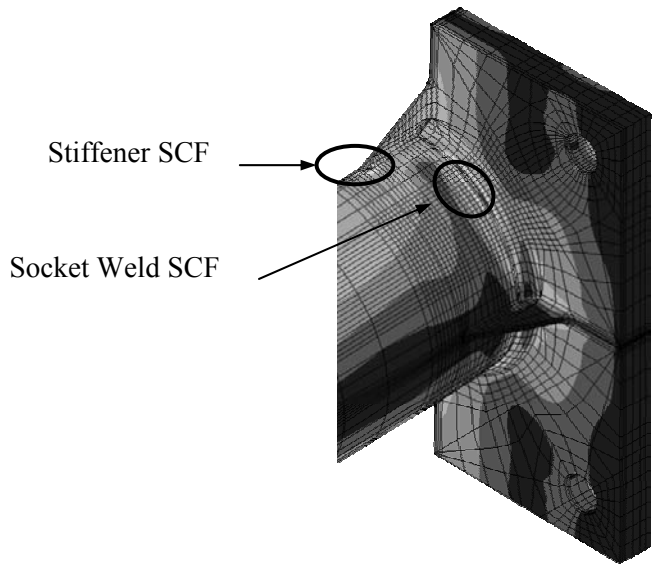


Figure 9.25 Typical Locations of SCFs on Stiffened Models

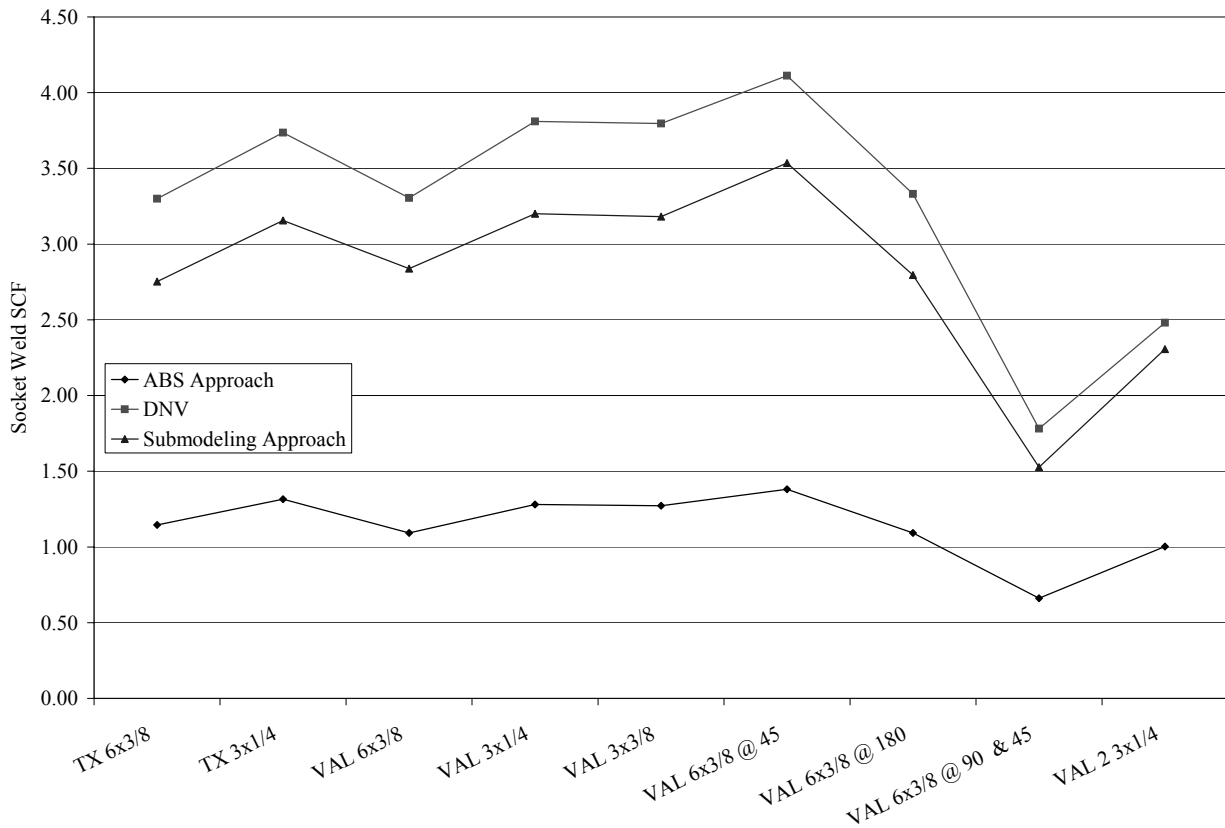


Figure 9.26 Socket Weld SCFs for Stiffened Model

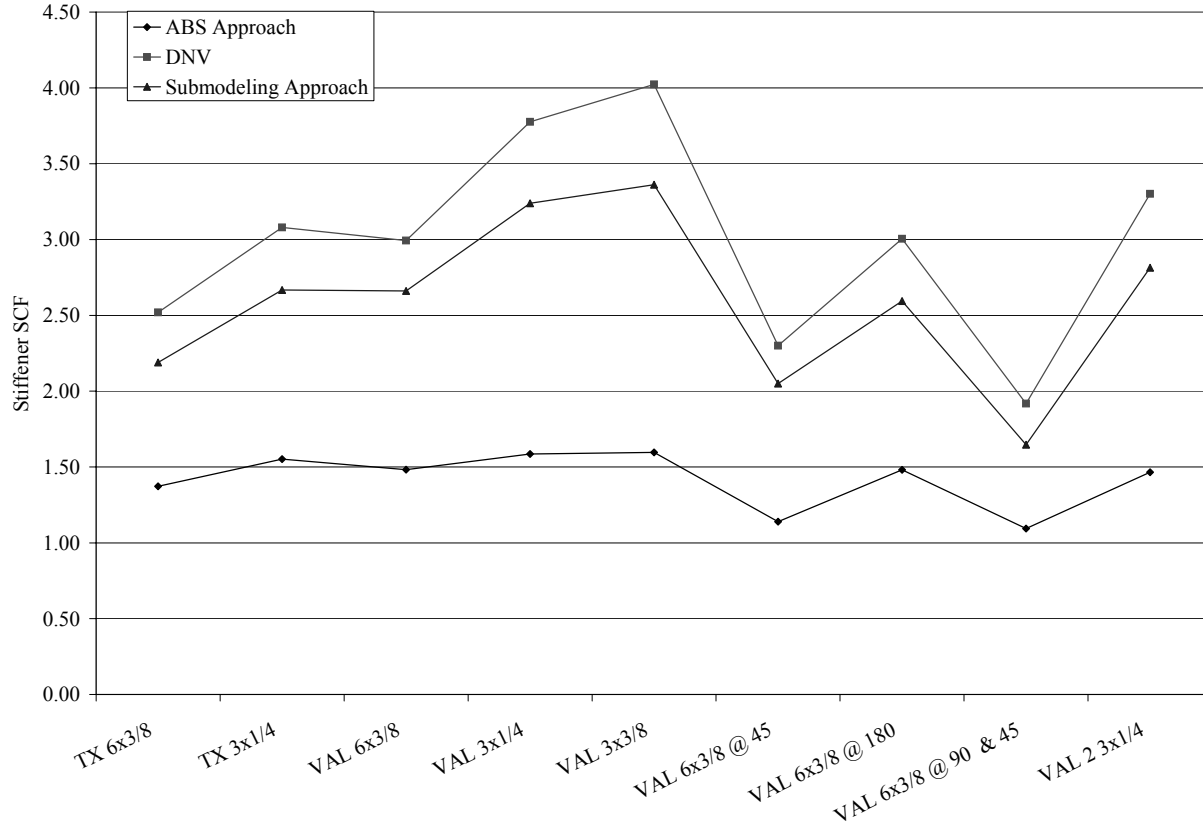


Figure 9.27 Stiffener SCFs for Stiffened Models

9.7.2 Effect of Mast Arm Wall Thickness on SCFs

The same two wall thicknesses are used for modeling the stiffened models: 0.179 in. and 0.239 in. Figure 9.28 shows the influence of the mast arm wall thickness on the socket weld and stiffener SCF respectively for models with 6 inch-long, 0.375 inch-thick stiffeners and models with 3 inch-long, 0.25 inch-thick stiffeners.

The results show that the mast arm wall thickness is not a variable in determining the socket weld SCF, however, increasing the mast arm wall thickness from 0.179 in. to 0.239 in. increases the stiffener SCF by 15-18%.

9.7.3 Effect of Stiffener Length on SCFs

The two stiffener lengths examined are 6 inches and 3 inches. Both stiffeners had a thickness of 0.375 in. and a mast arm wall thickness of 0.179. Figure 9.29 plots the influence of the stiffener length on the socket weld and stiffener SCFs.

Comparing results, the trend for both meshing approaches is that an increase in stiffener length decreases the socket weld and stiffener SCF. By increasing the stiffener length, the socket weld SCF is decreased by 13% and the stiffener SCF is decreased by 26%.

The stiffener SCF was reduced because the incident angle onto the mast arm for a 6.00 in. stiffener (18.3°) is half of that for a 3.00 in. stiffener (33.7°). The socket weld SCF was also reduced. An explanation for this is that the longer stiffener transfers more load directly to the baseplate than a shorter one, thus reducing the load carried by the socket weld.

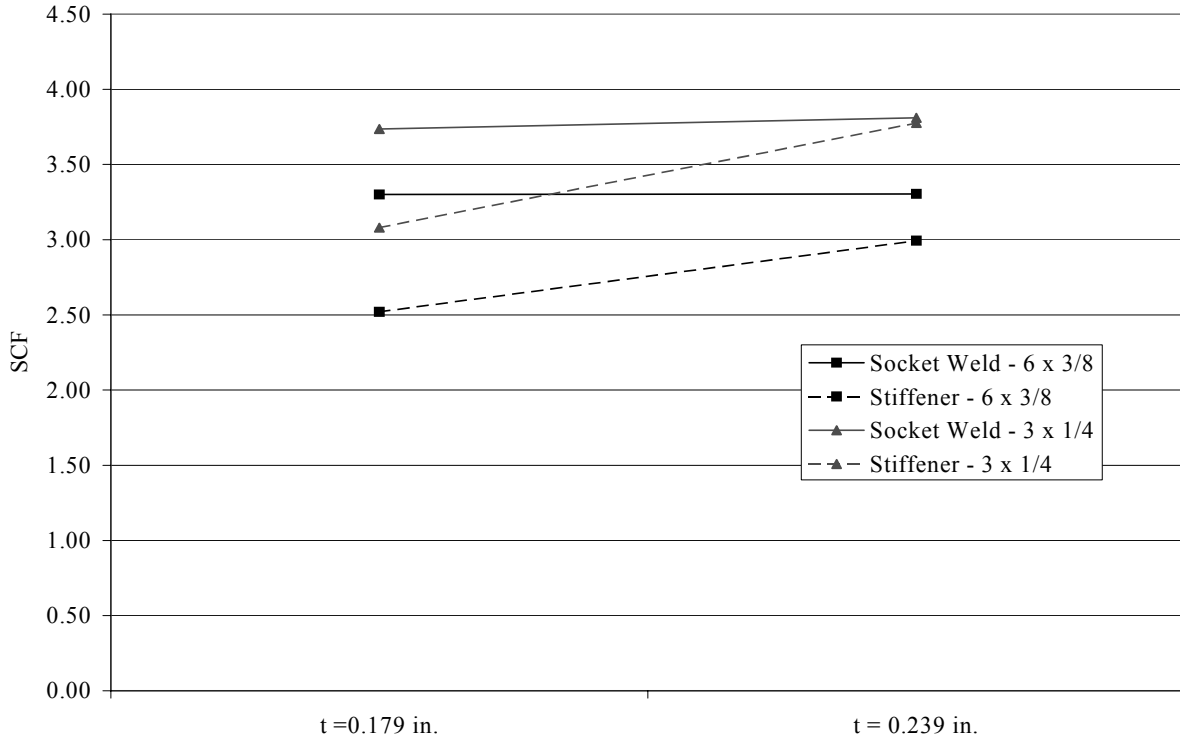


Figure 9.28 Effect of Mast Arm Wall Thickness on SCFs

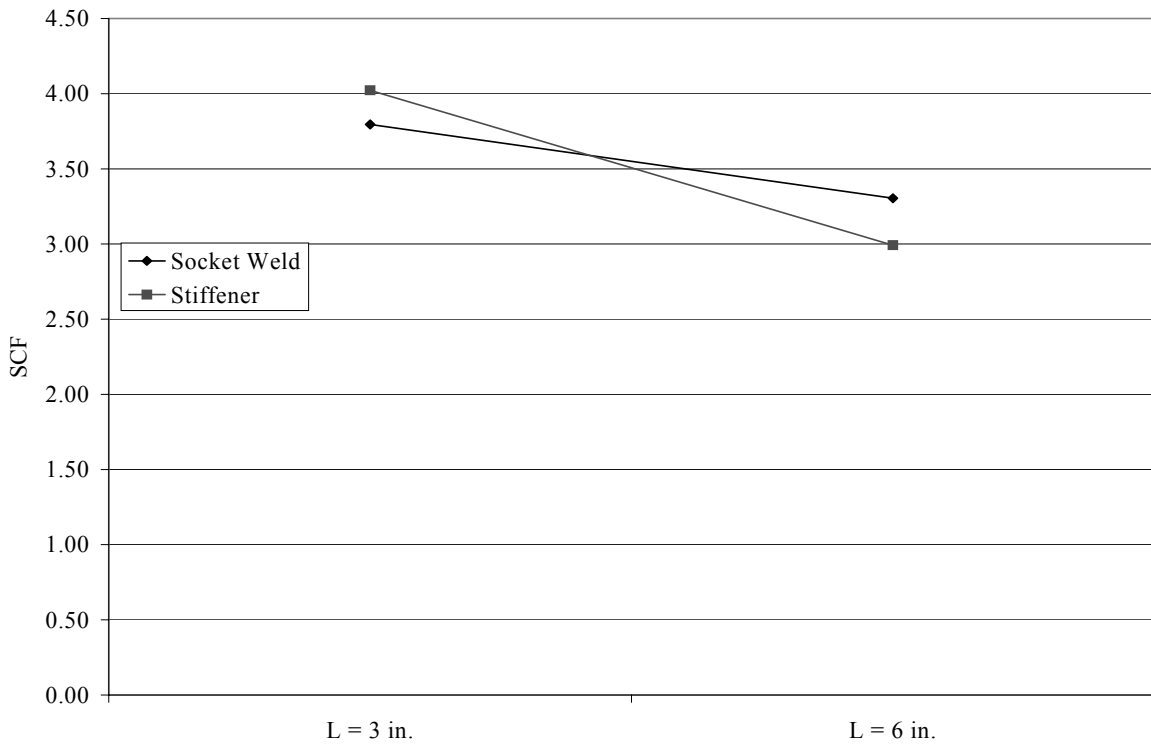


Figure 9.29 Influence of Stiffener Length on SCFs

9.7.4 Effect of Stiffener Thickness on SCFs

The effect of stiffener thickness was examined for 3-inch long stiffeners. Both 0.25 in. and 0.375 in.-thick stiffeners were analyzed. Figure 9.30 shows that changing the stiffener thickness has no significant affect on the SCFs at the socket weld. The stiffener SCF is elevated by 7% by increasing the stiffener thickness by 50%. Thus, the stiffener thickness has no influence on the socket weld SCF and a small affect on the stiffener SCF.

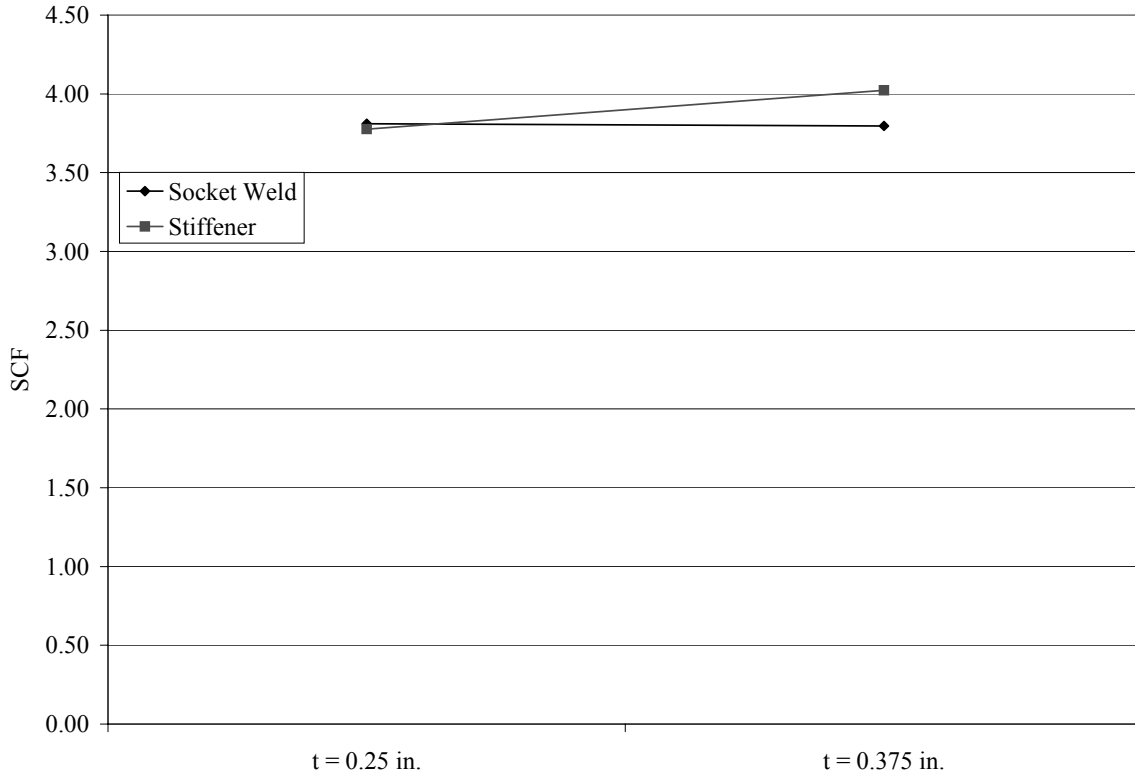


Figure 9.30 Influence of Stiffener Thickness on SCFs

9.7.5 Effect of Stiffener Thickness to Wall Thickness Ratio on SCFs

To show how punching shear affects the SCFs, the ratio of stiffener thickness to wall thickness is considered. Figure 9.31 compares two different thickness ratios (R): 2.10 and 1.05. The two models used to generate these two thickness ratios were VAL 3x3/8 (R = 2.10) and TX 3x1/4 (R = 1.05).

The trend shows that larger thickness ratios increase the stiffener SCF but do not affect the socket weld SCF significantly. The stiffener SCF is increased by 31% while the socket weld SCF is increased by less than 2%.

9.7.6 Effect of Baseplate Thickness on SCFs

Based on the results for the unstiffened models, it is expected that the baseplate will be an important variable in determining the SCFs for the stiffened models. Figure 9.32 shows the effect of the baseplate thickness on the socket weld and stiffener SCFs for VAL 6x3/8.

Increasing the baseplate thickness from 1.50 in. to 2.00 in. decreases the socket weld SCF by 35% – less than in an unstiffened model – and the stiffener SCF by 13%.

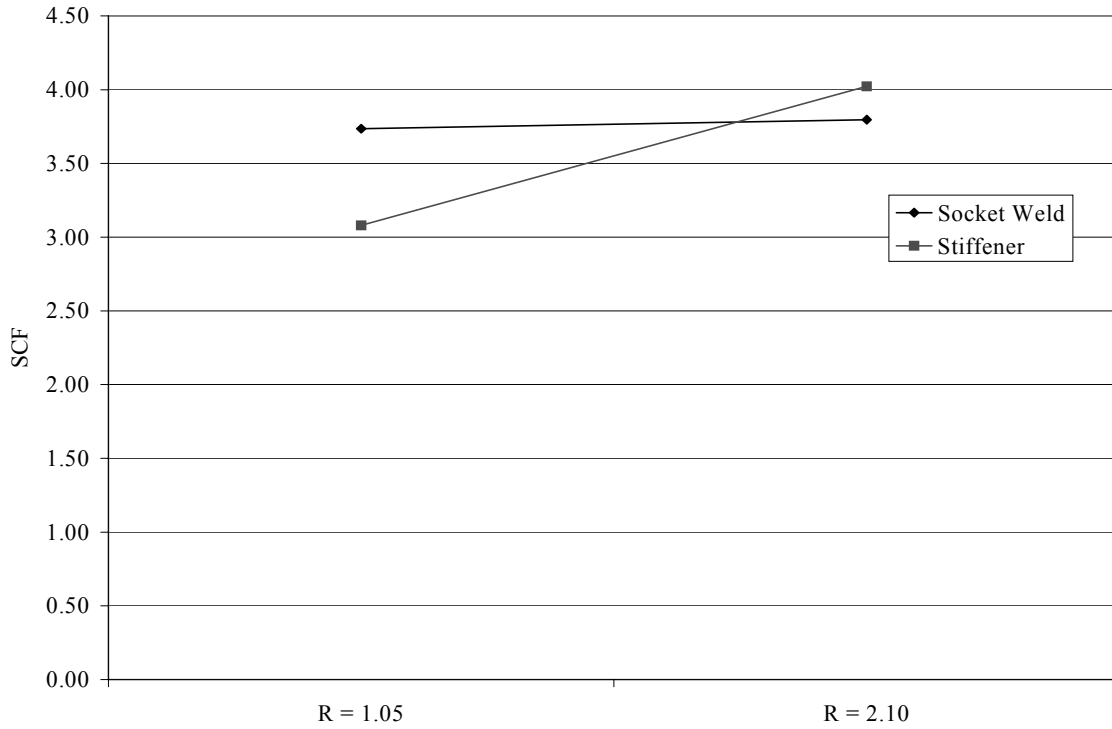


Figure 9.31 Influence of Thickness Ratio on SCFs

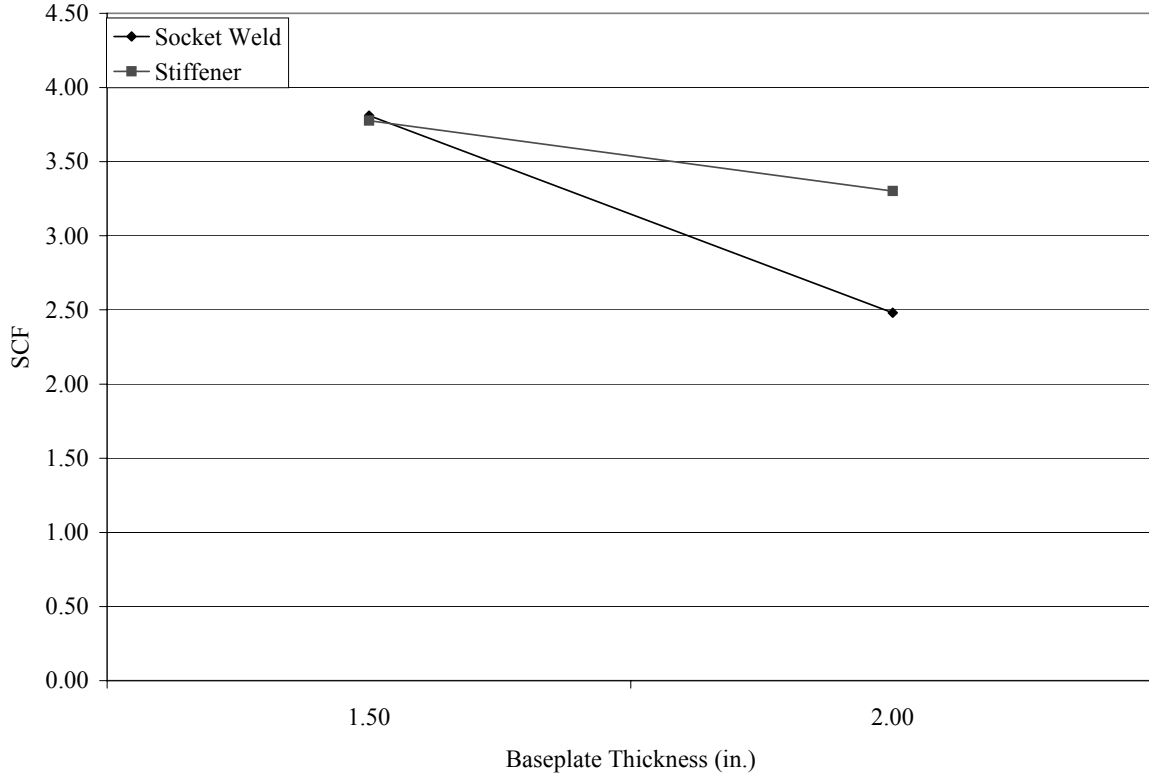


Figure 9.32 Influence of Baseplate Thickness on Socket Weld SCF

9.7.7 Effect of Number of Stiffeners and Stiffener Offset on SCFs

To examine the influence of the number and orientation of stiffeners, 3 models were created: a model with stiffeners offset at 45° from vertical, a model with 8 stiffeners placed around the perimeter of the arm, and a model with only 2 stiffeners – on the top and bottom of the arm. Figure 9.33 shows how these geometries influence the socket weld and stiffener SCFs.

As expected, the model with only 2 stiffeners gives the same SCFs as the models with 4 vertical and horizontal stiffeners. For the model with stiffeners offset at 45°, the stiffeners are located in a region with a lower stress range and the socket weld toe in a high stress range region. Thus, the trend is expected. The model with 8 stiffeners shows the best overall performance. This can be expected since the stiffeners reduce all deformations in the connection and each stiffener carries less load than models with 4 stiffeners.

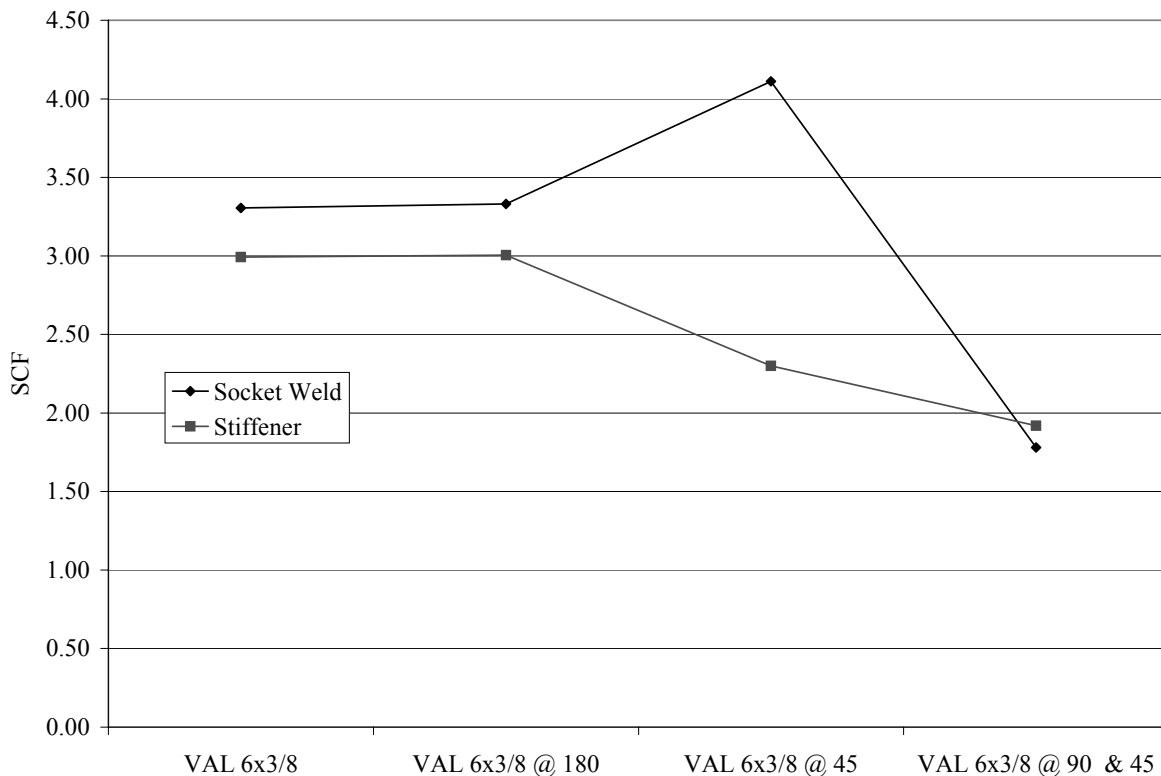


Figure 9.33 Influence of Stiffener Offset on Socket Weld SCF

9.8 COMPARISON OF STIFFENED AND UNSTIFFENED MODELS

The results presented in previous sections only compare stiffened models with other stiffened models and likewise for the unstiffened models. This section will briefly compare stiffened and unstiffened models to show that the results are reasonable.

Figure 9.34 compares socket weld SCFs for stiffened models and the corresponding unstiffened model. The figure shows that the socket weld SCF for the unstiffened model is greater than the SCF for the stiffened models. VAL 6x3/8 @ 45 is approximately equal to VAL u. This would imply that using the offset orientation of stiffeners negates the effect of the stiffeners. While this result does not correlate with the test results, the trend is correct; offsetting the stiffeners should improve the stiffener SCF and exacerbate the socket weld SCF.

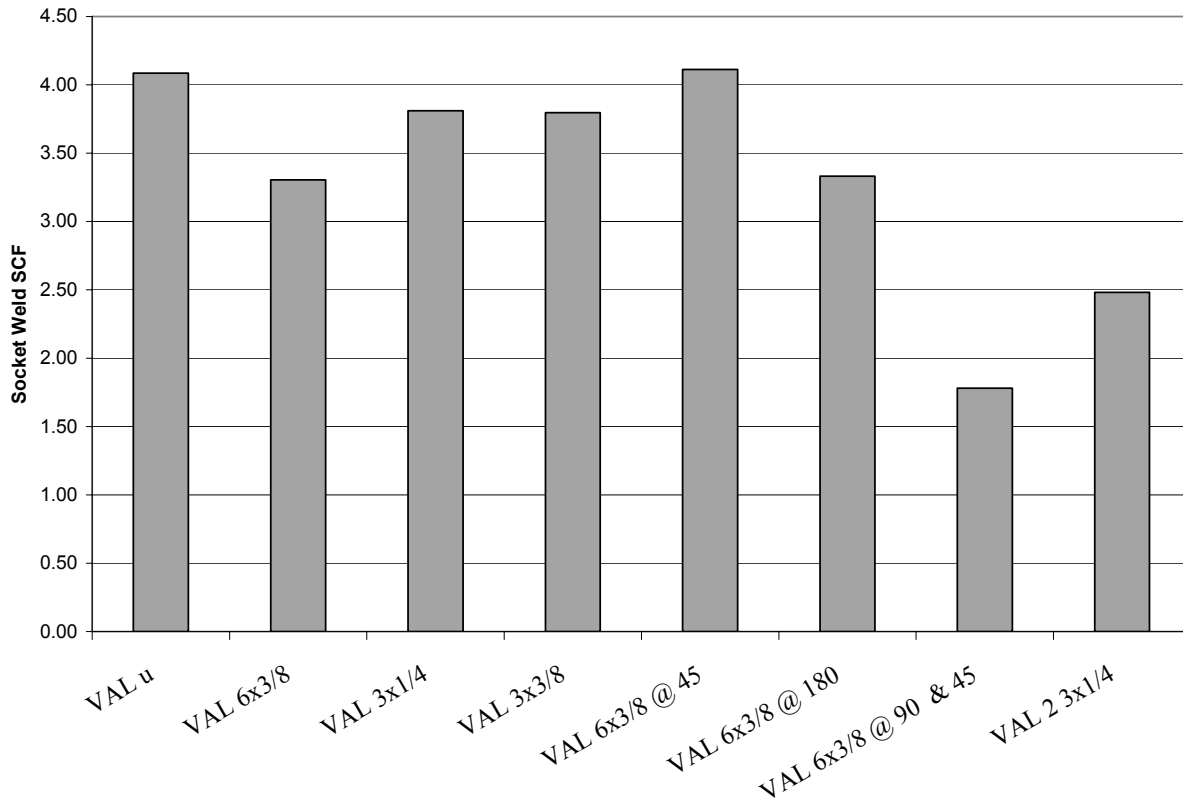


Figure 9.34 Comparison of Stiffened and Unstiffened Socket Weld SCFs

9.9 CONCLUSIONS

From the analyses, it was found that the stiffened models produce lower SCFs at the socket weld than unstiffened models. This means that for a given initial flaw, the fatigue life of the socket weld will be longer for a stiffened model than for an unstiffened model.

From the analyses of unstiffened models, baseplate properties were found to far outweigh other variables in determining the SCF at the socket weld. Models with a thicker baseplate had lower SCFs, as did models with solid baseplates and baseplates with increased fixity due to the bolt pattern.

From the analyses of stiffened models the following was found:

- Stiffener thickness, neutral axis stiffeners, and baseplate thickness were not found to have a major impact on the results. It should be noted however, larger baseplate and stiffener thicknesses – such as a 1.00 inch-thick stiffener and a 4.00 inch-thick baseplate – will significantly change the results.
- The mast arm wall thickness was not found to change the SCF at the socket weld much, but did change the SCF at the stiffener.
- The thickness ratio was also not found to influence the socket weld SCF, but models with large thickness ratios performed much worse at the stiffener than ones with small thickness ratios.
- Offsetting the stiffeners seems to cancel the effect of adding stiffeners by placing the stiffener in a lower stress range region and the weld in a higher stress range region.
- Placing eight stiffeners around the mast arm had the greatest effect on the socket weld and stiffener SCFs lowering them to 60% and 70% of the SCFs of a model with only 4 (non-offset) stiffeners.

CHAPTER 10: WELD SIZE MEASUREMENTS

10.1 INTRODUCTION

Welds on seventeen mast arms were examined in an effort to characterize their geometries. The weld geometries of the specimens were examined in an effort to 1) show variation from specified dimensions, 2) relate weld dimensions to fatigue strength, 3) identify variation between welds of similar specimens, and 4) examine the accuracy of field/inspection measurements. Particular socket welds were also subjected to Ultrasonic Impact Treatment (UIT). The influence of the treatment upon the weld geometry was explored.

10.2 DESCRIPTION OF STUDY

This study focuses on the failed, unstiffened specimens with a wall thickness of 0.179". The basic procedure of the study required taking molds of socket welds (typically at the location of failure), slicing the molds into thin sheets, and then examining the weld profiles under the magnification of digital imaging and National Instruments IMAQ Vision Builder 6 software.

The two weld length dimensions of interest are shown in Figure 10.1. The lighter colored area in the figure is the molding material. The side labeled "Pole" is the surface of the mast arm, while the perpendicular surface is the baseplate. The dark area enclosed by the perpendicular lines and the irregular surfaces is the profile of the weld. Each weld is specified as unequal leg, with the long leg at 0.44" and short leg at 0.25". For the study, very precise measurements were taken using IMAQ, followed by measurements using the G.A.L. Gage Adjustable Fillet Weld Gage.

Two methods of quantifying the incident angle of the weld onto the mast arm were utilized and compared. A *global* angle was defined as the angle that is calculated using the measured long and short leg dimensions and trigonometry, idealizing the weld as a right triangle (see Figure 10.2). The Valmont unequal leg specification for the 0.179" wall thickness (0.44" and 0.25") generates a 30 degree global angle. University of Missouri finite element analyses also call for a 30 degree maximum angle onto the pole (Alderman, 1999). The *local* angle is the angle between the tangent to weld at the weld toe and the mast arm surface (see Figure 10.3).

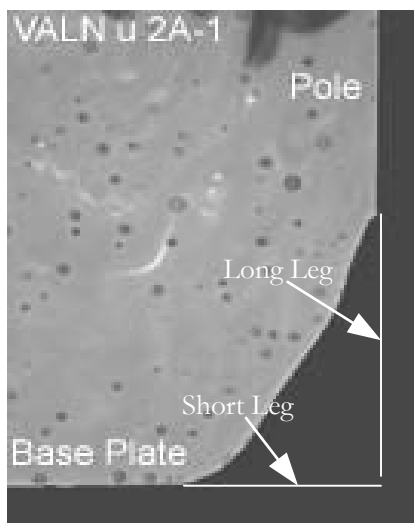


Figure 10.1 Length Dimensions of Interest

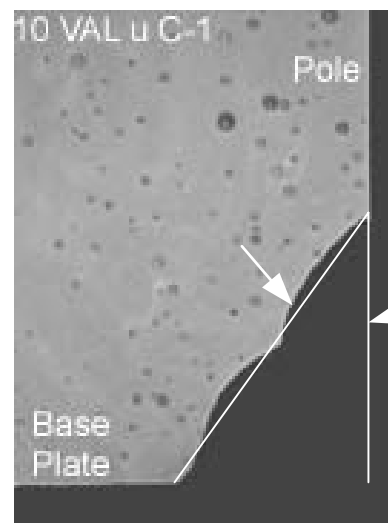


Figure 10.2 Global Angle

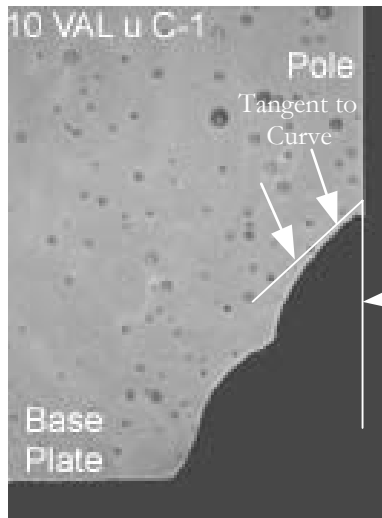


Figure 10.3 Local Angle

The UIT process involves multiple pins rapidly impacting the weld toe area. Two different pin diameters were used to treat the welds in the study, 3 and 5 mm (see Figure 10.4). The UIT process introduces a residual compressive stress and also modifies the geometry of the weld by shortening the long leg and imparting a radius to the toe area. Using IMAQ, circles were fit to these curves (see Figure 10.5) and their radii measured.



Figure 10.4 View of Pins on UIT Tool Head

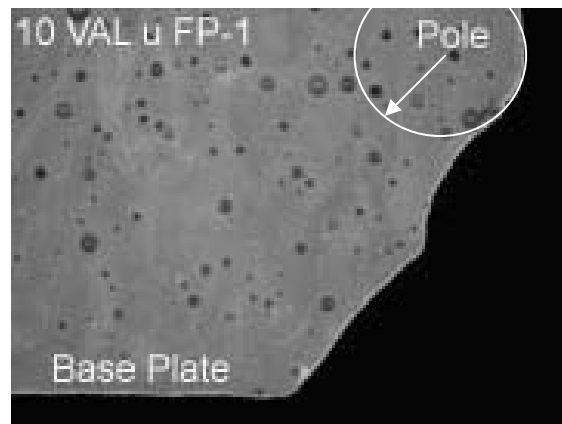


Figure 10.5 Curvature Due to UIT Process

10.2.1 Results of Study: Leg Dimensions

Although two specimens with a thicker wall (0.239") were examined in the study, the focus here will be on specimens with a wall thickness of 0.179", due to their majority in the fatigue testing. All measured data are available in Appendix F.

Standard weld dimensions for the VAL and VALN (the VAL specimens were fabricated in Texas and the VALN specimens were fabricated in Nebraska) specimens were 0.44 inches and 0.25 inches for the long legs and short legs, respectively. Figures 10.6 and 10.7 display the measured leg results. It should be

noted in Figure 10.6 that the long legs of UIT specimens were likely shortened by the treatment. The distribution of the leg lengths is shown in Figures 10.8 and 10.9.

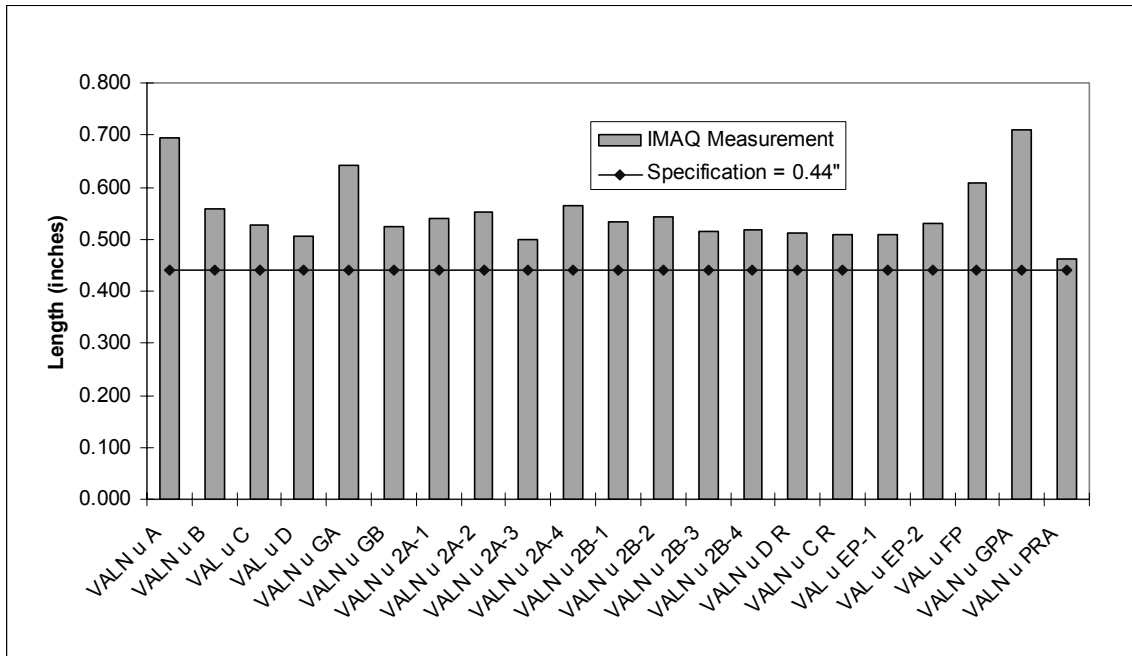


Figure 10.6 Long Leg Measurements for VAL Specimens

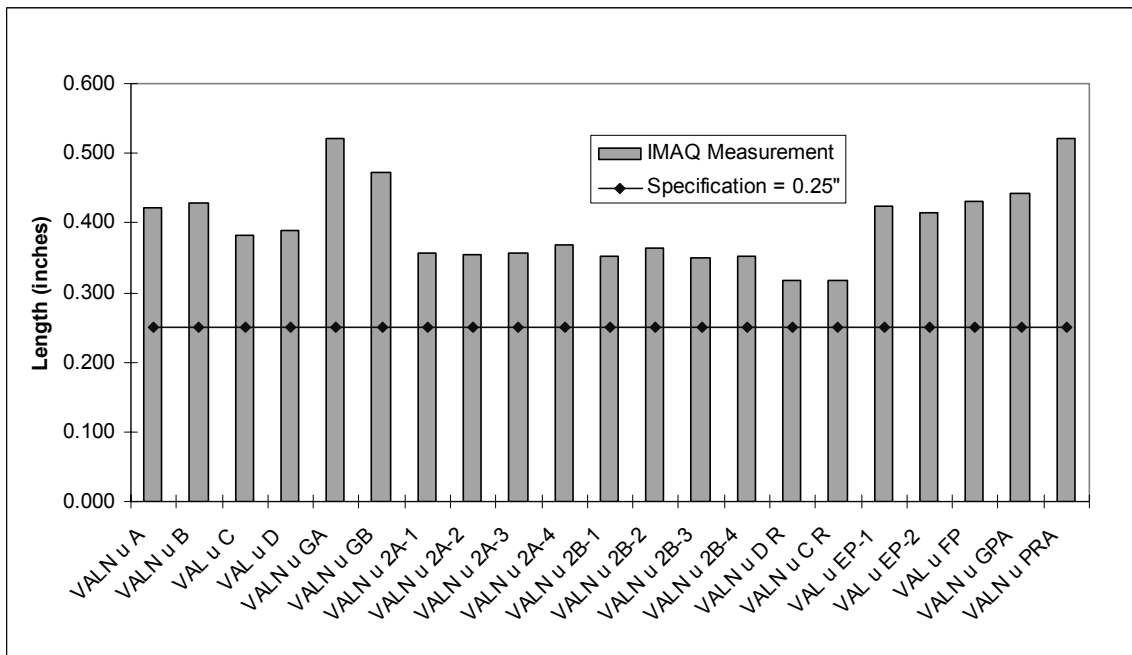


Figure 10.7 Short Leg Measurements for VAL Specimens

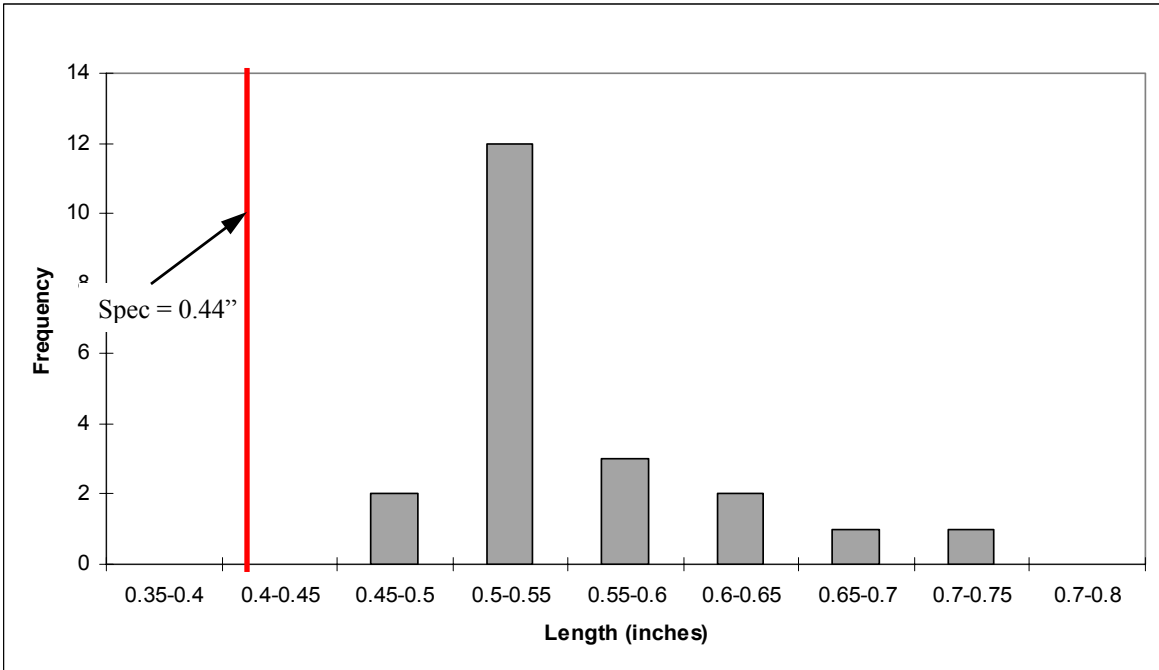


Figure 10.8 Distribution of Long Leg Measurements for VAL Specimens

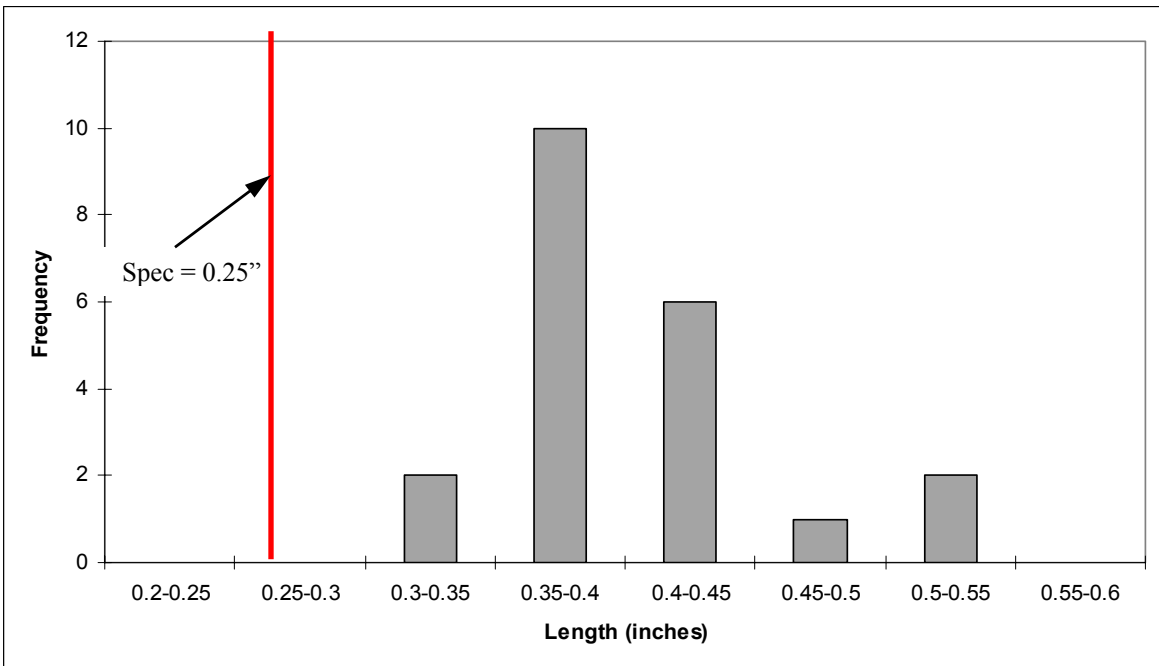


Figure 10.9 Distribution of Short Leg Measurements for VAL Specimens

In an effort to characterize the variation of the leg dimensions around a single pole, four molds were cast on both of the 2" baseplate specimens. Results of these measurements are found in Figures 10.10 and 10.11, noting the relation to the specified dimension.

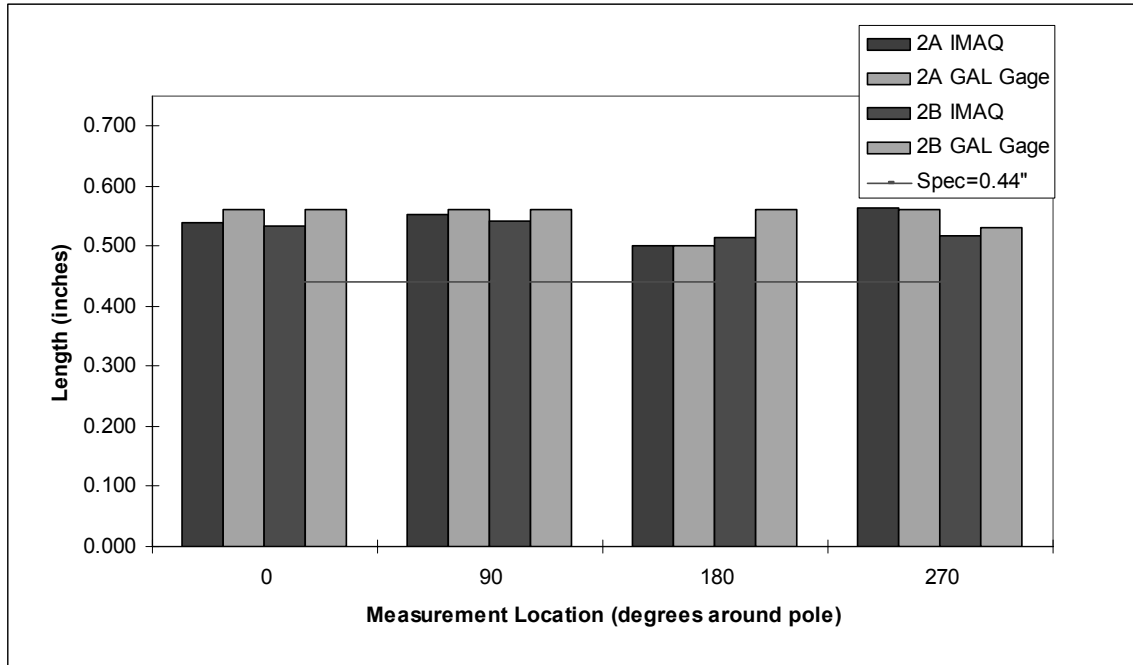


Figure 10.10 Variation of Long Leg Around Mast Arm

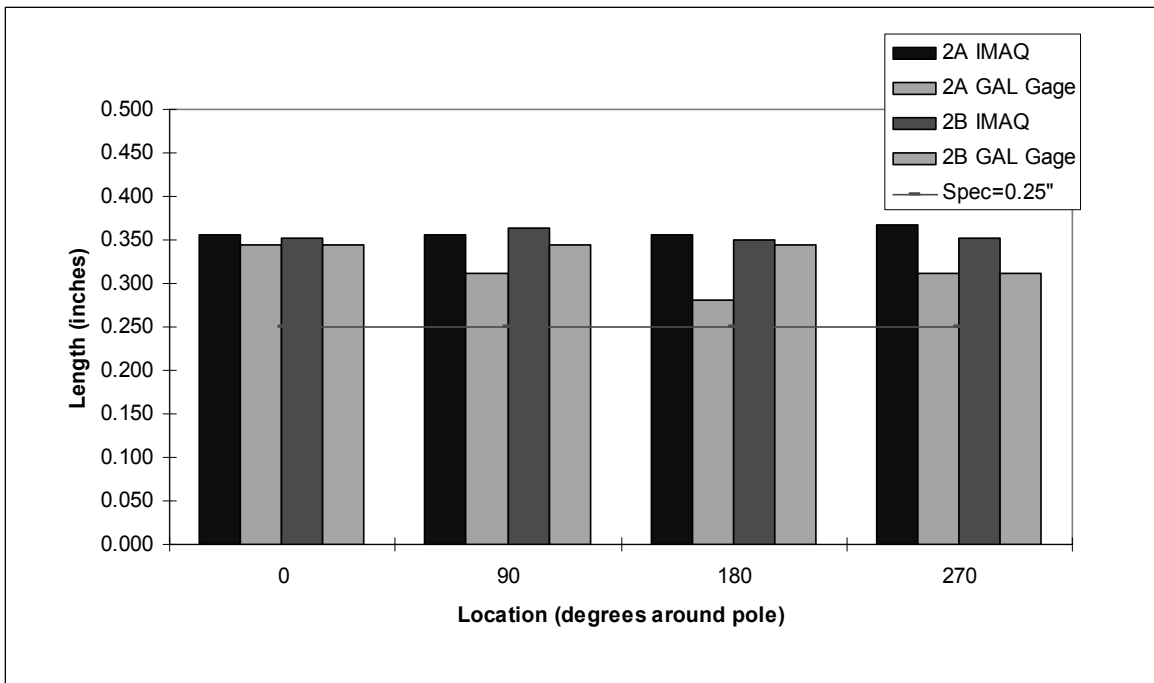


Figure 10.11 Variation of Short Leg around Mast Arm

10.2.2 Results of Study: Incident Angle onto Mast Arm

As with the leg lengths, angle variability will be examined throughout the test group as well as per specimen. Figure 10.12 shows the range of values for the global and local angles for the entire test group

against the aforementioned 30 degree target angle. Figure 10.13 focuses on the variability of the global and local angles at four locations on the 2" baseplate specimens.

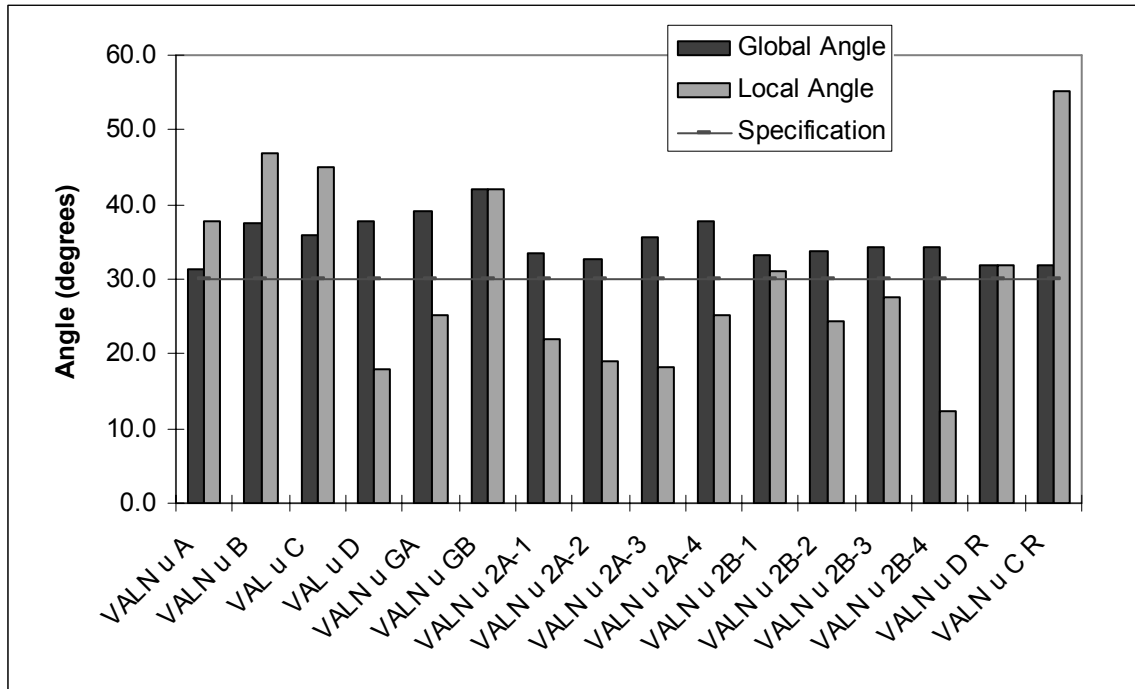


Figure 10.12 Global and Local Angle Measurements for the Study Group

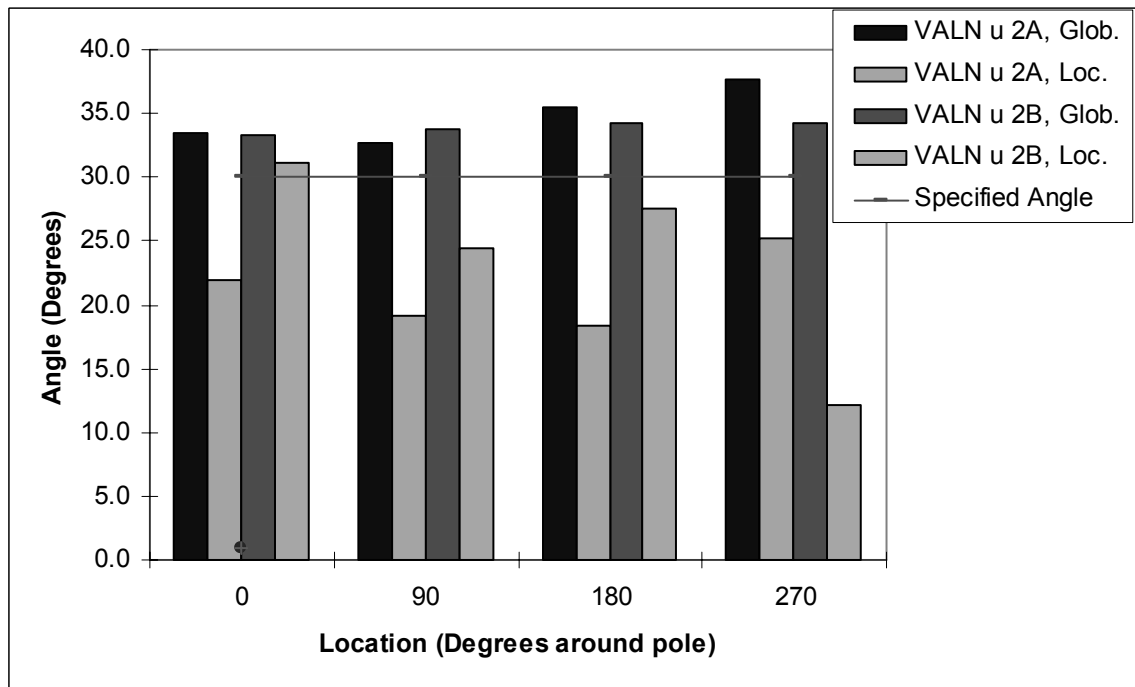


Figure 10.13 Global and Local Angle Measurements for 2" Baseplate Specimens

Figure 10.14 shows the effect of the local angle on the fatigue life constant, A . Results of testing of mast arms from Valley, Nebraska and Brenham, Texas were separated to reveal any effects of fabrication location on fatigue performance. Of note, 2" baseplate specimens and UIT specimens were not plotted in Figure 10.14 to preclude any additional parameters which may have an effect on the fatigue life.

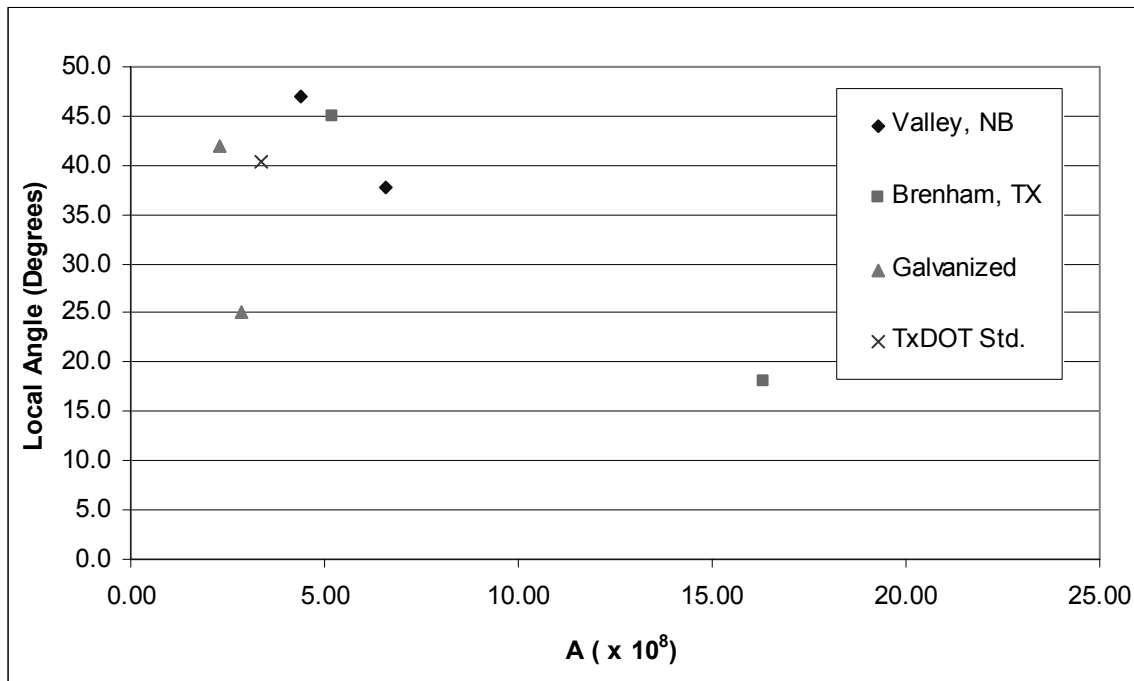


Figure 10.14 Influence of Local Angle on Fatigue Life

10.2.3 Results of Study: UIT Radius of Curvature

Table 10.1 shows the measured radii of circles fit to UIT specimens at the toe of the weld. Also recorded are the corresponding pin diameters used in the treatment. All measurements were taken using IMAQ software.

Table 10.1 Radius of Curvature at Toe of Weld and UIT Pin Diameter

Specimen	Radius, in.	Radius, mm	Pin Diam., mm
VAL u EP-1	0.115	2.93	5
VAL u FP	0.152	3.86	5
VALN u GPA	0.370	9.40	3
VALN u PRA	0.205	5.21	3

10.3 DISCUSSION: LEG DIMENSIONS

Data in Figures 10.6 and 10.7 show all welds exceeding the length specification for both the long and short legs, but still qualify as unequal leg fillet welds. Histograms in Figures 10.8 and 10.9 show the majority of long legs falling in the length range of 0.50-0.55" and the short leg majority in the range of 0.35-0.40". This exceeds the fabricator's long leg specification by 14-25% and the short leg specification by 40-60%. However, most significant is that although all welds examined in the study are unequal leg, the AASHTO specification does not require unequal leg fillet welds.

Not only do Figures 10.10 and 10.11 show little variation in leg lengths at locations around the pole, but also solid correlation between IMAQ measurements and GAL gage measurements. This consistency proves the GAL gage adequate for inspection purposes. Again, all legs exceed the specified lengths, but the leg lengths appear to be consistent. Therefore, if weld length were to affect fatigue life, and barring the presence of a start-stop in the top fiber, the orientation of the pole in the test set-up should be irrelevant.

10.4 DISCUSSION: INCIDENT ANGLE ONTO MAST ARM

Considerable differences exist between the global and local angles. Examining the data in Figure 10.12 for the 1.5" baseplate specimens reveals 50% of the welds having local angles larger than global angles, 37% have global angles larger than local, and in 13% (1 specimen), the two angles are equal. Hence, no generalization can be made correlating the global angles to local angles for 1.5" baseplate specimens. For the 2" baseplates, (2 specimens measured at 4 locations each), 100% of the welds exhibit a larger local angle than the corresponding global, allowing one to conclude that for "thicker" baseplates (2" and greater), the global angle will likely overestimate the local angle. This phenomenon may be attributed to the thicker plate requiring more preheating for the welding process, therefore producing more wetting. Furthermore, Figure 10.13 shows the global angles of the 2" baseplate specimens all hovered around the 30 degree target angle. Thus, although the long and short legs of the angles were previously shown to exceed the specification, the calculated angles show that the legs are staying in proportion to the specified lengths. However, it remains to be seen what effect this angle has on the fatigue life of the mast arm.

In Figure 10.14, a general trend running downward and to the right indicates that a smaller local angle onto the mast arm will improve fatigue life. Moreover, the plot supports the fabricator's weld specification, showing that an incident angle less than or equal to 30 degrees is ideal. At odds with this conclusion is the "galvanized" data point showing a local angle of 25 degrees. For this specimen, both the local angle and the fatigue strength are low. A visual inspection of the weld profile (Figure 10.15) reveals an odd geometry with a smaller throat dimension.

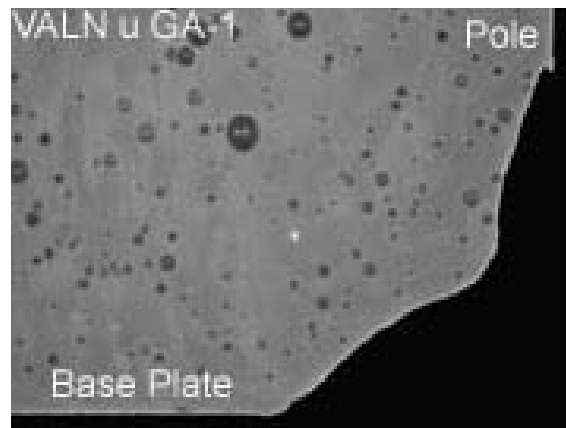


Figure 10.15 Profile View of VALN u GA Showing Smaller Throat Dimension

Further investigation is required to determine if the odd geometry of the weld was the cause of the poor fatigue performance. However, this weld shape resembles the ideal theoretical weld geometry developed from University of Missouri finite element analyses, seen in Figure 10.16. Missouri tests showed the idealized weld did not consistently improve fatigue life, with 1 of 2 tests falling well below the design Category E fatigue curve (Alderson, 1999).

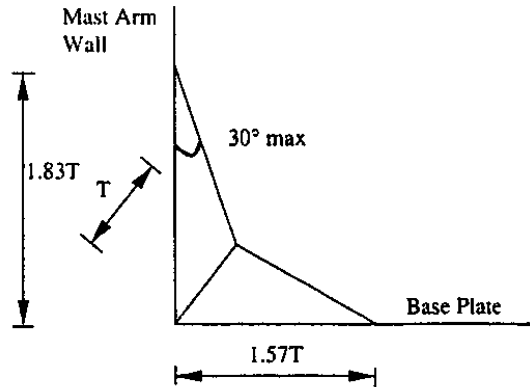


Figure 10.16 Ideal Weld Profile Developed in University of Missouri Finite Element Analyses (Alderson, 1999)

10.5 DISCUSSION: UIT RADIUS OF CURVATURE

Results listed in Table 10.1 show that a 5 mm pin diameter produced radii of curvature smaller than those produced by the smaller pin of 3 mm. It may be concluded from these data that the radius of the induced curvature is not necessarily a function of the size of the pin used in the treatment. Observation of the UIT process supports this conclusion, as the equipment operator has the option of “digging” the pins into the toe of the weld or spreading the treatment over a larger area around the toe. Thus, operator technique will dictate the resulting radius of curvature.

10.6 CONCLUSIONS

Although all exceeded fabrication specifications, measurements of the long and short legs of welds verify that all mast arms tested had unequal leg fillet welds at the socket connection. However, AASHTO broadly specifies a fillet-welded connection, not unequal leg. These measurements showed considerable variation throughout the test group, but multiple measurements per specimen showed little change throughout the weld length of a single mast arm. Global angle consistency with the fabricator’s specified angle show that in general, the legs’ lengths remain in proportion to the specification.

Generally, there was a significant difference between the global and local angles. In the case of the 2” baseplate specimens, *all* global angles were greater than local angles, allowing one to conclude that the global angle will generally overestimate the local angle. The 1.5” baseplate specimens showed an erratic relationship between the global and local angles, preventing any correlation between the two. Multiple measurements on single specimens revealed that although global and local angles are not similar to each other, they are consistent amongst their respective measurements. Notably, a trend between local angles and corresponding fatigue life constants reveals that a smaller local angle will generally produce greater fatigue strength.

Finally, UIT specimens showed varying radii of curvature at the toe of the long legs. Although two different pin diameters were used for the treatment, measurements show that the pin diameter has no effect on the radius.

CHAPTER 11:

CONCLUSIONS AND RECOMMENDED RESEARCH

11.1 CONCLUSIONS

Based on the results of the tests performed during this test program, the following conclusions can be made:

- The test results confirm the classification of the unequal leg fillet welded socket connection detail as an E' category detail, as originally established through testing at Lehigh University.
- The research shows that the design provisions for the stiffened connection details do not predict the actual behavior. The research shows that a longer stiffener is better than a shorter stiffener, contrary to the design provisions. The design equations also did not accurately predict the location of first crack initiation.
- The static tests of the socket connection details indicate that the pole section is deforming near the connection detail. The static test results showed that the linear strain vs. height relation did not accurately predict the measured strain behavior. This indicates that plane sections did not remain plane, and the section distorted. These observations were confirmed in the finite element analysis.
- The static tests of the stiffened connection details indicate that the stiffeners reduce the deformation of the cross section. This was clear as the measured strain values for the stiffened connection details were in good agreement with the predicted values.
- The results of the fatigue testing of the stiffened specimens indicated a relation between the fatigue life of the connection detail and ratio of the stiffener thickness to the thickness of the pole wall. The testing also indicated a relationship between the fatigue life and the angle of incidence of the stiffener. Neither of these factors is considered under the current design provisions.
- The UIT weld treatment process provided significant fatigue life improvement when the treatment was performed under certain conditions. Specifically, when the difference between the maximum stress in the treatment area and the stress when treated is low (less than approximately 10 ksi) the UIT weld treatment dramatically improves the fatigue life.
- The test results also indicate that the galvanizing process influences results of the UIT weld treatment. The test specimens that were treated prior to galvanizing did not benefit from the treatment, indicating that the galvanizing process negated any improvement due to the weld treatment process.
- The UIT weld treatment process was simple to perform. An operator with only a limited amount of training at performing the UIT weld treatment process treated the toe of one socket weld. This specimen showed a fatigue life that was equal to or exceeded the performance of the specimens treated by a professional operator.
- Although the UIT Retrofit procedure was the only retrofit solution tested, the results of these tests indicate a very significant fatigue life improvement through the use of this treatment method. At this time, the UIT Retrofit procedure is the best method for improving the fatigue life of a connection already in service without replacing the mast-arm.
- The Galvanized Prior to UIT treatment procedure provides the most significant improvement in the fatigue life of any connection detail or weld treatment process tested. This appears to be the most cost-effective method to improve the fatigue life, however further studies should be undertaken to determine the correct fatigue classification for treated welds.

- The test specimens with the 2" thick base plate exhibited a significant improvement in the fatigue life compared to a socket connection detail with a 1.5" thick base plate. This improvement is not represented in the current specifications, as the base plate thickness is not a variable in the fatigue design provisions. The finite element analysis confirmed the experimental result and indicated that the improvement in fatigue strength with increasing base plate thickness diminished with plate thickness beyond 2 inches.
- The galvanized socket connection specimens exhibited a reduced fatigue life as compared to the non-galvanized socket connection specimens. These results indicate that the remainder of the tests in the test program may overestimate the fatigue life of a connection detail.
- The U-Rib stiffener did not provide a significantly greater fatigue life following the nominal stress fatigue life analysis method of Chapter 7. However, through the value based design analysis method presented in Chapter 8, the U-Rib stiffener did exhibit an improved fatigue life compared to that of a socket connection detail. The failure at the stiffener to base plate weld in these specimens was not a critical failure. The fatigue life in this location may be improved with the use of a thicker plate for the stiffener.
- The external collar exhibited an improved fatigue life compared to that of a socket connection detail. The fatigue category of the base plate to collar weld was approximately the same as that of a socket connection detail, however, the reduced stress at the critical location due to the increased moment of inertia led to an improved fatigue life as indicated by the value based design analysis method.
- The static tests of the internal collar specimens exhibited nonlinear strain versus load behavior, which indicated that slip was occurring between the collar and the pole during loading.
- The internal collar proved to be a very poor connection detail. The fatigue category of the weld in this detail was below a category E'. This connection detail did not indicate a significant fatigue life improvement based on the Value Based Design Method.
- The static test of the full penetration weld connection details indicated that the backing bar was effectively reducing the stress in the area of the weld. In this way, the backing bar was acting as a short, but thick, internal stiffening collar.
- The full penetration weld exhibited a significant fatigue life improvement, however this may in part be due to the reduced stress caused by the thick backing bar.
- The Value Based Design Method provides a method to compare the benefits of the various connection details. This method allows for the selection of the most cost-effective connection detail by providing a measure of the fatigue life improvement compared to the fatigue life of a socket connection detail.

11.2 FURTHER RESEARCH

The suggested areas of future research based on the results of this testing can be divided into two distinct areas: research relating to the loading of traffic signal mast-arms and research relating to fatigue resistance of traffic signal mast-arms.

11.2.1 Loading Related Research

- The results of this research confirmed that the socket connection details, which are the most commonly used connection details, have poor fatigue lives. Using the fatigue resistances confirmed in this test program and the wind loading provisions of the current specification, an analysis of traffic signal structures currently in service would predict a very high rate of fatigue

related problems. While the occurrences of traffic signal structure failures are increasing, the rate of occurrence does not agree with the predicted number of incidents. This indicates that the wind loading side of the equation for these structures in the current specifications may not accurately enough represent the actual loading conditions. Based on this uncertainty, the wind loading of these structures should be investigated to a greater extent. Specifically, the phenomenon of galloping is not well understood, and should be the subject of further investigation.

- Aside from changes to the wind loading side of the fatigue design equation, the use of dampers or other mitigation devices should be studied in greater detail in order to prevent the accumulation of large numbers of stress cycles.

11.2.2 Resistance Related Research

- While the results of this research indicated some of the problems with the current specifications and indicated details or weld treatments that improve the fatigue life, the number of test results for any one connection detail or weld treatment is too small to use as the basis for a code revision. The connection details of this study that demonstrated improved fatigue lives should be studied in greater detail.
- While the results of this study provide fatigue categories for the specific connection detail geometries tested, the limits to the applicability of these results are not apparent. Prior to applying these fatigue categories to different geometries, further testing must be completed. The behavior of these connection details is not fully understood, such that the significance of what may seem to be a minor geometrical change is not completely known. The tests performed in this study attempted to isolate the influence of each specific variable. The combined influence of several variables was beyond the scope of this study.
- The test results indicated that a large number of variables influence the fatigue life of a connection detail. A standard fatigue category design method that accounts for each of these variables would be very cumbersome. Instead, the use of a finite element based design methodology, similar to the one used by API, should be investigated. While the use of this design method may complicate the analysis of a connection detail, this method may allow for a more straightforward and more accurate process to account for the large number of potential variables.
- The poor performance of the galvanized socket connection specimens when compared to the non-galvanized socket connection specimens indicates that all future fatigue testing should be performed on galvanized test specimens. As all mast-arms in-service are galvanized, testing galvanized specimens will more appropriately duplicate the in-service conditions.

APPENDIX A

Summary of Previous Testing

Table A.1 Description of Test Specimens Tested at Valmont Industries

Specimen Label	Connection Detail	Connection description
G1	Gusset	8-45 degree gussets, 3.25" tall x 3.25" wide x .3125" thick, fillet welded
G2	Gusset	8-45 degree gussets, 3.25" tall x 3.25" wide x .3125" thick, fillet welded
G3	Gusset	8-15 degree gussets, 6.00" tall x 3.25" wide x .3125" thick, full penetration weld to pole
G4	Gusset	8-Tangent Contour Gussets, 5.83" tall x 3.25" wide x .3125" thick, full penetration weld to pole
S1	Socket	Unequal leg fillet weld (.25" x .44", long leg on shaft)
S2	Socket	Unequal leg fillet weld (.25" x .44", long leg on shaft)

Table A.2 Results of Testing Performed by Valmont Industries

Specimen Label	Pole Diameter (in)	Pole Thickness (in)	Stress range at Base of Pole (ksi)	Load Cycles at First Crack	Load Cycles at Failure
G1	10	0.179	13.4	802,620	1,287,000
G2	10	0.179	13.4	376,740	475,020
G3	10	0.179	13.4	950,040	3,046,680
G4	10	0.179	17.6	657,540	870,480
S1	10	0.179	13.4	no crack	no failure
S2	10	0.179	17.6	1,240,200	1,375,920

Table A.3 Description of Test Specimens and Results of Testing Performed at Lehigh University

Specimen Label	Connection Detail	Connection description	Load Cycles at Failure*	Location of Failure
A1	Socket	Equal leg fillet weld	36,100	Arm
A2	Socket	Equal leg fillet weld	117,800	Arm
A3	Socket	Equal leg fillet weld	1,892,400	Arm
A4	Socket	Equal leg fillet weld	174,200	Arm
A5	Socket	Equal leg fillet weld	1,208,700	Arm
A6	Socket	Equal leg fillet weld	1,472,900	Arm
A7	Socket	Unequal leg fillet weld (long leg on shaft)	3,751,600	Arm
A8	Socket	Unequal leg fillet weld (long leg on shaft)	3,573,400	Arm
V1	Socket	Unequal leg fillet weld (long leg on shaft)	87,000	Arm
V2	Socket	Unequal leg fillet weld (long leg on shaft)	317,500	Arm
V3	Socket	Unequal leg fillet weld (long leg on shaft)	5,244,000	Pole
V4	Socket	Unequal leg fillet weld (long leg on shaft)	198,100	Arm
V5	Socket	Unequal leg fillet weld (long leg on shaft)	5,186,500	Pole
V6	Socket	Unequal leg fillet weld (long leg on shaft)	8,832,300	Small Crack in Arm

*Failure is defined as a 2 kip reduction in the maximum load capacity, which corresponded to a fatigue crack that severed about half of the pipe at the connection.

Table A.4 Section Properties of Test Specimens Tested at Lehigh University

Specimen Label	Arm Diameter (in)	Arm Thickness (in)	Stress Range at Base of Arm (ksi)	Pole Diameter (in)	Pole Thickness (in)	Stress Range at Base of Pole (ksi)
A1	10.0625	0.3125	18.8	10.625	0.3125	18.9
A2	10.0625	0.3125	12.4	10.625	0.3125	12.5
A3	10.0625	0.3125	6.4	10.625	0.3125	6.4
A4	10.0625	0.3125	12.4	10.625	0.3125	12.5
A5	10.0625	0.3125	6.4	10.625	0.3125	6.4
A6	10.0625	0.3125	6.4	10.625	0.3125	6.4
A7	10.0625	0.3125	6.4	10.625	0.3125	6.4
A8	10.0625	0.3125	6.4	10.625	0.3125	6.4
V1	10.0625	0.2391	18.9	10.625	0.2391	19
V2	10.0625	0.2391	12.4	10.625	0.2391	12.6
V3	10.0625	0.2391	6.4	10.625	0.2391	6.5
V4	10.0625	0.2391	12.4	10.625	0.2391	12.6
V5	10.0625	0.2391	6.4	10.625	0.2391	6.5
V6	10.0625	0.2391	6.4	10.625	0.2391	6.5

Table A.5 Description of Test Specimens Tested at The Tokyo Institute of Technology

Specimen Label	Outer Diameter (nominal at the bottom) (mm)	Pole Thickness (nominal at the bottom) (mm)	Pole Type		Stiffener Type
			Production Procedure	Change in thickness	
FA -1a	180	4.5	bending	equal	Triangular Rib
FA -1b	180	4.5	bending	equal	Triangular Rib
FA -2a	180	4.5	spinning	equal	Triangular Rib
FA -2b	180	4.5	spinning	equal	Triangular Rib
FA -3	180	6	spinning	tapered	Triangular Rib
FA -4	180	4.5	spinning	equal	U shaped rib
FA -5	180	4.5	spinning	equal	Inner Tube
FA -6	180	4.5	spinning	equal	Outer Tube
FA -7*	180	4.5	spinning	equal	U shaped rib
FA -8*	180	4.5	spinning	equal	U shaped rib
FA -9*	180	4.5	spinning	equal	U shaped rib
FA -10*	180	6	spinning	tapered	U shaped rib
FA -11*	180	6	spinning	tapered	U shaped rib
FA -12*	180	6	spinning	tapered	U shaped rib
FA -13*	180	6	spinning	tapered	U shaped rib
FA -14*	180	6	spinning	equal	Triangular Rib

*Note: Specimens FA-7 to FA-14 were not fully labeled in Reference 6.

Table A.6 Description of Test Specimens Tested at The Tokyo Institute of Technology

Specimen Label	Force Amplitude Applied at Pole Top P (kN)	Nominal Stress Range (Mpa)	Number of Cycles N	Notes on Crack Development
FA -1a	7.4	115	268,396	crack at toe of rib edge welding
FA -1b	10.6	164	53,579	crack at toe of rib edge welding
FA -2a	7.4	115	746,691	crack at toe of rib edge welding
FA -2b	10.6	164	66,330	crack at toe of rib edge welding
FA -3	10.6	164	408,774	crack at toe of rib edge welding
FA -4	10.6	164	3,500,000	no cracking
FA -5	10.6	164	235,921	crack at toe of rib edge welding
FA -6	10.6	164	351,316	crack at the weld between outer tube and base plate
FA -7*		200	818,726	crack at weld between upper part of the rib and pole
FA -8*		200	1,984,240	crack at the lower part of the rib
FA -9*		150	1,936,776	crack at the lower part of the rib
FA -10*		250	1,513,589	crack at weld between upper part of the rib and pole
FA -11*		200	3,663,800	no cracking
FA -12*		300	277,950	crack at weld between upper part of the rib and pole
FA -13*		150	2,815,010	no cracking
FA -14*		150	76,501	crack at toe of rib edge welding

*Note: Specimens FA-7 to FA-14 were not fully labeled in Reference 6.

Table A.7 Description of Test Specimens from Testing at The University of Missouri - Columbia

Specimen Label	Connection Detail	Connection Description
254682	Socket	Unequal leg fillet weld (long leg on shaft)
BB 34970	Socket	Unequal leg fillet weld (long leg on shaft)
CB 12917	Socket	Unequal leg fillet weld (long leg on shaft)

Table A.8 Results of Testing Performed by The University of Missouri - Columbia

Specimen Label	Section Modulus (in³)	Mean Stress (ksi)	Critical Stress Range* (ksi)	Load Cycles at First Crack	Comments
254682	11.68	14	8	1,800,000	
BB 34970	13.65	14	8	2,100,000	
CB 12917	18.42	14	8	400,000	Lack of fusion defect observed.

* Note: Reported Stress Range is at the strain gauge location, 4" from the toe of the socket weld.

APPENDIX B

Measured Dimensions of Test Specimens

Table B.1 General Dimensions – Socket Connection and Stiffened Specimens

	Diameter Measures at Base (in.)				Out of Round	Calculated Taper (in./in.)	Pole Wall Thickness (in.)
	1	2	3	Average			
VALu A	9.938	10.00	9.938	9.958	0.63%	0.012	0.171
VALu B	10.000	9.969	9.938	9.969	0.63%	0.012	0.170
VALu C	10.000	10.00	9.938	9.979	0.62%	0.012	0.170
VALu D	10.000	10.00	10.00	10.00	0.00%	0.013	0.172
VALu EP	10.031	10.03	10.03	10.03	0.00%	0.012	0.175
VALu FP	10.000	9.969	9.969	9.979	0.31%	0.008	0.176
TXu A	9.938	10.00	9.969	9.969	0.62%	0.012	0.230
TXu B	9.969	9.938	9.938	9.948	0.31%	0.012	0.230
TXu C	10.000	9.938	9.969	9.969	0.63%	0.012	0.234
TXu D	9.938	9.969	9.938	9.948	0.31%	0.011	0.233
TXu EP	9.938	10.03	9.969	9.979	0.93%	0.012	0.236
TXu FP	10.000	9.938	9.969	9.969	0.62%	0.012	0.239
VAL 3x1/4	9.938	10.00	9.969	9.969	0.62%	0.012	0.177
VAL 3x1/4	9.906	10.00	10.00	9.969	0.94%	0.012	0.174
VAL 3x1/4	9.938	10.00	10.00	9.979	0.62%	0.012	0.172
TX 3x1/4 A	10.031	10.00	10.00	10.01	0.31%	0.013	0.230
TX 3x1/4 B	10.000	9.969	9.969	9.979	0.31%	0.012	0.229
TX 3x1/4 C	9.938	9.969	9.938	9.948	0.31%	0.012	0.229
VAL 3x3/8	9.969	9.938	10.00	9.969	0.63%	0.012	0.169
VAL 3x3/8	9.969	9.938	9.969	9.958	0.31%	0.012	0.170
VAL 3x3/8	10.031	10.00	9.969	10.00	0.62%	0.012	0.171
TX 3x3/8 A	9.969	9.938	9.906	9.938	0.63%	0.012	0.233
TX 3x3/8 B	10.000	9.969	9.938	9.969	0.62%	0.012	0.234
TX 3x3/8	9.906	9.938	9.906	9.917	0.32%	0.011	0.227
VAL 6x3/8	9.938	9.969	10.00	9.969	0.62%	0.012	0.170
VAL 6x3/8	9.938	10.00	9.906	9.948	0.94%	0.012	0.170
VAL 6x3/8	9.969	9.969	10.00	9.979	0.31%	0.012	0.170
TX 6x3/8 A	9.969	9.969	9.969	9.969	0.00%	0.012	0.236
TX 6x3/8 B	10.000	10.00	9.969	9.990	0.31%	0.012	0.234
TX 6x3/8 C	9.938	9.938	9.969	9.948	0.31%	0.012	0.230
VALNu A	9.938	10.00	9.906	9.948	0.94%	0.012	0.170
VALNu B	10.000	9.938	10.00	9.979	0.62%	0.012	0.171

Table B.1 General Dimensions – Socket Connection and Stiffened Specimens (Continued)

	Diameter Measures at Base (in.)				Out of Round	Calculated Taper	Pole Wall Thickness
	1	2	3	Average			
TX 3x1/4 A	10.031	10.000	10.000	10.010	0.31%	0.013	0.230
TX 3x1/4 B	10.000	9.969	9.969	9.979	0.31%	0.012	0.229
TX 3x1/4 C LMS	9.938	9.969	9.938	9.948	0.31%	0.012	0.229
VAL 3x3/8 A	9.969	9.938	10.000	9.969	0.63%	0.012	0.169
VAL 3x3/8 B	9.969	9.938	9.969	9.958	0.31%	0.012	0.170
VAL 3x3/8 CP	10.031	10.000	9.969	10.000	0.62%	0.012	0.171
TX 3x3/8 A	9.969	9.938	9.906	9.938	0.63%	0.012	0.233
TX 3x3/8 B	10.000	9.969	9.938	9.969	0.62%	0.012	0.234
TX 3x3/8 CP	9.906	9.938	9.906	9.917	0.32%	0.011	0.227
VAL 6x3/8 A	9.938	9.969	10.000	9.969	0.62%	0.012	0.170
VAL 6x3/8 B	9.938	10.000	9.906	9.948	0.94%	0.012	0.170
VAL 6x3/8 C	9.969	9.969	10.000	9.979	0.31%	0.012	0.170
TX 6x3/8 A	9.969	9.969	9.969	9.969	0.00%	0.012	0.236
TX 6x3/8 B	10.000	10.000	9.969	9.990	0.31%	0.012	0.234
TX 6x3/8 C	9.938	9.938	9.969	9.948	0.31%	0.012	0.230
VALNu A	9.938	10.000	9.906	9.948	0.94%	0.012	0.170
VALNu B	10.000	9.938	10.000	9.979	0.62%	0.012	0.171
VALNu G A	10.031	10.000	10.000	10.010	0.31%	0.012	0.173
VALNu G B	10.031	10.000	9.969	10.000	0.62%	0.012	0.175
VALNu 2 A	9.969	10.000	10.000	9.990	0.31%	0.012	0.169
VALNu 2 B	9.969	10.000	10.000	9.990	0.31%	0.013	0.170
VALN 6x3/8@45	10.000	9.938	9.938	9.959	0.62%	0.012	0.170
VALN 6x3/8@45	10.031	9.938	9.969	9.979	0.93%	0.012	0.169
VALN 6x3/8@45	9.906	10.000	10.000	9.969	0.94%	0.012	0.169
VALN 6x3/8@45	9.969	10.000	10.000	9.990	0.31%	0.013	0.170
VALNu PR A	10.000	9.969	10.000	9.990	0.31%	0.012	0.174
VALNu PR B	9.969	10.031	9.938	9.979	0.93%	0.012	0.175
VALNu GP A	10.000	9.969	9.969	9.979	0.31%	0.012	0.174
VALNu GP B	9.969	9.969	9.969	9.969	0.00%	0.012	0.173
VALNu PG A	9.969	9.969	10.000	9.979	0.31%	0.012	0.175
VALNu PG B	10.000	10.000	10.000	10.000	0.00%	0.013	0.175

Table B.2 Socket Weld Dimensions – Socket Connection and Stiffened Specimens

Specimen Name	Long Leg (on Pole) (in.)					Short Leg (on Base Plate) (in.)				
	1	2	3	4	Average	1	2	3	4	Average
VALu A	0.490	0.550	0.509	0.509	0.515	0.347	0.411	0.367	0.392	0.379
VALu B	0.482	0.516	0.523	0.513	0.509	0.357	0.359	0.354	0.356	0.357
VALu C	0.522	0.579	0.505	0.536	0.536	0.437	0.523	0.540	0.438	0.485
VALu D	0.513	0.548	0.527	0.483	0.518	0.394	0.344	0.435	0.354	0.382
VALu EP	0.496	0.504	0.517	0.512	0.507	0.408	0.400	0.409	0.388	0.401
VALu FP	0.551	0.569	0.511	0.521	0.538	0.386	0.402	0.330	0.354	0.368
TXu A	0.788	0.714	0.688	0.715	0.726	0.458	0.483	0.437	0.474	0.463
TXu B	0.658	0.712	0.656	0.670	0.674	0.458	0.469	0.439	0.508	0.469
TXu C	0.850	0.810	0.733	0.821	0.804	0.677	0.632	0.737	0.724	0.693
TXu D	0.793	0.855	0.803	0.786	0.809	0.621	0.581	0.572	0.580	0.589
TXu EP	0.618	0.594	0.587	0.533	0.583	0.403	0.445	0.404	0.412	0.416
TXu FP	0.671	0.658	0.686	0.665	0.670	0.536	0.555	0.565	0.587	0.561
VAL 3x1/4	0.459	0.506	0.477	0.540	0.496	0.367	0.348	0.323	0.381	0.355
VAL 3x1/4	0.574	0.578	0.576	0.573	0.575	0.409	0.387	0.418	0.329	0.386
VAL 3x1/4	0.495	0.518	0.498	0.458	0.492	0.380	0.384	0.360	0.385	0.377
TX 3x1/4	0.711	0.684	0.728	0.815	0.735	0.501	0.542	0.444	0.534	0.505
TX 3x1/4	0.606	0.705	0.640	0.617	0.642	0.428	0.423	0.450	0.420	0.430
TX 3x1/4	0.812	0.778	0.791	0.785	0.792	0.486	0.544	0.522	0.570	0.531
VAL 3x3/8	0.523	0.529	0.501	0.538	0.523	0.323	0.348	0.332	0.349	0.338
VAL 3x3/8	0.596	0.591	0.530	0.575	0.573	0.275	0.287	0.274	0.266	0.276
VAL 3x3/8	0.636	0.635	0.644	0.622	0.634	0.427	0.426	0.446	0.428	0.432
TX 3x3/8	0.860	0.805	0.814	0.839	0.830	0.504	0.498	0.523	0.491	0.504
TX 3x3/8	0.670	0.676	0.662	0.690	0.675	0.415	0.412	0.381	0.491	0.425
TX 3x3/8	0.701	0.705	0.697	0.664	0.692	0.486	0.504	0.499	0.523	0.503
VAL 6x3/8	0.481	0.455	0.484	0.503	0.481	0.350	0.369	0.377	0.376	0.368
VAL 6x3/8	0.580	0.527	0.533	0.563	0.551	0.350	0.317	0.359	0.340	0.342
VAL 6x3/8	0.562	0.527	0.659	0.590	0.585	0.365	0.390	0.357	0.368	0.370
TX 6x3/8	0.755	0.874	0.805	0.871	0.826	0.514	0.513	0.470	0.565	0.516
TX 6x3/8	0.600	0.602	0.615	0.529	0.587	0.355	0.355	0.416	0.440	0.392
TX 6x3/8	0.600	0.643	0.581	0.631	0.614	0.420	0.400	0.385	0.382	0.397
VALNu A	0.730	0.615	0.633	0.734	0.678	0.390	0.402	0.378	0.435	0.401
VALNu B	0.614	0.664	0.625	0.610	0.628	0.380	0.345	0.351	0.387	0.371
VALNu G	0.605	0.594	0.582	0.575	0.589	0.466	0.382	0.398	0.367	0.403
VALNu G	0.640	0.506	0.508	0.533	0.547	0.433	0.407	0.356	0.426	0.406
VALNu 2	0.552	0.595	0.501	0.518	0.542	0.373	0.364	0.340	0.327	0.351
VALNu 2	0.561	0.518	0.511	0.469	0.515	0.346	0.337	0.320	0.350	0.338
VALN	0.522	0.550	0.655	0.578	0.576	0.382	0.366	0.381	0.373	0.376
VALN	0.541	0.562	0.557	0.493	0.538	0.398	0.472	0.418	0.383	0.418
VALN	0.539	0.541	0.503	0.502	0.521	0.420	0.392	0.347	0.441	0.400
VALN	0.565	0.556	0.508	0.558	0.547	0.417	0.355	0.360	0.364	0.374

Table B.2 Socket Weld Dimensions – Socket Connection and Stiffened Specimens (Continued)

Specimen Name	Long Leg (on Pole) (in.)					Short Leg (on Base Plate) (in.)				
	1	2	3	4	Average	1	2	3	4	Average
VALNu PR A	0.539	0.58	0.630	0.605	0.591	0.486	0.450	0.458	0.371	0.441
VALNu PR B	0.601	0.44	0.419	0.557	0.506	0.444	0.429	0.422	0.396	0.423
VALNu GP A	0.703	0.68	0.593	0.551	0.632	0.368	0.401	0.440	0.426	0.409
VALNu GP B	0.482	0.47	0.511	0.532	0.501	0.470	0.382	0.404	0.455	0.428
VALNu PG A	0.566	0.57	0.653	0.765	0.641	0.475	0.440	0.485	0.467	0.467
VALNu PG B	0.710	0.70	0.693	0.659	0.691	0.591	0.615	0.454	0.414	0.519

Table B.3 Stiffened Specimens – Stiffener Dimensions and Weld Sizes

	Length (in.)	Width (in.)	Thick-ness (in.)	Weld – Right Side of Stiffener (in.)					Weld – Left Side of Stiffener (in.)				
				1	2	3	4	Avg.	1	2	3	4	Avg.
VAL 3x1/4 A	3.36	2.33	0.252	0.399	0.332	0.277	0.372	0.345	0.335	0.295	0.337	0.401	0.342
	3.30	2.43	0.245	0.337	0.329	0.250	0.268	0.296	0.436	0.435	0.271	0.256	0.350
	3.34	2.32	0.244	0.381	0.313	0.254	0.277	0.306	0.348	0.293	0.321	0.329	0.323
	3.38	2.38	0.248	0.387	0.299	0.294	0.317	0.324	0.476	0.527	0.605	0.346	0.489
VAL 3x1/4 B	3.42	2.39	0.257	0.313	0.264	0.262	0.271	0.278	0.313	0.303	0.255	0.294	0.291
	3.40	2.34	0.252	0.290	0.290	0.266	0.362	0.302	0.279	0.286	0.284	0.228	0.269
	3.42	2.29	0.248	0.344	0.326	0.316	0.298	0.321	0.301	0.293	0.254	0.256	0.276
	3.44	2.32	0.252	0.322	0.400	0.289	0.281	0.323	0.312	0.289	0.295	0.258	0.289
VAL 3x1/4 C	3.39	2.53	0.248	0.332	0.239	0.279	0.305	0.289	0.348	0.395	0.320	0.311	0.344
	3.43	2.48	0.245	0.335	0.335	0.326	0.378	0.344	0.340	0.310	0.304	0.305	0.315
	3.37	2.38	0.245	0.328	0.289	0.303	0.328	0.312	0.351	0.334	0.338	0.309	0.333
	3.37	2.47	0.245	0.312	0.298	0.292	0.261	0.291	0.342	0.346	0.329	0.329	0.337
TX 3x1/4 A	3.49	2.32	0.245	0.405	0.438	0.373	0.330	0.387	0.425	0.476	0.461	0.470	0.458
	3.43	2.50	0.246	0.374	0.370	0.423	0.348	0.379	0.438	0.370	0.486	0.461	0.439
	4.55	2.30	0.246	0.407	0.434	0.441	0.384	0.417	0.412	0.340	0.380	0.360	0.373
	4.53	2.32	0.244	0.408	0.335	0.428	0.411	0.396	0.395	0.389	0.405	0.366	0.389
TX 3x1/4 B	3.38	2.32	0.243	0.416	0.373	0.498	0.450	0.434	0.532	0.505	0.427	0.390	0.464
	3.38	2.40	0.246	0.353	0.353	0.534	0.472	0.428	0.597	0.506	0.425	0.380	0.477
	3.44	2.34	0.244	0.376	0.387	0.521	0.465	0.437	0.458	0.516	0.458	0.408	0.460
	3.40	2.36	0.246	0.396	0.344	0.462	0.463	0.416	0.548	0.482	0.434	0.396	0.465
TX 3x1/4 C LMS	3.42	2.62	0.241	0.440	0.429	0.462	0.456	0.447	0.628	0.642	0.422	0.424	0.529
	3.48	2.40	0.244	0.438	0.436	0.462	0.421	0.439	0.546	0.660	0.559	0.430	0.549
	3.48	2.33	0.244	0.477	0.468	0.399	0.406	0.438	0.500	0.563	0.435	0.401	0.475
	4.50	2.27	0.243	0.463	0.452	0.467	0.430	0.453	0.593	0.519	0.447	0.437	0.499
TX 3x1/4 C LMS	3.42	2.62	0.241	0.440	0.429	0.462	0.456	0.447	0.628	0.642	0.422	0.424	0.529
	3.48	2.40	0.244	0.438	0.436	0.462	0.421	0.439	0.546	0.660	0.559	0.430	0.549
	3.48	2.33	0.244	0.477	0.468	0.399	0.406	0.438	0.500	0.563	0.435	0.401	0.475
	4.50	2.27	0.243	0.463	0.452	0.467	0.430	0.453	0.593	0.519	0.447	0.437	0.499

Table B.3 Stiffened Specimens – Stiffener Dimensions and Weld Sizes (continued)

	Length (in.)	Width (in.)	Thick-ness (in.)	Weld – Right Side of Stiffener (in.)					Weld – Left Side of Stiffener (in.)				
				1	2	3	4	Avg.	1	2	3	4	Avg.
VAL 3x3/8 A	3.18	2.27	0.365	0.200	0.233	0.294	0.273	0.250	0.213	0.274	0.290	0.285	0.266
	3.40	2.26	0.369	0.238	0.215	0.319	0.324	0.274	0.228	0.208	0.304	0.260	0.250
	3.54	2.24	0.369	0.236	0.227	0.249	0.278	0.248	0.258	0.245	0.264	0.261	0.257
	3.25	2.36	0.369	0.285	0.318	0.308	0.310	0.305	0.256	0.238	0.208	0.221	0.231
VAL 3x3/8 B	3.36	2.35	0.370	0.281	0.211	0.281	0.260	0.258	0.248	0.285	0.259	0.220	0.253
	3.42	2.18	0.367	0.255	0.270	0.349	0.318	0.298	0.306	0.265	0.279	0.272	0.281
	3.25	2.29	0.375	0.245	0.293	0.259	0.284	0.270	0.302	0.298	0.312	0.262	0.294
	3.42	2.38	0.372	0.251	0.210	0.295	0.249	0.251	0.237	0.282	0.228	0.269	0.254
VAL 3x3/8 CP	3.22	2.31	0.377	0.283	0.313	0.302	0.363	0.315	0.355	0.280	0.244	0.241	0.280
	3.29	2.29	0.377	0.287	0.278	0.269	0.264	0.275	0.375	0.319	0.368	0.326	0.347
	3.16	2.17	0.378	0.335	0.272	0.300	0.200	0.277	0.334	0.378	0.270	0.211	0.298
	3.42	2.28	0.377	0.325	0.326	0.312	0.278	0.310	0.341	0.297	0.264	0.309	0.303
TX 3x3/8 A	3.40	1.99	0.372	0.516	0.453	0.583	0.561	0.528	0.302	0.287	0.392	0.340	0.330
	3.48	2.40	0.370	0.504	0.425	0.510	0.606	0.511	0.364	0.353	0.449	0.448	0.404
	3.35	2.34	0.369	0.424	0.377	0.465	0.513	0.445	0.354	0.385	0.453	0.420	0.403
	3.41	2.95	0.367	0.433	0.348	0.347	0.528	0.414	0.402	0.473	0.493	0.615	0.496
TX 3x3/8 B	3.62	2.38	0.372	0.333	0.307	0.496	0.437	0.393	0.433	0.437	0.423	0.479	0.443
	3.65	2.39	0.372	0.382	0.368	0.567	0.446	0.441	0.442	0.416	0.386	0.394	0.410
	3.51	2.36	0.370	0.322	0.344	0.495	0.443	0.401	0.412	0.433	0.432	0.437	0.429
	3.54	2.37	0.373	0.365	0.442	0.469	0.498	0.444	0.382	0.371	0.401	0.398	0.388
TX 3x3/8CPLMS	3.59	2.31	0.369	0.366	0.382	0.285	0.280	0.328	0.423	0.446	0.327	0.409	0.401
	3.50	2.44	0.373	0.357	0.388	0.346	0.253	0.336	0.448	0.425	0.372	0.398	0.411
	3.31	2.48	0.373	0.375	0.472	0.384	0.255	0.372	0.401	0.412	0.480	0.472	0.441
	3.51	2.39	0.364	0.335	0.340	0.314	0.304	0.323	0.467	0.430	0.400	0.326	0.406
VAL 6x3/8 A	6.53	2.31	0.373	0.378	0.303	0.376	0.424	0.370	0.419	0.378	0.309	0.366	0.368
	6.62	2.40	0.367	0.369	0.332	0.377	0.403	0.370	0.470	0.420	0.373	0.391	0.414
	6.52	2.41	0.371	0.369	0.345	0.363	0.441	0.380	0.385	0.411	0.381	0.339	0.379
	6.62	2.31	0.371	0.340	0.413	0.353	0.328	0.359	0.342	0.341	0.349	0.413	0.361
VAL 6x3/8 B	6.36	2.25	0.368	0.280	0.309	0.325	0.326	0.310	0.297	0.268	0.360	0.333	0.315
	6.42	2.25	0.370	0.341	0.332	0.281	0.281	0.309	0.336	0.351	0.277	0.282	0.312
	6.52	2.28	0.371	0.301	0.333	0.325	0.345	0.326	0.307	0.250	0.433	0.401	0.348
	6.36	2.30	0.370	0.422	0.372	0.282	0.234	0.328	0.284	0.280	0.324	0.361	0.312
TX 3x3/8 B	3.62	2.38	0.372	0.333	0.307	0.496	0.437	0.393	0.433	0.437	0.423	0.479	0.443
	3.65	2.39	0.372	0.382	0.368	0.567	0.446	0.441	0.442	0.416	0.386	0.394	0.410
	3.51	2.36	0.370	0.322	0.344	0.495	0.443	0.401	0.412	0.433	0.432	0.437	0.429
	3.54	2.37	0.373	0.365	0.442	0.469	0.498	0.444	0.382	0.371	0.401	0.398	0.388
TX 3x3/8CPLMS	3.59	2.31	0.369	0.366	0.382	0.285	0.280	0.328	0.423	0.446	0.327	0.409	0.401
	3.50	2.44	0.373	0.357	0.388	0.346	0.253	0.336	0.448	0.425	0.372	0.398	0.411
	3.31	2.48	0.373	0.375	0.472	0.384	0.255	0.372	0.401	0.412	0.480	0.472	0.441
	3.51	2.39	0.364	0.335	0.340	0.314	0.304	0.323	0.467	0.430	0.400	0.326	0.406

Table B.3 Stiffened Specimens – Stiffener Dimensions and Weld Sizes (continued)

	Length (in.)	Width (in.)	Thick-ness (in.)	Weld – Right Side of Stiffener (in.)					Weld – Left Side of Stiffener (in.)				
				1	2	3	4	Avg.	1	2	3	4	Avg.
VAL 6x3/8 A	6.53	2.31	0.373	0.378	0.303	0.376	0.424	0.370	0.419	0.378	0.309	0.366	0.368
	6.62	2.40	0.367	0.369	0.332	0.377	0.403	0.370	0.470	0.420	0.373	0.391	0.414
	6.52	2.41	0.371	0.369	0.345	0.363	0.441	0.380	0.385	0.411	0.381	0.339	0.379
	6.62	2.31	0.371	0.340	0.413	0.353	0.328	0.359	0.342	0.341	0.349	0.413	0.361
VAL 6x3/8 B	6.36	2.25	0.368	0.280	0.309	0.325	0.326	0.310	0.297	0.268	0.360	0.333	0.315
	6.42	2.25	0.370	0.341	0.332	0.281	0.281	0.309	0.336	0.351	0.277	0.282	0.312
	6.52	2.28	0.371	0.301	0.333	0.325	0.345	0.326	0.307	0.250	0.433	0.401	0.348
	6.36	2.30	0.370	0.422	0.372	0.282	0.234	0.328	0.284	0.280	0.324	0.361	0.312
VAL 6x3/8 C	6.34	2.23	0.368	0.294	0.376	0.283	0.288	0.310	0.295	0.263	0.315	0.287	0.290
	6.30	2.22	0.370	0.365	0.389	0.332	0.267	0.338	0.279	0.280	0.327	0.270	0.289
	6.34	2.24	0.371	0.348	0.311	0.239	0.228	0.282	0.281	0.333	0.308	0.254	0.294
	6.28	2.37	0.369	0.328	0.366	0.263	0.257	0.304	0.258	0.318	0.283	0.282	0.285
TX 6x3/8 A	6.57	2.24	0.375	0.390	0.396	0.394	0.370	0.388	0.464	0.418	0.525	0.491	0.475
	6.53	2.26	0.374	0.645	0.355	0.530	0.445	0.494	0.431	0.476	0.445	0.390	0.436
	6.32	2.27	0.372	0.590	0.585	0.433	0.363	0.493	0.411	0.363	0.426	0.512	0.428
	6.39	2.31	0.374	0.451	0.458	0.393	0.338	0.410	0.415	0.425	0.397	0.425	0.416
TX 6x3/8 B	6.46	2.44	0.379	0.419	0.437	0.355	0.318	0.382	0.501	0.479	0.385	0.406	0.443
	6.51	2.37	0.373	0.385	0.327	0.391	0.420	0.381	0.534	0.499	0.428	0.367	0.457
	6.52	2.41	0.377	0.405	0.351	0.377	0.385	0.380	0.504	0.508	0.421	0.409	0.461
	6.55	2.35	0.375	0.449	0.454	0.320	0.341	0.391	0.500	0.500	0.513	0.455	0.492
TX 6x3/8 C	6.45	2.43	0.368	0.290	0.368	0.378	0.343	0.345	0.437	0.452	0.362	0.327	0.395
	6.37	2.41	0.369	0.333	0.352	0.458	0.372	0.379	0.370	0.425	0.379	0.328	0.376
	6.47	2.40	0.369	0.345	0.285	0.435	0.400	0.366	0.426	0.421	0.385	0.322	0.389
	6.42	2.34	0.369	0.367	0.292	0.344	0.267	0.318	0.395	0.462	0.408	0.384	0.412
VALN6x3/8 @45A	6.34	2.18	0.370	0.392	0.315	0.265	0.279	0.313	0.233	0.321	0.271	0.315	0.285
	6.40	2.23	0.372	0.271	0.333	0.254	0.242	0.275	0.283	0.249	0.300	0.246	0.270
	6.25	2.21	0.371	0.283	0.286	0.285	0.244	0.275	0.253	0.281	0.280	0.275	0.272
	6.28	2.24	0.371	0.335	0.307	0.272	0.318	0.308	0.318	0.610	0.608	0.296	0.458
VALN6x3/8 @45B	6.38	2.19	0.377	0.298	0.326	0.338	0.260	0.306	0.283	0.244	0.276	0.340	0.286
	6.33	2.17	0.371	0.290	0.349	0.266	0.321	0.307	0.302	0.329	0.308	0.265	0.301
	6.35	2.28	0.373	0.287	0.396	0.260	0.308	0.313	0.283	0.238	0.361	0.316	0.300
	6.31	2.29	0.373	0.275	0.369	0.296	0.288	0.307	0.280	0.290	0.290	0.283	0.286
VALN6x3/8 @45C	6.34	2.25	0.370	0.261	0.335	0.377	0.332	0.326	0.310	0.338	0.321	0.284	0.313
	6.39	2.31	0.370	0.285	0.355	0.240	0.241	0.280	0.290	0.372	0.318	0.326	0.327
	6.35	2.26	0.372	0.333	0.262	0.327	0.353	0.319	0.276	0.366	0.282	0.322	0.312
	6.36	2.24	0.369	0.369	0.325	0.344	0.382	0.355	0.289	0.314	0.319	0.298	0.305
VALN6x3/8 @45D	6.18	2.26	0.371	0.391	0.333	0.315	0.316	0.339	0.305	0.262	0.291	0.265	0.281
	6.23	2.35	0.369	0.246	0.350	0.243	0.306	0.286	0.291	0.302	0.355	0.380	0.332
	6.21	2.22	0.377	0.245	0.365	0.316	0.276	0.301	0.327	0.361	0.271	0.284	0.311
	6.23	2.34	0.378	0.263	0.393	0.270	0.310	0.309	0.256	0.326	0.212	0.231	0.256

Table B.4 General Dimensions for External Collar Stiffened Specimens

	Diameter at Base Plate (in.)				Diameter of Pole Above Collar (in.)				Out of Round	Pole Taper (in/in)	Collar Length (in.)	Collar Thick. (in.)
	1	2	3	Avg.	1	2	3	Avg.				
VALN Col A	10.375	10.375	10.375	10.375	9.906	9.875	9.938	9.906	0.63%	0.013	3.880	0.170
VALN Col B	10.313	10.344	10.375	10.344	9.938	9.875	9.906	9.906	0.63%	0.013	3.807	0.170

Table B.5 Weld Dimensions for External Collar Stiffened Specimens

		Long Leg (on Pole) (in.)					Short Leg (on Base Plate) (in.)				
		1	2	3	4	Avg.	1	2	3	4	Avg.
VALN Col A	Base Plate to Collar	0.722	0.733	0.686	0.720	0.715	0.326	0.394	0.346	0.344	0.353
	Collar to Pole	0.561	0.719	0.704	0.647	0.658	0.230	0.225	0.308	0.215	0.245
VALN Col B	Base Plate to Collar	0.680	0.710	0.575	0.720	0.671	0.369	0.370	0.401	0.429	0.392
	Collar to Pole	0.638	0.650	0.753	0.625	0.667	0.238	0.208	0.227	0.230	0.226

Table B.6 General Dimensions for Internal Collar Stiffened Specimens

	Diameter at Base Plate (in.)				Out of Round	Pole Taper (in./in.)	Collar Thickness (in.)
	1	2	3	Average			
VALN IC	9.938	9.969	9.969	9.959	0.31%	0.012	0.171
VALN IC	9.938	9.969	9.938	9.948	0.31%	0.012	0.172

Table B.7 Socket Weld Dimensions for Internal Collar Stiffened Specimens

	Long Leg (on Pole) (in.)					Short Leg (on Base Plate) (in.)				
	1	2	3	4	Avg.	1	2	3	4	Avg.
VALN IC A	0.439	0.473	0.558	0.477	0.487	0.400	0.403	0.354	0.345	0.376
VALN IC B	0.515	0.543	0.481	0.477	0.504	0.360	0.333	0.358	0.363	0.354

Table B.8 Dimensions of Internal Collar on Internal Collar Stiffened Specimens

	Collar Thickness (in.)	Length of Internal Collar (Back of Base Plate to Termination) (in.)				
		1	2	3	4	Avg.
VALN IC A	0.172	13.313	13.563	13.438	13.438	13.438
VALN IC B	0.172	14.125	14.188	14.000	14.000	14.078

Table B.9 General Dimensions for Full-Penetration Weld Specimens

	Diameter at Base Plate (in.)				Out of Round	Taper (in./in.)	Thickness (in.)
	1	2	3	Average			
VALN W A	10.000	9.938	10.031	9.990	0.93%	0.013	0.172
VALN W B	9.938	10.063	9.969	9.990	1.24%	0.013	0.173

Table B.10 Socket Weld Dimensions of Full-Penetration Weld Specimens

	Long Leg (on Pole) (in.)					Short Leg (on Base Plate) (in.)				
	1	2	3	4	Avg.	1	2	3	4	Avg.
VALN W A	0.541	0.532	0.575	0.584	0.558	0.281	0.369	0.348	0.236	0.309
VALN W B	0.582	0.612	0.574	0.554	0.581	0.371	0.236	0.290	0.277	0.294

Table B.11 Dimensions of Backing Bar and Interior Fillet Welds of Full-Penetration Weld Specimens

	Backing Bar Thickness (in.)		Backing Bar Length (in.)		Fillet Weld – Backing Bar to Base Plate (in.)		Fillet Weld – Backing Bar to Pole (in.)	
	1	2	1	2	1	2	1	2
VALN W A	0.180	0.169	1.904	1.880	0.299	0.386	0.347	0.360
VALN W B	0.164	0.174	1.870	1.684	0.371	0.443	0.389	0.362

Table B.12 General Dimensions of U-Rib Stiffened Specimens

	Diameter at Base at Base Plate (in.)		Average Diameter at Base Plate (in.)	Out of Round	Taper (in./in.)	Pole Wall Thickness (in.)
	1	2				
VALN UR A	10.000	9.938	9.969	0.62%	0.012	0.173
VALN UR B	9.969	10.000	9.985	0.31%	0.012	0.173

Table B.13 Socket Weld Dimensions of U-Rib Stiffened Specimens

	Long Leg (on Pole) (in.)					Short Leg (on Base Plate) (in.)				
	1	2	3	4	Avg.	1	2	3	4	Avg.
VALN UR A	0.579	0.588	0.529	0.567	0.566	0.4	0.445	0.45	0.413	0.427
VALN UR B	0.451	0.531	0.532	0.500	0.504	0.422	0.408	0.475	0.431	0.434

Table B.14 Dimensions of U-Rib Stiffeners

	D* (in.)	L1 (in.)	L2 (in.)	L3 (in.)	L5 (in.)	L6 (in.)	L7 (in.)	Stiffener Thickness (in.)
VALN UR A	4.043	7.938	4.184	5.969	3.109	0.773	0.734	0.174
	4.095	7.906	4.360	5.907	3.105	0.792	0.811	0.175
	4.057	7.906	4.264	5.891	3.129	0.798	0.719	0.175
	4.089	8.000	4.364	5.969	3.140	0.804	0.781	0.176
VALN UR B	4.108	7.938	4.296	5.922	3.094	0.812	0.750	0.177
	4.113	7.969	4.319	5.891	3.083	0.785	0.781	0.177
	4.112	7.906	4.358	5.907	3.086	0.787	0.797	0.176
	4.043	7.938	4.230	5.938	3.112	0.815	0.797	0.177

* See Figure B1 for Locations of Dimensions on U-Rib Stiffeners.

Table B.15 U-Rib Stiffener Weld Dimensions of U-Rib Stiffened Specimens

	Stiffener to Base Plate Weld				Stiffener to Pole Weld					
	Base Plate		Stiffener Leg		Base Plate Leg (in.)			Stiffener Leg (in.)		
VALN UR A	0.229	0.249	0.255	0.277	0.179	0.279	0.210	0.387	0.235	0.378
	0.259	0.275	0.304	0.336	0.268	0.280	0.264	0.401	0.236	0.422
VALN UR B	0.251	0.227	0.257	0.270	0.289	0.242	0.211	0.461	0.246	0.386
	0.280	0.236	0.293	0.264	0.220	0.253	0.231	0.386	0.246	0.417

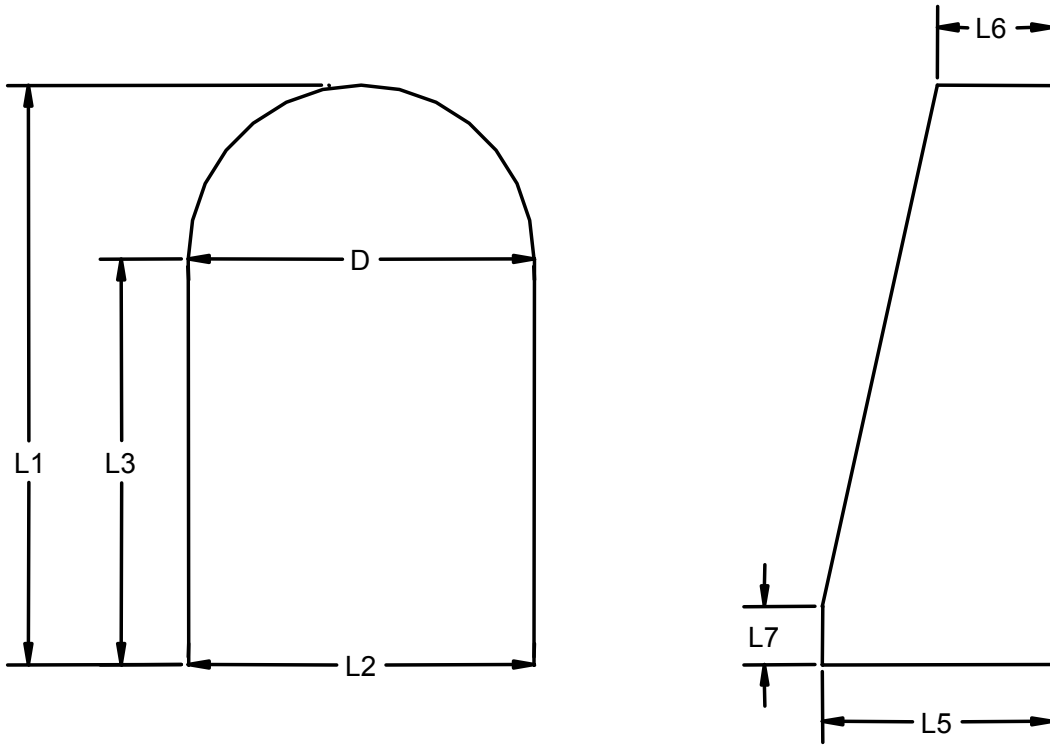


Figure B.1 Locations of Dimensions on U-Rib Stiffeners

APPENDIX C

Result Summary

Table C.1 Summary of Current Tests

Specimen Name	Nominal Stress Ranges			Controlling Stress Range (ksi)	N (cycles)
	At Socket Weld (ksi)	At Termination of Stiffener (ksi)	At Stiffener to Base Plate (ksi)		
VALu A	11.9			11.9	249,446
VALu B	11.9			11.9	453,948
VALu C	6.3			6.3	2,072,592
VALu D*	6.2			6.2	6,856,881*
VALu EP	11.4			11.4	393,767
VALu FP	11.5			11.5	353,103
TXu A	6.0			6.0	2,199,343
TXu B	6.1			6.1	2,816,706
TXu C	11.8			11.8	177,596
TXu D	12.0			12.0	194,694
TXu EP	11.8			11.8	320,915
TXu FP	11.7			11.7	141,155
VAL 3x1/4 A	6.8	11.1	10.0	11.1	476,269
VAL 3x1/4 B	6.8	11.4	10.1	11.4	696,326
VAL 3x1/4 C	3.6	6.1	5.4	6.1	3,592,372
TX 3x1/4 A	7.9	11.7	11.7	11.7	616,136
TX 3x1/4 B	8.0	11.8	11.8	11.8	416,146
TX 3x1/4 C LMS	7.8	11.9	11.9	11.9	523,397
VAL 3x3/8 A	6.0	11.7	8.7	11.7	386,253
VAL 3x3/8 B	5.8	11.6	8.6	11.6	410,410
VAL 3x3/8 CP	5.9	11.5	8.6	11.5	393,767
VAL 3x3/8 CP(2)	5.9	11.5	8.6	11.5	353,103
TX 3x3/8 A	7.0	11.7	9.9	11.7	473,735
TX 3x3/8 B	6.6	11.6	9.9	11.6	657,716
TX 3x3/8 CP LMS	6.7	12.1	9.9	12.1	1,707,128
VAL 6x3/8 A	5.7	11.2	8.4	11.2	242,728
VAL 6x3/8 B	5.9	11.3	8.7	11.3	653,392
VAL 6x3/8 C	3.2	5.9	4.6	5.9	3,592,372
TX 6x3/8 A	6.8	11.2	8.9	11.2	783,857
TX 6x3/8 B	6.4	11.3	9.7	11.3	783,857
TX 6x3/8 C	3.3	5.8	5.0	5.8	7,503,037

Table C.1 Summary of Current Tests (Continued)

Specimen Name	Nominal Stress Ranges			Controlling Stress Range (ksi)	N (cycles)
	At Socket Weld (ksi)	At Termination of Stiffener (ksi)	At Stiffener to Base Plate (ksi)		
VALNu A	11.9			11.9	389,428
VALNu B	11.8			11.8	265,540
VALNu G A	11.6			11.6	183,132
VALNu G B	11.5			11.5	151,679
VALNu 2 A	11.9			11.9	5,144,528
VALNu 2 B	11.8			11.8	1,683,127
VALN 6x3/8@45 A	9.0	12.0	9.2	12.0	238,515
VALN 6x3/8@45 B	8.9	12.0	9.2	12.0	161,843
VALN 6x3/8@45 C	3.2	4.3	3.3	4.3	6,066,817
VALN 6x3/8@45 D	3.1	4.3	3.2	4.3	6,066,817
VALN Col A	5.5	11.4		5.5	4,245,460
VALN Col B	5.7	11.4		5.7	2,363,152
VALN IC A	10.8	12.5		10.8	227,030
VALN IC B	10.7	12.3		10.7	227,030
VALN W A	17.7	17.5		17.7	422,400
VALN W B	17.6	17.3		17.6	422,400
VALN UR A (#4)	4.9	11.2	7.6	7.6	1,776,724
VALN UR B (#1)	5.0	11.2	7.6	7.6	950,670
VALN UR B (#2)	8.2	18.5	12.6	12.6	339,152
VALNu PR A*	11.6			11.6	4,557,126*
VALNu PR B*	11.5			11.5	4,557,126*
VALNu PR ul A	11.6			11.6	5,004,729
VALNu PR ul B	11.5			11.5	5,440,165
VALNu GP A	11.6			11.6	4,545,952
VALNu GP B	19.9			19.9	224,240
VALNu PG A	11.6			11.6	277,634
VALNu PG B	11.5			11.5	313,727
VALNu CP	19.9			19.9	1,301,077

* Test Stopped – Run-Out

APPENDIX D

Creating the Solid Models in AutoCAD 2002

The dimensions for the models were taken either from existing specifications and connection details or measurements taken from specimens. Appendix A tabulates the dimensions for the stiffeners, poles, welds, and baseplates and shows whether the dimensions were taken from details and or from measurements.

D.1 DRAWING THE BASEPLATE

The baseplate is created as a box¹ in AutoCAD with its center located at the origin and the bolt holes created by subtracting² cylinders from the box.

D.2 DRAWING THE POLE AND LOADING PLATE

The pole is a tapered ellipse that is socketed into the baseplate and is typically terminated 0.5 in. from the bottom of the baseplate. The shape of the pole is accomplished using the cone³ command in AutoCAD. For a given pole thickness, pole diameter at the face of the baseplate, and baseplate thickness, Equations 1-5 can be applied to calculate the required dimensions to draw the pole:

$$\text{Outer radius 1} = \frac{\text{Specified diameter}}{2} \quad (\text{Eq. 1})$$

$$\text{Outer radius 2} = (\text{Outer radius 1}) + 0.03125'' \quad (\text{Eq. 2})$$

$$\text{Inner radius 1} = (\text{Outer radius 1}) - (\text{Pole thickness}) \quad (\text{Eq. 3})$$

$$\text{Inner radius 2} = (\text{Outer radius 2}) - (\text{Pole thickness}) \quad (\text{Eq. 4})$$

$$\text{Outer cone height} = \frac{\text{Outer radius 1}}{\text{Taper}} + (\text{Socket Depth}) \quad (\text{Eq. 5})$$

$$\text{Inner cone height} = \frac{\text{Inner radius 1}}{\text{Taper}} + (\text{Socket Depth}) \quad (\text{Eq. 6})$$

Here Outer radius 1 is the radius parallel to the loading direction, and Outer radius 2 is the radius perpendicular to the loading direction. The cone height is the height entered into the cone command in AutoCAD.

Table D.1 shows the dimensions used for a 0.179 inch-thick pole with a diameter of 10.0 in., a 1.50 in. baseplate, and a 1.00 in. socket.

The distance from the bottom of the baseplate to the load point in the test setup was 94.85 in. The distance from the end of the pole to the center of the pin applying the load was 5.0 in. Therefore, a 5.0 inch-thick rigid loading plate is used to simulate this moment arm and to evenly distribute the load to the mast arm. The length of a typical pole is 89.35 in. This is found using Equation. 7:

$$\text{Pole Length} = 94.85 - 5.00 - (\text{Baseplate Thickness}) + (\text{Socket Depth}) \quad (\text{Eq. 7})$$

¹ 'Box' is a command in AutoCAD used to create cubes or cuboids

² 'Subtract' is a command in AutoCAD used to remove solids from other solids

³ 'Cone' is a command in AutoCAD used to create cones or elliptical cones

Table D.1 – Dimensions for VAL Pole

Parameter	Dimension (in.)
Baseplate thickness	1.50
Socket Depth	1.00
Taper	0.006
Pole thickness	0.179
Outer radius 1	5.00
Outer radius 2	5.03125
Inner radius 1	4.821
Inner radius 2	4.852
Outer cone height	834.33
Inner cone height	804.50
Pole length	89.35

To draw the loading plate, the outer cone is drawn and sliced⁴ at 94.35 in. and 89.35 in. from the base of the cone. To draw the pole, the inner and outer cones are drawn. The inner cone was subtracted from the outer cone and the result was sliced at 89.35 in. from the base of the cone.

D.3 DRAWING THE SOCKET WELD

The weld is drawn as a cone in AutoCAD and added⁵ to the pole and baseplate. The height of the cone used to draw the weld is computed using Equation 8:

$$H = \frac{(SL + \text{Outer radius } 1)(LL)}{SL \sqrt{(1 + \text{Taper}^2)}} \quad (\text{Eq. 8})$$

Here, H is the height of the cone, SL is the short leg of the weld, LL is the long leg of the weld, and the other variables are as defined in Equations 1 – 6.

D.4 DRAWING THE STIFFENERS

The stiffeners are drawn as boxes in AutoCAD to which the fillet welds – drawn using the wedge command – are added. The result is sliced to create a triangular stiffener. For the fillet weld connecting the stiffener to the baseplate, a small gap is left between the socket weld and the fillet weld to make meshing in Abaqus easier. For the fillet weld connecting the stiffener to the pole, a gap of 0.179” is left between the socket weld and the fillet weld for consistency in meshing.

D.5 EXPORTING MODELS

The models are exported as SAT files from AutoCAD found under *File – Export*.

⁴ ‘Slice’ is a command in AutoCAD used to remove portions of solid objects

⁵ ‘Union’ is a command in AutoCAD used to merge two or more solid objects

APPENDIX E ABS Technique

The following description is from the ABS report Rules for Building and Classing – Steel Vessels 2002, Part 5, Specific Vessel Types.

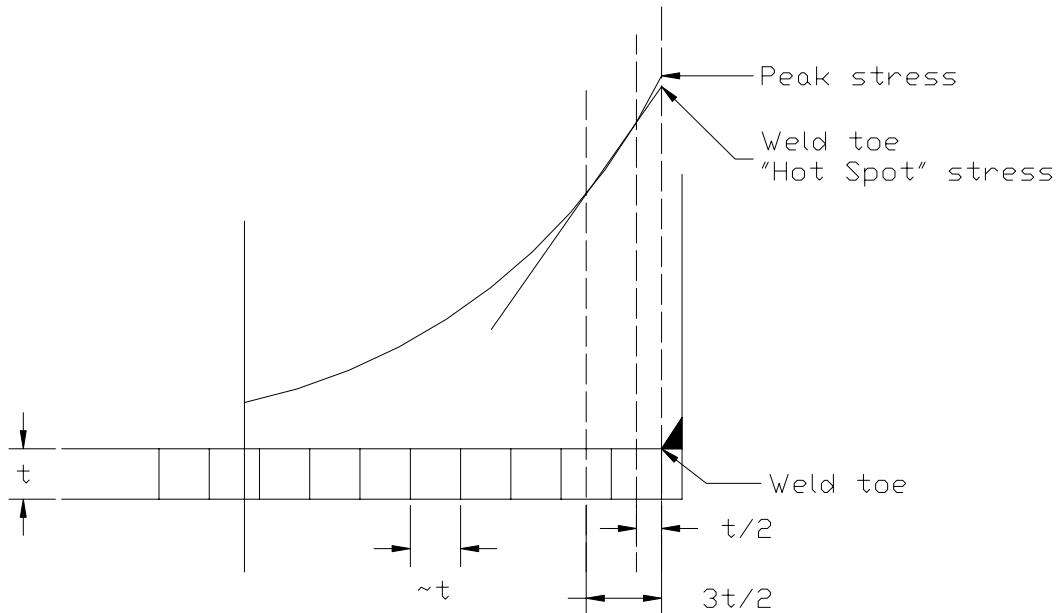


Figure A.1 ABS Technique

E.1 CALCULATION OF HOT SPOT STRESS FOR FATIGUE ANALYSIS OF SHIP STRUCTURES

The algorithm described in the following is applicable to obtain the hot spot stress for the point at the toe of a weld. The weld connects either a flat bar member or a bracket typically to the flange of a longitudinal stiffener, as shown in Figure A.1.

Consider the four points, P_1 to P_4 , measured by the distances X_1 to X_4 from the weld toe, designated as the origin of the coordinate system. These points are the centroids of four neighboring finite elements, the first of which is adjacent to the weld toe. Assuming that the applicable surface component stresses, S_i , at P_i have been determined from FEM analysis, the corresponding stresses at the “hot spot”, i.e., the stress at the weld toe, can be determined by the following procedure:

Select two points, L and R, such that the points are situated at distances $t/2$ and $3t/2$ from the weld toe; i.e.,

$$X_L = t/2, \quad X_R = 3t/2$$

where t denotes the thickness of the member to which elements 1 to 4 belong (e.g., the flange of a longitudinal stiffener)

Let $X = X_L$ and compute the values of four coefficients as follows:

$$C_1 = [(X-X_2)(X-X_3)(X-X_4)] / [(X_1-X_2)(X_1-X_3)(X_1-X_4)]$$

$$C_2 = [(X-X_1)(X-X_3)(X-X_4)] / [(X_2-X_1)(X_2-X_3)(X_2-X_4)]$$

$$C_3 = [(X-X_1)(X-X_2)(X-X_4)] / [(X_3-X_1)(X_3-X_2)(X_3-X_4)]$$

$$C_4 = [(X-X_1)(X-X_2)(X-X_3)] / [(X_4-X_1)(X_4-X_2)(X_4-X_3)]$$

The corresponding stress at Point L can be obtained by interpolation as:

$$S_L = C_1S_1 + C_2S_2 + C_3S_3 + C_4S_4$$

Let $X = X_R$ and repeat the step in 5-1-A1/13.7.2 to determine four new coefficients. The stress at Point R can be interpolated likewise, i.e.,

$$S_R = C_1S_1 + C_2S_2 + C_3S_3 + C_4S_4$$

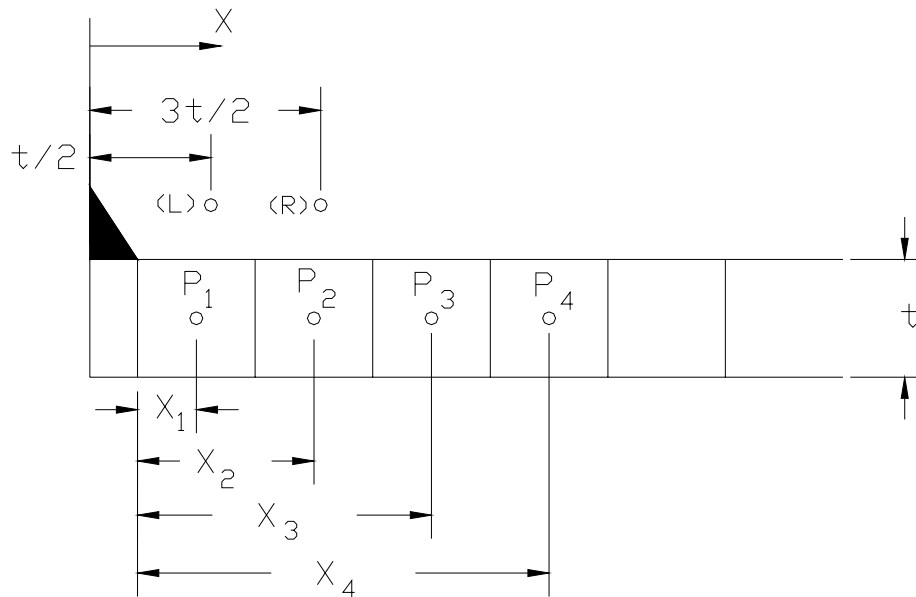
The corresponding stress at the hot spot, S_0 , is given by

$$S_0 = (3S_L - S_R)/2$$

Notes:

The algorithm presented in the foregoing involves two types of operations. The first is to utilize the stress values at the centroid of the four elements considered to obtain estimates of stress at Points L and R by way of an interpolation algorithm known as Lagrange interpolation. The second operation is to make use of the stress estimates, S_L and S_R , to obtain the hot spot stress via linear extrapolation.

While the Lagrange interpolation is applicable to any order of polynomial, it is not advisable to go beyond the 3rd order (cubic). Also, the even order polynomials are biased, so that leaves the choice between a linear scheme and a cubic scheme. Therefore, the cubic interpolation, as described in 5-1-A1/13.7.2, should be used. It can be observed that the coefficients, C_1 to C_4 are all cubic polynomials. It is also evident that, when $X = X_j$, which is not equal to X_i , all the C 's vanish except C_i , and if $X = X_i$, $C_i = 1$.



APPENDIX F

Measured Data

Table F.1 Measured Long Leg Dimensions (Inches)

Specimen	Specification	GAL Gage	NI IMAQ
VALN u A	0.44	0.69	0.696
VALN u B	0.44	0.56	0.557
VAL u C	0.44	0.53	0.528
VAL u D	0.44	0.53	0.505
VALN u GA	0.44	0.66	0.642
VALN u GB	0.44	0.53	0.525
TX u D	0.56	0.81	0.777
TX u E	0.56	0.56	0.659
VALN u 2A-1	0.44	0.56	0.538
VALN u 2A-2	0.44	0.56	0.552
VALN u 2A-3	0.44	0.50	0.500
VALN u 2A-4	0.44	0.56	0.564
VALN u 2B-1	0.44	0.56	0.535
VALN u 2B-2	0.44	0.56	0.543
VALN u 2B-3	0.44	0.56	0.516
VALN u 2B-4	0.44	0.53	0.517
VALN u D R	0.44	0.50	0.511
VALN u C R	0.44	0.53	0.509
VAL u EP-1	0.44	0.50	0.509
VAL u EP-2	0.44	0.53	0.531
VAL u FP	0.44	0.56	0.607
VALN u GPA	0.44	0.69	0.712
VALN u PRA	0.44	0.44	0.462

Table F.2 Measured Short Leg Dimensions (Inches)

Specimen	Specification	GAL Gage	NI IMAQ
VALN u A	0.44	0.41	0.422
VALN u B	0.44	0.41	0.428
VAL u C	0.44	0.28	0.382
VAL u D	0.44	0.34	0.390
VALN u GA	0.44	0.47	0.522
VALN u GB	0.44	0.41	0.473
TX u D	0.56	0.53	0.563
TX u E	0.56	0.34	0.398
VALN u 2A-1	0.44	0.34	0.356
VALN u 2A-2	0.44	0.31	0.355
VALN u 2A-3	0.44	0.28	0.356
VALN u 2A-4	0.44	0.31	0.368
VALN u 2B-1	0.44	0.34	0.352
VALN u 2B-2	0.44	0.34	0.363
VALN u 2B-3	0.44	0.34	0.350
VALN u 2B-4	0.44	0.31	0.352
VALN u D R	0.44	0.28	0.317
VALN u C R	0.44	0.31	0.317
VAL u EP-1	0.44	0.38	0.425
VAL u EP-2	0.44	0.38	0.415
VAL u FP	0.44	0.38	0.431
VALN u GPA	0.44	0.41	0.443
VALN u PRA	0.44	0.44	0.522

Table F.3 Long Leg Measurements (Inches), VALN u 2A

Parallels	GAL Gage	NI IMAQ
0.55	0.56	0.538
0.60	0.56	0.552
0.50	0.50	0.500
0.52	0.56	0.564
Average		0.538
Std Dev		0.028

Table F.4 Long Leg Measurements (Inches): VALN u 2B

Parallels	GAL Gage	NI IMAQ
0.56	0.56	0.535
0.52	0.56	0.543
0.51	0.56	0.516
0.47	0.53	0.517
Average		0.528
Std Dev		0.013

References

1. Alderson, Joseph L. “Fatigue Study of Cantilevered Traffic Signal Mast Arms.” Thesis. University of Missouri – Columbia, 1999.
2. American Association of State Highway and Transportation Officials. AASHTO Standard Specifications for Structural Supports for Highway Signs, Luminaires and Traffic Signals. 4th Edition. Washington, D.C.: AASHTO, 2001.
3. American Association of State Highway and Transportation Officials. AASHTO Standard Specifications for Structural Supports for Highway Signs, Luminaires and Traffic Signals. Interim Edition. Washington, D.C.: AASHTO, 2002.
4. ASTM Specification A595 “Standard Specification for Steel Tubes, Low-Carbon, Tapered for Structural Use”.
5. Cook, R. A.; Bloomquist, D.; Richard, D. S.; and Kalajian, M. A. “Damping of Cantilevered Traffic Signal Structures.” Journal of Structural Engineering ASCE, Vol. 127 (2001): 1476-1483.
6. Dexter, R. J., and Ricker, M. J. Fatigue-Resistant Design of Cantilevered Signal, Sign and Light Supports. NCHRP, TRB, National Research Council, Washington, D.C., June 2001.
7. Kaczinski, M. R.; Dexter R. J.; and Van Dien, J. P. NCHRP Report 412: Fatigue Resistant Design of Cantilevered Signal, Sign and Light Supports. TRB, National Research Council, Washington, D.C., 1998.
8. Macchietto, C. “Valmont Fatigue Testing: Gusset vs. Socket Weld Base Connection.” Presentation to Texas Department of Transportation. Austin, TX. September 2001.
9. Miki, Chitoshi; Fisher, J. W.; and Slutter, R. G. Fatigue Behavior of Steel Light-Poles. Report No. 200.81.714.1. Fritz Engineering Laboratory, Lehigh University, 1984.
10. Miki, C. and Masakazu, S. “A Study on U-Shaped Rib Configuration with High Fatigue Resistance.” Document No. XIII-1885-01. International Institute of Welding, 2001.
11. South, J. M. Fatigue Analysis of Overhead Sign and Signal Structures. Report No. 115. Illinois Department of Transportation Bureau of Materials and Physical Research, 1994.
12. Smith, J. W. Vibrations in Structures – Applications to Civil Engineering Design. New York: Chapman and Hall, 1988.